STUDIES IN PICOSECOND CHRONOSCOPY

A THESIS PRESENTED ON APPLICATION FOR THE DEGREE OF

DOCTOR OF PHILOSOPHY BY

STEWART FREDERICK BRYANT BSc

IMPERIAL COLLEGE LONDON 1978

TO MY WIFE

AND

TO MY PARENTS

STUDIES IN PICOSECOND CHRONOSCOPY

S F BRYANT

Abstract

The range of wavelengths over which picosecond time resolution can be obtained has been extended into the UV, by the construction of a Photochron 2 streak camera with a sapphire entrance window, and cathode substrate. Third harmonic generation in calcium of the mode-locked output of a Rhodamine 6G dye laser provided a test source of 3.5 psec. pulses at 200nm.

A streak camera with a higher effective intensifier gain was constructed by fibre-optically coupling a channel-plate image intensifier to the output of the streak tube. This streak camera is free from the effects of a large magnetic field, and is more compact.

Applications of the streak camera in the picosecond domain were demonstrated. Ultra-short pulses from an actively modelocked, flash-lamp pumped dye laser were investigated. It was found that in the middle and latter stages of the output train single pulses of duration 2-6 psec were generated. The characteristic delay, rise and decay times of the recombination radiation from a Cd-Se crystal at 77K were measured and found to be 34 ± 6 psec, 9 ± 2 psec, and 16 ± 3 psec respectively.

The dynamic range of operation of the Photochron type of streak camera was investigated, and was found to vary between 180 for 35 psec pulses, and 30 for 2 psec pulses. It was shown that on a 2 psec timescale no accumulative saturation effects occur.

A comparison was made between film and a vidicon system as the recording medium for a single shot streak camera. When the Mk. 3 streak camera was used in conjunction with an optical multichannel analyser, but without any image intensification the time resolution was less than 3 psec., and a dynamic range of 25 was measured for 4 psec pulses.

CONTENTS

CHAPTER 4 THE MK.3 STREAK CAMERA

CHAPTER 5 THE DYNAMIC RANGE OF THE PHOTOCHRON STREAK CAMERAS

CHAPTER 6 APPLICATION OF A PICOSECOND STREAK CAMERA

CHAPTER 7 THE USE OF A VIDICON READOUT SYSTEM

CHAPTER 8 FUTURE DEVELOPMENTS IN PICOSECOND DIAGNOSTICS

CHAPTER 1

THE GENERATION AND MEASUREMENT OF PICOSECOND PULSES

1.1 Introduction

Techniques for the generation and measurement of picosecond optical pulses have numerous applications in both science and engineering. Picosecond pulses have three primary properties that make them extremely useful : ultrashort duration, very high peak power when required, and a precisely reproducible pulse separation, inherent in the method of generation. The ultrashort temporal property of these pulses has enabled significant advances to be made in the fields of chemistry (107), biology (108), and physics (109, 114), where many of the fundamental processes occur on a picosecond timescale. The engineering application of these pulses ranges from the generation of picosecond electronic pulses (115, 116) to laser induced fusion (117).

Advances in pulse generation and pulse measurement are closely interrelated. Following the production of picosecond pulses for the first time (118, 119) came reports of sub-picosecond pulse durations. It was not until the advent of the picosecond streak camera (16), that an unambiguous analysis of the modelocking process became possible (65, 120 - 122), enabling a distinction to be made between a discrete pulse and a short burst of noise. The testing of the ultimate performance of an ultrafast streak camera has only been possible with the aid of reliable modelocked lasers, and pulse shortening techniques (19).

1.2 Modelocking

There are two completely organised states of operation of a laser: single frequency operation, and perfect modelocking. For each transverse mode of a laser cavity there corresponds a set of longitudinal modes limited in number by the bandwidth of the lasing medium, and separated in frequency by c/2L, where L is the cavity length, and c the velocity of light. In single frequency operation oscillation in only one longitudinal mode is permitted. If however the longitudinal modes are rigerously phaselocked to each other the laser output becomes a well defined function in time, and gives rise to the so-called "modelocked pulse train". This consists of a series of ultra-short pulses separated in time by the double-transit time (2L/c) of the resonator. In practice the duration of these pulses is limited by the bandwidth of the laser, since from the Uncertainty Principle

$$\Delta\nu \,.\, \Delta t \geq K$$

where $\Delta\nu$ is the bandwidth of the laser, Δt is the pulse duration, and K is a constant of the order of unity, whose value depends on the temporal profile of the pulse. The product $\Delta\nu.\Delta t$ is increased by the presence of amplitude or frequency modulation of the pulse, and is a figure of merit indicating the quality of the modelocking.

Modelocking is physically achieved by the application of gain or loss modulation to the cavity with a periodicity equal to or an integer multiple of its round trip time. This may be accomplished actively, by

externally providing a gain or loss at the round trip frequency, or passively by placing an intensity dependent loss within the cavity. A laser is usually actively modelocked either by optically pumping the active medium of the laser with a laser which is itself modelocked (gain modulation - 63), or by the inclusion of an acousto-optic modulator driven by a stable electrical oscillator (loss modulation - 123). Passive modelocking is accomplished by including a saturable absorber dye in the cavity (118). In the case of an actively modelocked laser accurate matching of the two frequencies is required (63, 61), while in the case of a passively modelocked laser the pulse provides its own modulation and hence synchronization is automatically achieved.

The laser systems with which picosecond pulses can be reliably produced may be divided into two principal groups, (a) giant pulse systems such as Nd: glass, Nd: YAG and ruby lasers, and (b) continuous or quasi-continuous lasers such as the dye laser.

1.3 Modelocked Solid State Lasers

Picosecond pulses were first obtained by passively modelocking ruby (118) and Nd: glass (119) lasers with an intra-cavity saturable absorber. The evolution of ultra-short pulses in these lasers has been the subject of extensive study both theoretical (125-127) and experimental (45), and is now well understood (124).

Pulses are generated by the action of the saturable absorber on the low intensity noise within the cavity. The loss experienced by a pulse passing through the saturable absorber depends on its intensity. The most intense noise pulses can saturate the absorption of the modelocking dye and subsequently be preferentially amplified in the gain medium.

The design and operation of this type of laser is extremely critical. For reliable operation the design must include optical compensation for thermal effects in the laser rod (5, 49), and a saturable absorber with a high value of low level light transmission contained within a thin dye cell contacted against one mirror (18). It is also important to only pump the laser close to threshold. Before the recent introduction of host glasses, with a low dn/dT (44) the statistics of the process limited the success rate of obtaining single trains of high quality modelocked pulses to $\sim$ 80%. A practical Nd: glass laser incorporating these features is described in Section 5.5.

The shortest pulses (3 - 8 psec) are produced by the Nd: glass laser. The pulse duration of other solidstate lasers is restricted by the bandwidth of the active medium to 20 - 30 psec (ruby and Nd: YAG respectively). Bandwidth-limited pulses are produced by the Nd: silicate glass laser only at the beginning of the pulse train (45). As the pulse train develops nonlinear interactions between the intense laser pulse and the laser glass give rise to self-phase modulation (128) causing pulse structure. The Nd: phosphate glass laser, with a lower nonlinear refractive index, is capable of producing bandwidth limited pulses for the entire output train, provided the power density is restricted to $\sim$ 150 MW cm^{-2} (42).

1.4 The Flashlamp Pumped Dye Laser

The passively modelocked dye laser (Cf Chapter 2) has several advantages over the giant pulse systems. It is capable of producing shorter pulses (> 1.5 psec -(4)), it is frequency tunable over the range 465 nm - 805 nm (18), and it is more reliable. The mechanism of dye laser modelocking differs from that occuring in giant-pulse systems. In a dye laser saturable amplification plays a more dominant role in the formation of short

pulses. The front edge of the pulse is sharpened by the absorption in the passive medium. The leading portion of the pulse then depletes the gain in the amplifier, which is then unable to amplify the back of the pulse. These two pulse shortening mechanisms combine to produce rapid pulse compression (120 - 122, 129). The presence of this second pulse shortening mechanism permits the use of saturable absorbers with long recovery times. Studies of the properties of the commonly used saturable absorbers show that dye laser pulses several orders of magnitude shorter than the recovery time may be produced (120). This is in marked contrast with the giant pulse systems, where the aperture time of the saturable absorber largely determines the lower limit on the final pulse duration (121, 122).

1.5 The C. W. Dye Laser

Bandwidth limited pulses as short as 0.3 psec have been produced directly with the passively modelocked C. W dye laser (130). These are the shortest optical pulses produced by any process.

A diagram of a C. W dye laser is shown in Figure 1.1. The laser is pumped by an argon ion laser which is focused into a freeflowing jet of dye (usually a solution of Rhodamine 6G in ethylene glycol). The modelocking dye is contained within a 200 μm dyecell in optical contact with the 100% mirror. The laser beam is focused into the absorber solution by a 2.5 cm focal length lens, increasing the power density by a factor of 4. Frequency selection is provided by a low dispersion prism within the cavity. With this arrangement short pulses are produced up to 20% above threshold. If a second free-flowing jet is used for the saturable absorber good pulses are only obtained close to threshold (131).

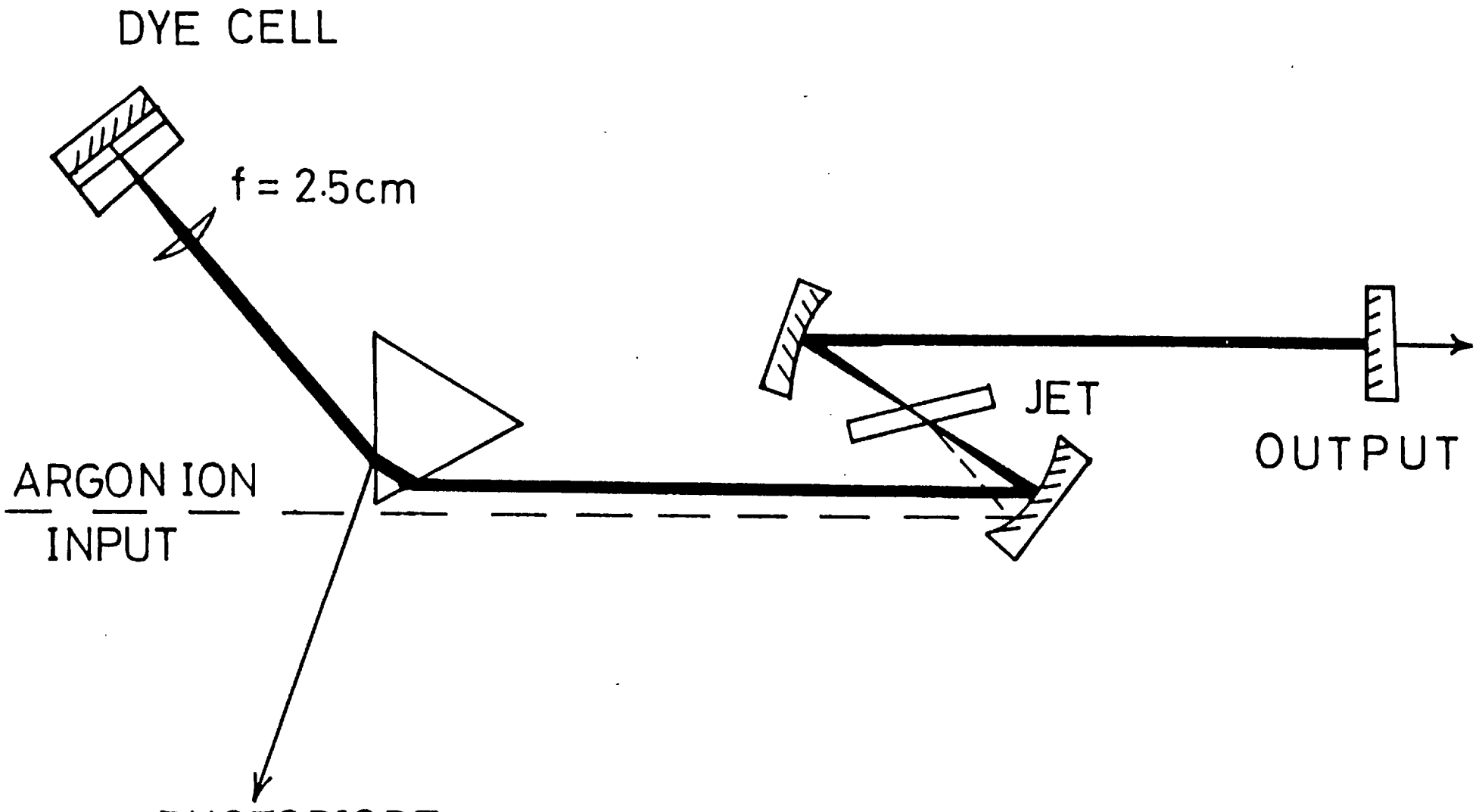

Fig.1.1 CW dye laser

Experiments have shown that as in the case of the Nd: glass laser, the pulse duration from this type of laser is dependent on the thickness of the absorber cell. Increasing the thickness of the cell to 500 μm increases the pulse duration from 0.3 psec to > 1.0 psec (130).

The pulses from the passively modelocked C.W. dye laser have a $sech^2$ intensity profile, peak powers of up to 300 W, and are sub-picosecond over a tuning range 598-615 nm.

1.6 Pulse Measurement - Non - linear Methods

The principle non-linear methods of pulse measurement are second harmonic generation (SHG - 133) and two photon fluorescence (TPF - 132). With these techniques the second order autocorrelation function of the pulse is measured. In normalized form this is given by

$$G^2(T) = \frac{\langle I(t)\, I(t+T) \rangle}{\langle I^2(t) \rangle}$$

where the brackets indicate an average over a long time. If I(t) is a single pulse, $G^2(T)$ vanishes for large values of the relative delay , and its halfwidth provides a measure of the duration of I(t). The function $G^2(T)$ is always symmetric regardless of any asymmetry in I(t). With these techniques it is not possible to determine the actual pulse shape, or readily estimate the level of inter-pulse noise (18).

Although background free SHG techniques are possible, the function normally measured in SHG and TPF is actually

$$S(T) = 1 + 2G^2(T) + r_1(T)$$

where S(T) is the recorded second harmonic signal or fluorescence intensity, and r_1 (T) is a rapidly varying fringe-like term that averages to zero. The shape of the recorded signal S(T) gives information about the quality of the pulses. A summary of these shapes is given in Figure 1.2.

The earliest technique used to determine the duration of a picosecond pulse was SHG in a Michelson interferometer (Figure 1.3(a)). An incoming pulse is split into two components each of which travel over a different path before being recombined in a non-linear crystal. The amount of second harmonic signal generated is proportional to the square of the instantaneous intensity, which will be a maximum when the two pulses arrive at the crystal simultaneously. The pulse width can hence be obtained by monitoring the dependence of the second harmonic signal upon the relative delay of the two sub-pulses. If the two sub-pulses are orthogonally polarized, and propagate through a K D P crystal as the ordinary and the extraordinary ray, then for an appropriate crystal cut the second harmonic frequency will only be generated when both pulses are simultaneously present. This gives a background-free SHG signal.

The triangular arrangement normally employed for the TPF technique is shown in Figure 1.3 (b). The input pulse is divided into two sub-pulses which travel co-linearly through an organic dye solution in opposite directions. Fluorescence from the dye is proportional to the two-photon absorption, which is a maximum at the point where the two sub-pulses are coincident in time. The spatial distribution of the fluorescence intensity may be recorded either on film or on an optical multichannel analyser (OMA), and the pulse duration deduced.

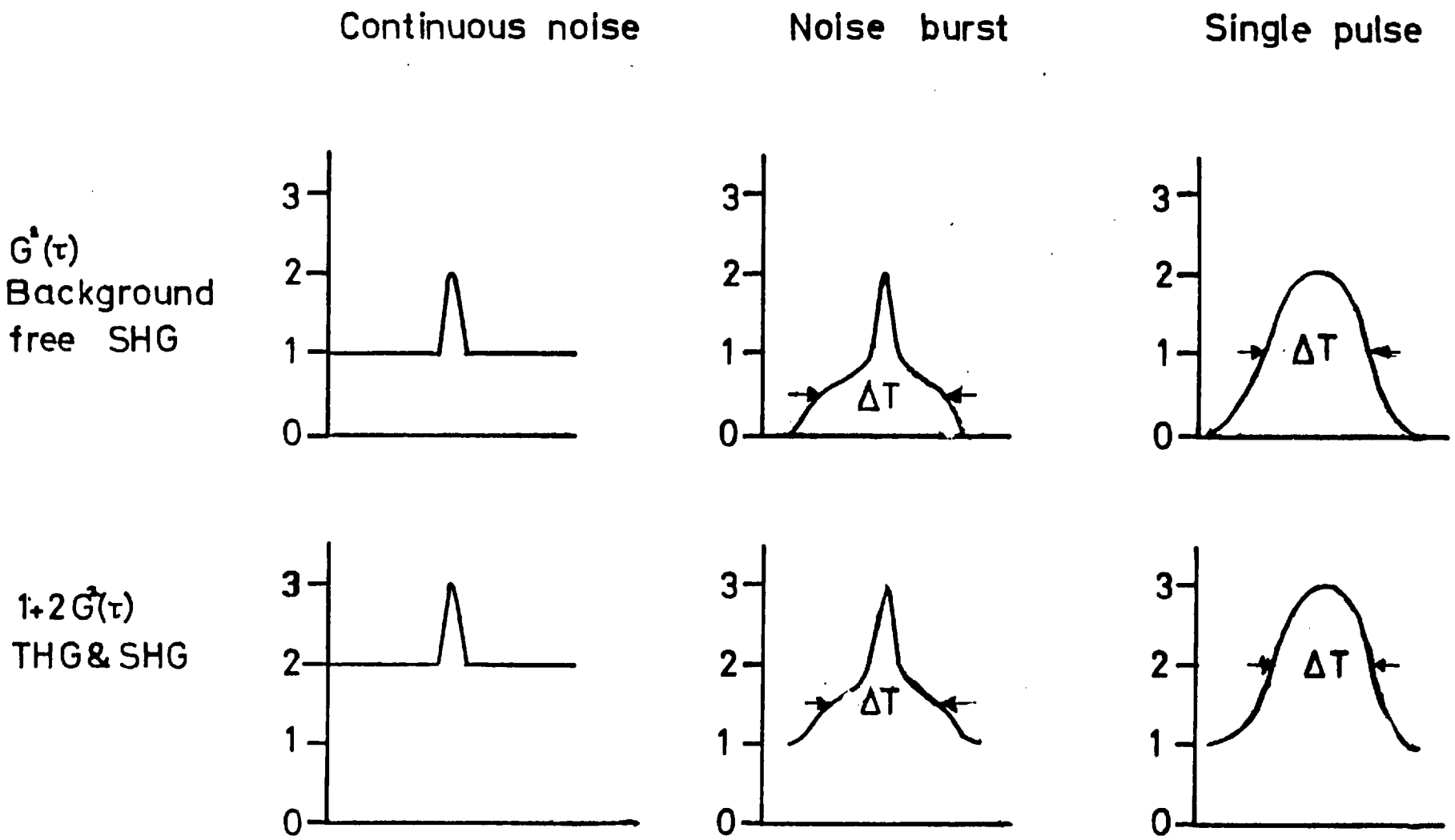
Continuous noise
Noise burst
Single pulse
G⁴(τ)
Background
free SHG
1+2G²(τ)
THG& SHG
3
2
1
0
ΔT

Fig. 1.2

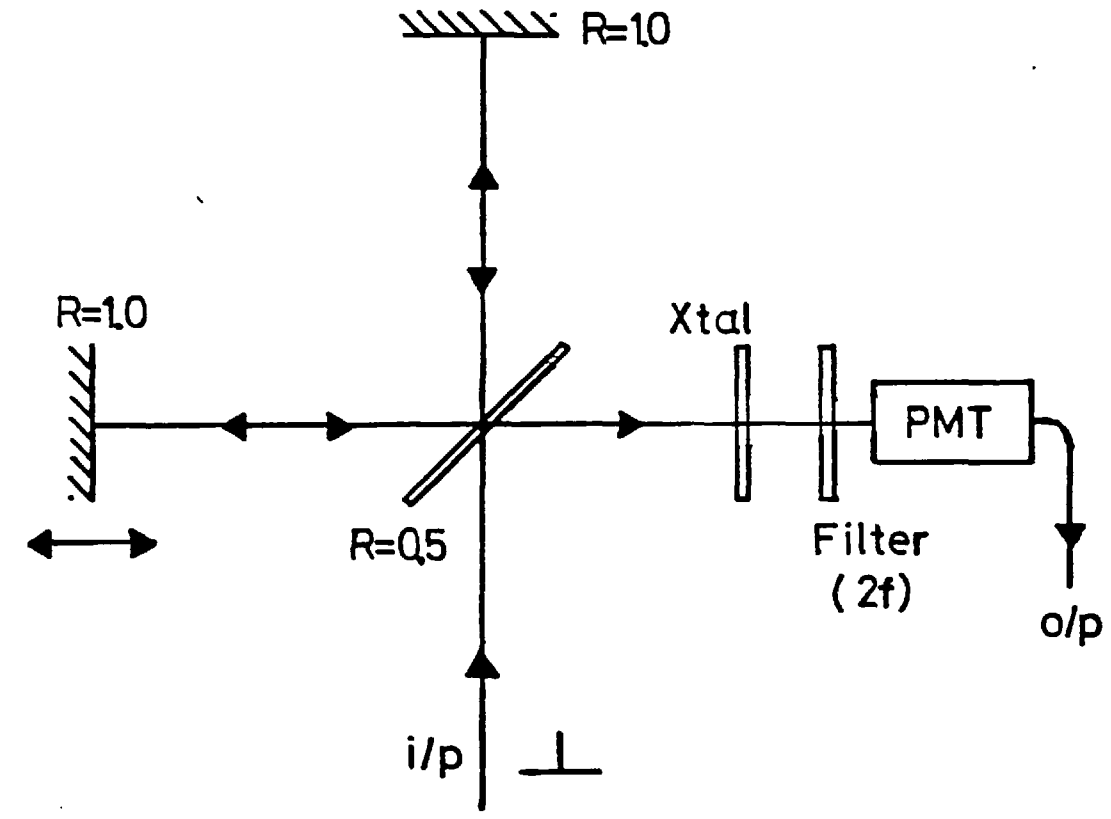

(a) SHG Autocorrelator

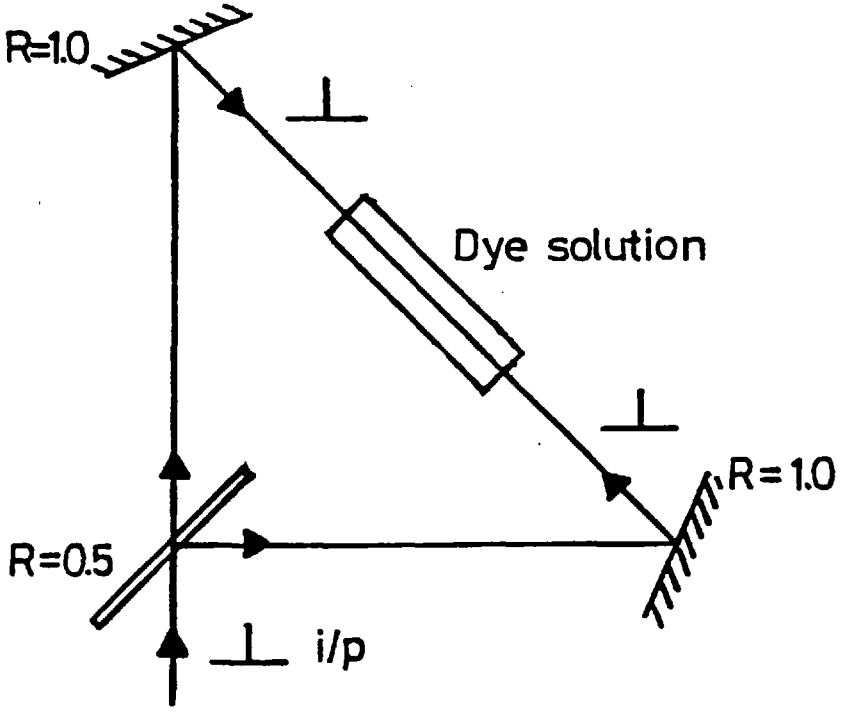

(b) TPF Autocorrelator

Fig.1.3

The principle disadvantage of using SHG in conjunction with a pulsed laser is that many individual laser firings are required to plot the temporal profile of a pulse. This method has hence largely been superceded by the TPF technique. The SHG method is however usually employed to measure the duration of the pulses from a modelocked CW laser. In this instance it is preferred since it does not introduce the non-linearities associated with film, or the expense of an OMA.

1.7 Pulse Measurement - The Streak Camera

The only linear technique capable of picosecond time resolution is the ultrafast electron-optical streak camera. Originally suggested by Zavoisky and Fanchenko in 1956 (40) the electron-optical streak camera is capable of unambiguously determining the temporal structure of an optical event on a picosecond timescale. The sensitivity of the streak camera is much higher than most of the non-linear techniques only being limited by the quantum efficiency of the photocathode, and photon statistics.

The principles of operation of the streak camera may be demonstrated with reference to Figure 1.4. Light from a picosecond optical source is incident on the slit of the streak camera, which in turn is imaged onto the photocathode. The optical pulse is thus converted into a pulse of electrons. These electrons are in turn imaged on the centre of the phosphor of the streak tube in the 'focus' or 'static' mode. By deflecting the slit image across the phosphor of the streak tube, temporal information is converted into spatial information. The optical intensity as a function of time can hence be obtained by examining the recorded intensity as a function of position. The two most significant parameters influencing

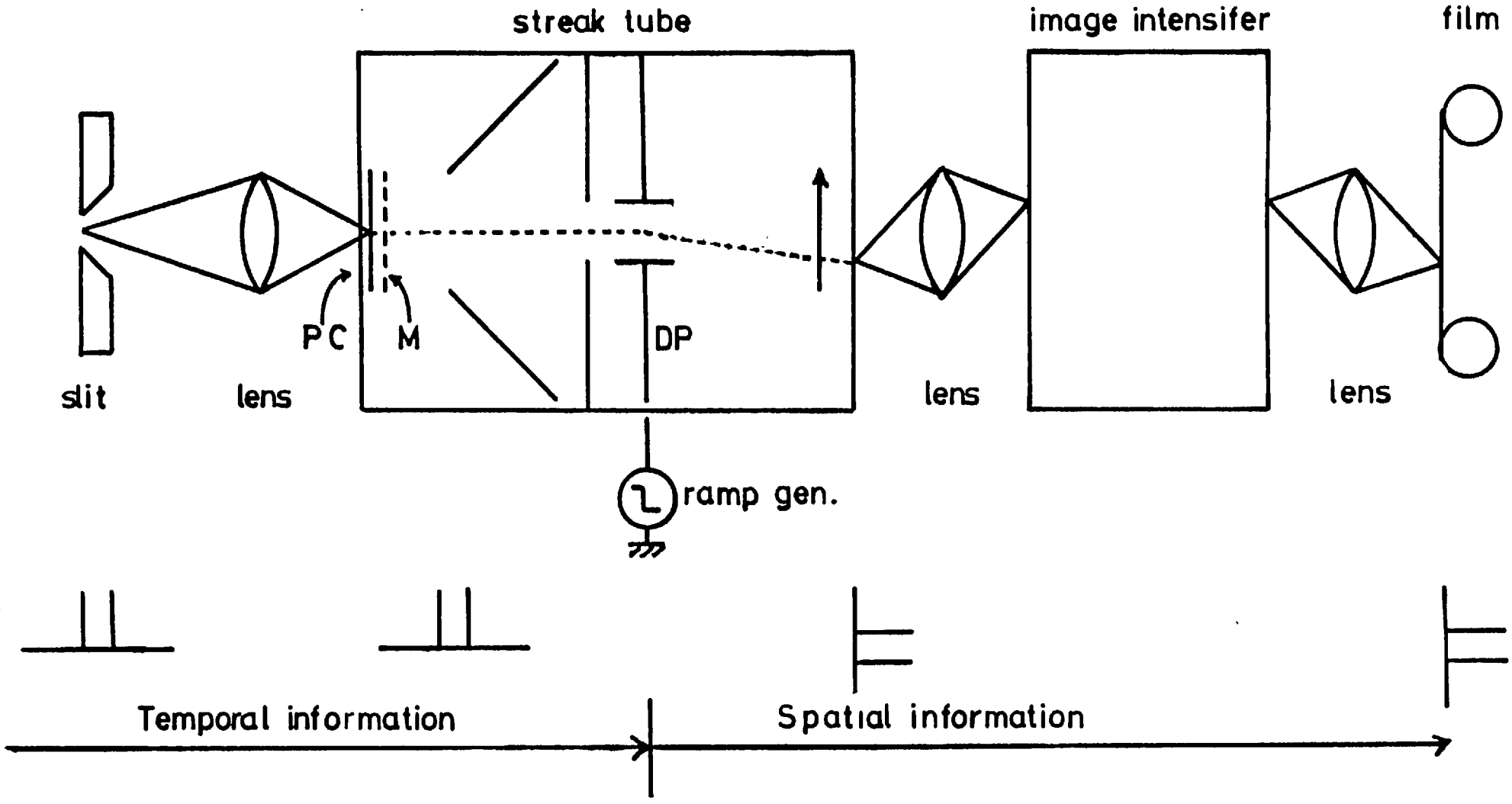

Fig.1.4 A streak camera

the resolution of these cameras are the initial electron energy distribution of the photoelectrons, and the length of time taken to deflect the slit image by a resolution element. The significance of the electron energy spread is reduced by rapidly accelerating the electrons to a high energy, whereupon they "forget their initial energy spread". This is normally accomplished by applying a high voltage to a mesh electrobe close to the photocathode (33).

For optimum temporal resolution the streak tube of the camera must be coupled to a high gain image intensifier, in order to reduce the photoelectron current to an acceptably small value. (A more complete discussion on the design and operation of these ultra-high speed cameras is given in Chapter 2).

The different types of streak camera developed may be divided into three basic classes. Those with streak tubes developed from the original Russian PIM design (134), those based on the RCA C73435 streak tube (31), and those based on other types of streak tube. The most highly developed streak cameras are those having the PIM type of electrode configuration, and include the U.K. Photochron type of tubes, and the Japanese Hamamatsu N895 tube. This is the only class of streak tube with a proven temporal resolution of 1 psec (19). With modifications to the photocathode these streak tubes have been used at a variety of wavelengths from 1.06 μm in the near infra-red to 12 Å in the X-ray region of the spectrum (135).

Although the RCA C73435 streak tube has been shown to be capable of 6 psec temporal resolution (31) it has a dynamic spatial resolution inferior to that of the Photochron type of streak tubes, and is less highly developed. The Thompson - CSF TSN 504-04 streak tube (136) is similar to the RCA tube. Although further developed to the point of incorporat-

ing an internal channel plate electron multiplier, this tube still only has a time resolution of $\sim$ 7 psec.

A number of other streak tube designs have been proposed and constructed, incorporating such features as proximity, quadropole lens (137) or magnetic focusing (138). Although these designs all have various merits, the only one in current production is the American Pico-V design (Figure 1.5). This is a proximity focused streak tube incorporating a passive micro-channel plate both to provide a high cathode extraction field and to act as an electron collimator. A time resolution of less than 2 psec has been claimed for this type of streak camera. Two particularly distinguishing features of this design are the high cathode extraction field, which at 100K V/cm is higher than used on any other tube, and its extremely small size ($\sim$ 8 cm long). An X-ray version of this streak tube, the pico-X (139), has also been constructed. This tube has a photocathode extraction field pulsed to over 400 KV/cm, and a time resolution of better than 3 psec.

1.8 Conclusion

Unfortunately space has limited this description of picosecond techniques to include only the main points of the more important techniques of optical pulse generation and measurement. The characteristics of the Photochron type of streak camera are discussed in greater depth in the later chapters of this thesis. For a more detailed description of picosecond techniques in general the attention of the reader is drawn to Reference 18, and the other chapters of the same book.

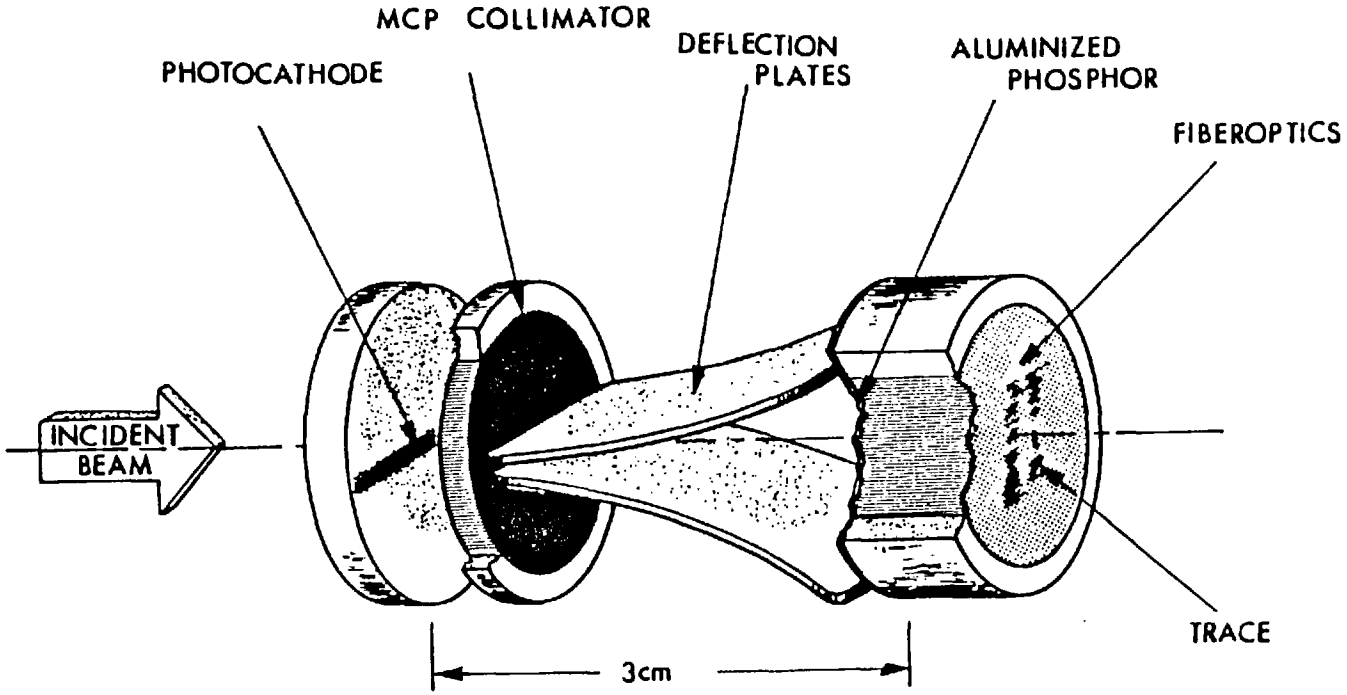

Fig. 15 The Pico-X streak camera

CHAPTER 2

THE MODELOCKED FLASHLAMP PUMPED DYE LASER AND THE MK.2 PHOTOCHRON STREAK CAMERA

2.1 Introduction

In order to develop a new type of picosecond streak camera it is essential to have available a reliable source of test pulse, having a duration comparable to, or preferably much less than the resolution limit of the streak camera. The modelocked, flashlamp pumped dye laser (1,2,3) is a convenient source of such ultrashort pulses.

To produce good test pulses however, adequate diagnostics must also be available. The Mk.2 Photochron streak camera (4,5) provides both a convenient method of pulse monitoring, and a suitable basis for further streak camera development.

As much of the work described in this thesis requires a basic understanding of the laser and streak camera, a description of each is given in this chapter.

2.2 The Modelocked Rhodamine 6G Dye Laser

The modelocked flashlamp pumped dye laser used has already been described in detail (3,6). This laser is capable of producing pulses of duration 2 - 4 psec. over most of the tuning range of Rhodamine 6G (620 - 575 mm).

The optical configuration of the laser is shown in Figure 2.1. The laser head consists of a double elliptical cylinder, machined from dural, polished and vacuum coated with aluminium. The dye cell (a quartz tube with 5 mm bore, 1 mm wall, 150 mm long, and with windows attached at each end, set at Brewster's angle) is located at the common foci of the ellipses. A second quartz tube (10 mm bore, 1.25 mm wall) through which cladding liquid is pumped surrounds the dye cell. This increases the apparent area of the dye cell which consequently increases the (optical) pumping efficiency, and also prevents long term thermal gradients between dye and dye cell wall.

The dye is optically pumped by two 6" capillary 4.5 mm bore flashtubes (T.W. Wingent GAA 10), located at the outer foci of the ellipses. The laser head is positioned roughly in the centre of the optical cavity, formed by two plane mirrors separated by 65 cms. One mirror has a reflectivity of 99% and is in optical contact with a saturable absorber in the 2 mm thick modelocking dye cell. The output mirror has a reflectivity of 50%. Both mirrors have 1^{o} wedges to prevent the occurence of subcavities. Frequency selection and narrowing are achieved by including a 5 μm gap intra-cavity Fabry-Perot etalon. The etalon is given a slight tilt about its horizontal axis to prevent the formation of satellite pulses, and the laser frequency is changed by rotating it about its vertical axis.

To minimize the effects of both thermal and u.v. degradation of the active medium (7,8,9) the dye is pumped through the dye cell from a 2 litre reservoir placed in a constant temperature bath. A filter membrane with 2 μm pores (Millipore BSWP 14200) is inserted in the dyecell feed line to inhibit the passage of bubbles through the dyecell, since they would destroy the homogeneity of the active medium. The dye normally used in

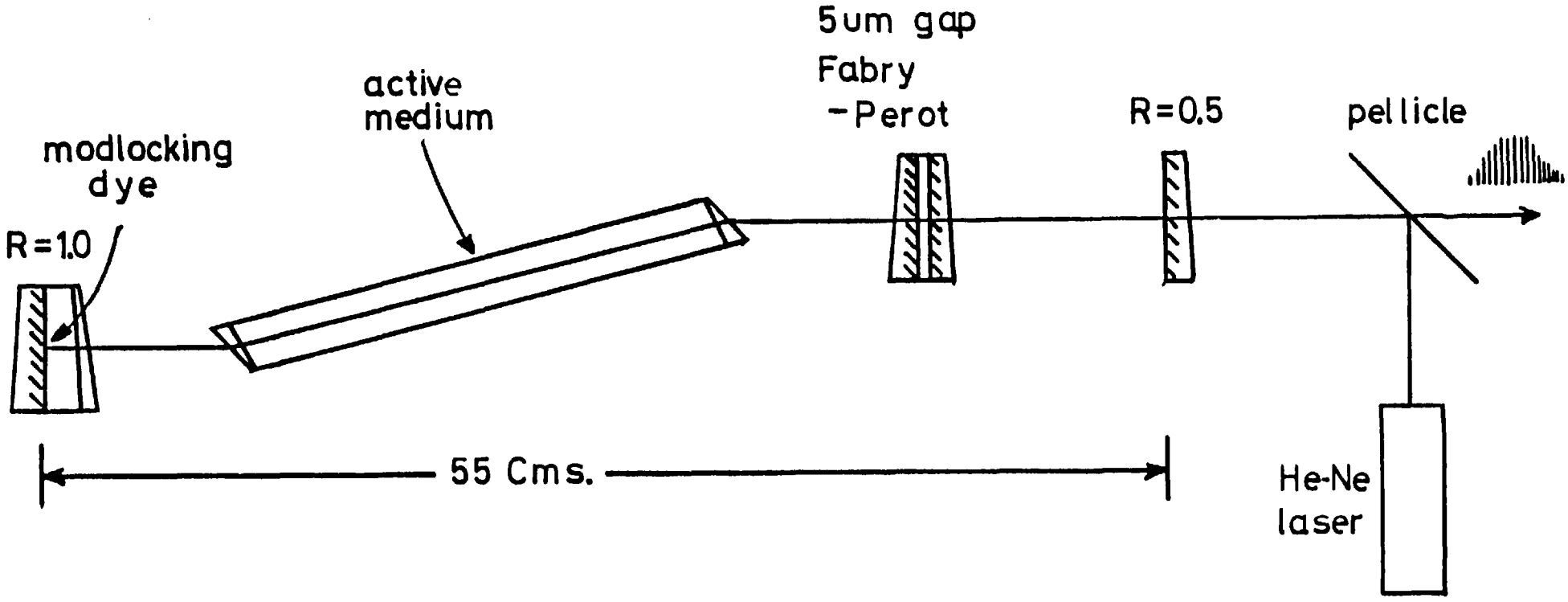

Fig 2.1 Dye laser

this system is an aqueous solution of Rhodamine 6G (1.2×10^{-4}M) to which 10% surfactant (N, N dimethyldodecylamine - N - Oxide, commercial name Ammonyx - LO) had been added to prevent the formation of non-fluorescing dimers (10).

The electrical circuit used to provide the fast discharge through the flashlamps is shown in Figure 2.2. A high current, high voltage power-supply (20 mA, 0 - 30 KV) charges the energy storage capacitors C1 and C2 through the charging resistance R1, and the two flashlamp bypass resistances R3 and R4. Since the lamps (filled to 100 Torr with pure Xenon) have a breakdown voltage of ~10 KV it is necessary to include a switch in the discharge circuit. This can either be a spark gap (5) or a hydrogen thyratron. Thyratrons have the advantage that their triggering characteristics are less dependant on the applied voltage (11, 12), and that they can be used at a higher repetition rate. Since they are physically larger, and the circuitry more inductive than their sparkgap counterpart, thyratron discharge networks tend to have a longer risetime. With this laser, flashlamp output risetimes were ~1 μs for an EEV CX1159 thyratron, compared to 0.6 μs for an EGG GP-12B spark gap. This is not a serious disadvantage however for the Rhodamine 6G laser.

The flashlamps are fired by applying an 800V pulse to the grids of the hydrogen thyratron V1, causing it to conduct. The whole of the voltage on each capacitor hence appears across its associated lamp. Since this voltage is greater than the holdoff voltage for the lamp a discharge takes place. To ensure that the two lamps fire simultaneously, they are preionized by applying the high voltage output from a trigger transformer to a nichrome wire spiral surrounding their capillaries. This preionizing pulse is applied ~4 μs before the main trigger pulse to the thyratron.

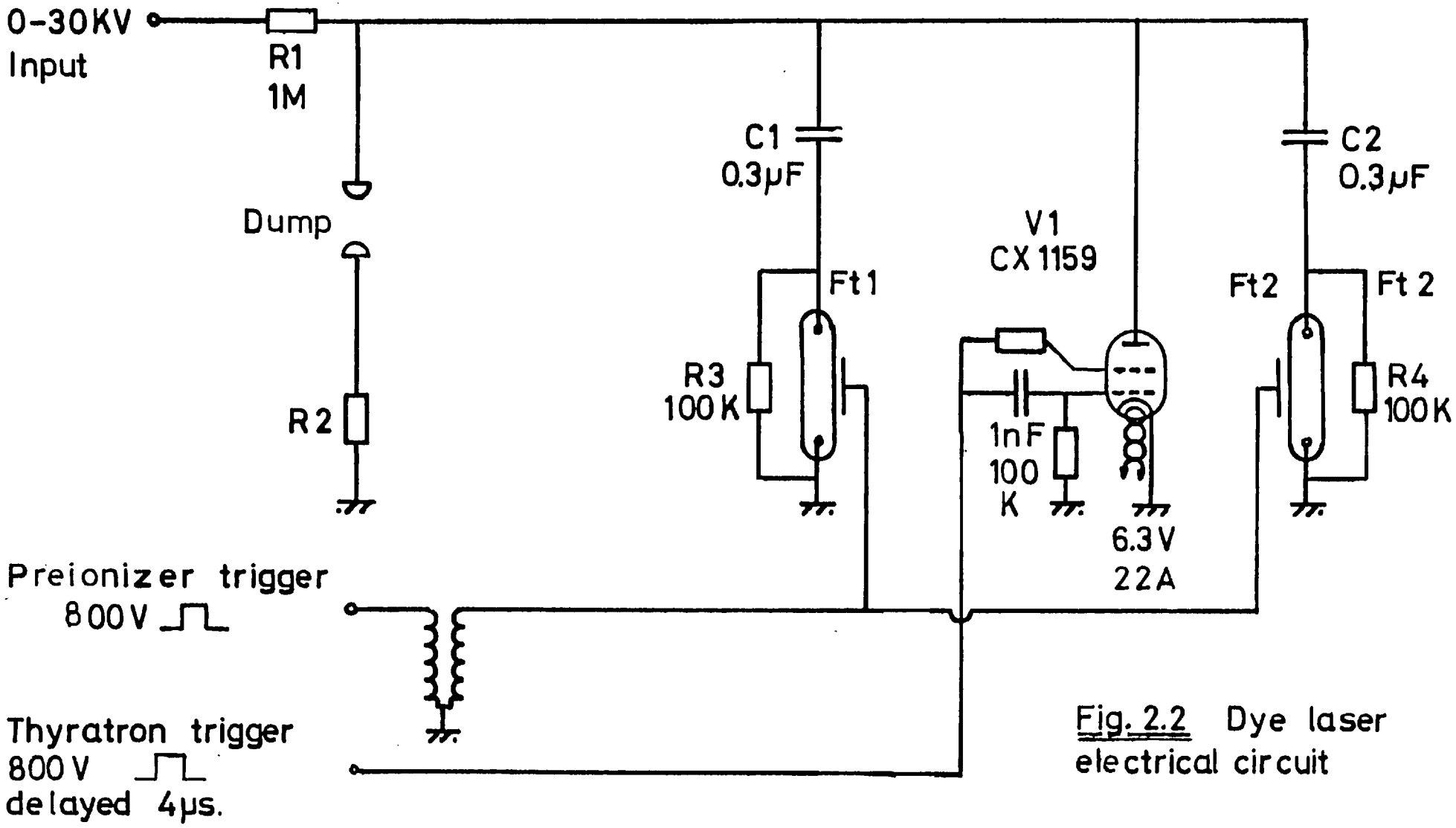

Fig. 2.2 Dye laser electrical circuit

For efficient laser action it is important that the risetime of the flashlamp light output be as short as possible (<1 μs). This is necessary because of the very short radiative lifetime of the lasing dye, and also to ensure that lasing takes place before the onset of severe thermal effects. Previously this fast risetime had been thought to be necessary to enable lasing to take place before the accumulation of level crossing effects, but is now known that atmospheric oxygen adequately quenches the triplet state in Rhodamine 6G (13, 14). The requirement for a fast risetime from the discharge circuit means that it must be constructed in a low inductance configuration, employing either short thick leads, or coaxial assemblies. An example of a flashlamp output profile for a circuit with a 75 cm long, 50Ω coaxial feed for each flashlamp is shown in Figure 2.3 (a).

The laser is normally modelocked by an ethanolic solution of either DQOCI when operating in the range 575-600 nm (4,6), or DODCI in the range 600 - 625 nm (4,15). Shorter pulses can be expected in the case of DQOCI (typically 1.5 - 3 psec) than in the case of DODCI (typically 2 - 3 psec), although this occurs at the cost of a lower output energy (3). Optimum operation is found to occur at 600 nm and 605 nm respectively. A typical modelocked train for each case is shown in Figure 2.2b, and 2.2c respectively.

DQOCI - 1,3' - DIETHYL 4,2' - QUINOLYLOXACARBOCYNINE IODIDE

DODCI - 3,3' - DIETHYLOXADICARBOCYANINE IODIDE

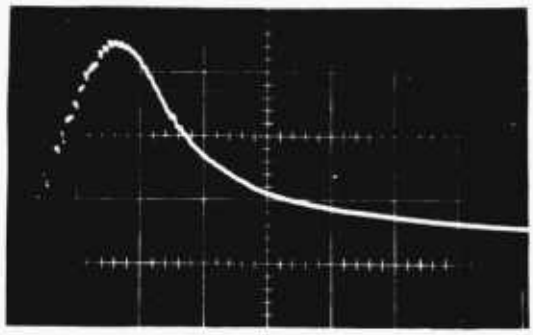

(a) Flashlamp profile 1μs/div.

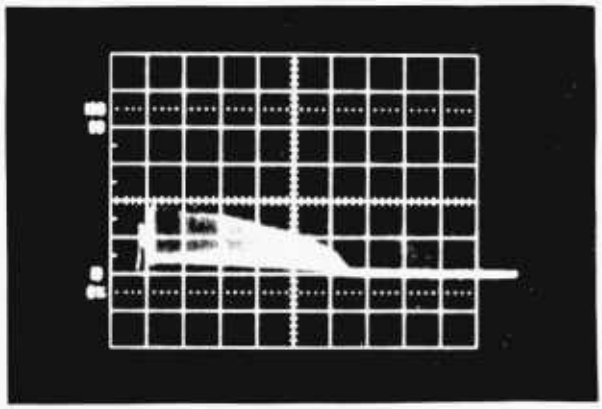

(b) Modelocked train DODCI 605nm 200ns/div.

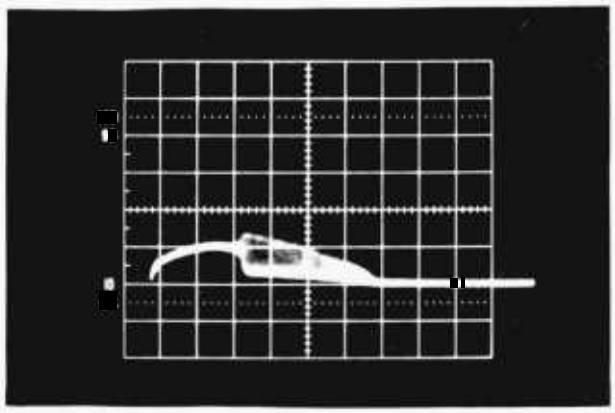

(c) Modelocked train DQOCI 600nm 200ns/div.

Fig 2.3

2.3 The Pulse Selector

It is frequently necessary to select one or more pulses from a modelocked pulse train. This is because in most cases it is desirable to exclude from a measurement the effects of the build-up and longer duration pulses at the start of a modelocked train, or to eliminate the accumulative effect of many pulses. When a streak camera is used in conjunction with a modelocked laser superfluous pulses induce a high background. This is because some of the photoelectrons produced whilst the slit image is biased off screen scatter onto the phosphor of the streak tube (5).

Ideally only one pulse would be switched out, however it is convenient to switch out several when working with a streak camera and pulsed dye laser. This is because the ramp generator circuit in a streak camera has an inherent delay of 20 - 25 ns. There are three possible ways of overcoming this delay :-

(a) Switch out several pulses, trigger the ramp generator from the first pulse, and streak a later one.

(b) Trigger the ramp generator and then send the modelocked pulse through a 25 ns optical delay line.

(c) To only gate the streak tube on for a few nanoseconds.

The construction of a Photochron 2 streak tube is unsuitable for fast gating, since long inductive leads connect the cathode and mesh electrodes to the external connector pins (this is for manufacturing reasons).

Any gating pulse used would have to be entirely free from high voltage spikes, since these would induce a cathode-mesh breakdown, giving rise to excessive noise on the output, and eventually destroy the shutter tube. It was thus considered expedient to adopt solution (a) above.

A diagram of the pulse selector is shown in Figure 2.4. The output from the laser, which is mainly horizontally polarized, is passed through a Glan-Thompson prism (GT1) to reject any residual vertical component. The second Glan-Thompson 'analysing' prism (GT2) is set to only pass vertically polarized light, thus initially the output from the laser is rejected and is incident on a fast vacuum photodiode (ITL Planar 125 Ω). The laser output is monitored on a Tektronix 519 oscilloscope.

At some predetermined time after the oscilloscope has triggered, avalanche transistors TR1 - TR6 are triggered, triggering in turn the krytron (EGG KN 22B). This avalanche transistor and krytron combination are similar to the arrangement used to generate the streak ramp in the streak camera (5).

Cable Ca1 and resistance R1 are a Blumlein pulse forming network. Cable Ca1 is charged to the halfwave voltage of the Pockel cell (PC), and R1 is chosen to be twice the surge impedance of the coaxial line. The action of the krytron switch is to produce a pulse across the Pockel cell equal to its halfwave voltage and having a duration $t = \frac{l}{ck}$, where l is the total length of the cable, c is the velocity of light, and k is the velosity factor for the cable. Thus for some time t the plane of polarization of the light is rotated, and a number of pulses n (where $n = t/tr$ and tr is the round trip time of the laser) are switched out.

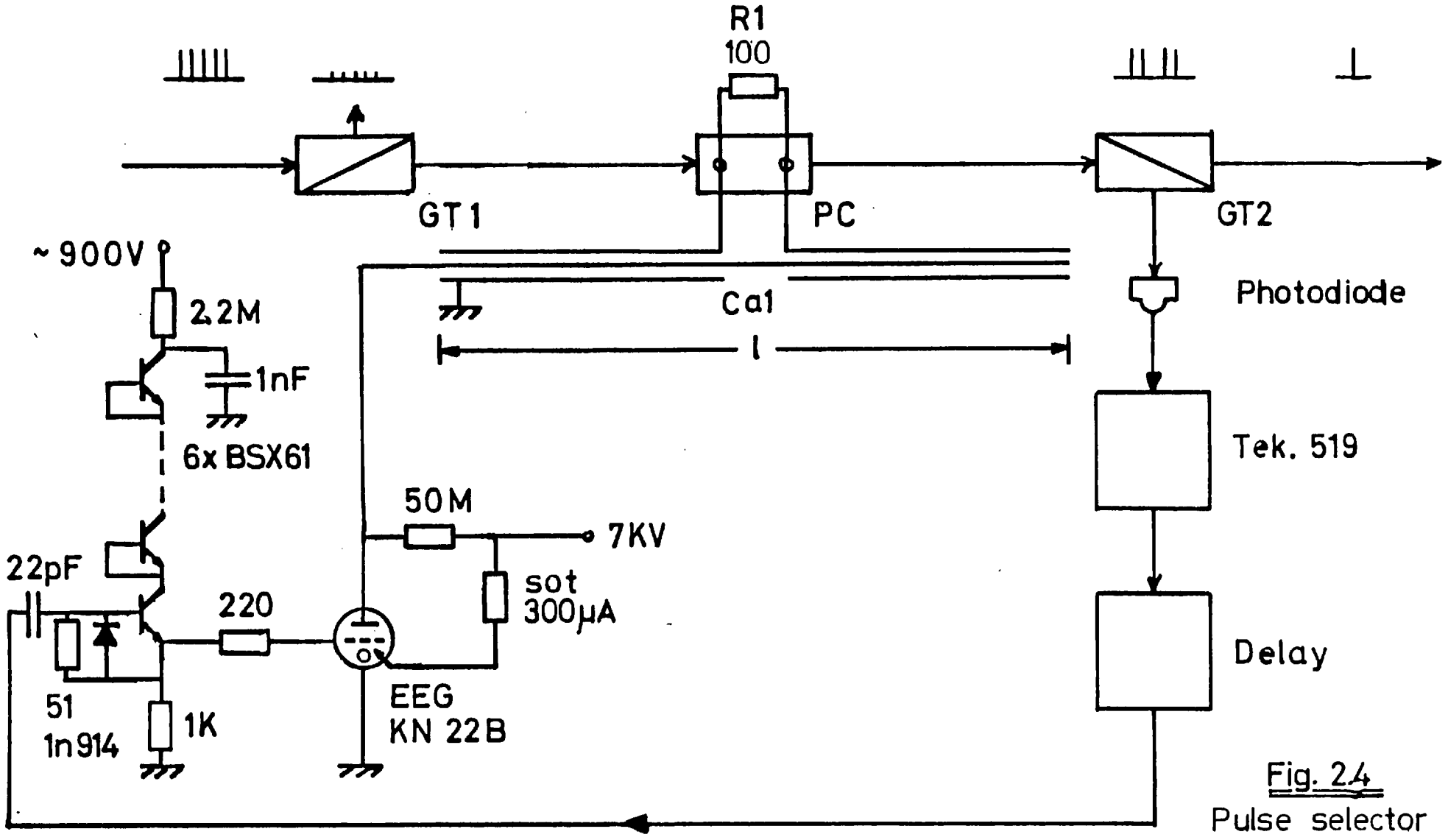

Fig. 2.4
Pulse selector

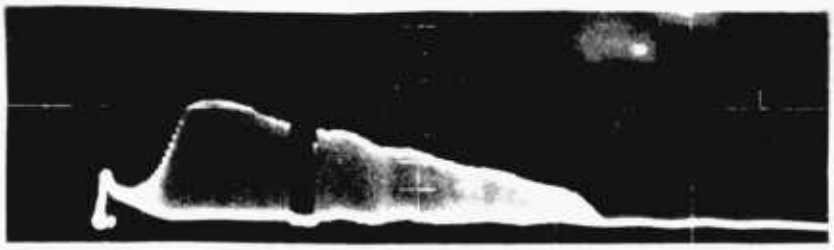

(a) Rejected train 200ns/div.

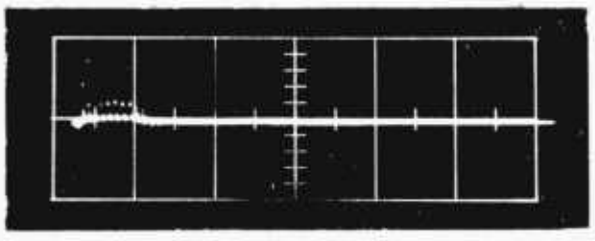

(b) Switched out pulses 50ns/div.

Fig. 2.5

An example of a modelocked pulse train with a switched out pulse packet, and the selected pulses is shown in Figure 2.5.

To enable the alignment of the optics after the switch it is necessary to permanently rotate the plane of polarization of the light before the second Glan-Thompson prism. This may be acheived either by applying the halfwave voltage from the EHT supply directly across the Pockel cell, or by introducing a halfwave plate after the Pockel cell. The use of a halfwave dc voltage is preferred in that it avoids any redirection of the beam through the switch.

2.4 The Streak Camera

Both the Photochron 1 and Photochron 2 streak cameras have been described in detail elsewhere (4, 16, 17). This type of camera has been adapted for operation over a large range of wavelengths (18), and it has been shown that when operated close to the photocathode cutoff wavelength it is capable of subpicosecond time resolution (19). The Photochron 1, and Photochron 2 streak cameras are similar in all respects, except that in the latter case modifications were made to the front of the streak tube to reduce both the electron transit time-spread, and the electron-optical magnification. In deference to Sibbett (5) the Photochron 2 streak tube lens coupled to a cascade image intensifier is known as the Mk 2 streak camera.

Figure 2.6 is a diagram of a photochron 2 streak tube. A 3 times demagnified image of the 50 μm slit at the front of the camera is focused onto the photocathode of the image tube, by a Biotar 75 mm f/1.4 lens. The photoelectrons liberated at the photocathode are rapidly accellerated to an energy of 1 KeV by a fine mesh (750 cpi) located 0.5 mm from the cathode surface. This is necessary to reduce the effect of the spread in their initial energies. Although a number of electrons may be generated simultaneously the more energetic ones will reach the deflection plates before the slower ones, and hence will appear at different positions on the phosphor of the tube. The inclusion of a mesh in this type of tube reduces the transit time spread from 50 psec for the early tubes with no mesh, to ~0.5 psec with the type of tube described here, when operating at say 735 nm with an S20 photocathode (19). The method for calculating the transit time spread is given in section 2.5.

The slit image on the photocathode is focused on to the phosphor of the image tube by the combined action of the electron-optical lenses constuted by the electrostatic fields set up by the mesh, cone and anode. The image may be brought into focus by adjusting the voltage applied to the cone, which is nominally 875V. The region after the anode is a drift zone, and is held at +18KV. In a grade one Photochron 2 tube a static resolution of 40lp/mm at the cathode and a magnification of 1.95 have been measured. A pair of deflection plates, mounted after the anode, in the drift zone, enable the slit image to be deflected across the phosphor with a deflection sensitivity of 300 V/cm.

The image of the slit is initially deflected off screen by the application of a bias of 20.5 kV through a 50 MΩ resistance to one of the deflection plates. The output of the ramp generator, a negative going

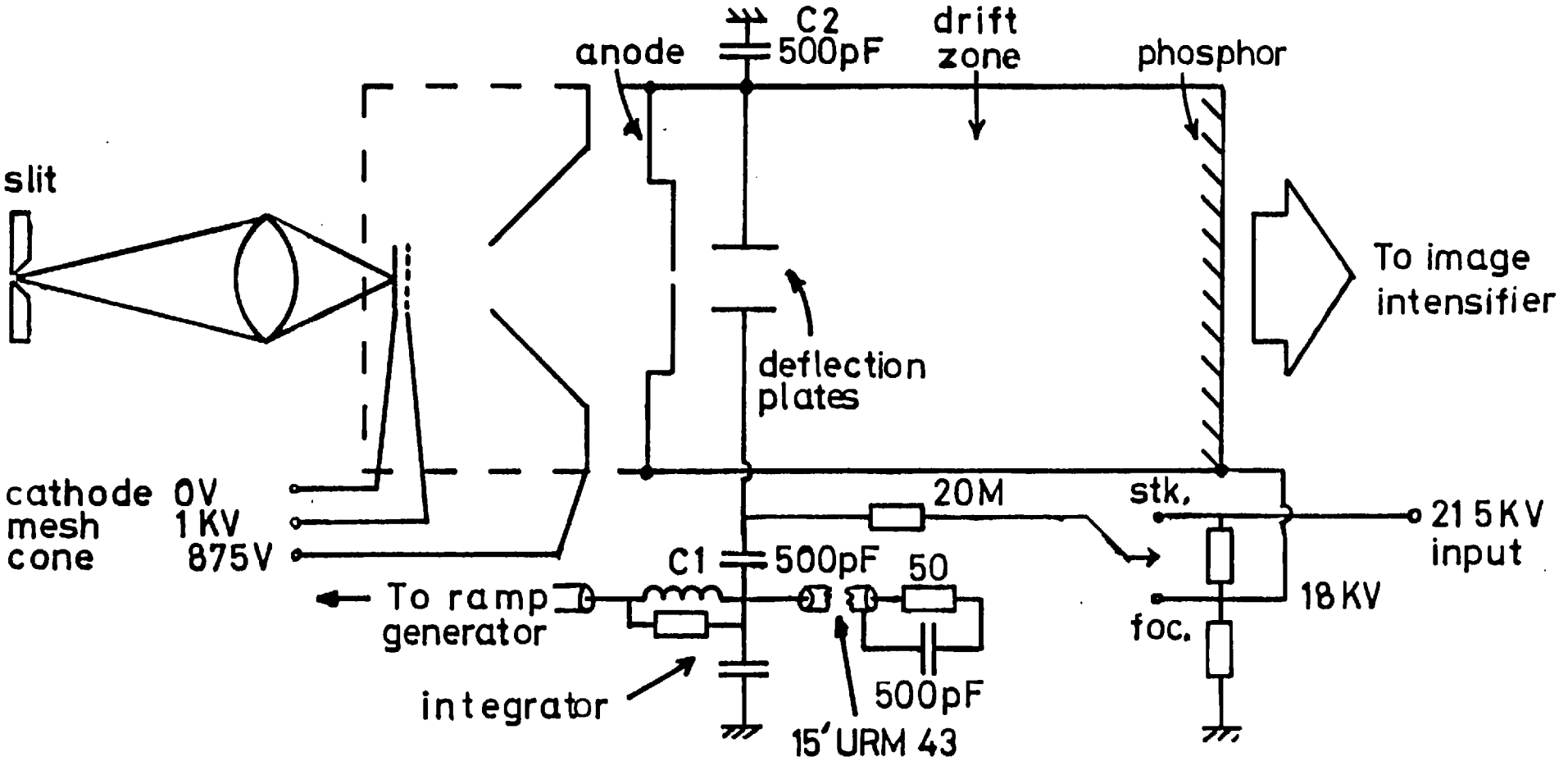

Fig.2.6 Photochron 2
streak tube

5KV ramp, is launched down a 50Ω coaxial line 12' long, terminated in a 500 pF capacitor in series with a 50Ω resistance. The deflection plate that is subjected to the bias voltage is capacitively coupled via C1 to the centre of the coaxial cable a few inches away from the ramp generator. The instantaneous bias applied is the superposition of the dc bias, and the ramp voltage. The image of the slit is thus swept across the phosphor, converting temporal information into spatial information. The other deflection plate is maintained at the anode voltage, but is decoupled to ground via C2. In order to reduce the streak speed an integrator is inserted between the output of the ramp generator and the coaxial line, which increases the falltime of the ramp. The streak camera is normally used at a streak speed of 1×10^{10} cm s^{-1}, giving a technical time resolution of 1 ps. A streak velocity of 2×10^{10} cm s^{-1} has also been employed. The flyback is both delayed and slow. When the streak camera is used in conjunction with a pulsed laser, the flyback takes place long after the end of the pulsetrain. However this slow flyback or reset leads to complications when streaking a modelocked CW laser, since gating of the photocathode - mesh voltage is required to prevent overwriting the initial trace (48). A detailed description of the ramp generator electronics is given in Chapter 4.

The phosphor of the streak tube is a P11 type settled onto the output faceplate before it is stichwelded onto the main body. The phosphor is given a thin aluminium backing to improve its conductivity and to promote the forward scatter of light, thereby improving its efficiency.

It was observed at an early stage (20 - 23, 41) that under conditions of high photoelectron currents the streak tube gave poor time resolution. This was due to the high photocurrent being drawn in the ultrashort pulses in order to provide adequate intensity at the recording film. To overcome this problem, the streak tube is usually coupled to a high gain

image intensifier. The reason for this loss of resolution is still the subject of controversy, and is discussed in some detail in Chapter 5.

In both the MK 1 and MK 2 streak cameras, the streak tube is lens-coupled to an EMI 9912 image intensifier. This is a magnetically focused 4 stage cascade intensifier, having a gain of 10^6 and a usuable diameter of 42 mm. When used in the recommended 2 loop focus mode, it has a resolution of 30lp/mm, and a magnification of 0.95. The intensifier is coupled to the shutter tube by an 80 mm f/1.5 lens (Dallmeyer Octac) positioned to give a magnification of 0.7. This demagnification is used, because it enables the entire length of the streak tube output phosphor to be imaged onto the photocathode of the intensifier, without significantly compromising the resolution of the overall system. A diagram of a cascade image intensifier is shown in Figure 2.7(a). It consists of 4 similar sections each an image converter, proximity coupled to both the preceeding and succeeding stages. The optical image is focused onto the input photocathode (Type S20, chosen because of its high quantum efficiency) liberating photo-electrons, which are accelerated by a uniform electric field. These are focused by a uniform axial magnetic field (generated by a constant current flowing in a surrounding air cooled solenoid), to form an image on the phosphor of the first multiplying screen.

The secondary electrons generated at the screen are then imaged onto the second multiplication screen, and so on. A final image is produced by high energy electrons at the output phosphor. A gain of ~30 per stage is normally achieved in a tube.

The construction of a multiplying screen is shown in Figure 2.7 (b). It consists of a thin sheet of mica, 4 μm thick with a P11 phosphor de-

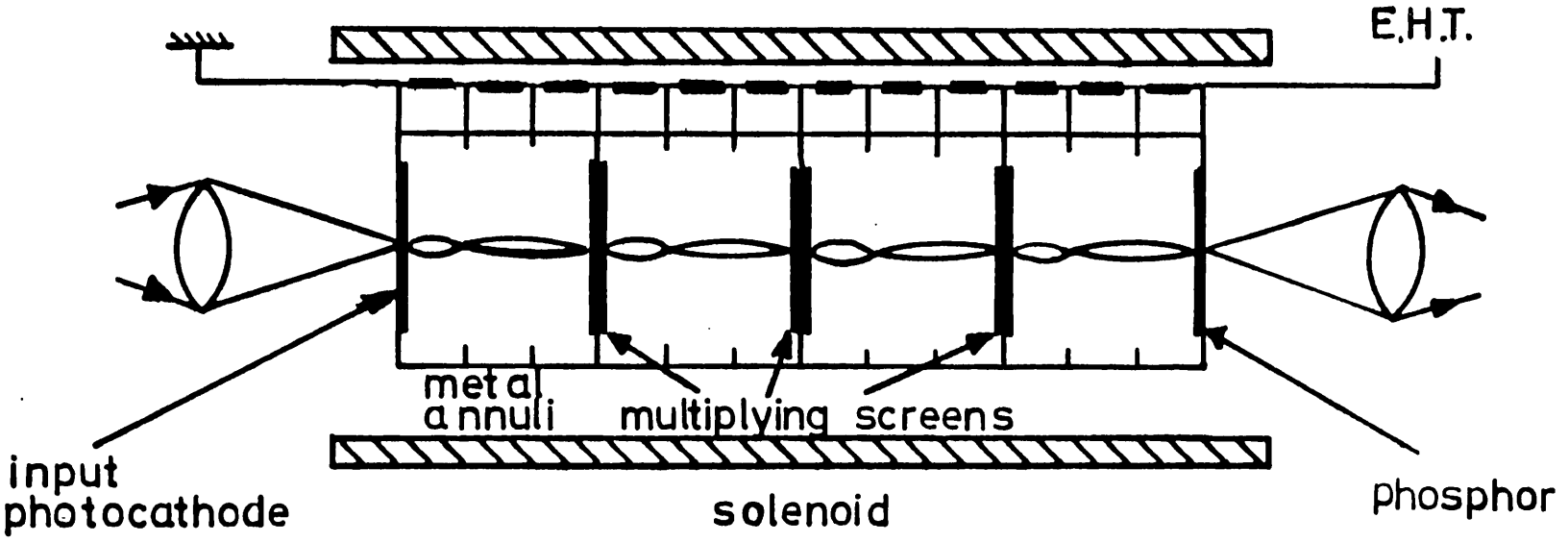

(a) Image intensifier

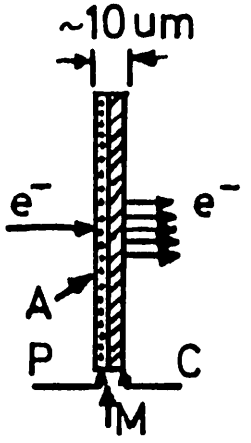

(b) Multiplying screen

Fig.27 Magnetically focused image intensifier

posited on one side, and a semi-transparent photo-cathode formed on the other. The phosphor is overlaid with a thin layer of aluminium, which in turn is coated with a thin light absorbing film to prevent the back reflection of light from the preceeding photocathode (25). The thickness of the phosphor (~ 4 μm) is a compromise, since it must absorb most of the electron energy, and yet neither absorb or scatter much of the phosphorescence.

A second 80 mm lens, similar to the first, operated at unit magnification, couples the output of the image intensifier to the recording film. The streak images may be photographed on either Polaroid or 35 mm film. Type 410 Polaroid film has the advantage that it is extremely sensitive (ASA 10,000), and has a short development time. Although it is extremely useful in the initial stages of an experiment, the high gamma, and opacity make it impossible to take quantitative results from this type of film. Accurate measurement of intensity profiles are therefore taken on 35 mm HP5 film, which is then developed in Microphen for 25 mins giving it an ASA of $\sim$3000. This film is then microdensitometered on a Joyce Loebl MK III CS dual beam recording microdensitometer, which gives a display of density against position on the film. Each roll of film is calibrated by photographing a neutral density step wedge illuminated by a white light source. By microdensitometering the photograph of the stepwedge it is possible to determine the change of density corresponding to a change of input intensity of say 2 .

2.5 The time resolution of the streak camera

For any chronographic instrument there exists a minimum temporal resolution limit.

This limit (Tinst) may safely be ignored when measuring time durations ~ 10 Tinst, but as the measured time interval approaches Tinst, it becomes increasingly important to apply a correction for it in the final measurement. In the case of the ultrafast fast streak camera Tinst has two principle components, the technical time resolution (Ts), and the transit time dispersion (Td).

The technical time resolution limit is the time taken, for the deflected slit image to be displaced by one resolution element at the phosphor of the streak tube. It is given by the equation $Ts = \frac{1}{vS}$, where v is the writing speed at the phosphor of the shutter tube, and S is the corresponding dynamic spatial resolution in lp/mm. Although Ts can always be reduced by increasing v, there exists a practical limit of 0.5 - 1 psec in the present system (corresponding to a writing speed of $1 - 2 \times 10^{11}$ mm s^{-1}, and a dynamic spatial resolution of 10 lp/mm). This arises because as the camera writing speed increases, the current required to maintain the film exposure also increases. A point is reached where the improvement in technical time resolution is negated by the deterioration of tube performance at the excessively high photocurrents (see Chapter 5). The maximum writing speed is also constrained by the speed and jitter of the ramp generator, and by the desired overall time interval that is to be monitored. It is also possible to reduce Ts , by increasing the dynamic spatial resolution of the system, in which case the constraints mentioned earlier do not apply.

The time taken by an electron to travel between the photocathode of the streak tube, and the deflection plates is dependent on its initial energy. The spread in initial photoemission energies consequently gives rise to transit time dispersion Td within the streak tube. The distribution of initial electron energies (ΔE about a mean energy Eav) varies both with wavelength and cathode type, and has been the subject of study in the solid-state physics associated with photoemission (26 - 31).

Measurements of these distribution functions are normally by the a.c. method described by Leder and Simpson (32).

In the absence of an exact measurement at the wavelength of interest it is necessary to make an approximation of the type described in Appendix 1. Fortunately the time resolution of the system is a function of the form $\sqrt{\Delta E}$, thereby reducing the significance of any error in the value of ΔE.

Most of the transit time dispersion occurs near the photocathode of the streak tube, the region where the photoelectrons move very slowly. This time dispersion is reduced by placing a mesh held at +1KV above the cathode potential (Photochron 2) very close to the photocathode. This mesh rapidly accelerates the electrons to an energy of ~1 KeV, thus minimising the build-up of time dispersion (33).

In order to calculate the transit time dispersion of an image tube it is necessary to know the electric field strength along the axis of the streak tube as a function of position. This may be obtained either by direct measurement in an electrolytic tank (34), or a resistance network (34,35), or by the numerical solution of Laplace's equation (34,35).

Because the streak camera shutter tube has circular symetry, the solution to Laplace's equation is obtained in polar co-ordinates. If a matrix of points is used to represent the geometry of the streak tube (Fig. 2.8), it can be shown that the potential Vo at a given point Po is given by

$$Vo = \frac{1}{4}\left\{ V_1 + V_2 + \left(1 + \frac{1}{2H}\right) V_3 + \left(1 - \frac{1}{2H}\right) V_4 \right\} \qquad H \neq 0$$

Eq 2.1

where H is the number of mesh points between Po and the axis. When H = 0 equation 2.1 becomes

$$Vo = \frac{1}{6} \ (V_1 + V_2) + \frac{2}{3} \ V_3$$

Eq 2.2

The potential distribution is determined by applying Eq 2.1 to each point in the matrix in turn and calculating a new value of Vo from its neighbouring points V_1 - V_4 . The axis is similarly dealt with by the application of equation Eq 2.2. The other boundries are represented either by a direct approximation to the correct potential, or are allowed to 'float' to the correct potential. Because of the geometry of the streak tube the axis potentials, the only ones of interest here, appear fairly insensitive to the exact boundary potentials used.

The system for solving Laplace's equation described above is known as successive displacement, since each value of Vo is immediately replaced by the new approximation derived from equation Eq 2.1. This method is slow to converge and so successive over-relaxation is employed.

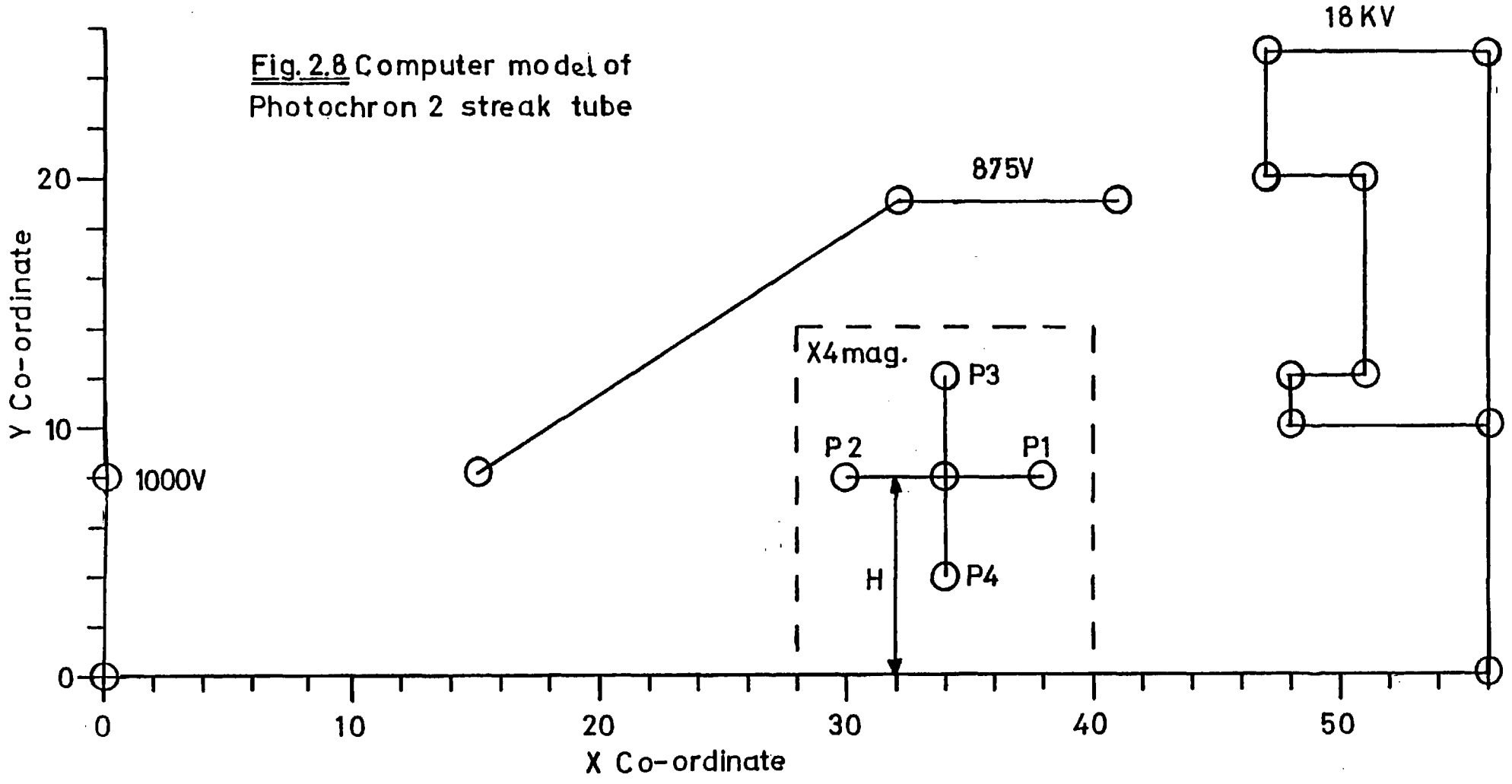

Fig. 2.8 Computer model of Photochron 2 streak tube

Here the new approximation for Vo is given by

$$Vo\ (new) = Vo\ (calculated) + \gamma\,(Vo\ (calculated) - Vo\ (old))$$

Eq 2.3

a process of 'helping Vo on its way'. The term γ must be chosen such that the solution rapidly converges without becoming unstable. A complex procedure is outlined for calculating γ in Ref. 84. A more direct approach is to start the programme running with a small value for γ (say $\gamma = 0.7$), and after a few alterations increase γ to ~ 0.9.

Using the procedure outlined above, a matrix of points (a 25 x 50 array - 2mm per element) was used to represent the Photochron 2 streak tube (Figure 2.8), and after $\sim$600 alterations a stable solution for the axial potentials was obtained (Fig 2.9 (a)).

By performing a numerical integration of the transit time difference of a pair of electrons at the full width half maximum points (FWHM) of the initial electron energy distribution, the transit time spread for the tube as a whole can be estimated.

From elementary mechanics it can be shown that under conditions of acceleration the time taken by an electron to travel a distance d is given by :-

$$t = \frac{d}{V}\sqrt{\frac{2}{e/m}}\left\{\sqrt{V + E_i} - \sqrt{E_i}\right\} \qquad \text{Eq 2.4}$$

where V is the applied voltage, E_i is the initial energy of the electron, and e/m is the electronic charge to mass ratio. The transit time spread

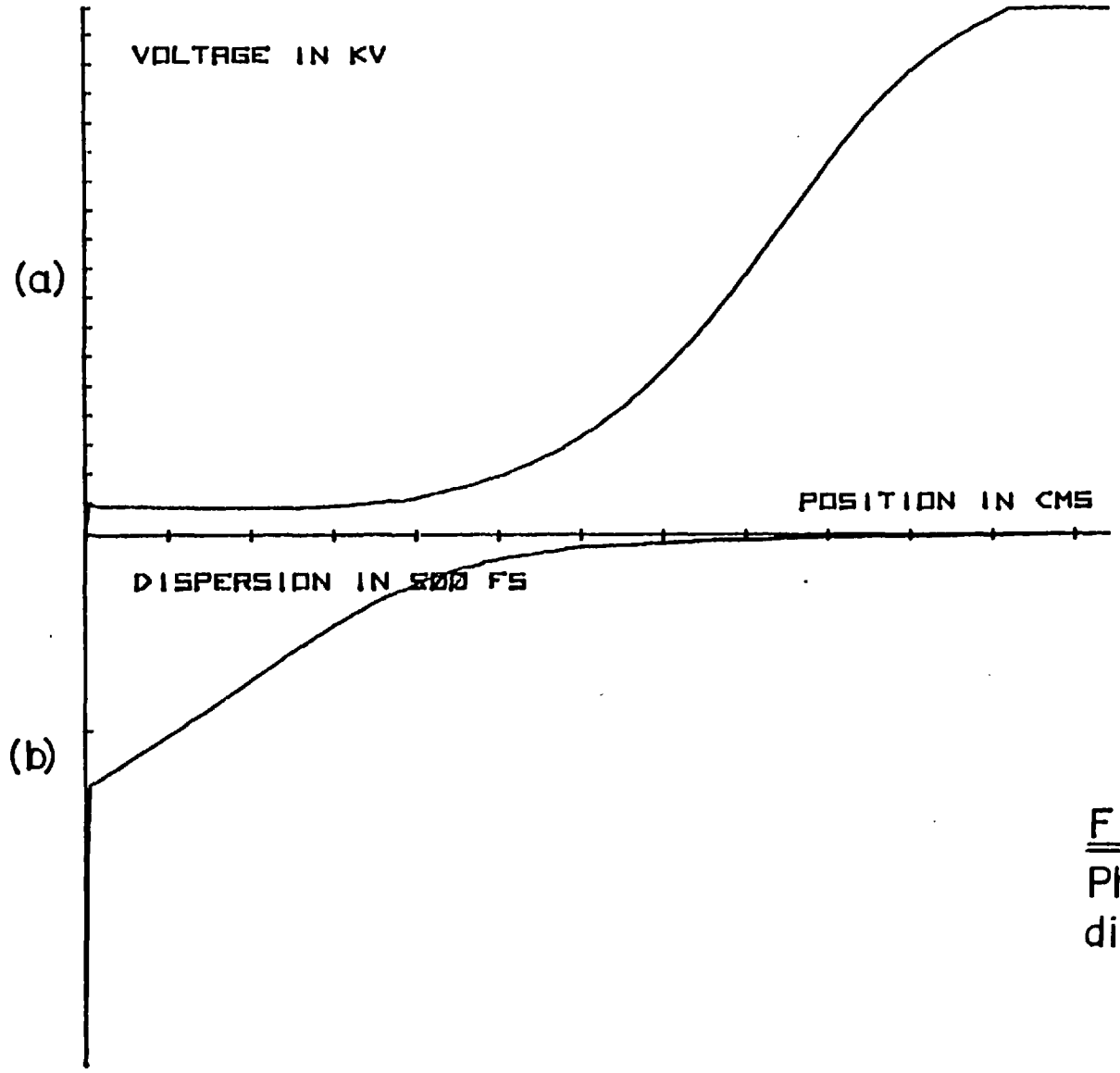

Fig.2.9 (a) On axis potentials of Photochron 2, and (b) time-dispersion S20 600nm

T_d is hence given by :-

$$T_d = \sum_{\substack{\text{along} \\ \text{the tube axis}}} \frac{d}{V}\sqrt{\frac{2}{e/m}}\left\{\sqrt{V + E_{i_1}} - \sqrt{V + E_{i_2}} - \sqrt{E_{i_1}} + \sqrt{E_{i_2}}\right\}$$

Eq 2.5

where Ei_2 and Ei_1 correspond to the upper and lower FWHM points on the initial energy distribution curve.

In the case that $Ei_1 \sim 0$ and $V \gg Ei_2$ this reduces to

$$Td = \frac{d}{V}\sqrt{\frac{2}{e/m}\,\Delta E}$$

Eq 2.6

which leads to the well known approximation (18, 37)

$$Td = \frac{d}{V} \times \frac{\Delta U}{e/m}$$

Eq 2.7

where ΔE is the FWHM of the electron energy distribution and ΔU is its velocity equivalent.

By applying equation 2.5 to the axial potentials of a Photochron 2 streak tube (Fig 2.9a), and substituting the values Ei_1 = 0.15 eV, Ei_2 = 0.45 eV (cf Appendix 1 S20 photocathode at 600 nm), we get a value of Td = 0.8 psec. (Fig 2.9b).

While in its present state of development, Ts and Td are by far the most important terms in determining the camera instrument function, it is important to note that both the photocathode response time ($\sim$ 0.15psec), and the time dispersion in the optics (0.05 - 0.1 psec, 37) will represent fundamental limits to the ultimate resolution capability of the streak camera.

The time resolution of a photocathode has been estimated by several authors (38-40). Although Spicer (39) calculated the cathode response time his method may also be used to calculate the resolution time. An estimate of the inherent cathode time resolution may be made by considering the initial and final energies of an electron, and calculating the time taken to loose the energy difference. Assuming that prior to emission an electron has an energy Ei + Ea, where Ei is a FWHM point on the electron energy distribution curve, and Ea is the electron affinity, then the cathode resolution is given by the time it takes an electron to loose the energy difference $(Ei_1 + Ea) - (Ei_2 + Ea)$

Taking a mean free path of 30Å, the values of Ea, Ei_1 and Ei_2 quoted in Appendix 1 for an S20 photocathode at 600 nm, and using them in a simple itterative programme the value for T res is $\sim$ 0.15 psec.

If it is assumed that both the slit image, and the form of the time dispersion curve are gausian, then from (36) Tinst is given by

$$T\,inst^2 = Ts^2 + Td^2$$

For a Photochron 2 streak camera with a writing speed of 10^{10} cm s^{-1}, a static resolution of 10 lp/mm, and an S20 photocathode at 600 nm, an instrument time resolution of 1.3 psec is indicated. When this camera is used to measure the duration (Tp) of pulses having a gausian intensity profile, the camera instrument time can be removed from the recorded pulse duration (Tr) by the application of the equation

$$T_r^2 = Tp^2 + Ts^2 + Td^2 \qquad \text{Eq 2.8}$$

Confirmation of these results is indicated by the work of Sibbett (4) who

recorded pulses with a recorded duration of 1.5 psec from a dye laser mode-locked with DQOCI, and tuned to 605 nm.

CHAPTER 3

THE ULTRA - VIOLET STREAK CAMERA

3.1 Introduction

In order to extend the range of wavelengths over which picosecond diagnostics are available, an ultra-violet sensitive streak camera has been constructed and tested. The Mk.2 streak camera was modified for operation in the U.V. by the construction of a Photochron 2 streak tube equiped with a sapphire entrance window and photocathode substrate.

Test pulses at 200 nm were provided by frequency tripling the pulses from a modelocked Rhodamine 6G dye laser in calcium vapour. These frequency tripled pulses were found to have a pulse duration ~ 3.5 psec which was comparable to the duration of the fundamental pulses.

The parametric process of stimulated Raman scattering competes with third harmonic generation, and produces an output at ~ 422 nm. An investigation of this process showed that under some circumstances 6 psec pulses were produced with $\sim 0.5\%$ conversion efficiency.

3.2 The Test Source

It is desirable that an S-20 ultra-violet streak camera be tested at a wavelength shorter than 210 nm since this wavelength represents the limit at which the production of low energy photoelectrons by pair production is nearly complete (26). Any degradation of time resolution

caused by pair production should hence be clearly evident.

The shortest wavelength at which picosecond pulses have been directly generated by modelocking is 465 nm (18). In order to generate such pulses at shorter wavelengths non-linear techniques are required.

Although in principle it is possible to generate picosecond pulses at wavelengths down to $\sim$ 200 nm by harmonic generation or mixing techniques in a crystal, 200 nm represents the limit where crystals can no longer be used (90). Thus to extend the wavelength range further into the U.V. it is therefore necessary to employ a gas (97) or metal-vapour as the non-linear medium (90).

The third harmonic generation (THG) of picosecond pulses in metal vapours has been reported by a number of authors (98-102). Streak camera measurements of the quality and duration of these pulses are of particular interest since no measurements are yet available showing that short discrete pulses are indeed produced by this technique.

The use of a modelocked dye laser as a source of fundamental pulses has the advantage that short pulses are reliably produced, and can be tuned to a two-photon resonance in the non-linear medium to maximise conversion efficiency (101, 102). Calcium vapour is a suitable material for third harmonic generation. It has a strong two photon resonance at 600 nm, corresponding to the $4\,S^2$ (ground state) to 4S 5S level separation and autoionizing levels in the continuum which enhance third harmonic generation. The use of the forbidden dipole transition $4\,S^2$ to 4S 5S to provide resonant enhancement means that there is no linear absorption associated with this process. The small

absorption cross-section of metal vapours above their ionization potential ensure that the third harmonic is not reabsorbed by the vapour itself. This ultraviolet transparency allows the generation of radiation in spectral regions inaccessable to non-linear optical crystals (90). The optimum wavelength of a modelocked Rhodamine 6G dye laser is $\sim$ 600 nm, and the third harmonic pulses at 200 nm can propagate in air thus simplifing the experimental system.

Although a number of classical explanations for third harmonic generation exist (90, 91), the physics of the process is still under debate (88, 89).

For the case of ultra-short pulse excitation, in particular, coherent effects have to be taken into consideration. A laser tuned close to the two-photon resonance (Figure 3.1) will exite the calcium atoms into a mixture of real and coherent states. The amplitude of these states then beats against the incoming wave to produce the third harmonic. The intermediate coherent state acts as an energy store (88), and a second pulse may extract part of this energy (thereby producing third harmonic) at any time during the coherence dephasing time of the atoms. There is no requirement however for the two pulses to be concurrent. Experiments by Matsuka et al (95), and Royt et al (96) have demonstrated this effect.

3.3 The Ultra-Violet Sensitive Streak Tube

The near ultra-violet (U.V.) sensitivity of a conventional streak tube

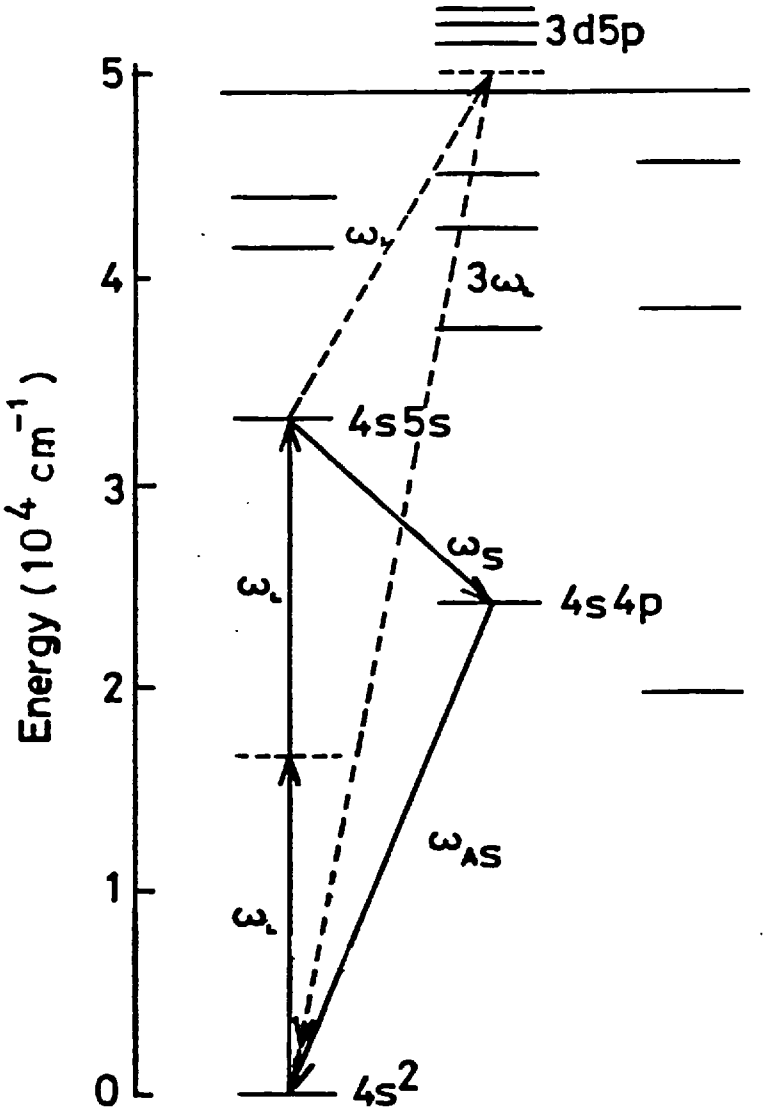

Fig.3.1 Term diagram of calcium

is entirely limited by the cutoff wavelength of its entrance window and cathode substrate. The spectral response of the photocathode may hence be extended simply by using U.V. transparent window and substrate materials. Although materials such as Li F, Ca F_2 and Mg F_2 have shorter cutoff wavelengths (105 nm, 125 nm and 135 nm respectively), sapphire was preferred for both the entrance window and cathode substrate, giving the tube a response down to only 140 nm.

The large difference between the coefficient of expansion of glass and that of Li F necessitates a joint incorporating an elastic material such as silver chloride cement (93). Unfortunately silver chloride photodisociates under U.V. radiation to form silver and chlorine. The free chlorine that would eventually be given off into the streak tube would contaminate, and ultimately destroy the photocathode.

Unlike Li F, Mg F_2, or Ca F_2, sapphire may be braized into place producing a stable seal. In the construction of the U.V. streak tube, the sapphire window was first brazed to a Nilo-K ring using a copper-silver eutectic (Nilo - K is an Iron-Cobalt-Nickel alloy commonly used as a part of a glass-to-metal seal). This Nilo - K ring was then argon arc welded to a second similar ring joined to the front of the streak tube body by conventional glass-to-metal seal techniques. The top-hat shaped cathode substrate was ground from a sapphire blank, but in all other respects the streak tube was similar to a conventional Photochron 2 design.

3.4 The experimental arrangement

The experimental arrangement used to test the U.V. streak camera is shown in Figure 3.2. The flashlamp pumped dye laser described in Section 2.2 (modelocked with DODCI) was used as a source of fundamental pulses at 600 nm. These pulses were amplified to powers of 100 - 200 MW in a single amplifier stage. The amplifier was a 6" capillary laser head similar to the oscillator except for an increase in the size of the energy storage capacitors to 0.5 μF. These capacitors were charged to 28KV, and an electrical energy of ∿ 200 J was discharged into each flashlamp. The active medium of the amplifier was a 2.4×10^{-4} M solution of Rhodamine 6G in water. A single pass gain of ∿ 10 was achieved.

A 30 cm lens focused the pulses into a heatpipe oven containing a mixture of calcium vapour at 3 Torr and Xenon phasematching gas at ∿ 15 Torr. The beam divergence of the laser was ∿ 3 mR (5) and so power densities of 4 - 8 GW cm^{-2} were achieved at the focal spot.

The construction of the heatpipe-oven (103) is shown in Figure 3.3. The outer heatpipe section (104) contained a mixture of calcium vapour and argon at 3 Torr, and maintained a 20 cm section of the inner oven at a constant uniform temperature of ∿ 1150K. A water jacket at each end of the oven, creates a pair of cold zones containing relatively dense buffer gas. This buffer gas acts as a barrier to the hot calcium atoms, preventing them from condensing on the windows of the oven. Operation of the heatpipe-oven for > 8 hours was possible before the build-up of calcium at the cold zone boundary obscured the passage the light through the oven.

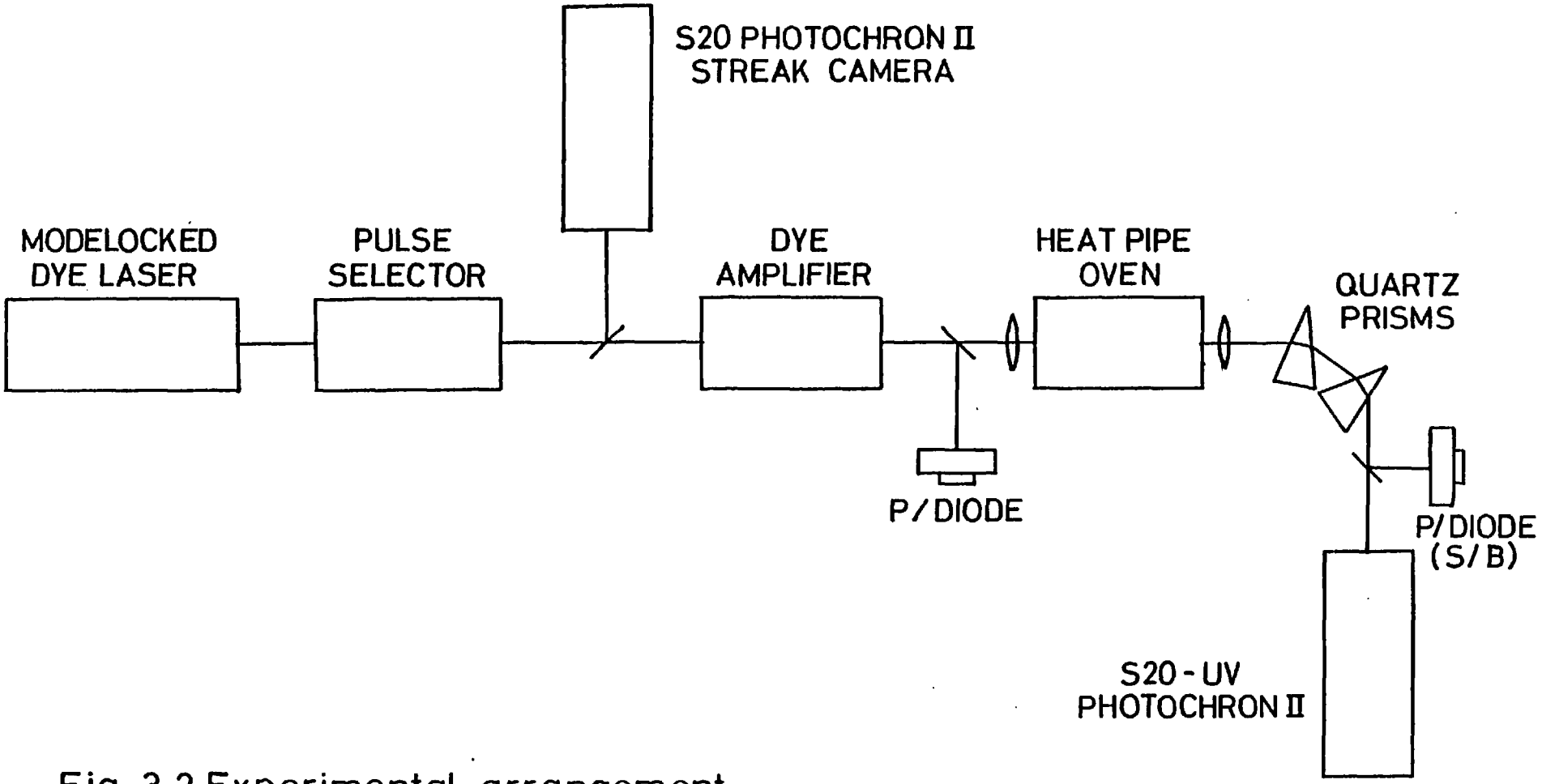

Fig. 3.2 Experimental arrangement

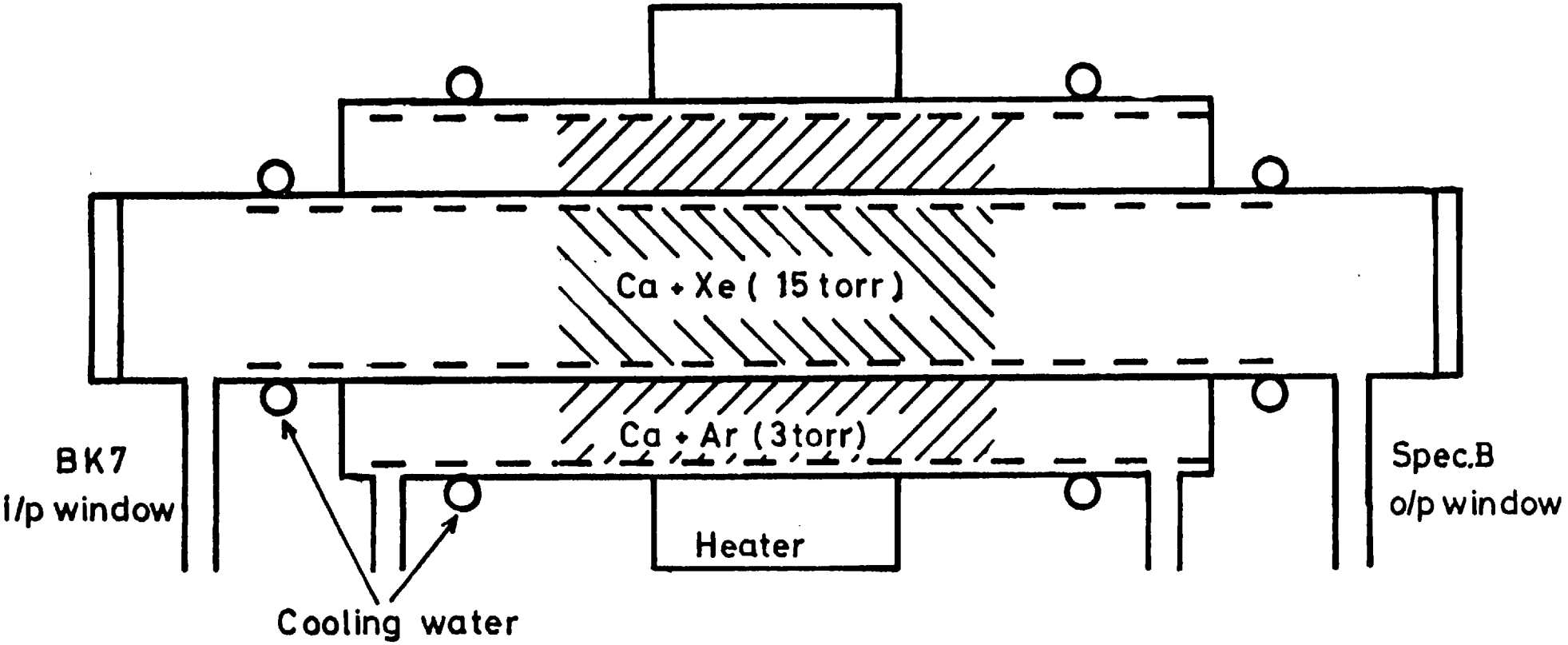

Fig. 3.3 Heatpipe - oven

At these temperatures calcium is extremly reactive, and the materials used in the construction of the hot sections of the heatpipe oven must be carefully chosen. Heat resistant stainless steel tubing type 310 - 25/20 quality (Philip Cornes & Co., Worcs) was used for over a year without any noticeable reaction with the calcium.

The outer heatpipe section was heated by a spiral nichrome heating element connected to the mains via a variac. This heating element was cemented into place by a mixture of aluminium oxide and potassium silicate. Insulation for this hot section of the system was provided by a 3 inch thick layer of glass wool held in place by a layer of aluminium foil.

The light from the output of the heatpipe oven was recollimated by a 30 cm Spectrocil B lens. A simple prism spectrograph spatially separated the third harmonic from both the fundamental and the parametric outputs. The U.V. radiation was directed onto the slit of the streak camera by tracing its path with a scintilator such as solium salicylate, over a number of laser shots. The U.V. streak camera was triggered by the signal from a photodiode monitoring the fundamental pulses. The discrimination between the U.V. pulses and the visible pulses was checked by covering part of the slit of the streak camera with a glass slide, in which case the corresponding part of the streak image vanished.

3.5 The Third Harmonic Pulses

The third harmonic pulses were initially monitored on a coaxially mounted solar blind biplanar photodiode. The laser was tuned until maximum third harmonic was obtained, corresponding to a wavelength of $\sim$ 600 nm

An example of a typical third harmonic pulse train, is shown in Figure 3.4 (a). The spectrum of these pulses was measured with a Monospek 1000 spectrograph. The recording film used was Ilford HP3 which had adequate sensitivity at this wavelength. Figure 3.4 (b) shows a microdensitometer trace of the spectrum of these pulses. The recorded linewidth was 50 cm^{-1}. These results may be compared with the corresponding fundamental pulsetrain (Figure 3.5 (a)), and spectrum (Figure 3.5 (b) and 3.5 (c)). As can be seen the recorded linewidths are similar. The quality and duration of the amplified fundamental pulses was checked with an S20 Photochron 2 streak camera. Pulses with a duration of $\sim$ 4 psec were consistantly recorded (Figure 3.6). The conversion efficiency of the process was estimated from oscilloscope traces of both the fundamental and third harmonic taken simultaneously. The results taken indicate a conversion efficiency of $\sim 10^{-4}$ for the process.

The writing speed of the U.V. streak camera was calibrated by streaking the quasi-normal reflections of a fundamental pulse from a series of glass plates 5.0 mm thick (Figure 3.7). This arrangement gave a subpulse separation of 50 psec. The writing speed was found to be 7×10^{9} cm/sec at the phosphor of the streak tube.

The focusing of the slit of the streak camera onto the photocathode of the streak tube is wavelength dependent. The focusing was hence adjusted by illuminating the slit of the streak camera with the complete train of third harmonic pulses, and with the camera switched to "static", adjusting the lens to photocathode distance whilst monitoring the recorded slit width.

The recorded duration of the third harmonic pulses was found to be $\sim$ 4 psec. A typical streak record with corresponding microdensitometer

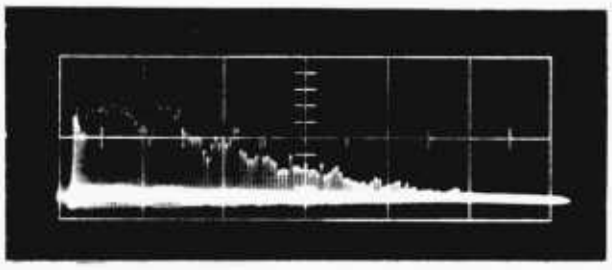

(a) Third harmonic modelocked train
(100 ns/div)

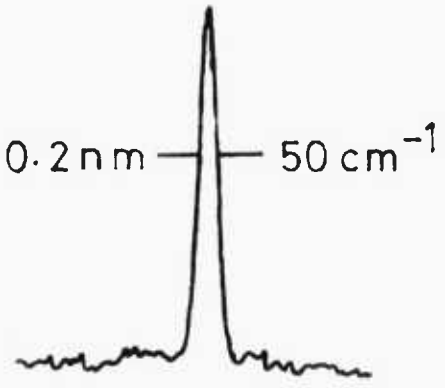

(b) Third harmonic spectrum (200nm)

Fig. 3·4

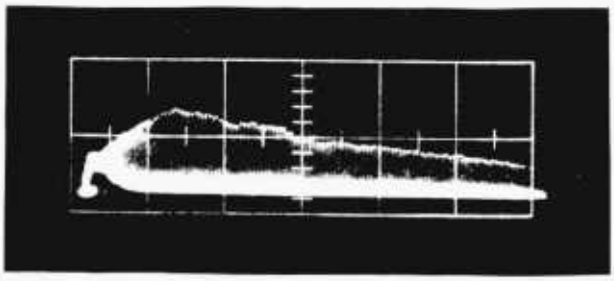

(a) Fundamental modelocked train
(100ns/div)

(b) 626, 625 604 593 nm

633nm 600nm

(c) 1.7nm 50 cm^{-1}

(b),(c) Fundamental spectrum (600nm)

Fig. 3.5

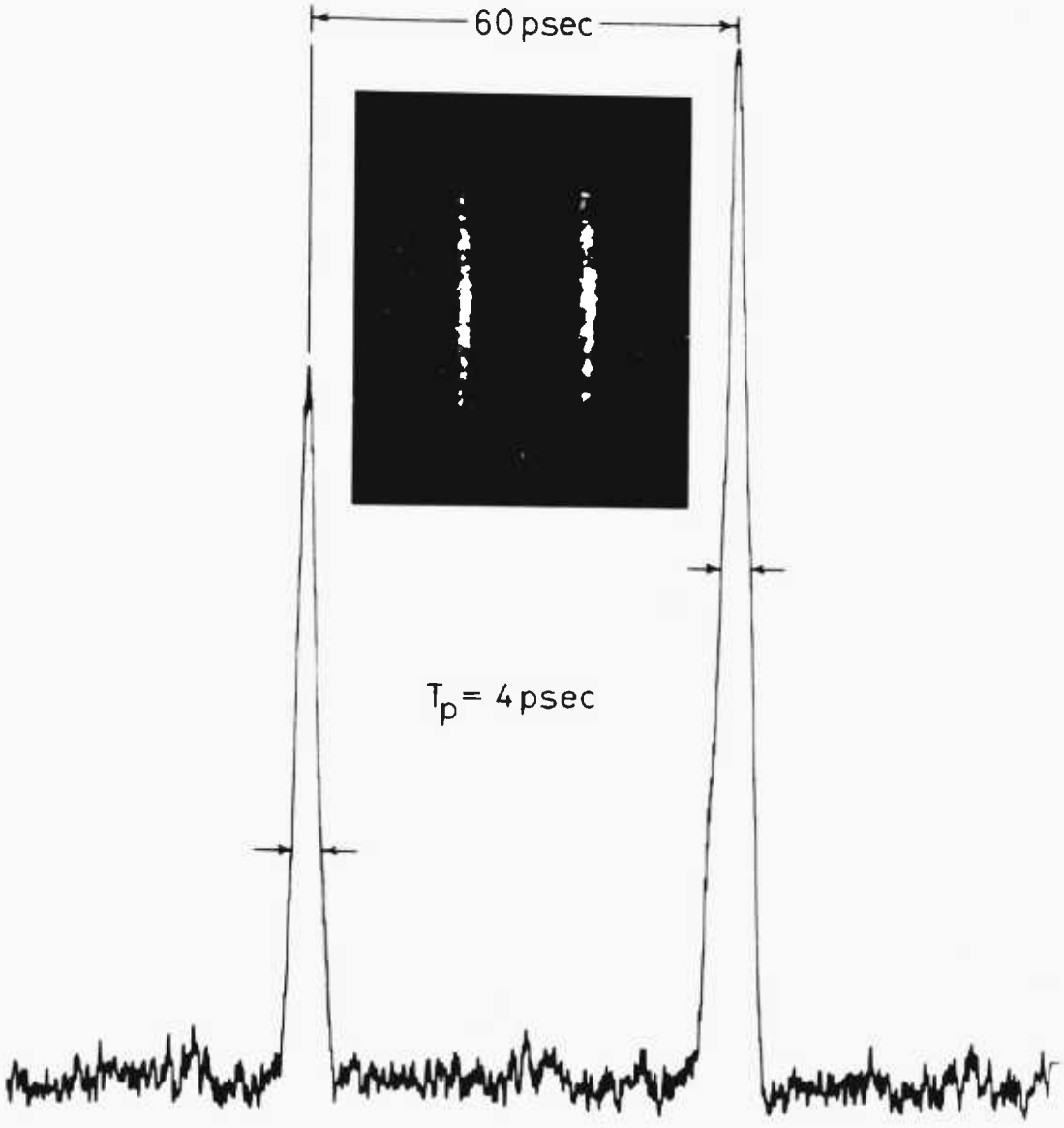

Fig. 3.6 Fundamental pulse

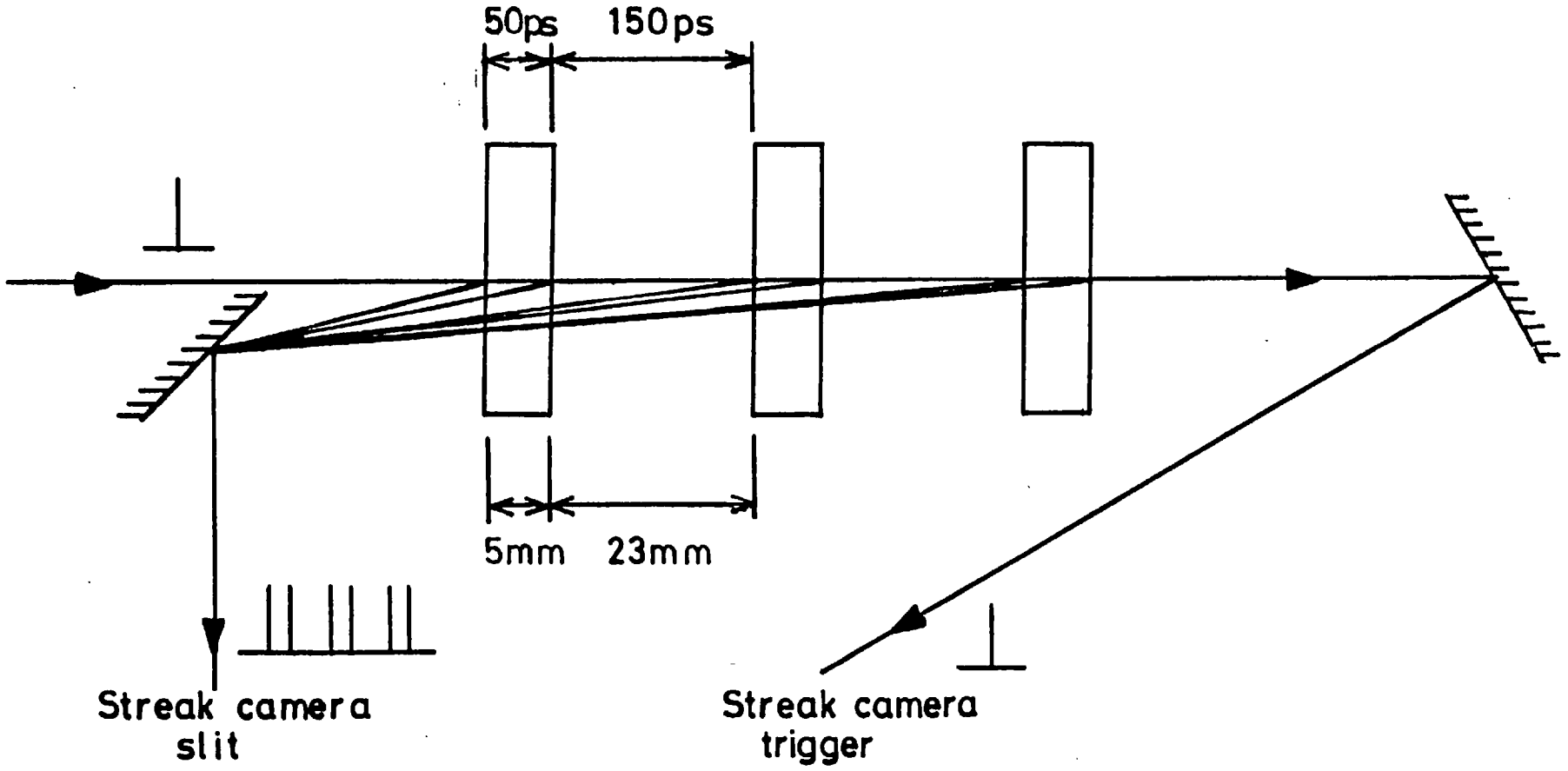

Fig. 3·7 Calibration delay line

trace is shown in Figure 3.8. The photoelectron energy distribution for an S20 photocathode at 210 nm has been measured by Spicer (26) and found to have a F.W. H.M of $\sim$ 1.0 eV centred on $\sim$ 0.6 eV. Applying these values to equation 2.5 the transit-time spread is estimated to be $\sim$ 1.2 psec. When the technical time resolution of the streak camera is taken into consideration the overall instrument limited time resolution is $\sim$ 1.9 psec. By deconvolution (c.f. equation 2.8) the third harmonic pulse duration can be estimated to be $\sim$ 3.5 psec.

3.6 The Parametric Process

The spectrum of the light from the heatpipe-oven was examined for evidence of processes competing with third harmonic generation. Upon scanning between 650 nm and 240 nm (the useful range of Polaroid type 107 film) a single line at $\sim$ 422 nm was observed, indicating just one competing process.

The 422 nm line is generated by a four-wave parametric process (94), in which two laser photons are converted into a signal photon plus an idler photon i.e.

$$2\,W_L \longrightarrow W_s + W_i$$

The idler photon (W_i at 1.03 μm) corresponds to the 4s5s - 4s4p transition in calcium (Figure 3.1), and the signal photon (W_s at 422 nm) corresponds to the 4s4p - $4s^2$ ground-state transition. The spectrum of the 422 nm line is shown in Figure 3.9 (b), and the corresponding

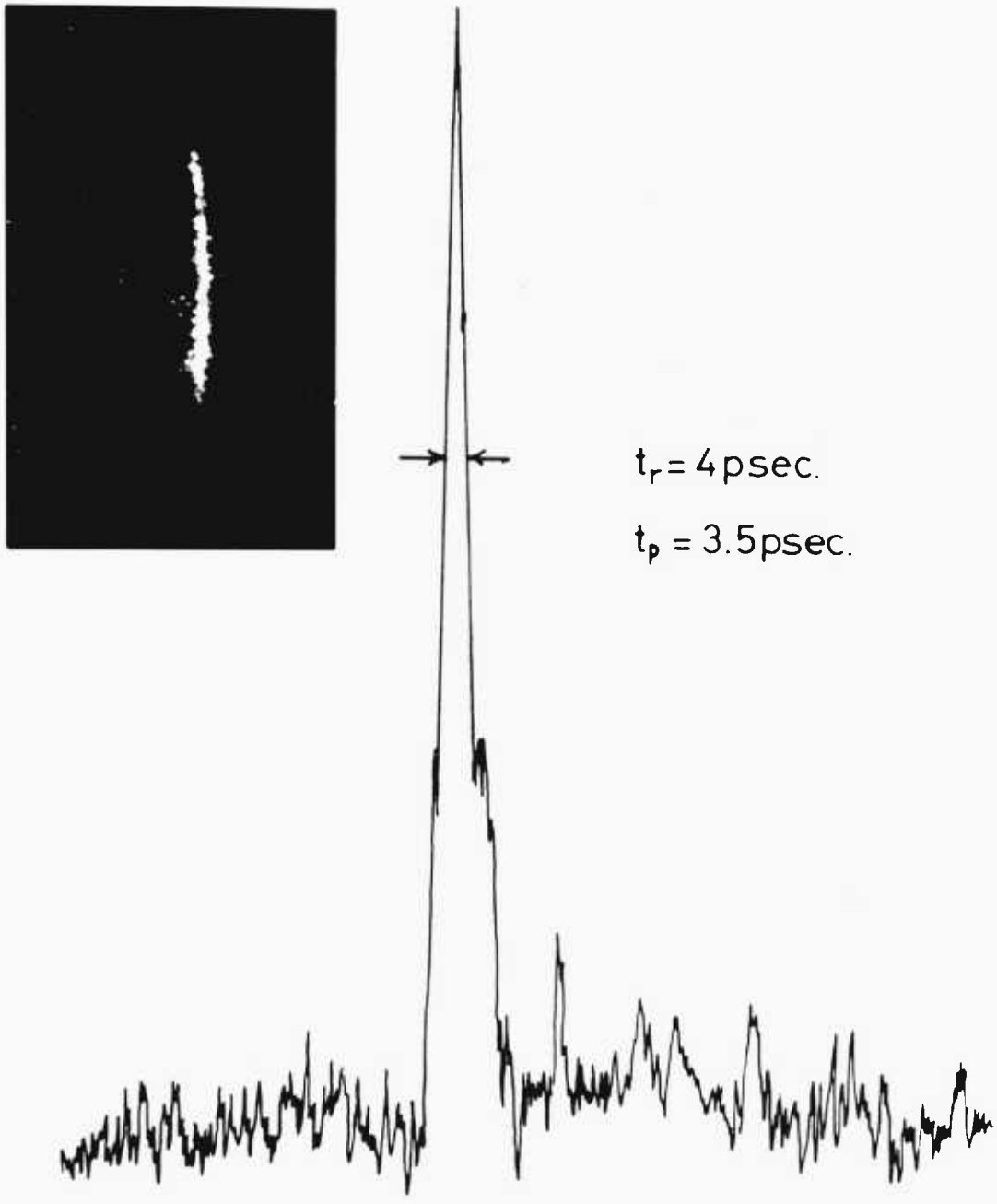

Fig.3.8 Third harmonic pulse

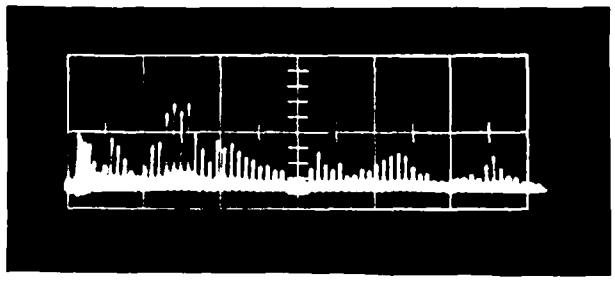

(a) Parametric modelocked train
(422 nm - 50 ns/div)

(b)

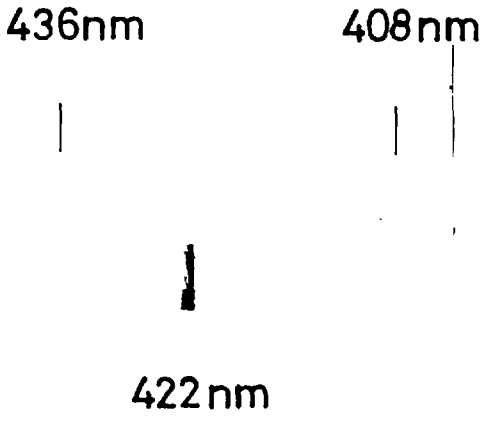

(c)

(b), (c) Parametric spectrum (422 nm)

Fig. 3.9

microdensitometer trace in Figure 3.9 (c). The measured linewidth is $\sim 55\ cm^{-1}$.

The temporal behaviour of the 422 nm line was initially investigated using an S20 biplanar photodiode and fast oscilloscope (Tektronix 519). The laser light was excluded by a Schott BG3 glass filter. Although this filter shows a second transmission peak at $\sim$ 850 nm this was not a problem, since the photocathode of the photodiode does not have significant sensitivity at this wavelength. A typical pulsetrain is shown in Figure 3.9 (a). The sharp fluctuations in output intensity demonstrate the non-linarity of the process. By inserting glass beam splitters before and after the heatpipe - oven, and monitoring the intensity at each point on alternate shots, the conversion efficiency of this process was estimated to be $\sim$ 0.5%.

The duration of these parametric pulses was investigated using a Mk.2 S-20 streak camera. The light from the output of the heatpipe-oven was directed into the calibration delay line (Figure 3.7), and then onto the input slit of the streak camera. Again the Schott BG3 filter was used to exclude the laser light. The streak camera was triggered from the gate output of a Tektronix 519 oscilloscope which was used to monitor the fundamental pulse trains. A typical streak record of the pulses at 422 nm is shown in Figure 3.10. From a number of such microdensitometer traces of streak records, the duration of these pulses was found to be $\sim$ 6 psec.

Under some circumstances the pulses at 422 nm were long (15 - 20 psec) and were accompanied by a highly structured tail (Figure 3.11). The removal of the BG3 input filter enabled the fundamental pulses from the same part of the modelocked train to be monitored. The fundamental pulses were both short and free from any structure. Despite careful

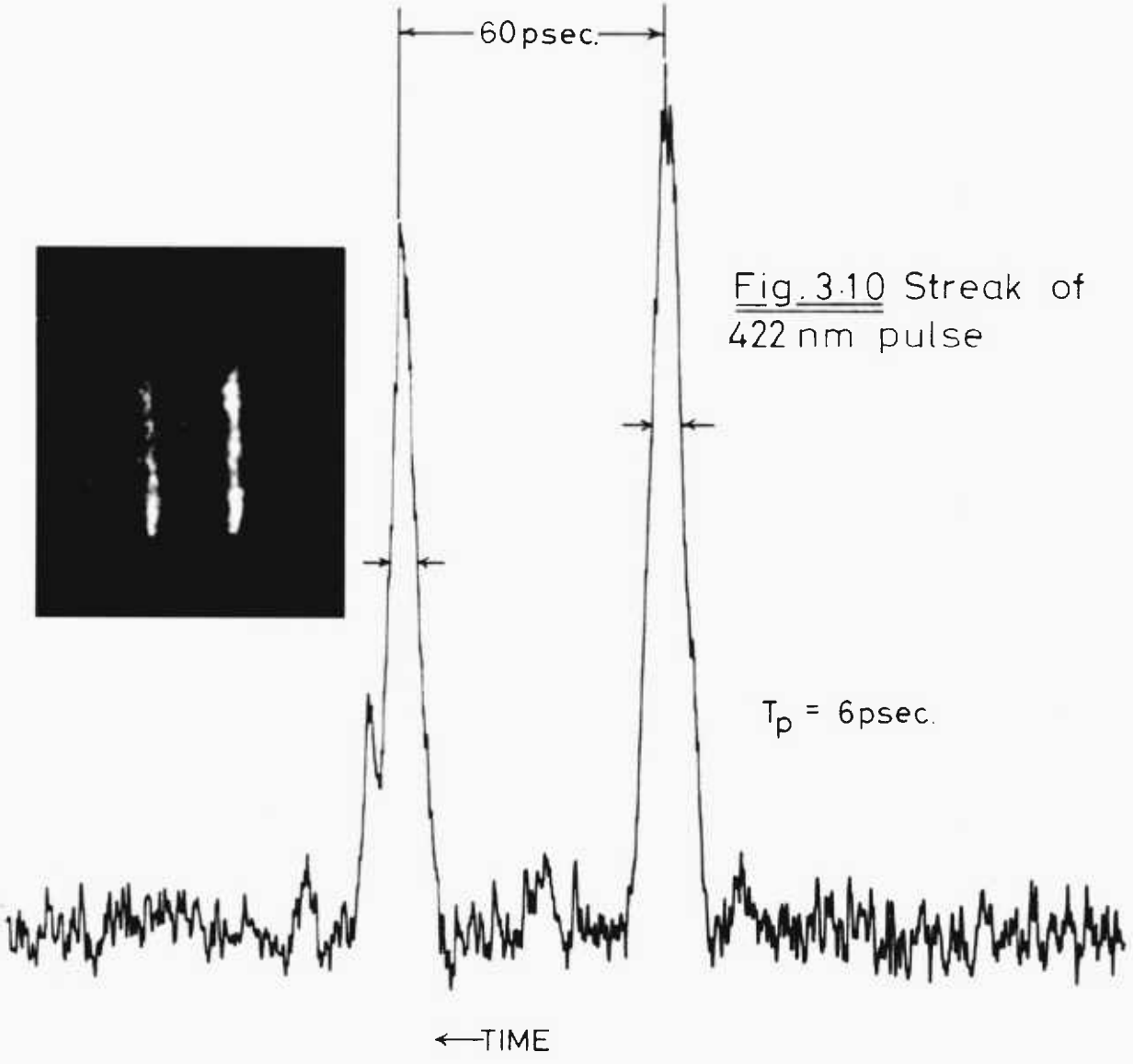

Fig. 3.10 Streak of 422 nm pulse

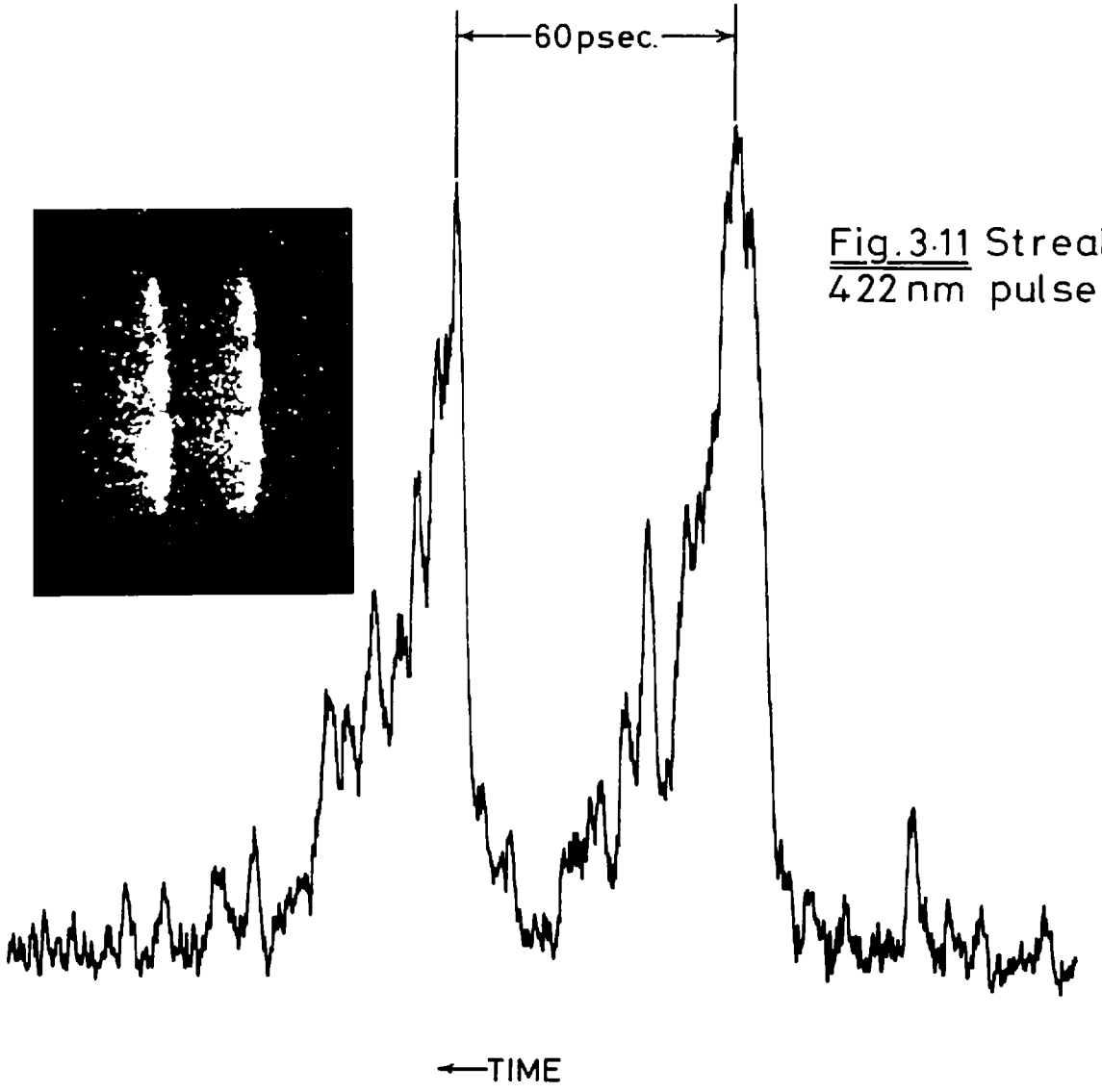

Fig. 3.11 Streak of 422 nm pulse

investigation the nature of this pulse broadening mechanism remains unclear although it has been speculated that it is simply due to linear dispersion.

The angle phase matching of the parametric process (94) was demonstrated by observing the annular structure of the radiation at 422 nm. The light from the heatpipe was incident on a glass slide covered with a semi-transparent layer of sodium salicylate powder, acting as both a scintillator and a diffuser. A BG3 filter placed behind the glass slide removed any fundamental light. Figure 3.12 shows a photograph of the fluorescence caused by third harmonic radiation, surrounded by the 422 nm parametrically generated light.

The idler signal pulses at 1.03 μm were detected using an S1 photodiode. A Schott RG 830 filter was used to remove any signals with a wavelength < 750 nm. As would be expected a pulse train similar to the one generated at 422 nm is observed (Figure 3.13 (a)). The spectrum of this second pametrically generated line was examined using a Monospek 1000 spectrograph with a Kodak I-Z plate as the recording medium. These plates must be sensitized prior to use by washing them in a 4% ammonia solution for 15 secs. They were developed for 10 mins. in Kodak D-19 developer. A microdensitometer trace of the spectrum of the 1.03 μm pulses integrated over several shots is shown in Figure 3.13 (b). The measured linewidth was $\sim 2\ cm^{-1}$. Whilst this is sufficient to support the generation of pulses as short as 6 psec, the reason why this linewidth is much narrower than that of the other processes is again unclear.

3.7 Conclusion

The Mk.2 streak camera has been shown to be capable of picosecond

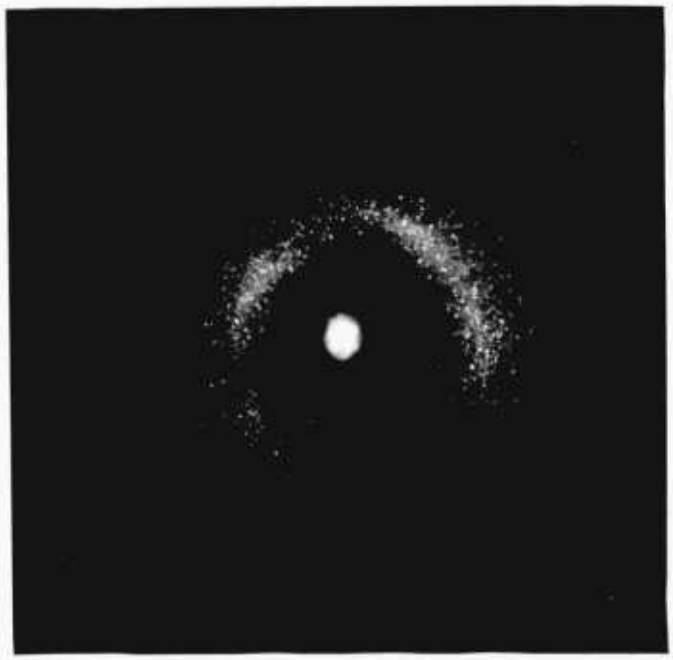

Fig. 3·12 Angle phase-matching
200nm (inner), 422nm (outer)

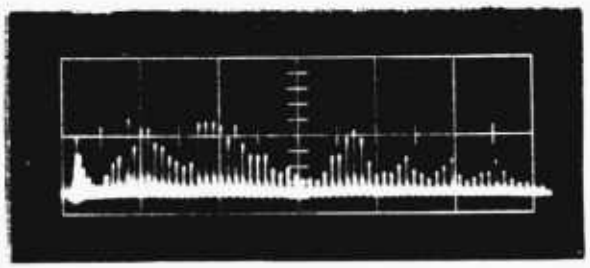

(a) Parametric modelocked train
(50 ns/div - 1·03μm)

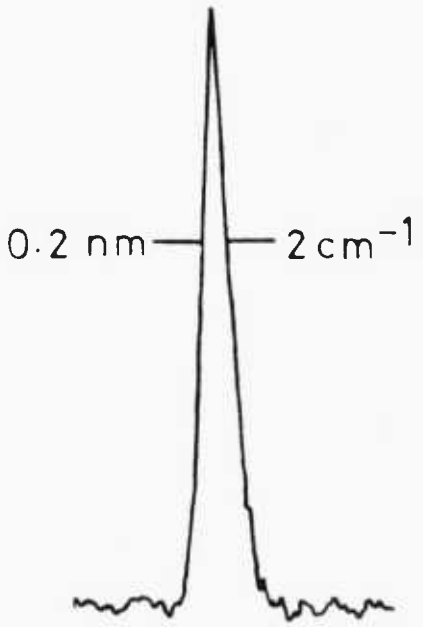

(b) Parametric spectrum (1·03μm)

Fig. 3·13

performance at 200 nm. Although the primary method of photoelectron energy loss within the photocathode is pair production, this has no adverse influence on the temporal performance of the instrument, which should be capable of time resolution < 5 psec up to the transmission limit of the photocathode substrate (140 nm).

In proving the capability of the streak camera this experiment has also shown that third harmonic generation in a metal vapour is a reliable means of generating ultra-violet picosecond pulses.

CHAPTER 4

THE MK.3 STREAK CAMERA

4.1 Introduction

The advantages of the channel plate image intensifier for night vision applications have long been appreciated (78). In order to determine whether or not these advantages might be applied to streak camera usage, a Mk.3 streak camera has been constructed in which a Mullard XX1332 channel plate image intensifier was fibre-optically coupled to a Photochron 2 streak tube. Despite the differing requirements of these quite distinct applications [1], this image intensifier was found to be quite suitable for use in conjunction with an ultrafast streak camera.

In this chapter the design and construction of the Mk.3 streak camera is described, together with details of the static and dynamic performance of both the image intensifier and the system as a whole. Details of the dynamic range of the system for short pulses are however given in a later chapter (cf Chapter 5).

1. The Mullard XX1332 image intensifier was designed for incorporation in passive night viewing systems.

4.2 The Channel Plate Image Intensifier

The construction of a channel plate image intensifier of the inversion type (Mullard XX1332) is shown in Figure 4.1 (a). It can be seen that this is a conventional electrostaticaly focused image converter tube, in which a microchannel-plate electron multiplier has been substituted for the phosphor. The phosphor has been moved back a short distance, and now forms part of a proximity focussed stage, receiving electrons from the output of the channel plate. The S25 photocathode is formed on the concave side of a plano-concave fibre-optic plate. This enables the tube to be fibre-optically coupled to its input, and yet provides the curved photocathode required by the electron-optics for optimum focussing. An image of the photocathode is focused onto the input of the channel plate by the electrostatic field set up by the focusing electrodes. The image may be brought into sharp focus by altering the tube focus voltage.

A section through a channel in the micro-channel plate is shown in Figure 4.1 (b). The channel is internally coated with a material having both a high resistivity and a high secondary emission coefficient. By the application of a potential across the channel-plate a potential gradient is maintained along the channels. An electron entering the channel collides with the wall, producing secondary electrons, which are then accel erated down the channel. These secondary electrons in turn produce further secondaries, the process being repeated until finally the electron bunch leaves the channel and is further accellerated towards the phosphor.

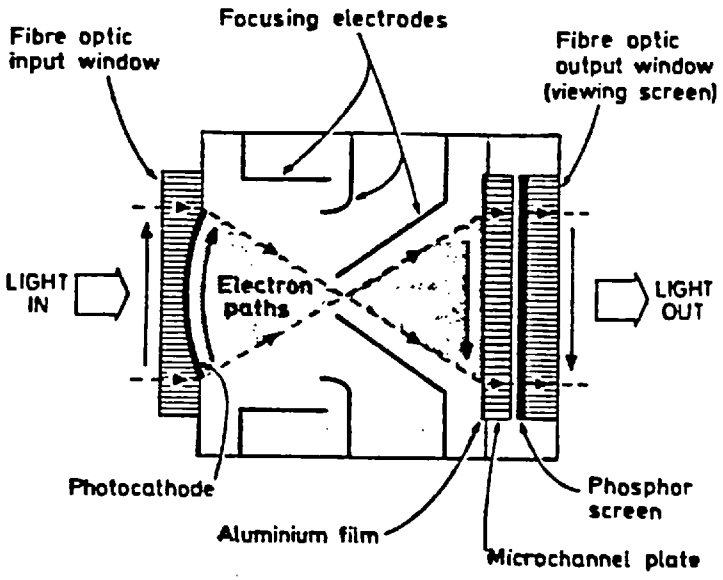

(a) Channel plate image intensifier

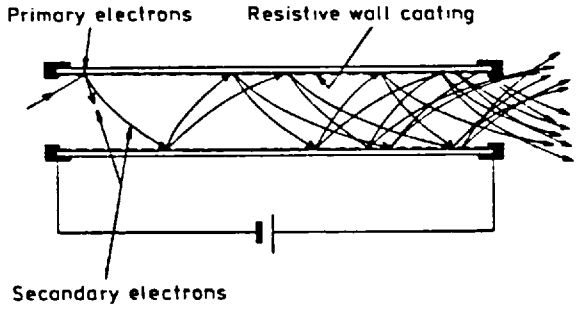

(b) Channel electron multiplier

Fig. 4.1

Because an electron travelling pa rallel to the axis of the tube may pass through the channel plate without colliding with the wall, the channel plate is cut from the boule in such a manner that the channels are inclined at a small angle to the axis of the image tube.

The gain of a channel is a function of both the applied voltage and its length to diameter ratio (85). The length to diameter ratio of the channels in the Mullard XX1332 tube is 60:1. This corresponds to the peak of the 1200v curve on the 'Channel Plate Universal Gain Curve' (85). Under these circumstances the gain of the channel plate itself will be $\sim 10^4$, and will be relatively independent of the channel diameter. The independence of gain and channel diameter under these conditions enables the production of tubes with uniform gain characteristics.

The gain of the channel-plate may be adjusted by altering the voltage applied along the channels. Unlike many cascade intensifiers (e.g. EMI 9693) the gain and focus controls of the channel-plate intensifier are independent. This is particularly useful when initially focusing the intensifier, since it is possible to focus it under conditions of high contrast and low noise (i.e. at low gain).

The inverter type of channel plate intensifier is not the only type available. A so-called proximity tube, in which both photocathode and phosphor are proximity focussed to the channel-plate, is also manufactured. This type of tube is shorter than the inverter tube, and free from pincushion distortion. It has a number of major disadvantages however, both technical and economic (78).

Only a limited field strength may be applied to the front proximity stage before serious field emission takes place. The outcome of this is to significantly reduce the spatial resolution of the system. Blooming effects take place caused by light passing through the semi-transparent photocathode and being reflected back to the cathode by the channel plate, and by electrons scattering from the front surface of the channel plate into the wrong channel. In some cases these electrons generate secondaries, further degrading the image quality. A further serious problem with this type of tube is that ions generated inside the channels feed back to the photo-cathode producing secondary electrons, which in turn produces a bright scintillation at the output. This ion bombardment eventually destroys the photocathode, and consequently tubes of this type normally have a short useful life.

These latter problems may be prevented in the inverter tube by covering the front of the channel-plate with a thin conducting foil. This foil, usually an evaporated layer of aluminium, is readily penetrated by the high energy photoelectrons (79).

In the proximity tube the large potential required across the gap between the photocathode and the channel-plate, to obtain the required electron energy, necessitates an increased spacing, resulting in a further loss of resolution, and an increase in blooming in the front section of the tube.

Because of the small gap between the photocathode and the channel plate, the photocathode of the proximity tube must be processed prior to incorporation within the device. This automaticly leads to an expensive tube. The price of the inverter tube however is reduced due to its application in night-viewing devices. These users find the inversion, and indeed the pincushion distortion an asset (78). This is unfortunate,

since this distortion compounds the streak camera slit curvature problem, and is a principal handicap in our application.

4.3 The advantages of channel plate intensification

Previous ultra-fast streak camera designs have incorporated an EMI 9693, 9694 or 9912 4 stage cascade image intensifier . This type of intensifier is bulky, requires a solenoid to provide the magnetic focusing field, and is incompatable with fibre-optic coupling to a streak tube.

In deciding on an image intensifier for a streak camera the designer must give consideration to three basic types: the magnetically - focussed cascade intensifier, the electrostatically-focussed cascade intensifier, and the channel plate intensifier.

Although the magnetically-focussed cascade tube has slightly better spatial resolution ($\sim$ 35 lp/mm) than either of the electrostatically focused tube designs ($\sim$ 30 lp/mm), and has much lower image distortion (by a factor of 5-10, Ref 80), a physically large solenoid is required, needing either air or water cooling. The high voltage (35 KV), and high current (12A for the solenoid of the EMI 9912 tube) requirement of this design necessitates considerable ancillary electronics. The large magnetic field needed to provide focussing limits the proximity of the intensifier and the streak tube to about 25 cms. This effectively prohibits the use of fibre-optical coupling.

Assuming that the streak tube phosphor emits with a Lambertian distribution (81), the lens coupling efficiency (Ce) can be calculated from the equation,

$$Ce = \frac{Tr\ M^2}{4(F/n)^2\ (1 + M)^2} \times 100\%$$

where Tr is the transmission factor of the lens, F/n is the f number of the lens (f/d), and M is the magnification (82). Taking values of F/n = 1.4 Tr = 1 and M = 0.7 (typical values used in the Mk.2 streak camera) the coupling efficiency is found to be 2.2%. This reduces the overall gain of the intensifier stage, from the streak tube phosphor to the film, to 700 (assuming an intensifier gain of 10^6, and a film camera with a single f/1.4 lens set for a magnification of unity).

The electrostatically focused cascade tube whilst not having the problems associated with a large magnetic field is still unsuitable for complete fibre-optic coupling, since there is a potential of $\sim$ 45Kv across its end plates (140). Lens coupling would hence be required at one end and for a typical tube such as the Mullard XX1603 with a gain of 7×10^5, an overall phosphor to film gain of only 2800 would be realized (This assumes that fibre optic coupling is 25% efficient, and that it is possible to use an f/1.2lens pair, which is 10% efficient, for the output coupling). Even if by internally re-arranging the voltage on the cascade tube module full fibre-optic coupling were possible, some form of shutter action would have to be devised in order to prevent fogging of the contacted film by background noise. Short of a mechanical lens shutter this is not easily accomplished. A further problem encountered with this type of intensifier is the severe distortion, which can be as high as 20% (80).

Many of the disadvantages of these tube types are overcome in the channel plate image intensifier. It is far more compact than either of the previously described types, and its modest E.H.T. requirement ($\sim$ 10Kv), and absence of magnetic field permit fibre-optic coupling at both ends.

Tubes such as the Mullard XX1332 are available with a luminous gain of $5 - 10 \times 10^4$, giving a phosphor to film gain of up to 1.3×10^4. The availability of this extra gain allows the sensitivity of the camera to be increased, with a possible increase in the dynamic range of the streak camera. The intensifier is readily gated by the modulation of the voltage applied to the channel plate. The recording film may thus be held in contact with the output faceplate, and the intensifier only gated on during the period when information is present at the output phosphor of the streak tube. From an operational point of view the gain saturation of this type of intensifier is useful, since it removes the possibility of damaging the output phosphor by accidental over-exposure. It also enables a streak record to be taken without flare, even though part of the image is over-exposed. Unfortunately this effect is also a potential limit to the dynamic range of the system (c.f. Chapter 5).

Due to the lower detection efficiency of a channel plate, compared to a phosphor, the channel plate intensifier itself has a noise figure greater than that of a cascade tube by a factor of 4. The greatly improved efficiency of fibre-optic coupling however more than compensates for this. Figure 4.2 shows a schematic diagram of both a cascade intensifier and a channel plate intensifier, indicating the noise and signal level at each stage. The noise figure (N F) of a system is defined such that

$$N\,F = \frac{SNR\ i/p^2}{SNR\ o/p^2} = \frac{1}{D}$$

where SNR i/p and SNR o/p are the input and output signal to noise ratios respectively, and D is the detection effeciency. The noise figure for a cascade tube is ~ 10, caused by the quantum efficiency of the input photo-

Channel plate intensifier

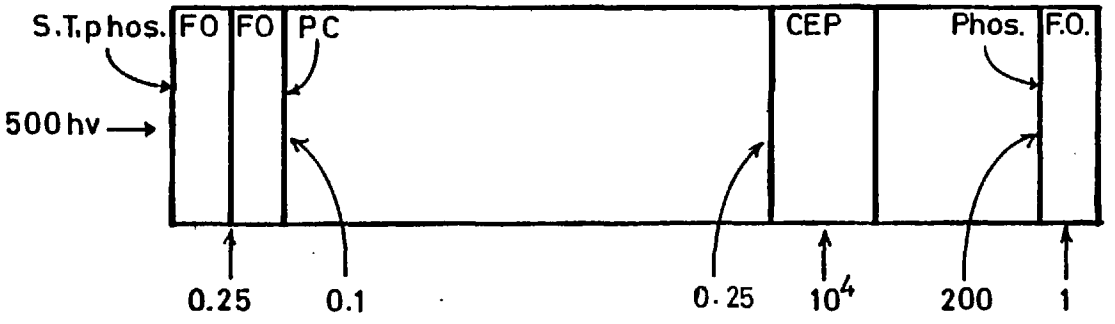

Cascade intensifier

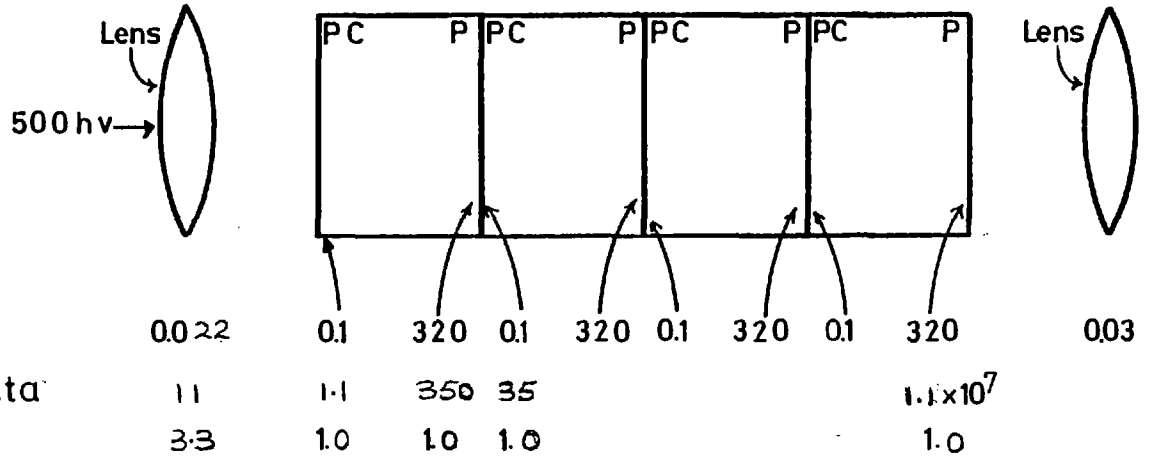

Fig.4.2 Intensifier noise figure

cathode, whilst the noise figure for a channel plate intensifier is ∿ 40 (the noise figure of the photocathode will be 10, and the noise figure of the channel plate is 4). The channel plate noise figure arises from two sources, (i) a factor of 2 due to the open area of the channels and (ii) a further factor of 2 due to the probability of an electron being detected.

The input coupling lens on a cascade system will typically be only ∿ 2% efficient, increasing the noise figure to ∿ 4600.

A coupling efficiency of ∿ 25% may be expected for a pair of fibre optic plates, giving a noise figure of ∿ 160 for a channel plate intensifier. Taking the coupling efficiencies and gains indicated in Figure 4.2 the overall system gain for a channel plate intensifier system will be ∿ 20 times larger than that of a cascade intensifier system, whilst the noise figure will be ∿ 3 times smaller.

4.4 The system as a whole

A diagram of the streak camera as a whole is shown in Figure 4.3. The shutter tube is a modified Photochron 2 type, in which a fibre-optic face plate set in a supporting metal flange is stitch-welded to an additional metal flange near the rear of the streak tube, such that the position of the phosphor is unaltered.

The tube mountings are in contact with the flange joining the phosphor cap to the main body (i.e. not the phosphor flange), and the cone flange.

Since a film was to be contacted against the output face of the channel plate intensifier it was desirable that it be maintained at earth

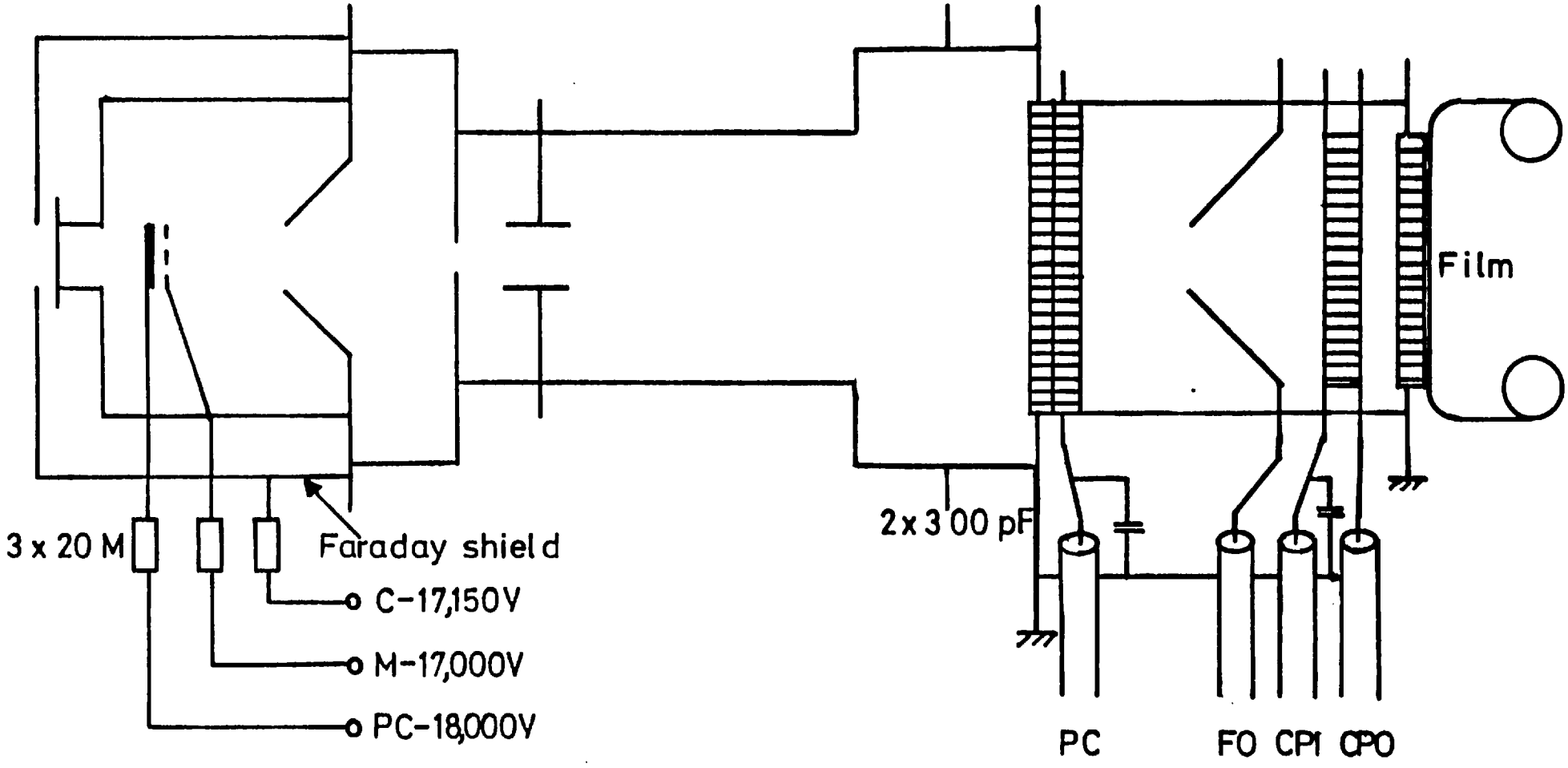

Fig.4.3 The Mk3 streak camera

potential, resulting in an intensifier photo-cathode potential of - 10KV. The potential between the streak tube phosphor and its photocathode is also - 18KV. Thus unless a potential of 10KV is retained across the two fibre-optic face plates, the streak tube photocathode would be required to run at - 28KV. To reduce the insulation requirements of the system the phosphor of the streak tube was also grounded enabling a cathode potential of -18KV to be used. This made the physical construction of the camera much simpler, with the added convenience that the deflection plates would operate close to ground potential.

The channel plate intensifier was mounted within a light-proof brass cylinder, supported at its ends by two plastic discs. This intensifier module was slid inside a dural cylinder attached to the rear of the streak tube housing. The image intensifier was held in place by a retaining ring screwed into a 40 t.p.i. thread at the end of the cylinder. Prior to assembly the two fibre-optic faceplates were thoroughly cleaned with lens tissue soaked in Iso-propol alcohol, and a few drops of microscope immersion oil were applied to ensure good optical contact. To avoid any oil leakage back along the edge of the fibre-optic faceplate to the cathode connector, a silicone rubber seal was included between the edge of the fibre optic plate and the end of the intensifier housing.

The voltages to drive the system were derived from a pair of bleeder chains driven from a Brandenburg Alpha type 807R power supply, set to give an output of -18KV (Figure 4.4). The -17.0KV, and -17.13KV points were tapped off and fed to the mesh and cone respectively. All three high voltage electrodes, cathode, mesh, and cone were fed through 20MΩ series resistances in order to limit the current in the event of a

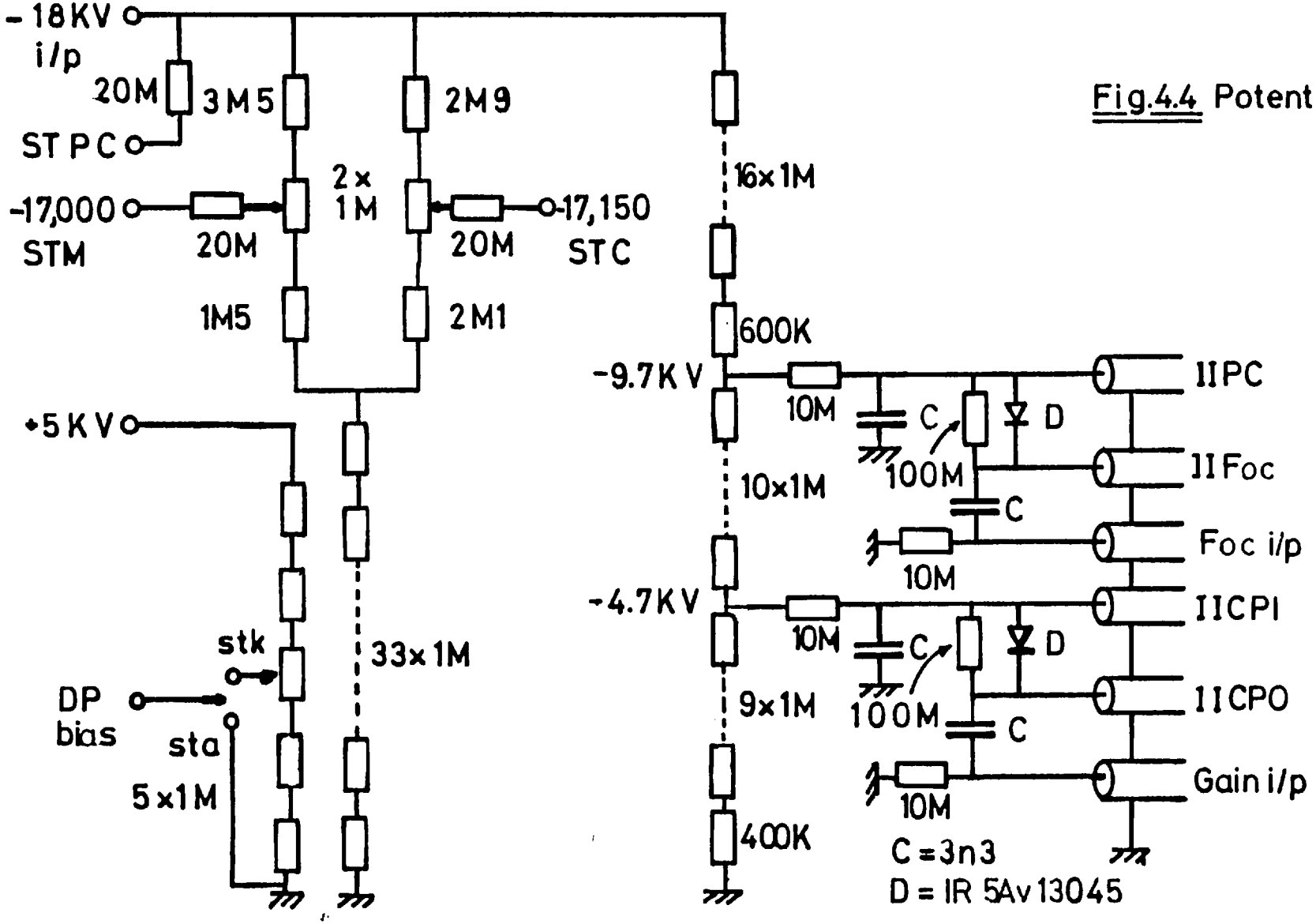

Fig.4.4 Potential dividers

breakdown.

In an improved version of this system a pure resistive bleeder chain would not be used, since it is difficult to monitor the mesh voltage with a precision of better than ∿ 10%. Cheap high-voltage zener diodes such as the Motorola IN5200 series (e.g. IN5281 - 200V 500 mW, IN5271 - 100V 500 mW) are now a more attractive means of deriving the mesh voltage. Such a system would self-compensate for any voltage monitor, prevent any variations in the EHT supply overvolting the mesh, and are less likely to be adversly affected by age.

A separate bleeder chain supplied the channel plate intensifier. A voltage of - 9.7KV was supplied to the cathode, and 5KV to the input of the channel plate, again via 20M Ω feed resistances. The focus electrode was tied to the cathode, and the channel plate input and output were tied together through 20M Ω resistances. The cathode and channel plate were each decoupled to ground through a 1nF 30KV capacitor. Positive going pulses were supplied to the focus electrode and the channel plate output when gain was required from the intensifier. The amplitude of these pulses ∿ 220V and ∿ 1KV respectively were independently variable, the former being adjusted for optimum focussing, and the latter for the desired gain. These pulses were coupled to the image intensifier electrodes via a second pair of 1nF 30KV capacitors. A diode across the channel plate prevented a pulse of the wrong polarity being applied, since this was known to be seriously detrimental to the intensifier tube life.

Measurements of the voltages at the tube electrodes showed that very careful screening was required to prevent crosstalk between the electrodes as the channel plate was gated on. Miniature coaxial cable type UR95 was used to feed the voltages to the intensifier

electrodes, the screening being taken well inside the housing. The cathode and channel plate input were further decoupled by 300pF 12KV disc ceramic capacitors soldered to the electrode connectors themselves.

The use of pulsed focus and channel plate voltages enables the production of these voltages accurately, and without the need for a variable high voltage output from the power supply. Nominal values for gain as a function of channel plate voltage are as follows :-

Gain	Channel Plate Voltage
10^5	1200 V
10^4	1000 V
10^3	800 V

The slit of the streak camera was focused onto the photocathode of the streak tube by a lens. Because the streak tube was the U.V. sensitive tube previously described (c.f. Chapter 3), it was fitted with a short 'snout' to which its sapphire entrance window was attached. This made the distance between the front of the tube and the photocathode longer than usual. It was thus necessary to accept a slit demagnification of 2.2 instead of the normal demagnification of 3.

4.5 The Faraday Shield

With the cathode of the shutter tube operating at -18KV it was found necessary to enclose the front end of the tube within a Faraday shield held at either mesh or cone potential. In the absence of this, the glass at the front of the streak tube charged up in an irregular manner, and the non-uniform electrostatic field interacted with the comparatively slow moving electrons in the mesh-cone region, causing both de-

focussing and image deflection. In this proto-type streak camera the front of the streak tube was surrounded by a copper "can", clad with nylon to prevent corona, and attached to the cone support. A 2 cm diameter hole in the front allowed access to the photocathode. In later commercial versions of this system the glass at the front of the tube was painted with a conductive paint such as silver-dag. It was found that providing this shield was attached to either the mesh or the cone potential its exact shape or position was not critical. This can be understood by examining the tube potentials (Figure 2.9 (a)) and noting that the mesh-cone section is virtually a drift zone at a potential somewhere between that of the mesh and that of the cone. With this in mind two other tube designs evolved. In the so-called Rutherford X-ray streak camera, the electron-optics of which were designed at Imperial College, a 7.5 cm diameter copper "can" was mounted from the mesh support pillars by means of two 1.5 cm metal spacers. The Faraday shield was thus contained within the tube body itself. Mounting from the cathode support pillars was also tried, but as might be expected serious defocussing took place. As this type of construction is unsuitable for a sealed-off tube, and also in reply to the need for an X-ray streak tube with a more streamlined front end, an alternative variation has been proposed, in which the mouth of the focus cone is extended forward in the shape of a cylinder, until it is $\sim$ 1 mm from the mesh. This cylinder could of course be used as a mount for the mesh, which would have a number of advantages in electrode alignment in the construction of the tube. Whilst initially the idea was that the cylinder be physically separate from the cone, and at an independently variable voltage, preliminary experimental and theoretical studies (83) with a cylinder in physical and electrical contact with the cone have been very encouraging. This work has not yet however advanced to the stage where a sealed-off tube has been made.

4.6 The channel plate gating generator

The channel plate gating circuit and laser control systems are integrally connected. The control system is complicated by the requirements of the Optical Multichannel Analyser (OMA) to be used in conjunction with this streak camera at a later stage (c.f. Chapter 7).

Although the circuit diagrams are complete, the operation of the system is described as if it were being used without the OMA, and any differences to this mode of operation are described in appropriate later sections.

A block diagram of the channel plate intensifier, streak camera and laser control systems is shown in Figure 4.5. A command signal from the control logic causes the gating generator to produce a low voltage pulse with a duration equal to the desired gating duration $\sim$ 200 μs (chosen such that the channel plate intensifier has gain for the whole of the streak tube phosphor decay time). This pulse controls the gating output stage, producing a 225V pulse for the intensifier focus electrode, and an 800 - 1200V pulse for the channel plate output. A laser trigger pulse is also produced, and is coupled to the laser via two opto-isolators used to eliminate earth currents. The omission of these insolators was found to produce severe electrical interference problems. The streak camera ramp generator is then triggered by the laser in the normal manner.

The control logic and gating generator are shown in Figure 4.6. The system is 'armed' by pressing the reset button, which sets the three latches (IC 3a and 3b - laser inhibit, IC 4a and 4b - reset hold, and IC 3c and 3d - test hold). When the OMA is not in use a short is applied to the DELINHD2 input. The application of a short to the AACUMSDO acts

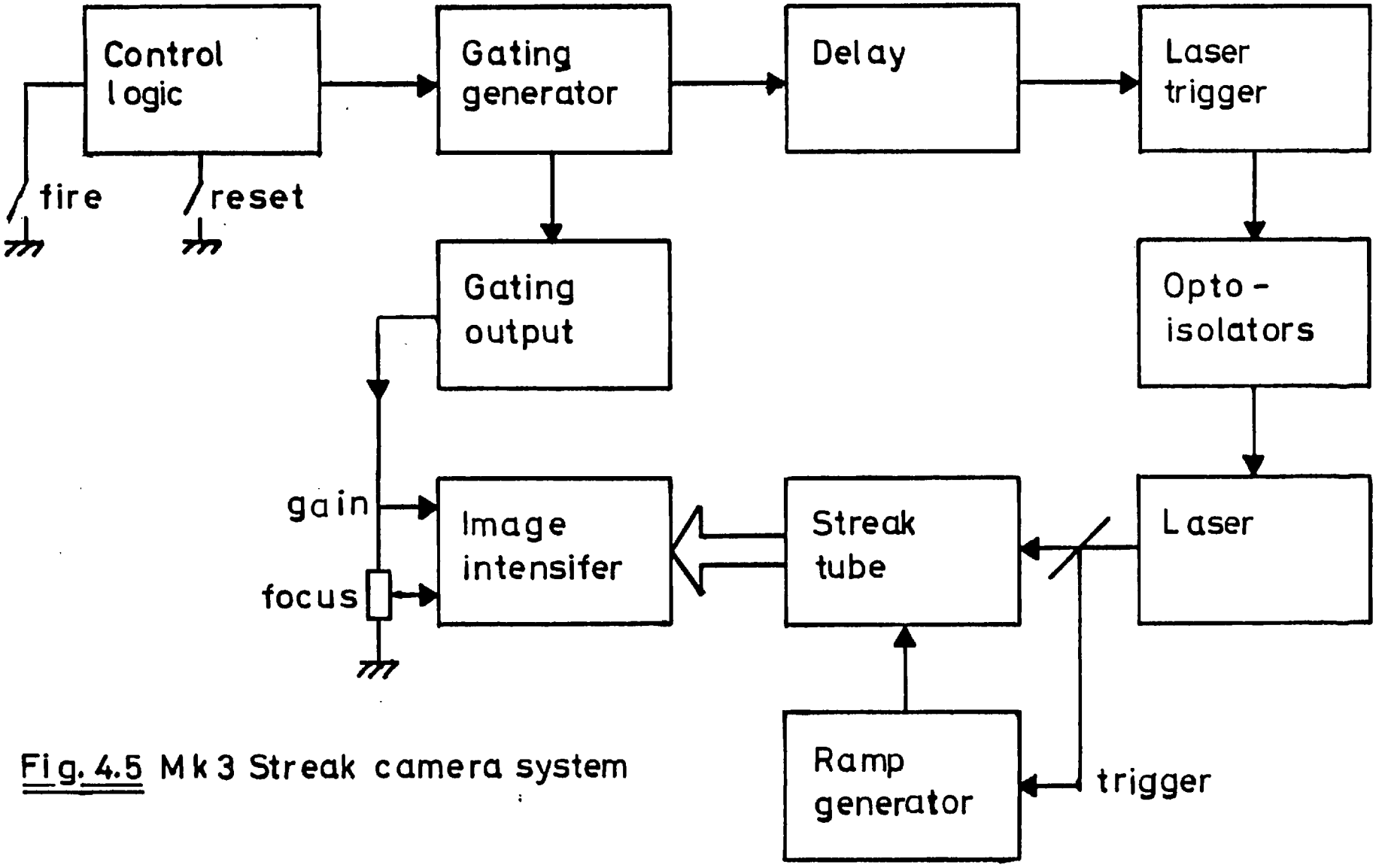

Fig. 4.5 Mk 3 Streak camera system

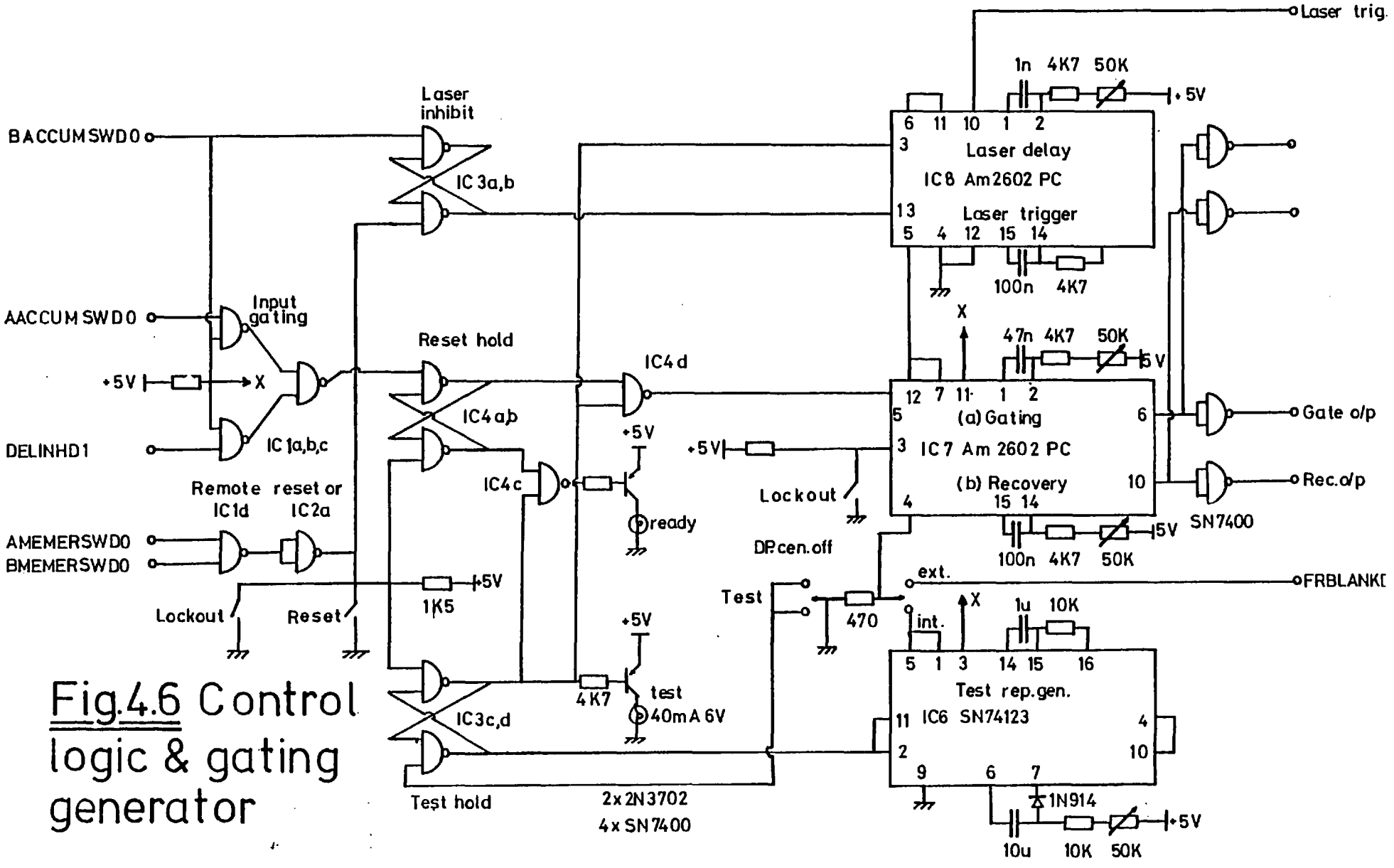

Fig.4.6 Control logic & gating generator

as a trigger for the system by tripping the reset latch, and triggering the gating generator monostable (IC7a). At the end of the gating period the recovery generator (IC7b) generates a pulse used to steepen the fall of the gating pulse output. These pulses are coupled to the gating output stage via two inverters (IC 5a and 5b). The gating generator also triggers the laser trigger delay monostable which in turn triggers the laser trigger monostable, producing the opto-isolator drive pulse.

In order to focus the electron optics a 30 Hz pulse generator (IC6), is used to repeatedly trigger the gating generator, continuously pulsing the intensifier on to give a flicker-free image. A logical 0 output from the test hold latch (IC 3c) is applied to the reset pin of the laser delay monostable, preventing the laser being fired when the system is in this mode.

The push-pull gating output stage is shown in Figure 4.7. A negative-going pulse from the gating generator switches Tr_1 on, which then turns Tr_2 on, driving a current through the primary of pulse transformer T1. The secondary of the pulse transformer is coupled to the base of the output transistor Tr_5, which is hence turned on, effectively connecting one side of C7 to the EHT supply. As the gating generator pulse ends, Tr_1 and Tr_2 turn off, removing the drive from the base of Tr_5. A negative pulse from the recovery generator is simultaneously applied to the base of Tr_3. Tr_3 and Tr_4 thus switch on bringing the output voltage to zero. A positive-going pulse with a voltage equal to the EHT supply, and a duration determined by the gating generator is thus produced. The amplitude of this pulse is varied by adjusting the output voltage of the EHT regulator.

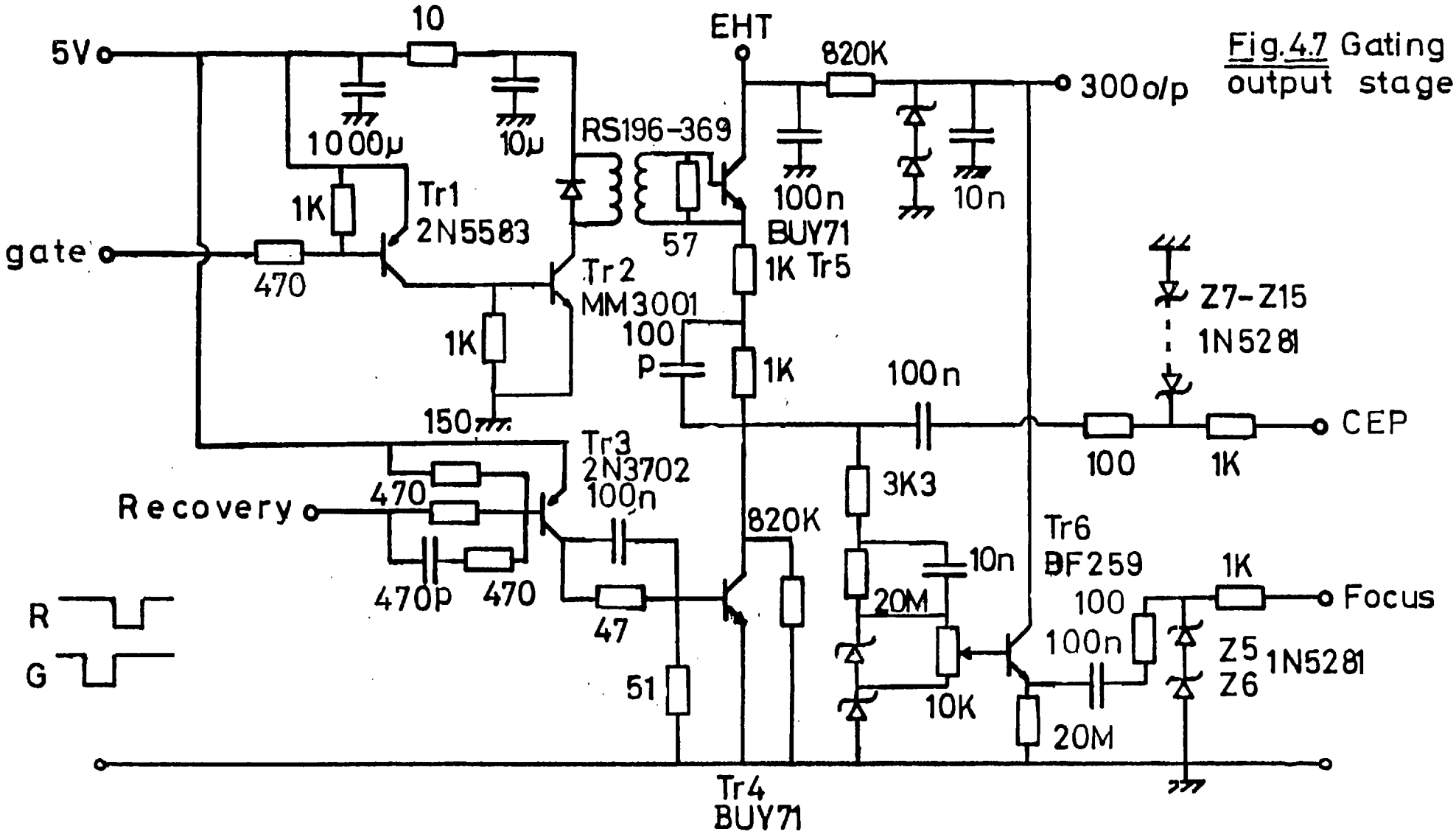

Fig.4.7 Gating output stage

By applying this voltage pulse to a current limiting resistance in series with a string of 100V zener diodes, and tapping the voltage across one of the zener diodes with a 10K potentiometer, a variable amplitude pulse (200 - 300V) is generated concurrent with the main gating pulse. This pulse is applied to base of Tr_6 the focus voltage emitter follower output transistor. The collector of Tr_6 is connected to the cathode of zener diode Z_3, which is used to provide a 300V voltage supply.

The two strings of zener diodes (Z_5 - Z_6 and Z_7 - Z_{15}) across the output are used to suppress any large voltage spikes that might arise as the result of a breakdown within the image intensifier, or one of its connectors.

The main EHT supply was generated by voltage doubling the output of a 700V mains transformer, to produce a 2KV d.c. supply. This voltage is fed to the input of the EHT regulator (Figure 4.8).

This is a series regulator in which Tr_8 acts as a series pass transistor, IC9 acts as a differential voltage to current converter, and Tr_7 acts as a voltage amplifier. A fraction of the output voltage from the regulator is compared with a fraction of the voltage across zener diode Z_{16}. The output voltage of IC9 is determined such that its two input voltages are identical. The output voltage of IC9 determines the base and hence collector current of Tr_7, which in turn determines the base voltage of Tr_8. Since Tr_8 is an emitter follower the regulator output voltage is approximately equal to its base voltage.

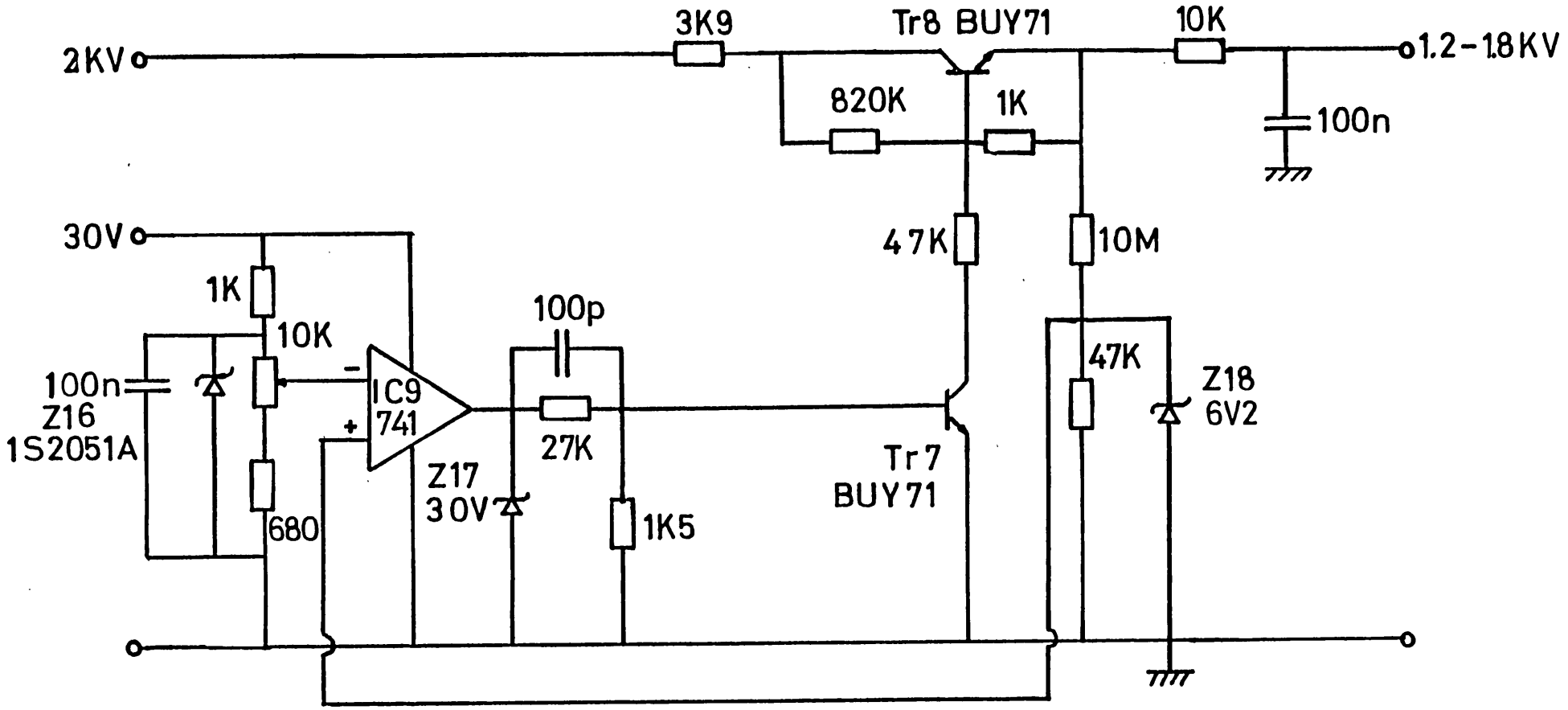

Fig.4.8 EHT Regulator

4.7 The opto-isolator circuits

The two opto-isolator circuits used are shown in Figure 4.9 (a) and 4.9 (b). The laser trigger output from the channel plate gating generator is used to drive the light emitting diode (led) of an integrated circuit opto-isolator (HP 5082 - 4351), via two nand gates used as a buffer (Figure 4.9 (a)). Because of the high output impedance, and low guaranteed output voltage of a T T L gate with a logical 1 output (2.4V of which 0.7Vwill be dropped across the led), the led was connected between the gate output and Vcc, and driven in logical 0 state, being pulsed off at the application of the trigger pulse. This was reckoned to produce more reliable operation of the system. The power for this part of the unit was taken from the + 5V supply of the channel plate gating generator.

The receiver section of this circuit is a light sensitive diode activated switch, and is battery powered. When the led pulses off the resistance of the diode changes from low to high turning the internal transistor Tr_1 off, and the output transistor Tr_2 on. The resulting -9V pulse triggers the laser in place of the normal trigger button.

Although the use of this isolator prevented the wholesale destruction of the integrated circuits in the channel plate gating unit, when the laser was fired a high voltage spike was capacitively coupled into the streak camera, occasionally inducing a breakdown inside the channel plate image intensifier. This spike was suppressed by including a second isolator in the laser trigger line (Figure 4.9(b)). In this case the input and output stage voltage supplies were supplied from a pair of 9V batteries.

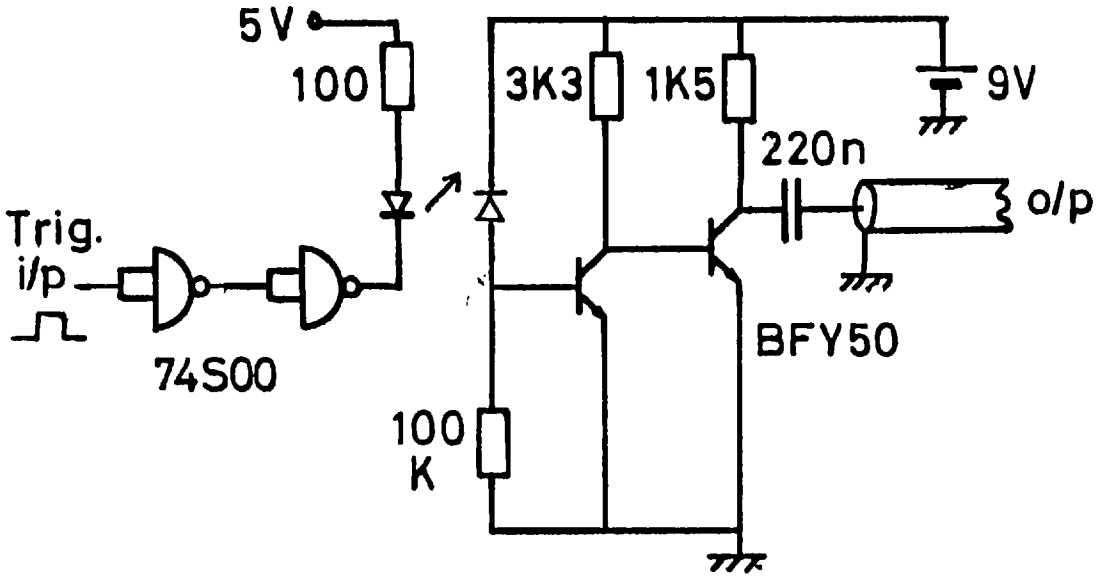

Fig.4.9 Opto-isolator circuit based on HP 5082-4351

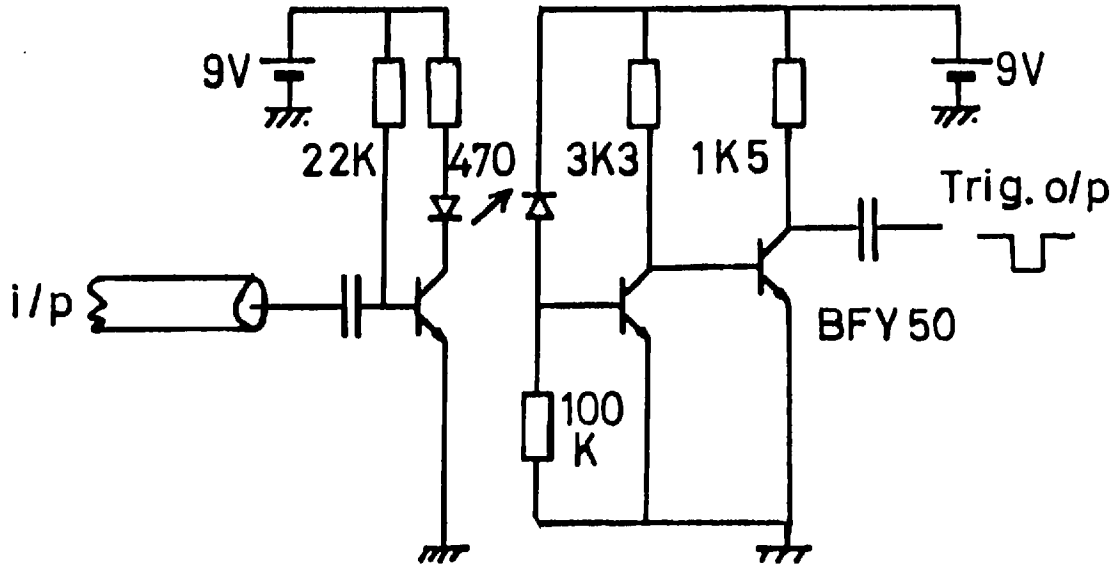

4.8 The Ramp Generator

There are two principal requirements placed on the ramp generator of an ultra-fast streak camera. It must be able to sweep the streak image across the phosphor of the streak tube at the desired writing speed, and it must have minimal jitter. Although spark gaps (24, 31) hard valves (142) and avalanche transistors have been used, spark gaps often tend to be too jittery for this application, and hard valves and avalanche transistors have so far failed to give the required writing speed. The Krytron trigger tube (5) is thus almost universally used as the ramp generator in streak cameras requiring the shortest possible time resolution.

For a writing speed of 10^{10} cm s^{-1} the ramp generator is required to produce a 1500V edge with a 500 psec linear rise or fall time. This can be obtained from a Krytron switch operating at 5KV, by taking only the linear part of its output.

A ramp generator of this type is described by Sibbett (5), who reported a jitter of $\pm$ 50 psec, and a maximum writing speed of 2×10^{10} cm s^{-1}. Unfortunately lat er copies of this ramp generator failed to reproduce this performance with any degree of consistency. A variation of this design was used in conjunction with this camera, and an attempt was made to locate the source of the jitter.

The ramp generator used is shown in Figure 4.10. A 10V pulse from an ITL 125 Ω S20 vacuum photodiode was used to trigger the avalanche transistors Tr_1 - Tr_6. The avalanche transistors were selected from a batch of 50 so that they exhibit identical avalanche voltages, when set for the fastest risetime. The transistor with the fastest risetime in the whole batch was used as the trigger transistor Tr_1.

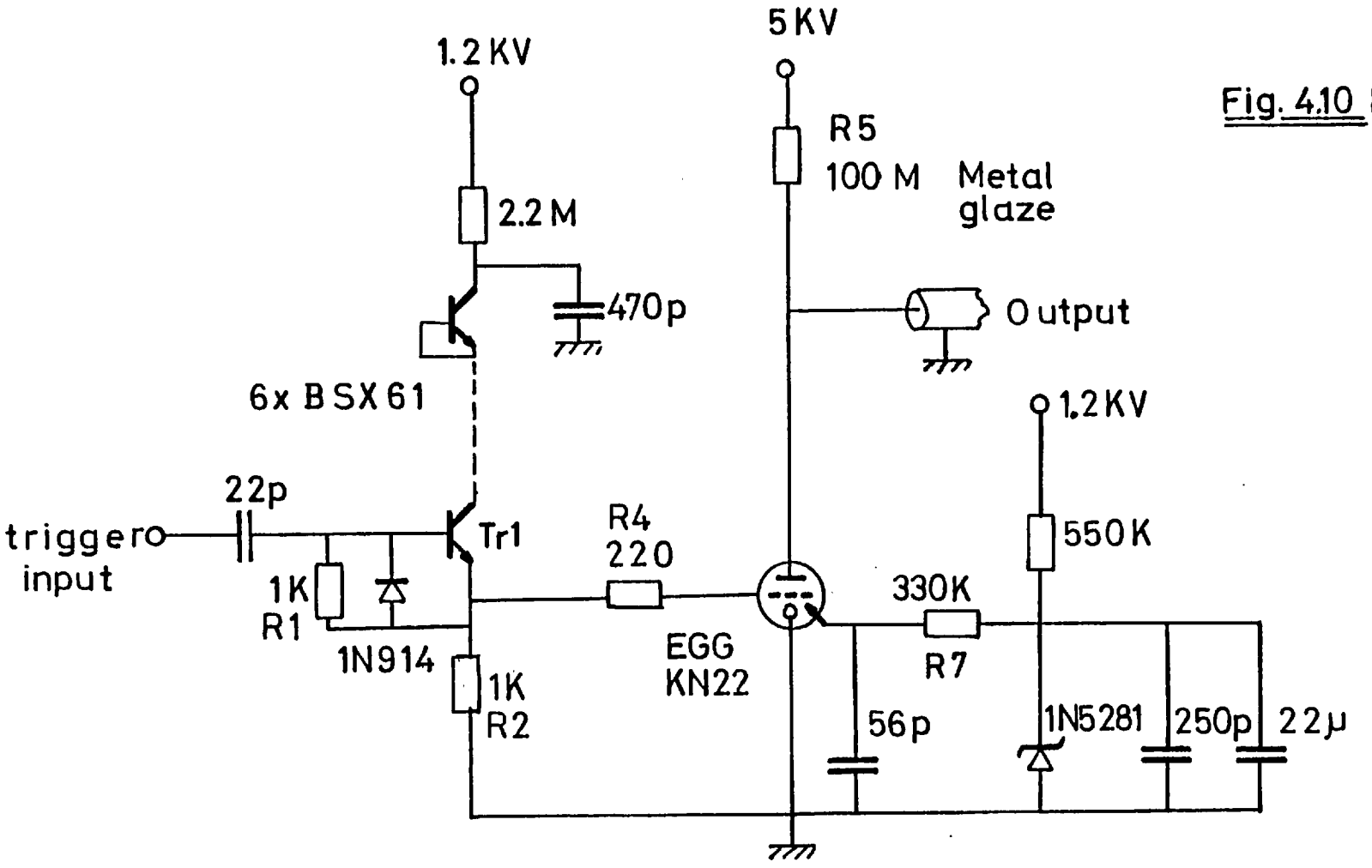

Fig. 4.10 Ramp generator

The positive voltage developed across a 1KΩresistance in the emitter of the trigger transistor was used to trigger the Krytron. In the circuit used by Sibbett this voltage was doubled by passing the pulse through a short piece of 50Ω coaxial cable with an open circuit at the Krytron grid. This cable increased the risetime of the front edge of the pulse, and it was thought to be better to trigger the Krytron from a lower voltage pulse with a faster risetime. The voltage to the avalanche transistors was derived from a very stable high voltage power supply (Fluke 412B - 0.005% stability 1mV ripple) and fed through metal glaze resistances used for their good high voltage and low noise properties. The Krytron keep-alive electrode was fed from a well decoupled zener diode, and was decoupled by a low inductance capacitor very close to its lead in. This capacitor was found to significantly affect the performance of the ramp generator, since its removal, or the inclusion of an antiparasitic bead on one of the leads of R7 increased the jitter by a factor of 4 - 5. Unfortunately there are restrictions on the maximum size of this capacitor, since if it is too large, the keepalive current goes into relaxation oscillations.

The use of an ultrastable power supply for the Krytron anode was also found to be important. Substituting a Fluke 408B power supply (-0.005% stability, 5mV ripple) for the usual Brandenburg Alpha type 507R power supply (0.01% stability 500 mV ripple) produced a significant reduction in jitter.

Typical figures for the jitter measured during these experiments was ± 30 psec. Although this was maintained for a period of several months, a gradual deterioration in performance was observed until eventually the jitter increased to ± 300 psec. This deterioration is thought to

arise from the aging of the avalanche transistors, since replacing the Krytron failed to restore the original performance.

4.9 Static performance of the system

Before any streak measurements were taken the static performance of the system was checked. A Baum pattern projector (141) was used to project a resolution chart onto the cathode of the streak tube. By observing the output phosphor of the system with a X10 microscope, and measuring the diameter of the pattern the resolution of the system could be determined at various stages of assembly.

The streak tube was found to have a spatial resolution of 11.5 lp/mm at its phosphor, with a magnification of 1.75 in the streak direction, and a spatial resolution of 16.3 lp/mm at the phosphor, with a magnification of 1.83 perpendicular to the streak direction. This spatial resolution is lower than set out in the specification for a Photochron 2 tube, but can be traced to problems concerning phosphor manufacture and electrode misalignment. A check made on the spatial resolution of the channel plate showed that it had a spatial resolution of 20 lp/mm at its photocathode, in agreement with the manufactures specification. When assembled, the static spatial resolution of the whole system was found to be equivalent to 9.3 lp/mm at the phosphor of the streak tube. This is slightly less than might be expected from a calculation of the resolution based on the resolution of the individual components (which predicts $\sim$ 10 lp/mm), and implies a slight loss of resolution across the fibre optic interface.

The static spatial resolution figure was confirmed by contacting Ilford Pan F film onto the fibre-optic output faceplate of the image intensifier.

This film, developed in Acutol for 8 minutes has a spatial resolution of > 80 lp/mm. The recorded image is shown in Figure 4.11. As can be seen the 30 lp/mm point on the chart can still be resolved. When the magnification of the pattern projector and the streak tube are taken into account (x3.25) this corresponds to a resolution of 9.2 lp/mm at the streak phosphor.

The shutter ratio of the channel plate intensifier was measured in order to determine the effectiveness of the gating system. Ilford HP5 film was contacted against the output faceplate of the image intensifier, and the time taken to expose the film to an arbitary density was measured, both with and without the application of gating pulses. The shutter ratio was thus found to be $\sim 10^5$.

4.10 Dynamic Performance of the System

The dynamic spatial resolution of the system was measured in order to be able to estimate the instrumental time resolution. The output from the modelocked flashlamp pumped dye laser (cf Chapter 2) was directed into the normal calibration delay line (cf Chapter 3). The output from the delay line was focussed onto a diffuser, and the diffused light recollimated before being directed onto the slit of the streak camera, which was opened to give a 2 mm wide slit.

The variable spatial frequency wedge from a 1 cm diameter Baum chart was held in contact with the slit of the streak camera, such that the resolution lines were parallel to the streak direction. A streak image of the slit was recorded at a writing speed of 10^{10} cm s^{-1}.

Fig.4.11 Baum chart through whole system
magnification at streak tube phosphor = 3.25

A typical streak record is shown in Figure 4.12(a) and 4.12(b). As can be seen it is possible to resolve at least 20 lines corresponding to a resolution of $\sim$ 6 lp/mm for this magnified chart. When the overall system magnification of 0.82 is taken into account this corresponds to a resolution of $\sim$ 7.3 lp/mm at the streak tube phosphor. Errors in alignment of the resolution bars with the streak direction, non-uniformities in illumination and the lower visibility of the resolution elements when compared to the whole slit (50) make this a pesimistic measurement of the streak camera dynamic spatial resolution.

If the dynamic spatial resolution is 7.3 lp/mm as is indicated, then a technical time resolution of 1.4 ps is to be expected at a writing speed of 10^{10} cm s^{-1}. It is more likely however that the spatial resolution has only apparently degraded, and remains at $\sim$ 9 lp/mm indicating a technical time resolution of $\sim$ 1.1 ps.

4.11 Conclusion

A description has been given of a streak camera incorporating a channel plate image intensifier fibre optically to the streak tube. Preliminary performance measurements have been made, and a technical time resolution of 1.1 - 1.4 psec predicted. The measurement of the dynamic range, and applications of this camera are the subject of Chapters 5 and 6.

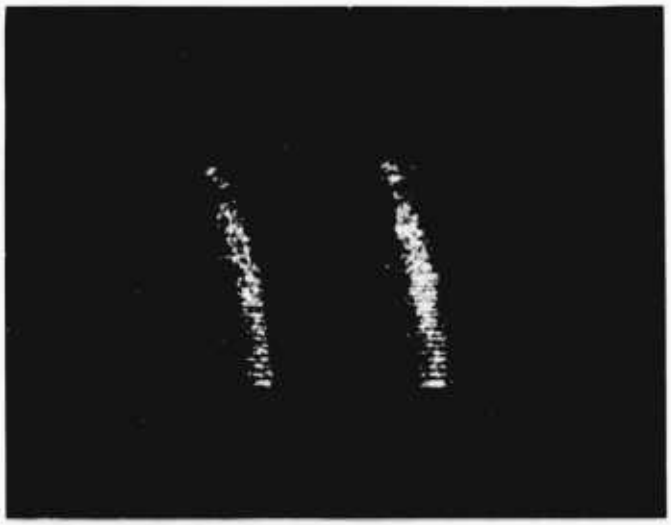

(a)

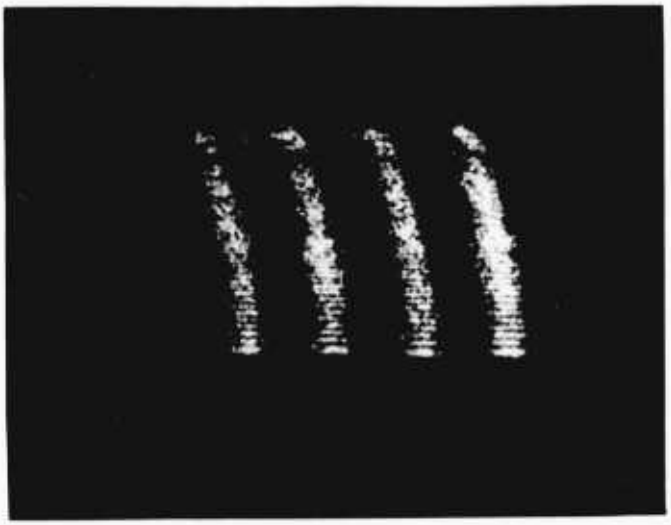

(b)

Fig. 4.12 Dynamic Spatial Resolution

CHAPTER 5

THE DYNAMIC RANGE OF THE PHOTOCHRON STREAK CAMERAS

5.1 Introduction

While extensive efforts have been made to reduce the temporal resolution of the ultrafast streak camera, and to increase the wavelength range over which picosecond resolution may be obtained, little work has been done on measuring the linearity and dynamic range of these devices. Such work as has been done, both theoretical (53) and experimental (47, 52, 105, 106) is the subject of some controversy (51). The increasing use of ultrafast streak cameras in the fields of, for example, laser-plasma physics (117), chemistry (107), biology (108) and solid-state physics (109), where experiments to observe luminescent phenomena demand both good time resolution and good dynamic range make an accurate study of these parameters essential.

The result of recent measurements (47) indicates a disappointingly low value for the dynamic range of the Photochron type of streak camera. Had these results been characteristic of this type of streak tube then it would not have been possible to obtain the high resolution and good signal-to-noise ratio reported by other users (19). It was hence necessary to resolve the apparent discrepancy between these results.

A study of the dynamic range is also of importance to the streak camera designer, since it yields information from which it may be possible to determine the fundamental physical processes which may limit the further development of this type of ultrahigh speed diagnostic instrument.

Measurements were made on the dynamic range of both the Mk.1 streak camera with an S1 photocathode, and the Mk.3 streak camera with an S20 photocathode. It was found that the dynamic range depended upon the time resolution employed. For events $\sim$ 2 psec a useful dynamic range of 30 is obtainable. This increases to a value of 180 for 35 psec events.

5.2 Streak Image Degradation

As the writing speed of an electron-optical streak camera increases then so does the current required to maintain a given film exposure. It was discovered at an early stage in the development of high speed cameras, that above a certain maximum current the temporal resolution of a streak was reduced (16).

With a comparatively slow streak camera for example the Hadland Imacon 790 (150 psec time resolution), the peak photoelectron current required to produce an exposure is normally well below this limiting current. This is not the case for the experimental ultrafast streak cameras described here. To attain picosecond resolution a streak camera must be coupled to a high gain image intensifier such as the EMI 9912 four stage cascade intensifier (16), or the Mullard XX1330/A channel plate intensifier.

The degradation of the streak image is shown in Figure 5.1 (a). The photograph shows a pair of streaks taken with a Mk.3 streak camera with an image intensifier gain $\sim 10^3$. Since too much photoelectron current has been drawn from the photocathode the images are broadened.

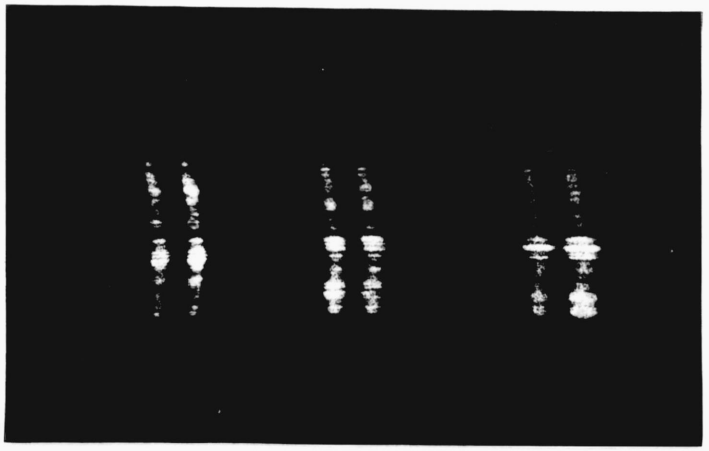

(a) Over - exposed streak images

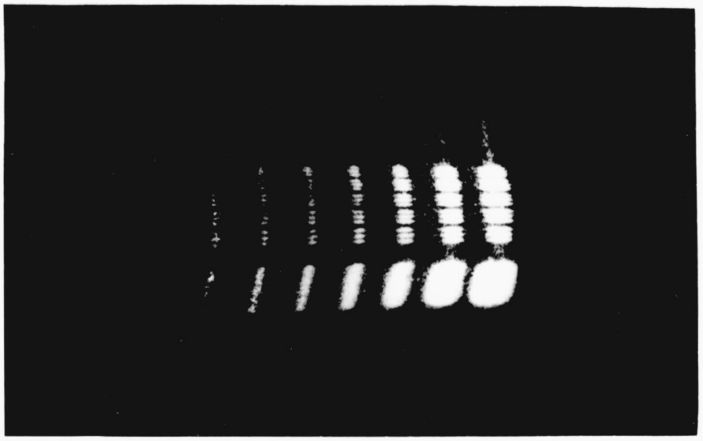

(b) Resolution chart streaked at various exposures

Fig. 5.1

Due to the non-uniformity in the slit illumination the broadening is also non-uniform, but it will be noticed that the structure in the beam appears to be reproduced with high spatial resolution. This is confirmed by increasing the intensifier gain to 10^5, and illuminating part of a USAF resolution pattern contacted against the slit, with a series of picosecond dye laser pulses of gradually reducing intensity (c.f. Section 5.4). It can be seen that as the intensity increases broadening takes place, but spatial resolution along the slit is maintained (Figure 5.1 (b)) (In fact due to the influence of contrast on resolution (50), the resolution actually increases !). It is also clear that the broadening is symetrical about a line defined by the position of a correctly exposed image.

Although it is somewhat difficult to quantify, it has been reported (47, 51, 110) that the intensity level at which pulse broadening takes place is dependent on the, sensitivity (51), spectral response, and resistivity (54) of the photocathode of the image tube. Unfortunately for practical reasons largely related to the cost and availability of streak tubes a thorough investigation of these parameters and their effect on dynamic range is not possible.

5.3 The Dynamic Range - definition

The dynamic range of a streak camera may be studied by plotting a graph of the ratio of the measured pulse duration (Tr') to the actual pulse duration (Tr), as a function of pulse intensity. The point at which the ratio Tr'/Tr departs from a value of 1.0, represents the point at which the streak tube is starting to approach its photoelectron current limit.

The accepted definition of dynamic range (D.R.) is the ratio of the intensity level at which a measured pulse duration (FWHM) exceeds its actual duration by 20%, to the noise level (In) of the whole system, i.e.

$$D.R. = \frac{I(T' = 1.2T)}{In}$$

A correction is made to both T' and T for the low intensity time resolution of the streak camera, before they are applied to the dynamic range criterion. The value of T may be obtained by measuring the duration of pulses whose intensity is sufficiently low, that the photoelectric current is well below the saturation current limit of the streak tube.

5.4 Dynamic Range - measurement

Early experiments to measure the dynamic range of a streak camera employed a calibrated neutral density step wedge contacted against the slit (Figure 5.2 (a) and Reference 111).

By uniformly illuminating the slit with a picosecond pulse, and microdensitometering the recorded streak image across each step, Tr' could be measured as a function of intensity. In principle one measurement will give the dynamic range of the camera. In practice this technique is unreliable, since it is difficult to ensure uniform illumination of the slit throughout the experiment. Problems of beam drift, calibration of the illumination to compensate for any non-uniformities across the slit, and flare from the neutral density wedges (111) have led to the use of other methods. The alternative to the use of a step wedge is to generate a sequence of pulses of differing

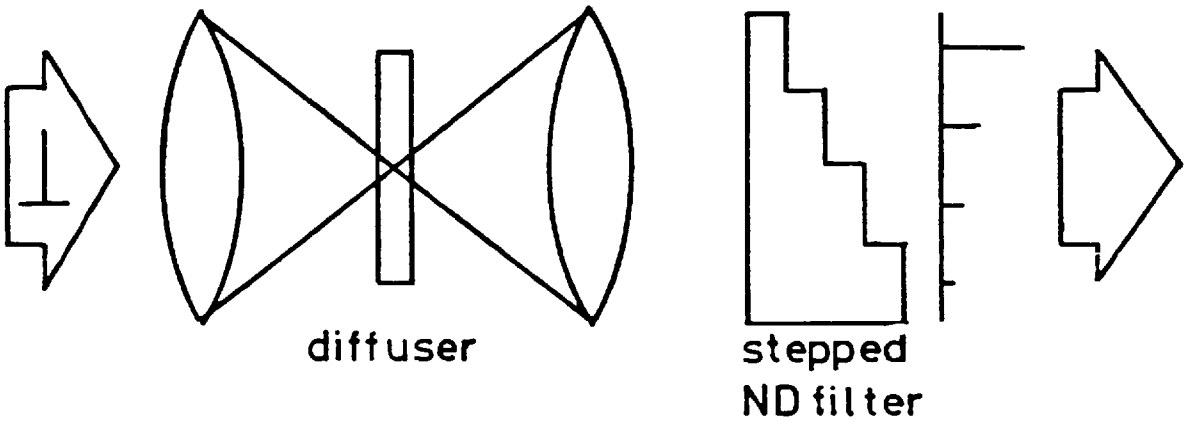

(a) Stepped filter method

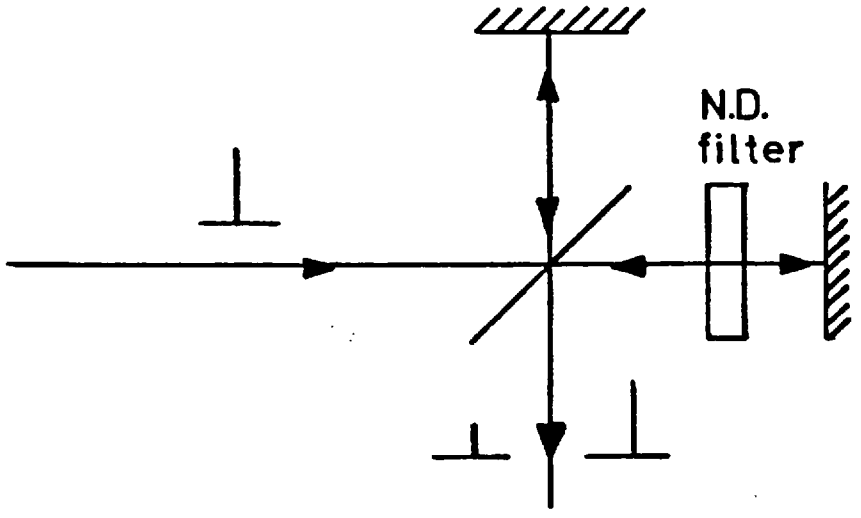

(b) Michelson method

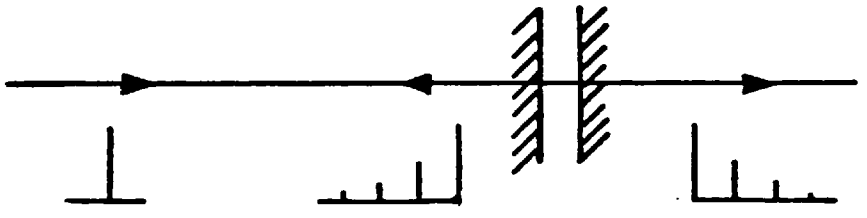

(c) Fabry-Perot method

Fig. 5.2 Test pulse generation

intensity in an interferometer (106). Either a Michelson or a Fabry-Perot etalon may be used.

A Michelson system is shown in Figure 5.2 (b). A picosecond pulse is directed towards a 50% beamsplitter, where two indentical sub-pulses are produced. Each sub-pulse is made to pass twice through a calibrated neutral density filter before being directed onto the slit of the streak camera. The two optical path lengths in the Michelson introduce a known time delay which provides a temporal calibration for the camera. The attenuation through one arm is kept high to provide a low intensity calibration, whilst the other attenuation is progressively decreased enabling the measurement of Tr'/Tr as a function of intensity to be made on a multi-shot basis.

A lossy Fabry-Perot may be either the equally reflecting type employing a pair of 70% reflecting mirrors (47, 106) (Figure 5.2(c)), or the differing mirror type(Figure 5.4 (b))employing a 50% reflecting mirror, and a 100% reflecting mirror. A picosecond pulse entering such a system, oscillates between the mirrors, and at each incidence with a transmitting mirror a low intensity replica of the pulse is transmitted, reducing the amplitude of the intra-cavity pulse. A train of sub-pulses is thus produced, each sub-pulse being half as intense as its predecessor, but having an identical shape and duration. The sub-pulse separation is twice the intra-cavity round-trip time and can be used to provide a temporal calibration for the streak camera. This technique has the advantage that it is only necessary to record one set of such streaks to make a complete measurement of the dynamic range.

5.5 Photochron 1 Streak Camera with S1 Photocathode

The Photochron 1 streak camera is in many respects similar to the

Photochron 2 system described in detail in Chapter 2. The main difference is an alteration in the cathode-mesh-cone spacing, with consequential changes in both operating voltages, and performance (19). These differences are summarised in Table 5.1. For the purposes of this work a streak-writing speed of 10^{10} cm s^{-1} was used wherever possible, giving the camera a time resolution of $\sim$ 2.5 psec (45).

A modelocked Nd: phosphate glass laser (42) was used as a source of test pulses from which the dynamic range of the streak camera was determined. A diagram of the laser is shown in Figure 5.3. The 167 mm Brewster-angled Nd: phosphate glass rod (3.3% doped Hoya LHG-5) was mounted inside a quartz jacket, through which cooling water was passed. The rod was optically pumped by a close-coupled air-cooled helical flashlamp in the arrangement described by Caughey (43). The electrical energy discharged through the flashlamp for multimode operation was $\sim$ 230 J, and the modelocked laser produced a train of $\sim$ 10 ps pulses with an energy of 1 mJ per pulse. For reliable operation, without multipulsing it was important to stabalize the flashlamp energy to better than $\sim$ 0.2%. The optical cavity consisted of a plane wedged 70% reflectivity output mirror, and a 2m radius-of-curvature concave 100% reflectivity mirror, separated by $\sim$ 1m. The curved mirror compensates for the thermal lensing of the glass laser rod (5,49), and enables a much longer pulse train to be produced. The mode-locking dye (an 2 x 10^{-5} M solution of Eastman Kodak 9860 in 1, 2 - dichloroethane) was contained in a 100 μm dye cell, and was in optical contact with the 100% mirror. The entrance window of the dyecell was fabricated from red filter glass to prevent photodecomposition of the dye by stray UV flashlight. Due to the low value of dn/dT of the host glass (44) this laser could be operated at 1 minute intervals with $\sim$ 90% reproducibility.

Table 5.1

	Photochron 1	Photochron 2
Cathode - mesh spacing	3 mm	0.5 mm
Mesh - cone spacing	3 mm	30 mm
Cathode voltage	0 V	0 V
Mesh voltage	2 KV	1 KV
Come voltage	550 V	875 V
Photocathode extraction field	6 KV/cm	20 KV/cm
Electron-optical magnification	x 3.6	x 2
Phosphor spatial resolution		
Static	8 lp/mm	18 lp/mm
Streaked	5 lp/mm	10 lp/mm

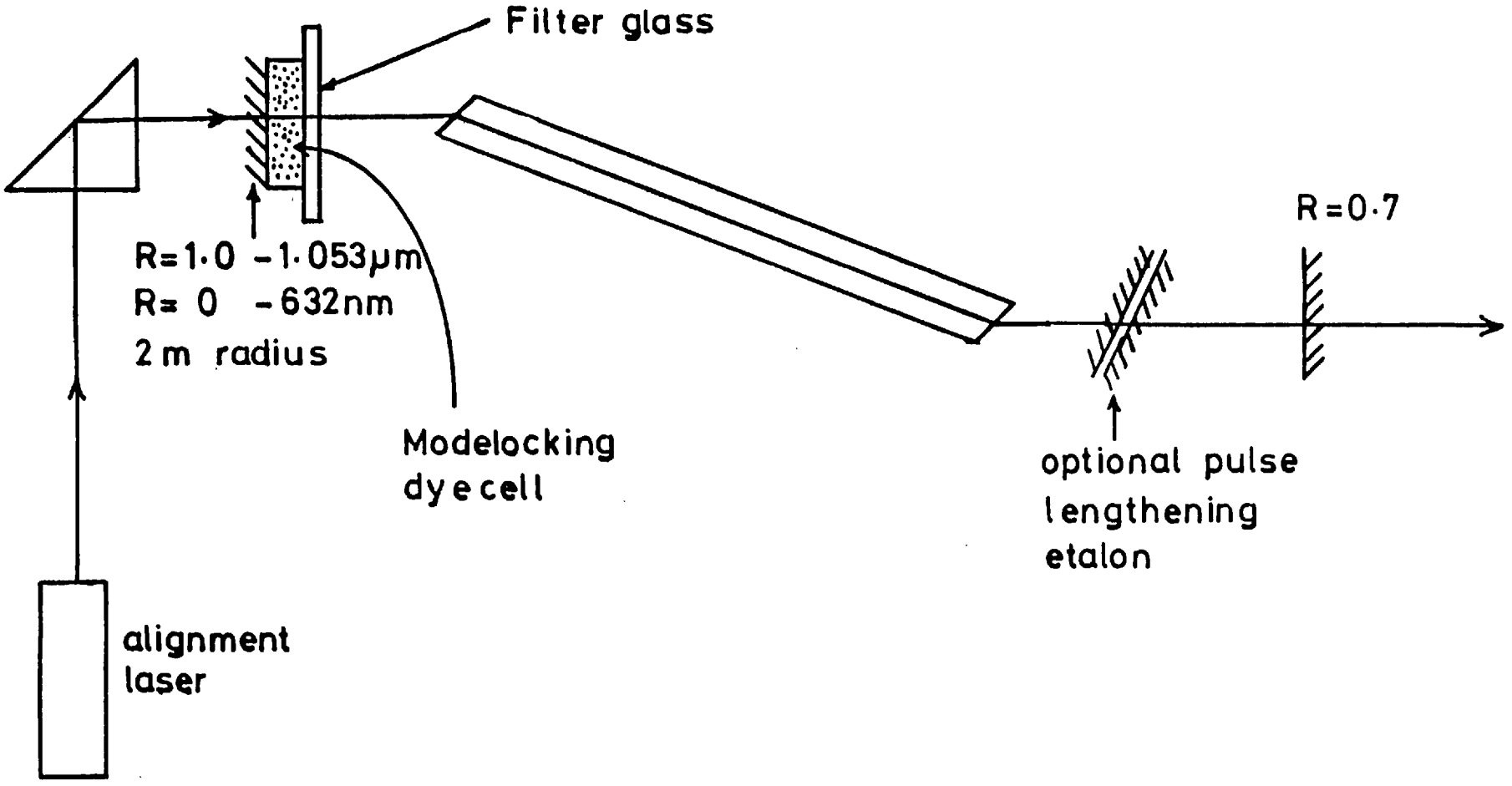

Fig. 5·3 Nd phosphate glass laser

A Pockels cell switch (c.f. Chapter 2.2) was used to select about five pulses from the middle of the pulse train. These pulses were injected into an air-gap Fabry-Perot etalon consisting of a 50% and 100% mirror (Figure 5.4). A train of test pulses of the type described earlier were thus produced. The sub-pulse separation time (the double transit time of the etalon) was set to be compatable with both the recorded pulse duration, and the required streak speed. Initially the mirrors were set 5.3 mm apart, corresponding to a round-trip time of 35 psec. To avoid the effect of structure in the beam changing position on the slit, with consequential difficulties in interpreting and analysing the results, the Fabry-Perot had to be aligned very accurately. This was readily accomplished by looking for the interference fringes of the He-Ne alignment laser on the slit of the streak camera. By altering the attenuation of the light entering the slit, the peak intensity level was set at $\sim$ 5 times the maximum linear response of the camera.

A typical streak photograph, and corresponding calibrated microdensitometer trace is shown in Figure 5.5. This was recorded on Ilford HP5 film (developed in Ilford Microphen for 25 minutes to an ASA rating of $\sim$ 3000), with an image intensifier gaim of $\sim 10^6$. From a series of 20 - 25 such results a graph of Tr'/Tr against pulse intensity (referred to film fog level) is plotted (Figure 5.6). The actual pulse duration Tr is determined by taking the mean duration of the lowest intensity pulses in a series (i.e. the pulses with a recorded intensity of less than 10 times the film fog level). Clearly from Figure 5.6 this camera has a dynamic range of 55:1 for 10 psec pulses, and 180:1 for 35 psec pulses. These longer pulses were produced by introducing into the laser cavity, a bandwidth limiting Fabry-Perot

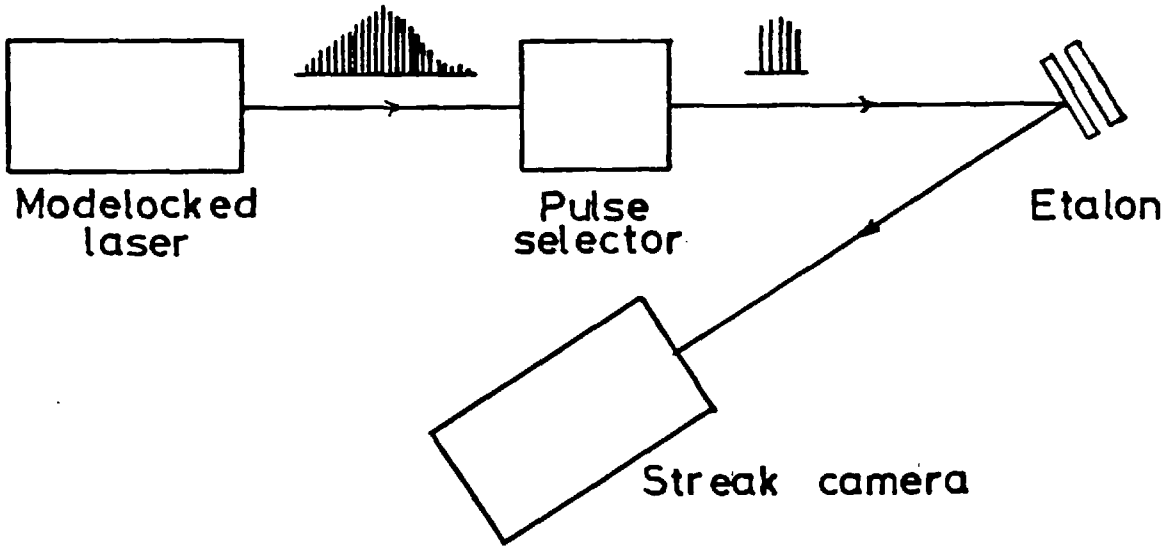

(a) Experimental arrangement

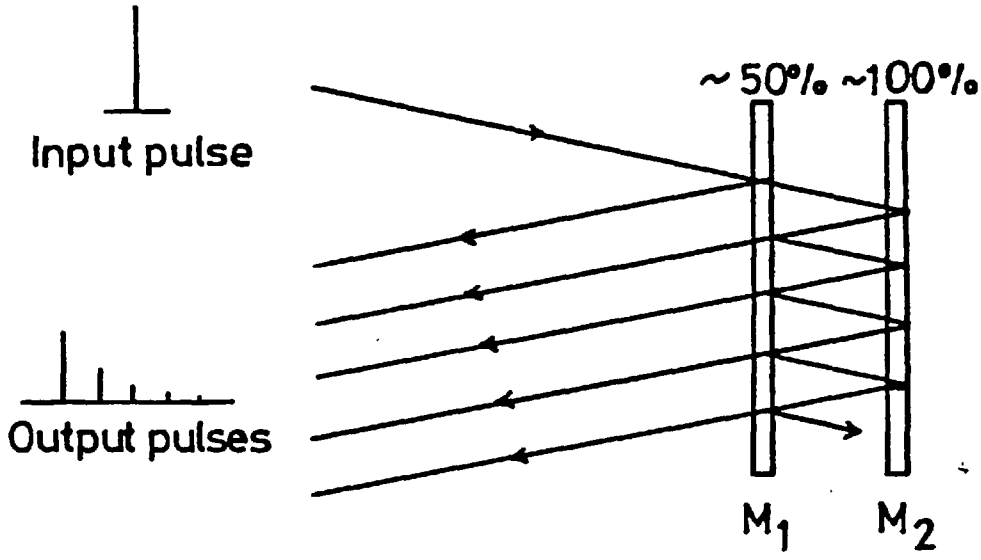

(b) Etalon

Fig. 5.4

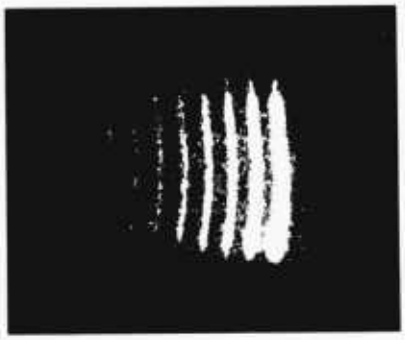

Fig. 5.10

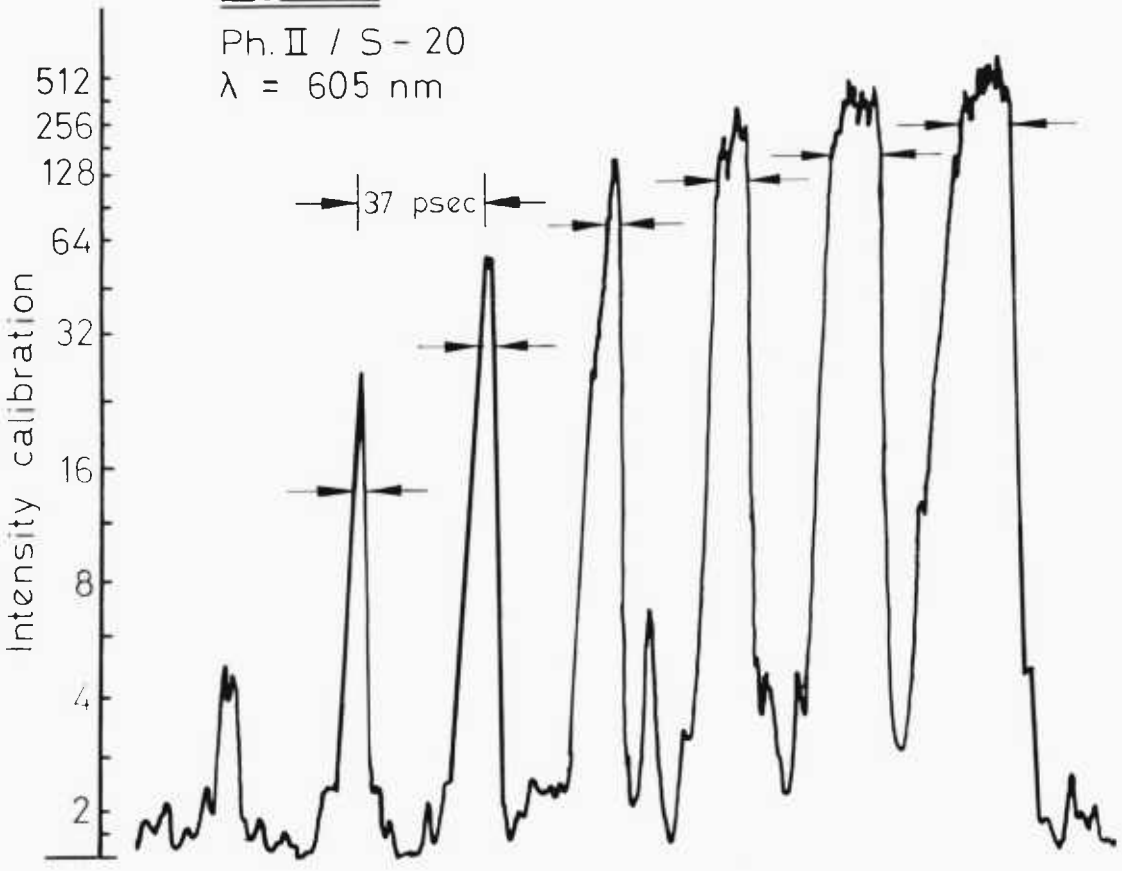
Ph. II / S - 20
λ = 605 nm
37 psec
Intensity calibration
512
256
128
64
32
16
8
4
2

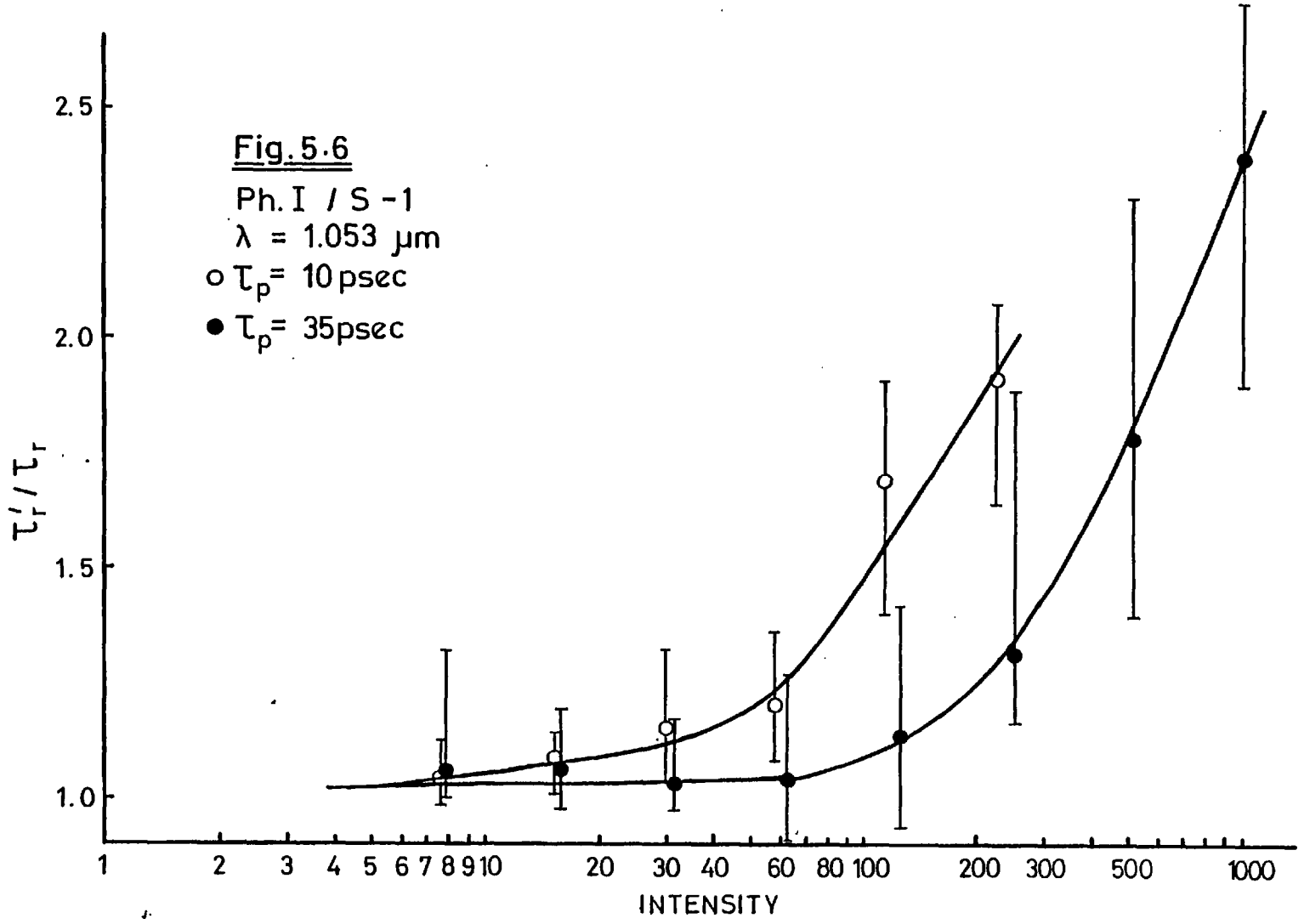
Fig. 5.6
Ph. I / S -1
λ = 1.053 μm
o τ_p= 10 psec
● τ_p= 35psec
τ_r'/τ_r
2.5
2.0
1.5
1.0
1 2 3 4 5 6 7 8 9 10 20 30 40 60 80 100 200 300 500 1000
INTENSITY

which was comprised of two 70% reflecting mirrors separated by $\sim$ 60 μm. In order to record these longer pulses it was necessary to increase the separation of the sub-pulses to 100 psec, and reduce the writing speed of the camera to 4×10^9 cm s^{-1}, in order to display the entire sequence of pulses on the phosphor of the streak tube. For this second set of results the camera had a time resolution of $\sim$ 5 psec.

These results are of particular significance since a great many similar cameras are used at this wavelength, to measure the pulses of duration 10 - 100 psec normally involved in laser plasma studies (117). Freidman et al (47) report a dynamic range of $\sim$ 5 and $\sim$ 20 for 10 psec and 30 psec pulses at 1.06 μm respectively. These results are at a considerable variance with those reported here.

As an independent check of these measurements the dynamic range was also measured using the Michelson method (c.f. Section 5.4). From a graph of Tr'/Tr against pulse intensity (Figure 5.7) a dynamic range of $\sim$ 44 was measured for 10 psec pulses. There is an agreement within an error of $\sim$ 20% between this result and the one obtained by the etalon method. This then demonstrates the validity of the use of an etalon to measure dynamic range of a streak camera.

The dynamic range of this S1 camera was also measured at 526 nm, by generating the second harmonic of the Nd: phosphate glass laser. The second harmonic was produced in a 15 mm long, 10 mm aperture ADP crystal placed after the pulse selector. The fundamental was removed by passing the output through a pair of Chance - Pilkington HA3 glass filters. A conversion efficiency of $\sim$ 10% was achieved giving an energy of $\sim$ 100 μJ per pulse. The increased electron energy spread at this

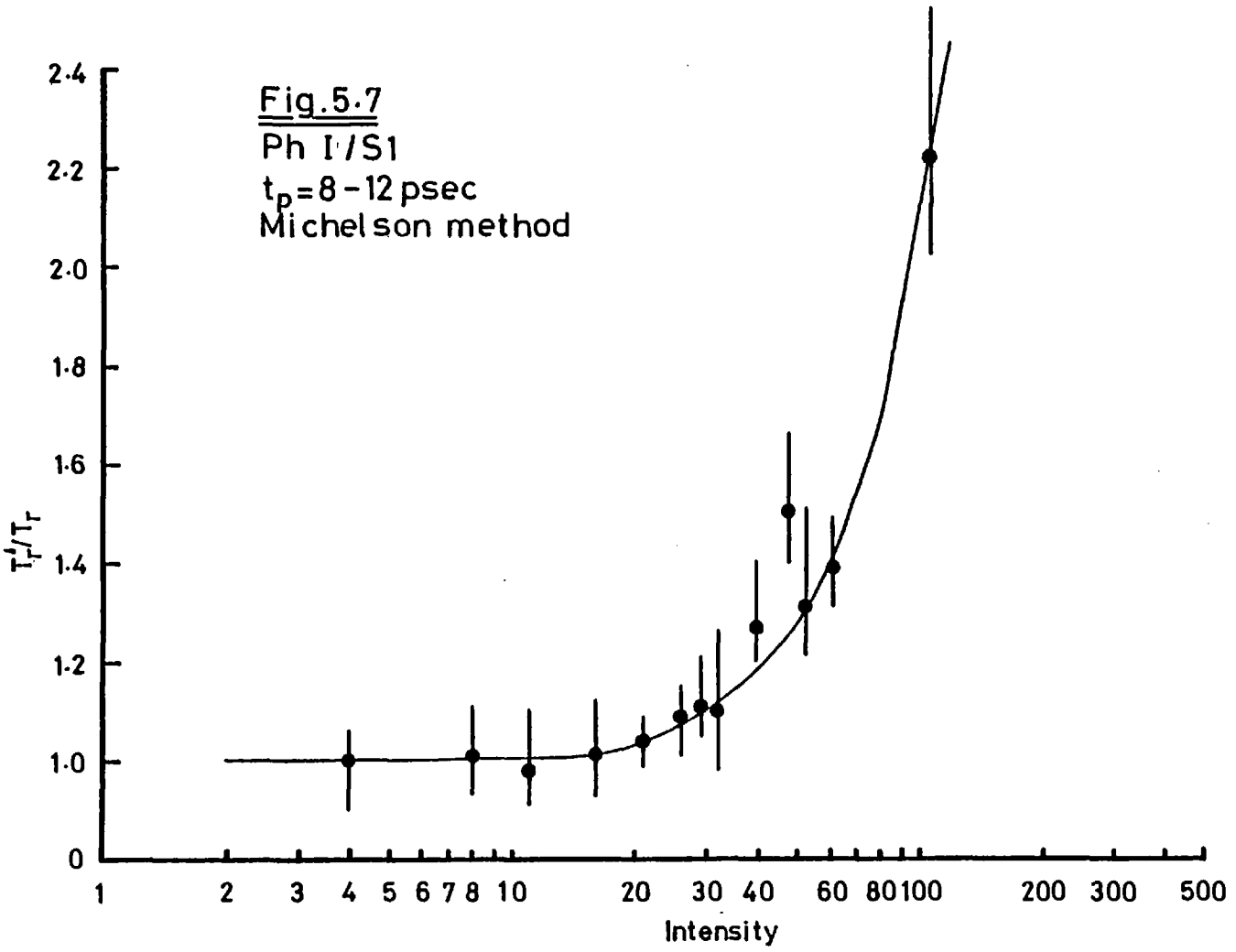
Fig.5.7
Ph I/S1
t_p=8-12 psec
Michelson method
T_r'/T_r
2·4
2·2
2·0
1·8
1·6
1·4
1·2
1·0
0
1
2
3
4
5
6
7
8
10
20
30
40
60
80
100
200
300
500
Intensity

wavelength (31) reduced the time resolution of the camera to $\sim$ 4 psec. The mirrors in the dynamic range etalon used previously were changed ones with 50% and 100% reflectivity in the visible and a further series of streak records (e.g. Figure 5.8) were obtained. From these results it was possible to determine the second harmonic pulse duration ($\sim$ 7 psec) and the dynamic range ($\sim$ 60) of the streak camera at this wavelength (Figure 5.9).

5.6 Photochron 2 Streak Camera with S20 Photocathode

Dynamic range measurements were also made on the fibre-optically coupled Photochron 2 (Mk.3) streak camera described in Chapter 4. This streak camera was initially operated at a writing speed of 6×10^9 cm s^{-1} giving it a time resolution of better than 2.3 psec. The modelocked Rhodamine 6G dye laser and pulse selector described in Chapter 2 were used as a source of test pulses. Tuned to $\sim$ 605 nm, and modelocked with DODCI this laser consistently produced 5 psec pulses.These pulses were injected into the Fabry-Perot etalon described earlier, from which a series of streak photographs displaying Tr' as a function of pulse intensity were obtained (Figure 5.10). Under these conditions the dynamic range was found to be $\sim$ 55 (Figure 5.11). Pulses of duration $\sim$ 2 psec were generated by employing DQOCI as a modelocking dye and tuning the laser to 600 nm. The camera writing speed was increased to 10^{10} cm sec^{-1} providing an instrumental time resolution of $\sim$ 1.4 psec (46). From Figure 5.12 it can be seen that even for pulses as short as 2 psec the dynamic ranges is as high as 30.

In previous analysis of the dynamic range of ultrafast streak cameras(47) an accumulative effect on the recorded pulse intensities was reported. The authors of Reference 47 measured the recorded intensity of three identical 30 psec pulses separated by 120 psec. They reported that the

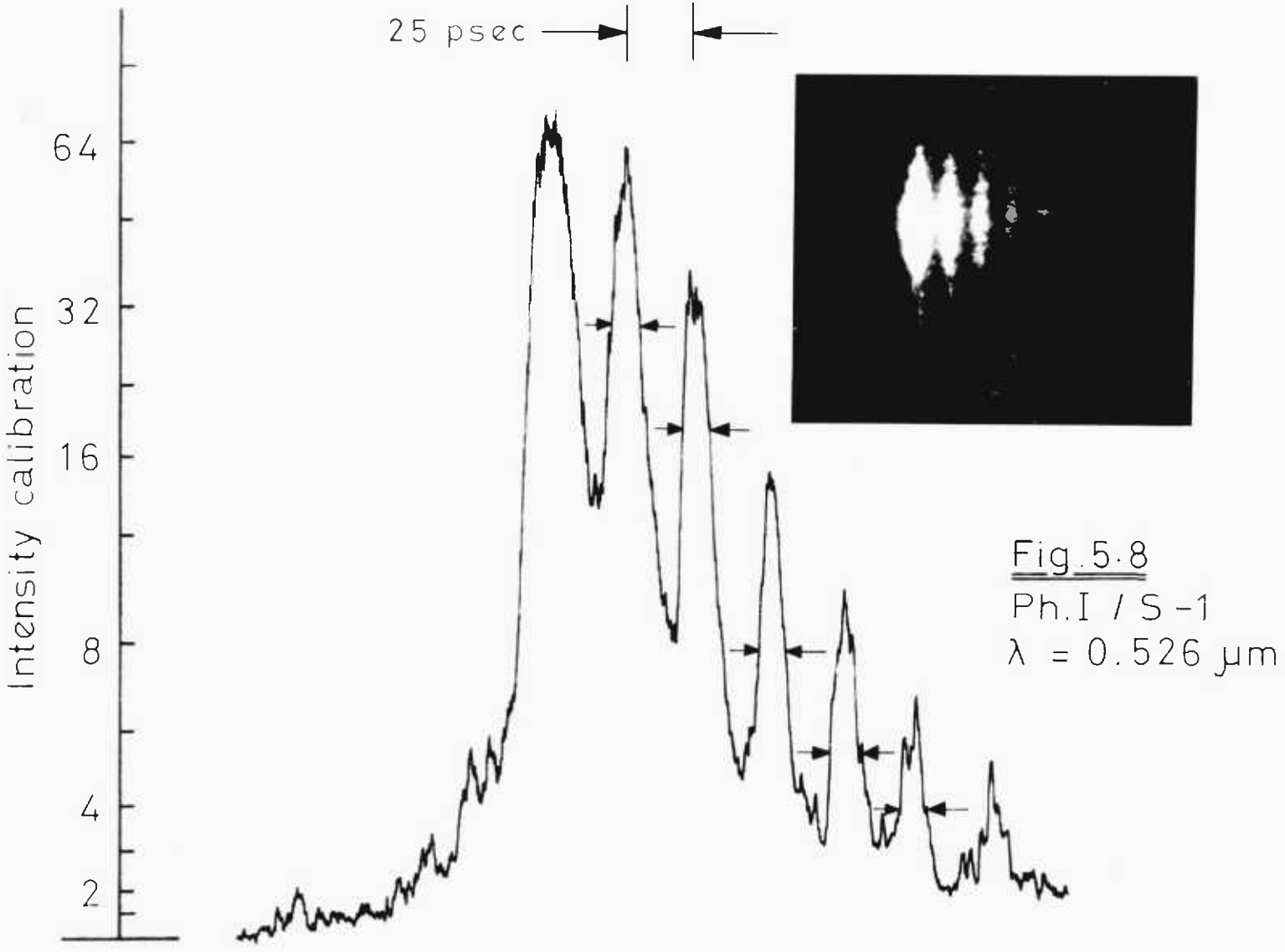

Fig. 5·8
Ph.I / S -1
λ = 0.526 μm

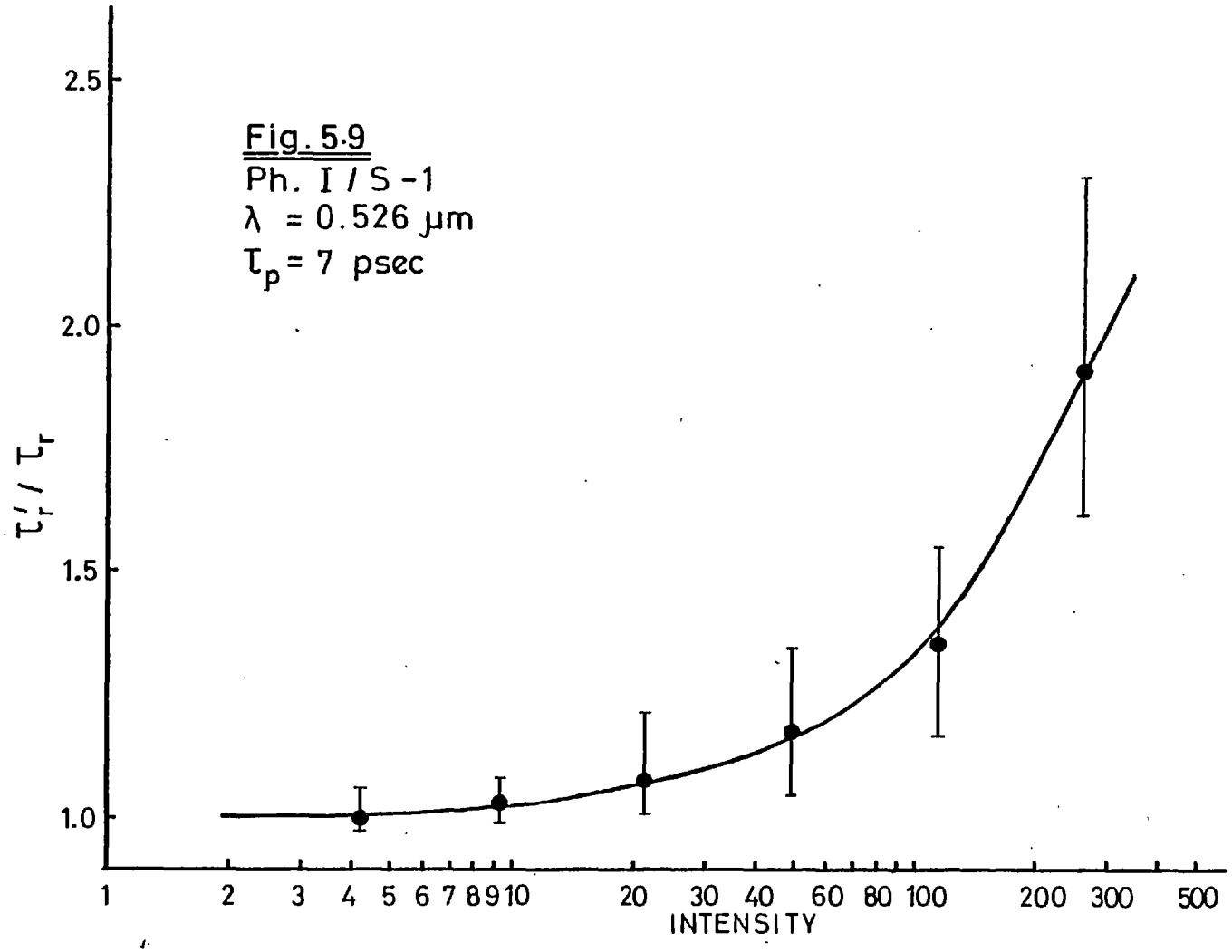
Fig. 5.9
Ph. I / S -1
λ = 0.526 μm
τp = 7 psec
τr' / τr
2.5
2.0
1.5
1.0
1 2 3 4 5 6 7 8 9 10 20 30 40 60 80 100 200 300 500
INTENSITY

Fig. 5.10

Ph. II / S - 20

λ = 605 nm

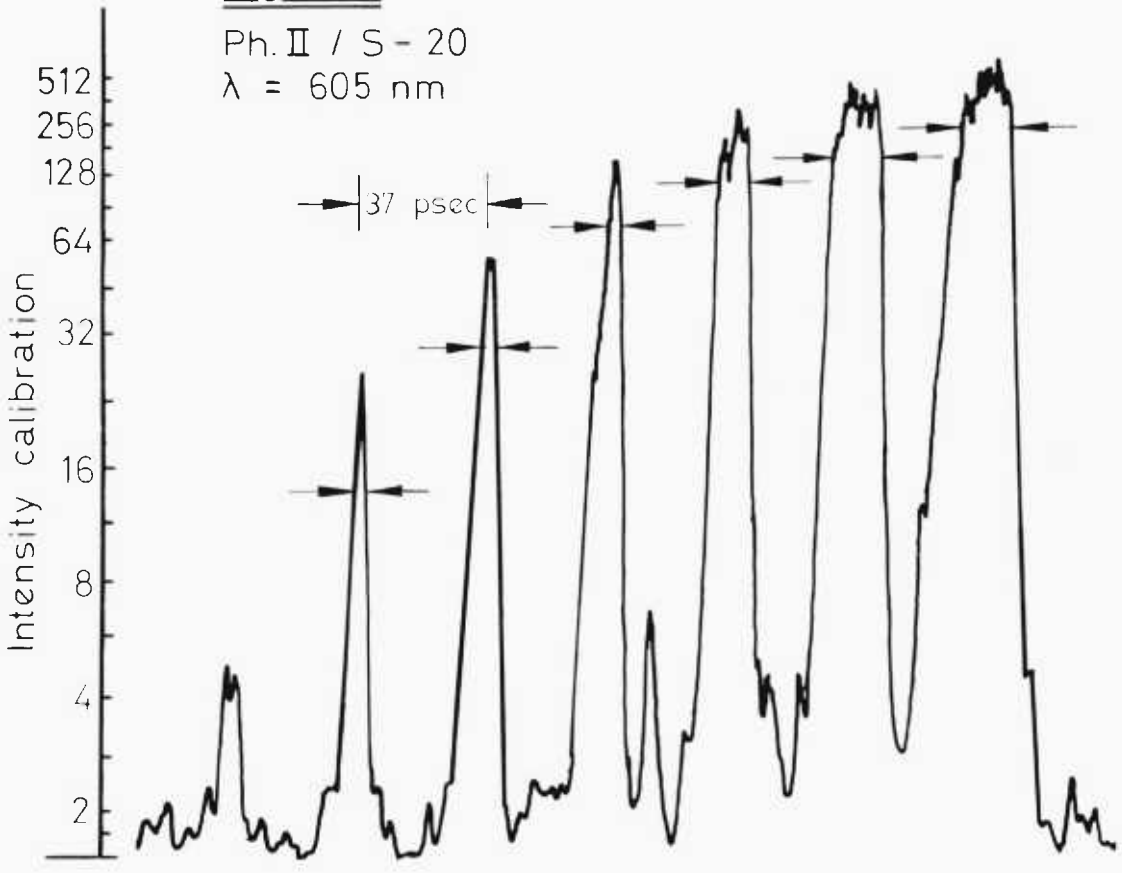

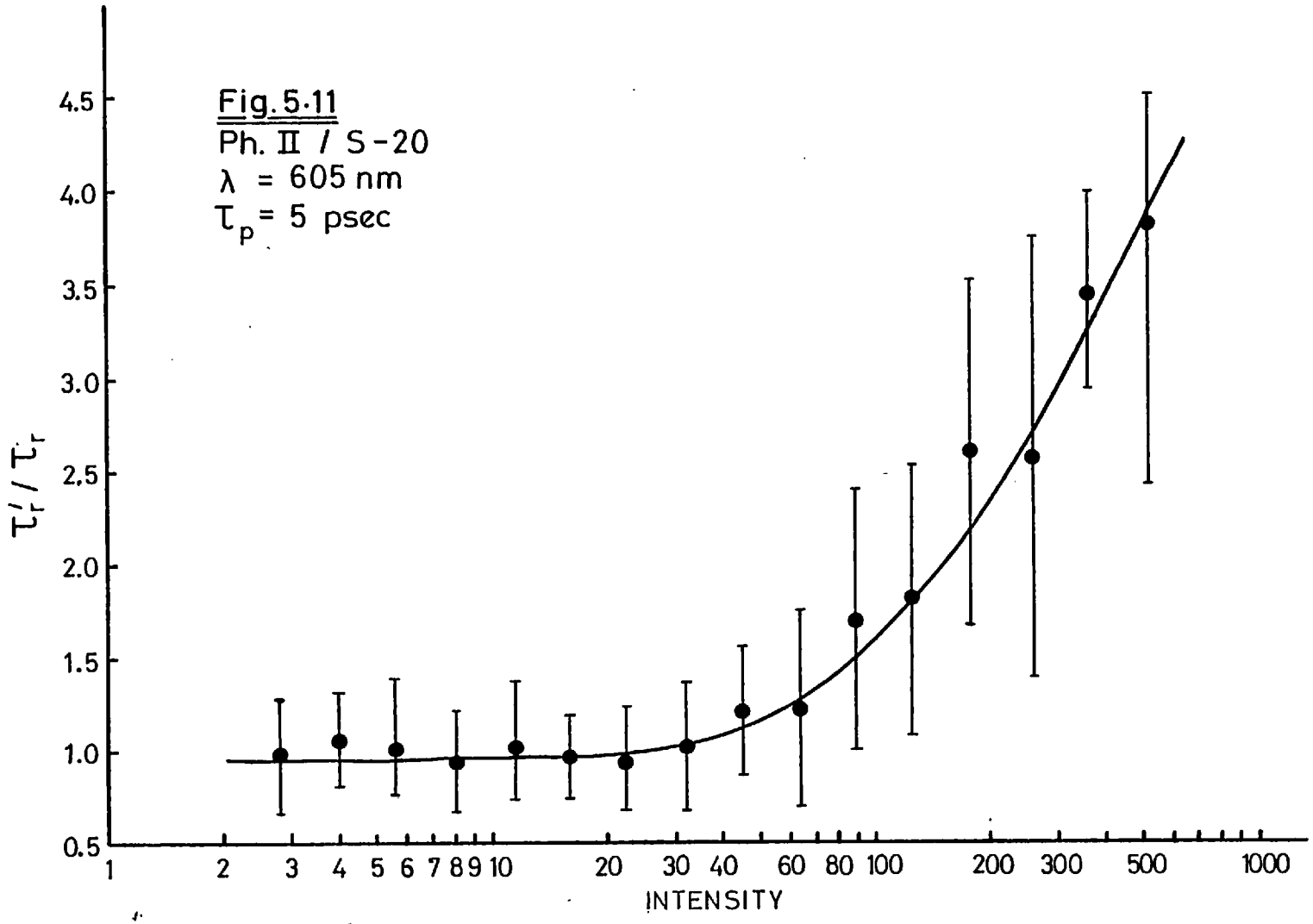
Fig. 5·11
Ph. II / S-20
λ = 605 nm
τ_p = 5 psec
τ_r' / τ_r
4.5
4.0
3.5
3.0
2.5
2.0
1.5
1.0
0.5
1
2
3
4
5
6
7
8
9
10
20
30
40
60
80
100
200
300
500
1000
INTENSITY

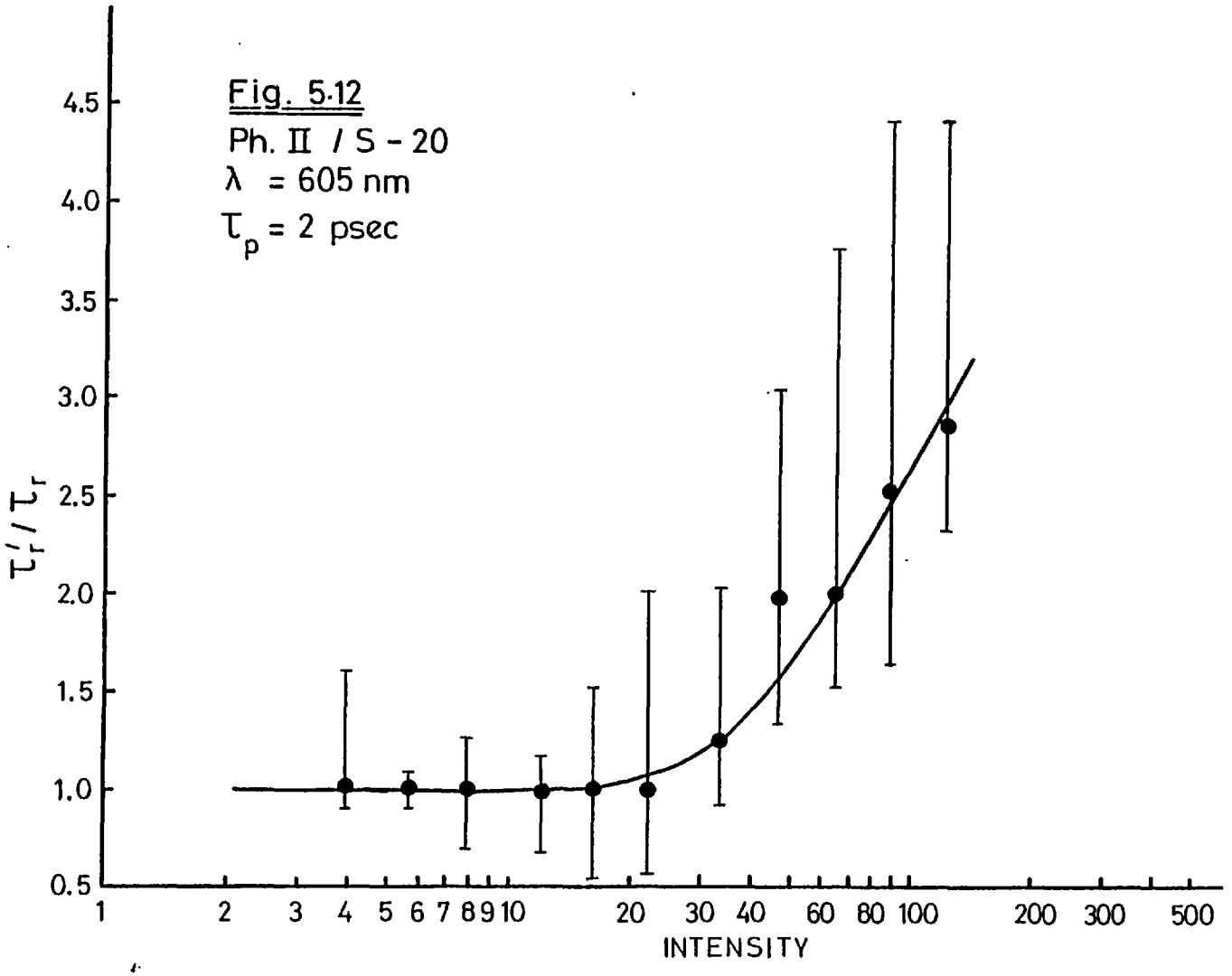
Fig. 5.12
Ph. II / S - 20
λ = 605 nm
τ_p = 2 psec
τ_r' / τ_r
4.5
4.0
3.5
3.0
2.5
2.0
1.5
1.0
0.5
1 2 3 4 5 6 7 8 9 10 20 30 40 60 80 100 200 300 500
INTENSITY

recorded intensity of a pulse appeared to be influenced and reduced by any preceding pulse/s. They further reported the worsening of the effect with increased pulse intensity. A similar experiment was tried by reflecting the 2 psec pulses from the dye laser off the front and back surfaces of a pair of glass flats 0.8 mm thick, separated by 1.2 mm. The resulting quartet of equal intensity 2 psec pulses separated by 8 psec were streaked with a writing speed of 10^{10} cm s^{-1}. A typical streak record, and corresponding microdensitometer trace are shown in Figure 5.13. It is evident that the camera faithfully reproduces the pulse profiles, and confirms that no accumulative photocathode saturation occurs on this timescale.

5.7 The Causes of the Photocurrent Limit

A number of mechanisms have been suggested to account for the photoelectron current limit, for example :

(a) The resistivity of the photocathode gives rise to a local potential gradient at the point of photoelectron emission, causing an electron optical defocusing of the image.

(b) A high electron density occurs in the electron beam cross-over region of the streak tube, and that this is sufficient for Coulomb repulsion of the electrons to defocus the image.

(c) In or near the photocathode, space-charge effects introduce defocussing or in someway effect the electron velocities.

Fig. 5.13

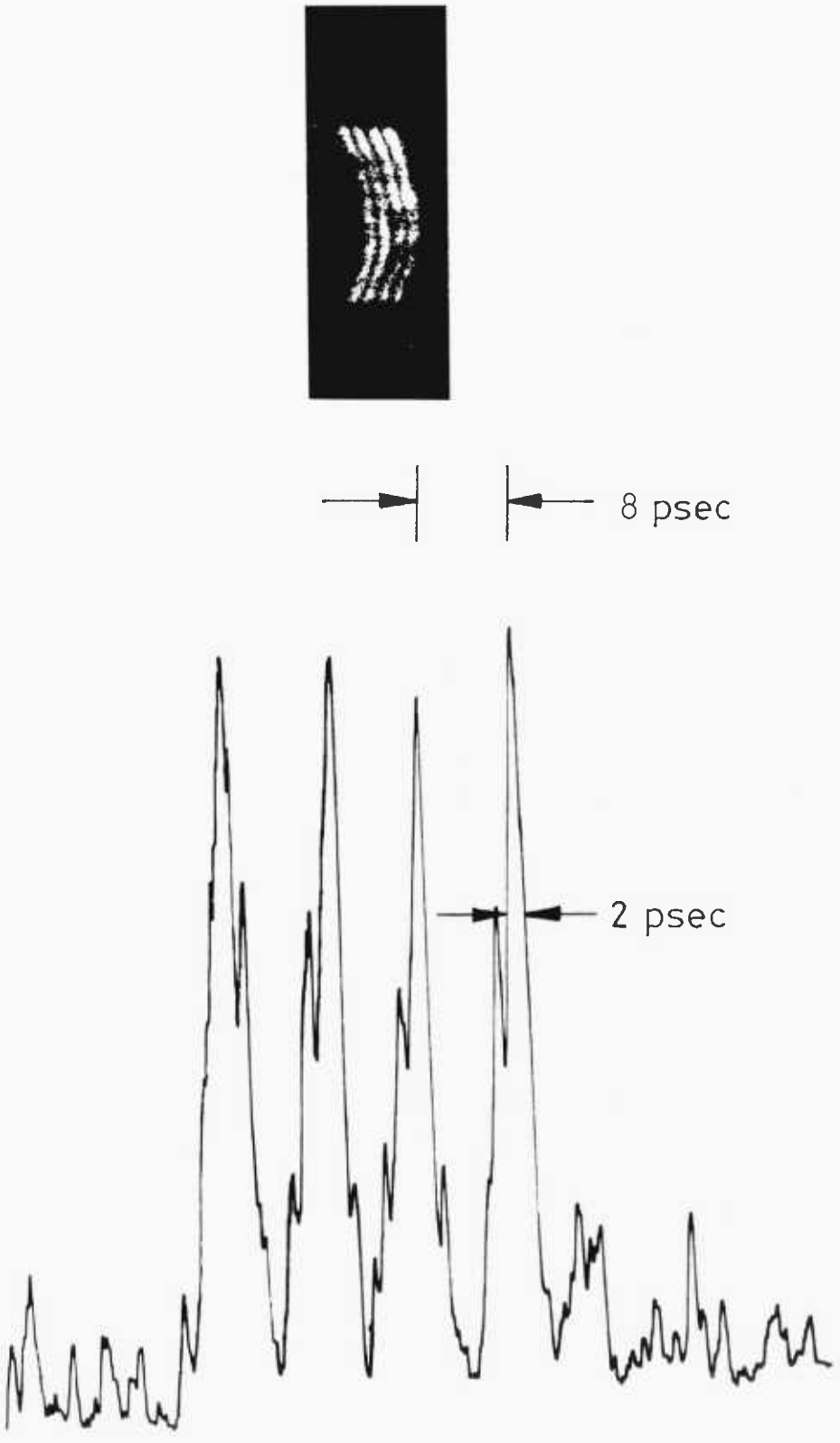

(d) An emission lifetime exists for the photocathode, and that this is dependent on the intensity of the incident illumination (53).

The correct mechanism must of course be entirely consistent with the experimentally observed effects. It is thus necessary to explain the sudden onset of the saturation effect, the dependence of the limiting current on cathode resistivity (54) and sensitivity (51), the apparent loss of resolution in the temporal direction only, and the symmetry of the distorted streak image about the position of a low intensity streak.

The insensitivity of the focussing of streak tube to changes of mesh voltage of up to 10V makes the cathode resistivity explanation (a) unlikely. It has been estimated (55) that for an S11 photocathode a photoelectron current of 2×10^4 e^-/resolution element/psec can be drawn for a change in cathode-mesh voltage of 4.5V. The silver coating upon which the S1 photocathode is made, and the chromium mesh upon which the S20 photocathodes in these streak tubes are made, should give these photocathodes a similar surface resistivity to the manganese oxide backed S11 photocathode. The connection between cathode surface resistivity and streak tube dynamic range is thus likely to be more subtle that a simple defocussing effect.

The theory of Majumdar (d) that the photoelectrons within the photocathode have an intensity dependent lifetime predicts that the dynamic range of a streak camera is proportional to the square of the time resolution. Although there is some support for this theory (57, 58), the work presented here and the work of Freidman etal (47) indicate a linear proportionality, implying some current density limiting phenomena as being the cause.

The work of Jones (56) indicates that the cross-section of the cross-over region of the streak tube has an area of $\sim 10^{-9}$ m^2. At this point the electrons have an energy of 18 KeV (a velocity of $\sim 0.25c$). They thus occupy a volume of $\sim 0.75 \times 10^{-13}$ m^{-3} psec^{-1}. The area of the photocathode illuminated by the slit is $\sim 10^{-7}$ m^2. Since the electrons emerge from the photocathode with an energy of $\sim$ 0.5eV corresponding to a velocity of $\sim 1.4 \times 10^{-3}$ c, they occupy a volume of $\sim 0.8 \times 10^{-13}$ m^{-3} psec^{-1}. Thus in the two most critical regions of the tube the electrons occupy a similar volume. Since however the electrons at the crossover are considerably more energetic, space-charge effects are more likely to be significant in or close to the photocathode.

The characteristics of the dynamic range limit appear almost contradictory. The symmetry of the streak images could suggest a defocussing effect, but it is known that at least perpendicular to the streak direction the spatial resolution is apparently unaffected.

5.8 Saturation of the Channel Plate Intensifier

Apart from the photoelectron current limit, the dynamic range of the Mk.3 streak camera is limited by the saturation current of the channel plate image intensifier. This saturation effect (112) arises because a short duration electron pulse will strip electrons from the walls of the channels faster than they can be replaced by the charging current. This accumulation of charge on the walls of the channels reduces the electric field within the channels thereby reducing their gain.

The maximum charge (Q max) that a single channel can supply is given by,

$$Q_{max} = \pi \varepsilon r^2 E$$

where r is the radius of a channel, and E is the electric field along it (112). Applying the parameters of the Mullard channel plate image intensifier type XX1332 to this equation (channel diameter 12 μm, channel length 0.8 mm, voltage applied to the channel for a tube gain of 10^5 = 1200V) the maximum charge per channel is $\sim 10^5$ electrons. Each of these electrons produce $\sim$ 200 photons at the phosphor (assuming 3.5 KeV electrons strike the P20 phosphor, and that this phosphor is 14% efficient (113)). Taking a 50% open area for the channel plate the saturation limit of the channel plate image intensifier is $\sim 10^{13}$ photons cm^{-2}. Taking the film sensitivity figures quoted by Liddy (24), and further assuming that HP5 (developed for 25 minutes in Microphen) and Polaroid type 47 film have similar sensitivities, saturation should occur at $\sim 10^4$ times film fog level.

In order to experimentally demonstrate this effect pulses from the dynamic range etalon (Section 5.4) were streaked with a slow writing speed ($\sim 10^9$ cm s^{-1}) at different channel plate intensifier gains. When the gain of the intensifier was only 10^3 the liniarity of the system can clearly be seen from the variation in the peak intensity of the subpulses (Figure 5.14 (a)). The gain of the image intensifier was increased to $\sim 10^5$. Since this would saturate the recording film, a thin gelatin neutral density filter (ND 2.0) was sandwiched between the fibre optic output faceplate of the image intensifier and the recording film. This filter should have offset the increase in gain in the image intensifier. A mirodensitometer trace of the subpulses on an expanded intensity scale (Figure 5.14 (b)) shows little variation in recorded intensity, indicating saturation. This saturation occurs at $\sim$ 4 times the film fog level. Taking the attenuation of the neutral density filter into consideration saturation occurs at an intensity corresponding to $\sim$ 400 times the film fog level. Whilst this figure is not in direct agreement with the predicted figure, there are considerable experimental errors to be

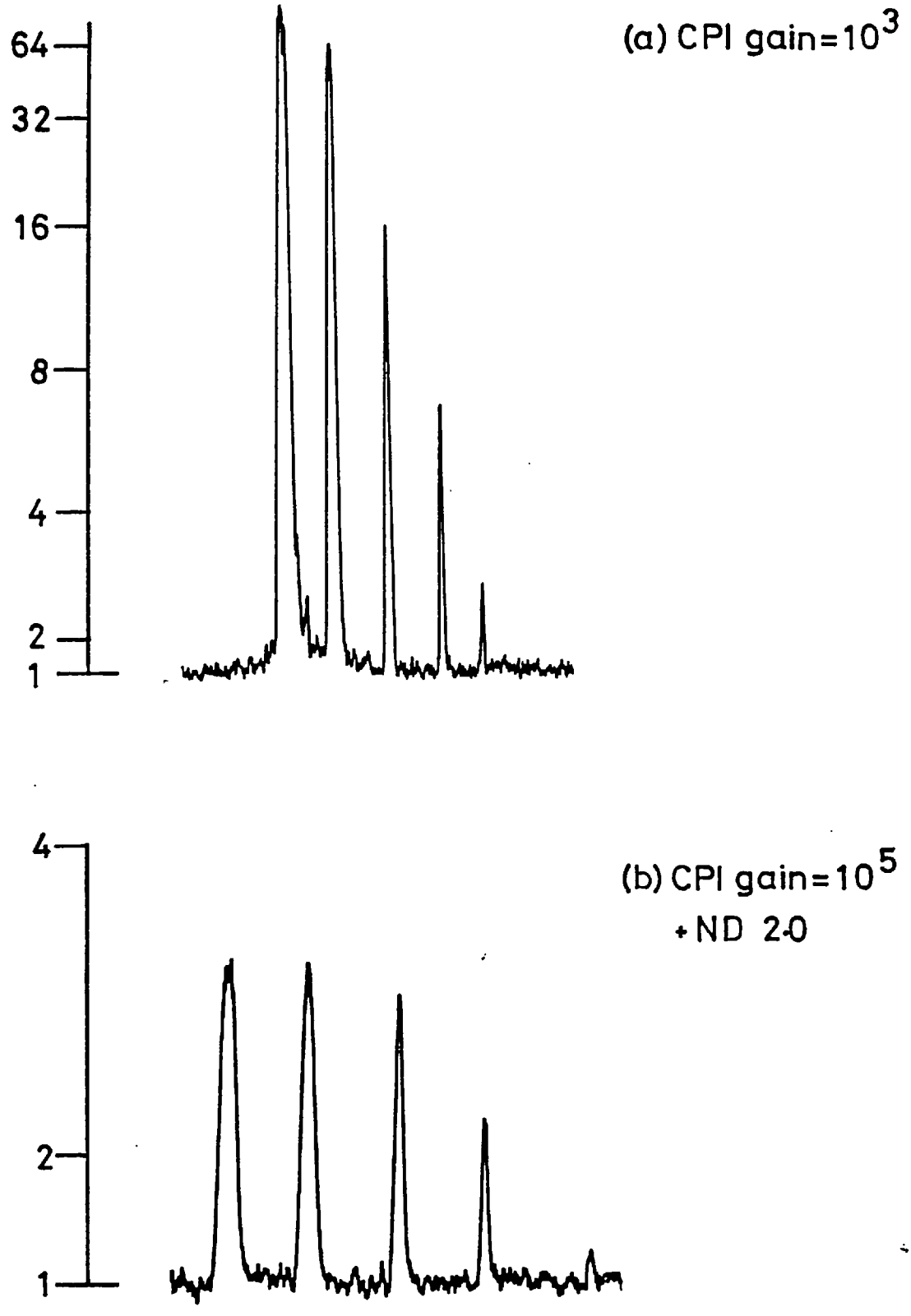

Fig.5.14 CPI Saturation

taken into consideration, the primary error being the estimate in the sensitivity of the recording film. Experiments conducted by Lotty (113) indicate liniarity of the channel plate up to ∿ 0.3 Q max. This indicates a maximum dynamic range of 120 for the Mk.3 camera at maximum gain.

5.9 Conclusion

A summary of the dynamic range results is shown in Table 5.2. These measurements indicate a dynamic range for the Photochron type of streak camera ∿ 10 times greater than previously reported (47). The dynamic range of a shortened Photochron 1 tube has been measured by the authors of Reference 52, who report a dynamic range of 220 for 50 psec pulses. This result is consistent with the results presented here.

At high resolution the dynamic range of the Mk.3 streak camera is limited by the photoelectron current limit while at low temporal resolution the dynamic range of the channel plate intensifier imposes a limit on the performance of the system.

Table 5.2

Parameters	Photochron 1 (S1) Camera			Photochron 2 (S20) Camera	
Test Laser Pulse Duration	35 psec	10 psec	7 psec	5 psec	2 psec
Wavelength	1.05 μm	1.05 μm	0.53 μm	0.6 μm	0.6μm
Photocathode Sensitivity	0.3 mA/W	0.3 mA/W	1.2 mA/W	24 mA/W	24 mA/W
Dynamic Range Measured	180	55	60	55	30

CHAPTER 6

APPLICATION OF A PICOSECOND STREAK CAMERA

6.1 The chosen applications

The Mk 3 streak camera has been applied to investigations in the picosecond domain where good time resolution, good dynamic range and high sensitivity are required.

Direct measurements have been made on the pulse duration of an actively modelocked flashlamp pumped Rhodamine 6G dye laser. It has been shown that in the middle and later stages of the output train single pulses of duration 2 - 6 psec can be reliably produced. It was found that measured pulsewidths were not critically dependent on the matching of the master and slave oscillator cavity lengths. Pulses at the beginning of the modelocked train were found to exhibit a complicated structure and are unsuitable for use as either excitation or probe pulse in most experiments.

The characteristics of the recombination radiation at high exciton densities in a Cd Se monocrystal at 77K have been investigated. By exciting the crystal with a picosecond dye laser pulse and monitoring both the pulse and the resultant luminescence, the delay, risetime and decay time of this recombination radiation were measured, and found to be 34 ± 6 psec, 9 ± 2 psec and 16 ± 3 psec respectively.

The capabilities of the Mk 3 ultra-fast streak camera as a picosecond diagnostic instrument have thus been demon strated by the results obtained during these studies.

6.2 An actively modelocked flashlamp pumped dye laser

6.2.1 Introduction

For many applications in monlinear optics and spectroscopy a source of independantly tunable synchronized picosecond pulses is highly desireable. These applications include the study of four wave mixing processes, such as the generation of tunable picosecond pulses in the U.V (60), excite-and-probe experiments, (68, 69), and measurements of coherence dephasing times (95).

The technique normally used to generate such pulses is the active modelocking of a dye laser by gain modulation (70, 71, 72). Here a modelocked laser such as an argon-ion laser, or a frequency doubled Nd: glass laser is used to pump a dye contained within an optical cavity. The optical path length of the dye laser cavity is adjusted to be either identical to that of the pump laser or an integer multiple of it. The matching of these cavity lengths has been found to be extremely critical (61, 63). By splitting the output of the pump laser it is possible to drive several such dye lasers, and hence synchronously generate pulses at a number of different wavelengths.

An alternative method reported by Lill et al (59) is to lock two flashlamp pumped dye lasers, by using the modelocked output of one laser to loss modulate the saturable absorber of the second laser. If the second laser has a longer cavity that the first a novel single shot excite and probe technique becomes possible, in which the first laser excites a

sample and the second probes it at successively later times (62). This modelocking technique can also be used to extend the tuning range of existing modelocked lasers and to provide picosecond pulses in spectral regions where suitable saturable absorbers are not yet available (59).

Initial measurements by the authors of Ref. 59 using the two photon fluorescence technique showed the duration of the actively modelocked pulses to be 5 ± 3 psec. These measurements necessitated the overall integration of the pulses in the modelocked train, providing no information on either pulse development or individual pulse duration and structure. With the availability of the Mk 3 picosecond streak camera it has been possible to make direct measurement of individual pulses from various parts of the modelocked pulse train.

Measurements of pulse duration as a function of cavity length have also been possible, and contrary to the findings of Frigo et al (63), and Ryan (61) (albeit with their rather different systems), it was found that large cavity mismatches ($\sim$ 10%) could be tolerated without significant pulse degradation.

6.2.2 The experimental arrangement

The experimental arrangement was similar to that described by Lill et al (59), and is shown schematically in Fig 6.1. Two identical 150 mm dye-cell flashlamp pumped modelocked dye lasers of the type already described in section 2.1 were used as the master and slave oscillators. In each case the active medium was a 1.0×10^{-4} M aqueous solution of Rhodamine 6G (+ 5% Ammonyx LO) and the modelocking dye was a 1.4×10^{-4} M ethanolic solution of DODCI. Laser 1, the master oscillator, had a 600mm optical cavity, and was tuned to 604 nm where it was known to reliably produce short pulses, and where the onset of modelocking was rapid (15,73,74).

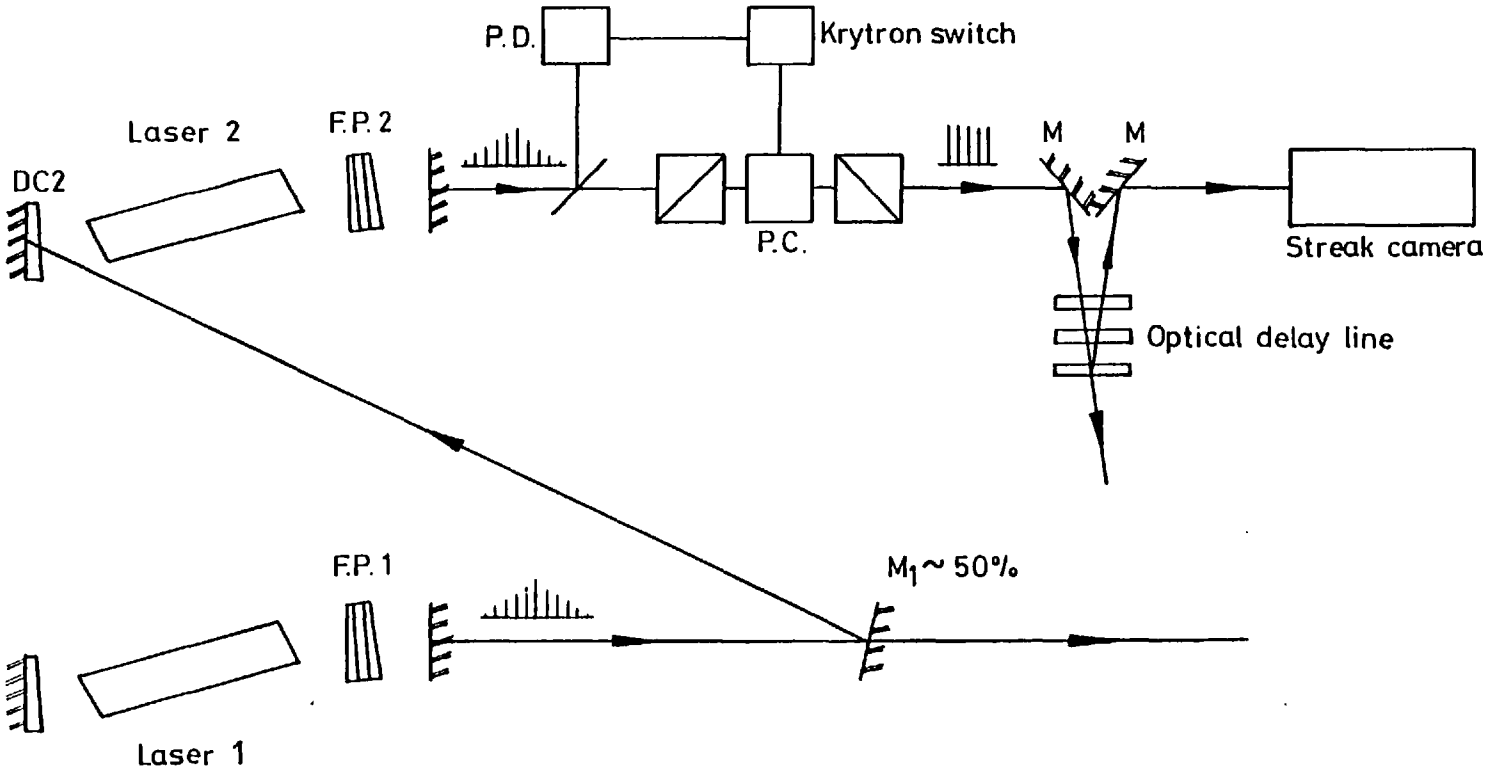

Fig.6.1 Actively modelocked dye laser

Part of the output of the master oscillator was directed onto the mode-locking dye cell of the slave oscillator (L2) by the 50% reflecting mirror M1. This second oscillator was pumped slightly below threshold, and so was incapable of oscillating on its own. The action of a piosecond pulse from the master oscillator on the saturable absorber of the slave oscillator, is to bleach it, reducing the cavity loss for a short period determined by aperture time (64). If the overall gain in the slave oscillator (L2) is sufficiently high, the actively modelocked pulse train rapidly builds up, and is synchronized with the driving pulse train.

A commercial delay unit was used to control the relative timing of the two flashlamp trigger pulses. The peak of the ~ 1 μs modelocked output from the master oscillator was set to coincide with the rising edge of the flashlamp profile of the slave oscillator (FWHM ~ 2.5 μs), ~ 500 ns before its peak.

Pulses were selected from various parts of the slave oscillator mode-locked train using the Pockels cell switch described in Section 2.2. These pulses were passed through a calibrated delay line (Section 3.5), and were then directed onto the slit of the Mk 3 ultrafast streak camera.

A writing speed of 10^{10} cm sec^{-1} was used giving a time resolution of ~ 1.5 psec.

The two cavity lengths were set by direct measurement with a metre rule, which for most purposes is sufficiently accurate. In the event that accurate synchronism of the two pulse trains is required they are both

simultaneously monitored on a fast photodiode, whereupon a beat pattern is observed superimposed on the pulse envelope. By reducing the number of beats in the pulse train envelope the cavity lengths can be matched.

6.2.3 The Pulse Evolution and Quality

As an initial check the pulses from the master oscillator were streaked. Typical pulses had a duration of 2 - 4 psec, and an energy of ~80 μJ. An example of a typical streak record of one of these pulses is shown in Figure 6.2. The slave oscillator was the laser used for the earlier work described in this thesis, and so was known to produce pulses similar in both energy and duration to those produced by the master oscillator.

The slave oscillator was tuned to 595 nm and the cavity length was set at 580 mm. When operated as a passively modelocked system the pulse formation time was ~100 ns at this wavelength. The length of the master oscillator cavity was varied in steps of ~66 psec (~ 22 mm) mismatch over the range 520 mm - 620 mm. Pulses were selected ~300 ns from the start of the ~800 ns long actively modelocked trains. Figure 6.3 shows a number of microdensitometer traces of typical pulses for master oscillator cavity lengths of (a) 620 mm, (b) 560 mm and (c) 520 mm. In each case short pulses evolved, and it was found that pulse quality was relatively independent of cavity length over this range of mismatch. Recorded pulse durations were in the range 2 - 7 psec.

The initial build-up phase of the actively modelocked pulse train was also examined. Pulses were selected ~ 80 ns from the start of the train, and streaked. In this case the slave laser had been tuned to 585 nm, where in passive operation the pulse evolution time was ~150 - 200 ns.

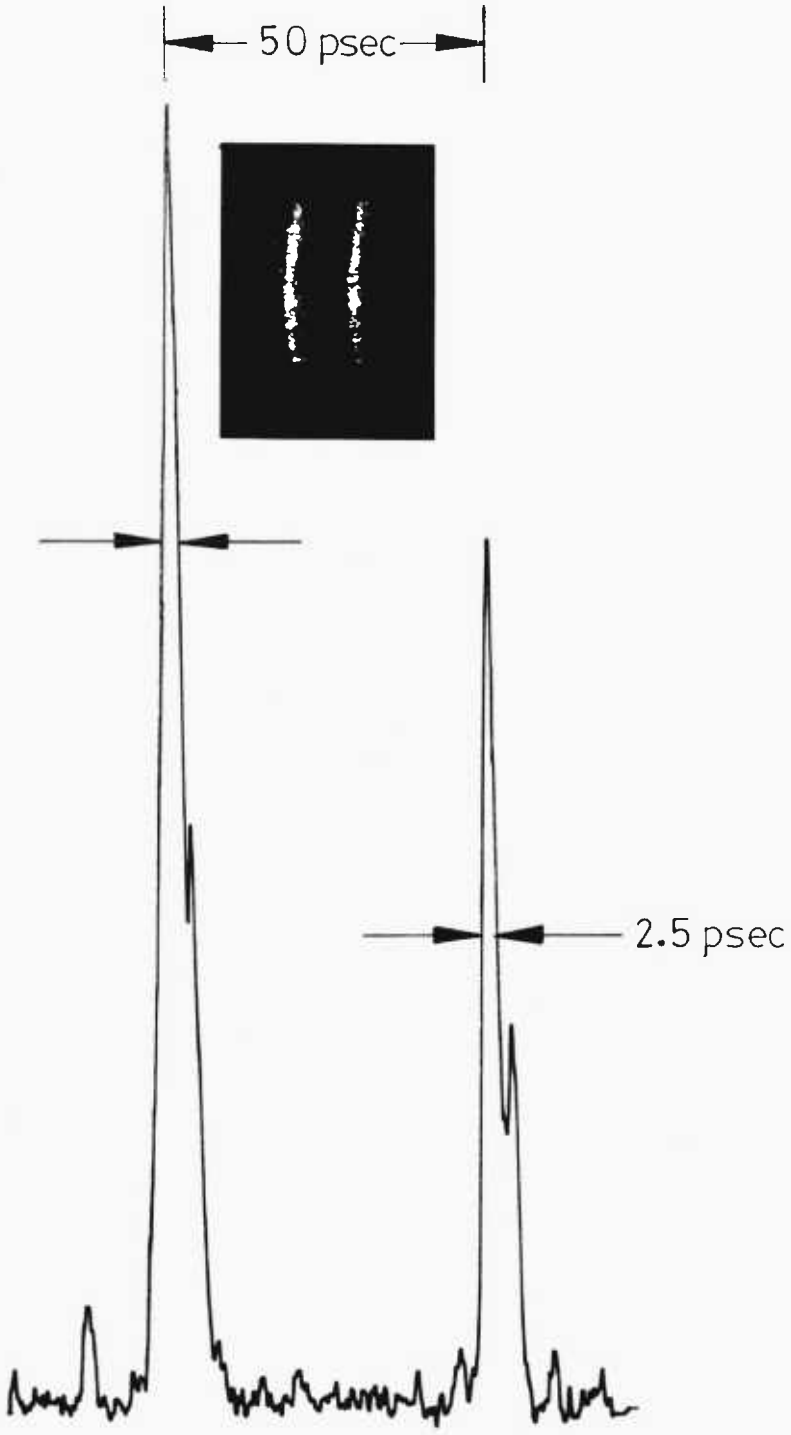

Fig. 6.2 Master oscillator pulses

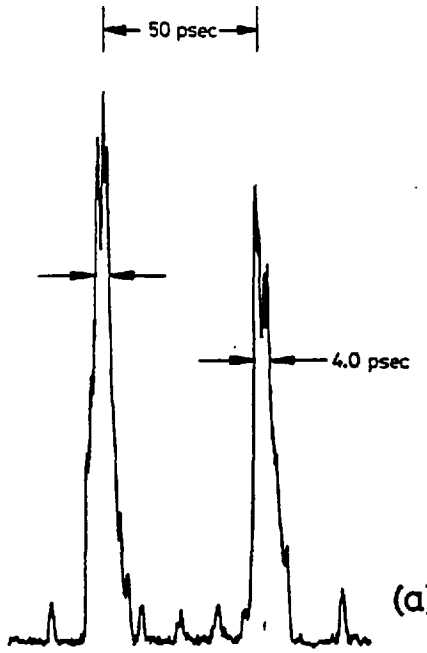

(a) Master CL = 620 mm

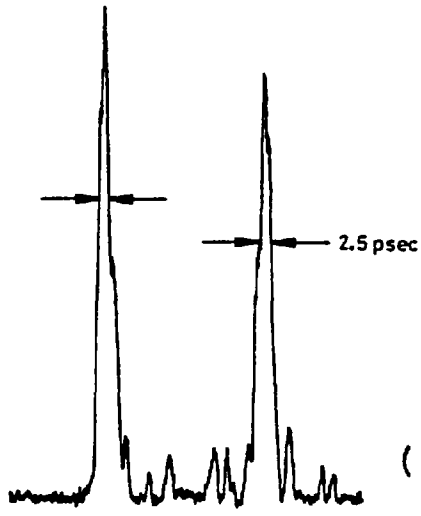

(b) Master CL = 560 mm

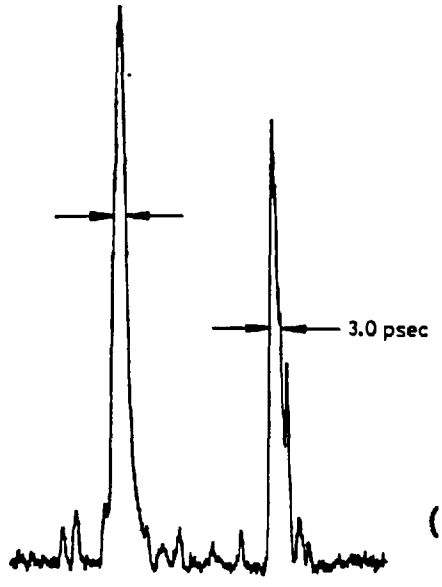

(c) Master CL = 520 mm

Fig.6.3 Actively modelocked pulses, 300ns from start of modelocked train.
Slave CL = 580 mm

With the length of the slave oscillator cavity maintained at 580 mm pulse durations were measured for master oscillator cavity lengths in the range 540 mm - 620 mm. Figure 6.4 shows microdensitometer traces of typical recorded pulses. In most cases a single pulse of duration 2.5 - 6 psec had started to form, but pulse evolution was however incomplete.

A large amount of intrapulse structure was present as can be seen from Figures 6.4 (a), 6.4 (c) and 6.4 (d), (corresponding to master oscillator cavity lengths of 620 mm, 580 mm and 560 mm respectively). Occasionally single pulses were recorded when the master oscillator cavity length was longer than that of the slave oscillator (e.g. Figure 6.4(b) recorded for a master oscillator cavity length of 600 mm), but this is probably due to small variations in the pump power, or jitter in the pulse selector caused by slight variations in the amplitude of the pulse train. Typically the pulses recorded for a 600 mm master oscillator cavity resemble Figure 6.4 (c). Single pulse evolution from this type of profile is very rapid (65, 66, 67). A typical pulse recorded for a master oscillator cavity length of 540 mm is shown in Figure 6.4 (e). In this case the pulses were much longer, and highly structured. Although these results indicate that the pulse quality is poor in the early stages of the actively modelocked pulsetrain, no indication of this would be given on an oscilloscope monitor, and the only indication on a T.P.F. pattern would be a reduction in the contrast ratio. It is obvious that this early portion of the modelocked train should not be used for experimental applications requiring picosecond pulses.

pulse evolution in the case of a large cavity mismatch is complicated.

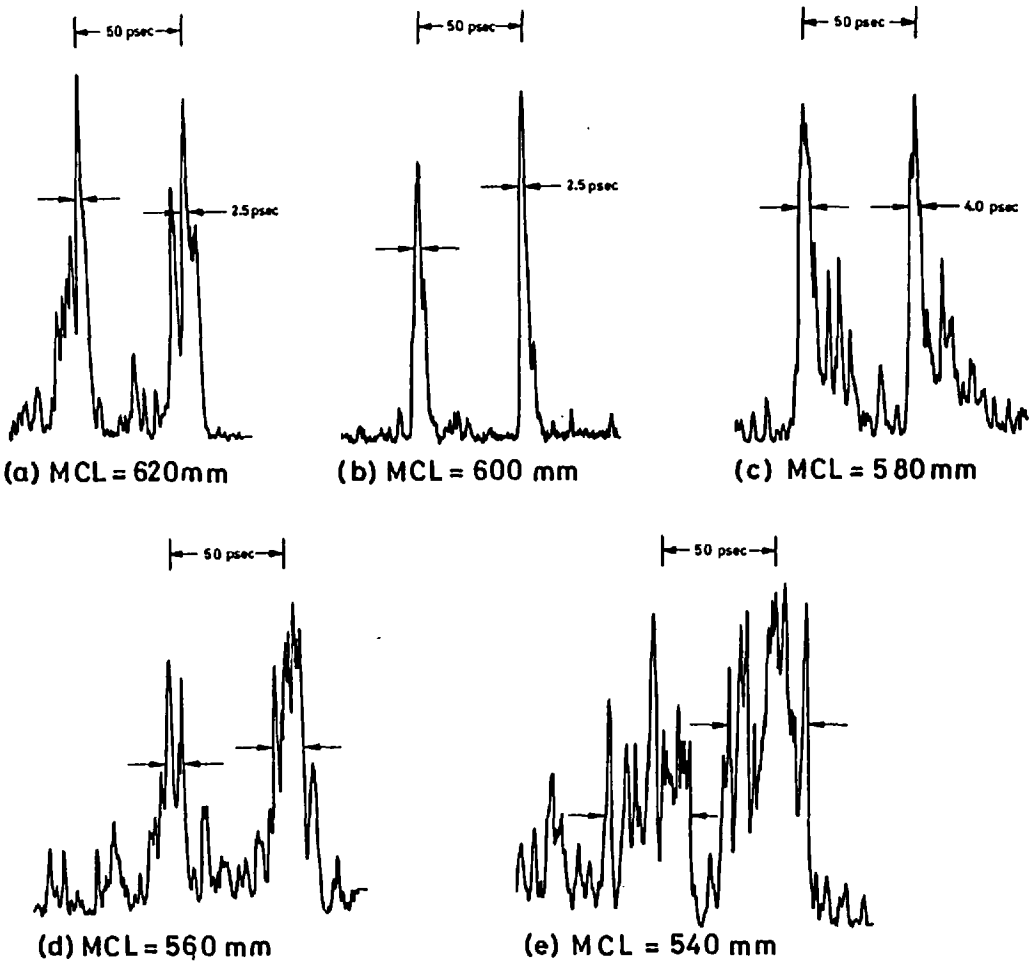

Fig.6.4 Actively modelocked pulses ~80ns from start of modelocked train. Slave CL = 580mm.

The actively modelocked laser pulse gradually looses synchronism with the driving pulse, and on progressing through the pulse train, the actively modelocked pulses arrive at successively later times during the period when the saturable absorber is "open". Complete saturable absorption does not take place, and the initial pulses are highly structured. In the latter stages of the pulse train however, saturable absorption and saturable amplification occur in the usual manner on the initial noise pulses created in the cavity by the reduced cavity loss. A single pulse thus evolves. This contrasts with the near perfectly matched case, where pulse build is extremely rapid.

6.2.4 Conclusion 1

These results have shown that short pulses are produced by the actively modelocked laser for most of its output train. Pulse evolution is rapid, and cavity matching uncritical. The initial pulses are highly structured and unsuitable for experimental work. As yet no measurements have been made on the pulse to pulse jitter of the two pulse trains, and it is expected to extend this work by performing these measurements in the near future.

6.3 An investigation of the luminescence from the CdSe P band

6.3.1 Introduction

The use of a Mk 3 streak camera has enabled the accurate measurement of the delay, rise, and decay time of the recombination radiation from a CdSe monocrystal excited by a picosecond optical pulse. A number of

previous attempts at making these measurements have been made. These include the use of an optical Kerr shutter (75), and the use of a 30 psec streak camera (76). In these cases the resolution was comparable with the duration of the effect being observed. In this case however the 2 psec resolution of the streak camera (at a writing speed of 7×10^9 cm s^{-1}) is a factor of five less than the risetime of the luminescence.

6.3.2 The Physical Process

An energy level diagram of CdSe is shown in Figure 6.5. A photon with an energy in excess of the bandgap creates an electron-hole pair. The hot electron rapidly thermalizes by the emission of longitudinal phonons and then binds to the hole forming an exciton. This is the formation of an exciton by interband transitions. A second exciton creation process occurs in the case of resonant excitation, in which case a photon with an energy equal to the exciton energy creates an exciton directly.

A number of decay processes are possible (Fig 6.5). An exciton may recombine emitting a photon and a longitudinal phonon (A - LO line); it may interact with an electron to form an excited electron whilst itself recombining with the emission of a photon (E line); or thirdly it may interact with a second exciton creating an excited exciton (which rapidly discociates), whilst itself decaying to produce a photon (P line). There are a series of possible P lines, but above 50K only the Pn = ∞ line appears in the emission spectrum. This indicates a complete ionization of the excited exciton into an electron-hole pair. As will be experimentally demonstrated the competition between the A - LO, E and P lines depends on the exciton concentration. At large exciton concentrations (corresponding to an intense excitation pulse) the P line is dominant.

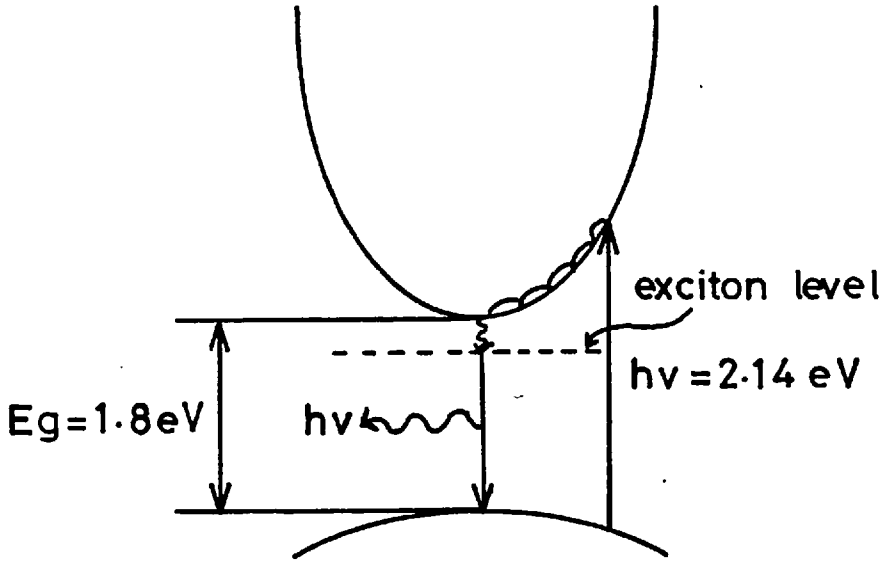

$$e_x \longrightarrow h\nu + LO + \boxed{e} \quad \text{A-LO line}$$

$$e_x + e \longrightarrow h\nu + e^* + \boxed{e} \quad \text{E line}$$

$$e_x + e_x \longrightarrow h\nu + e_x^* + \boxed{e} \quad \text{P line}$$

Fig. 6·5 Exciton processes in CdSe

6.3.3. The experimental arrangement

A schematic diagram of the experimental apparatus is shown in Figure 6.6. A platelet crystal of high purity CdSe, of stoichiometric composition, was attached to a small brass rod, by smearing the tip of the rod with grease, and pressing the back of the platelet against it. Extreme care was taken not to touch the crystal with the fingers at any time. The platelet was immersed ~ 2 cm from the bottom of a ~ 4 cm diameter dewar containing liquid nitrogen. The sample was excited by the complete train (~ 600 ns) from a flashlamp pumped dye laser, modelocked with DQOCI, and tuned to 580 nm (cf Section 2.2). The bandgap of the crystal is ~ 1.8 eV. The energy of the exciting photons is thus 340 meV greater than the bandgap energy.

The focussed laser beam was incident at an angle of $\sim 75^{\circ}$ to the $(1\ \bar{2}\ 1\ 0)$ plane of the crystal. The luminescence and the reflected part of the laser beam were focused onto the slit of the streak camera by an f/1.0, 5 cm focal length lens. Part of this light was passed through a Schott RG 630 filter to eliminate the laser component, and the rest was attenuated by a large neutral density filter (ND 3.0). Streak images of both the excitation pulse and the resultant luminescence were thus simultaneously displayed on the phosphor of the streak camera. Part of the laser output was used to trigger the streak camera. A commercial delay unit (TRW Model 46A) was used to delay the trigger pulse by ~ 400 ns so that only the effects of short pulses were recorded.

Initial checks were made on the quality and duration of the laser pulses,

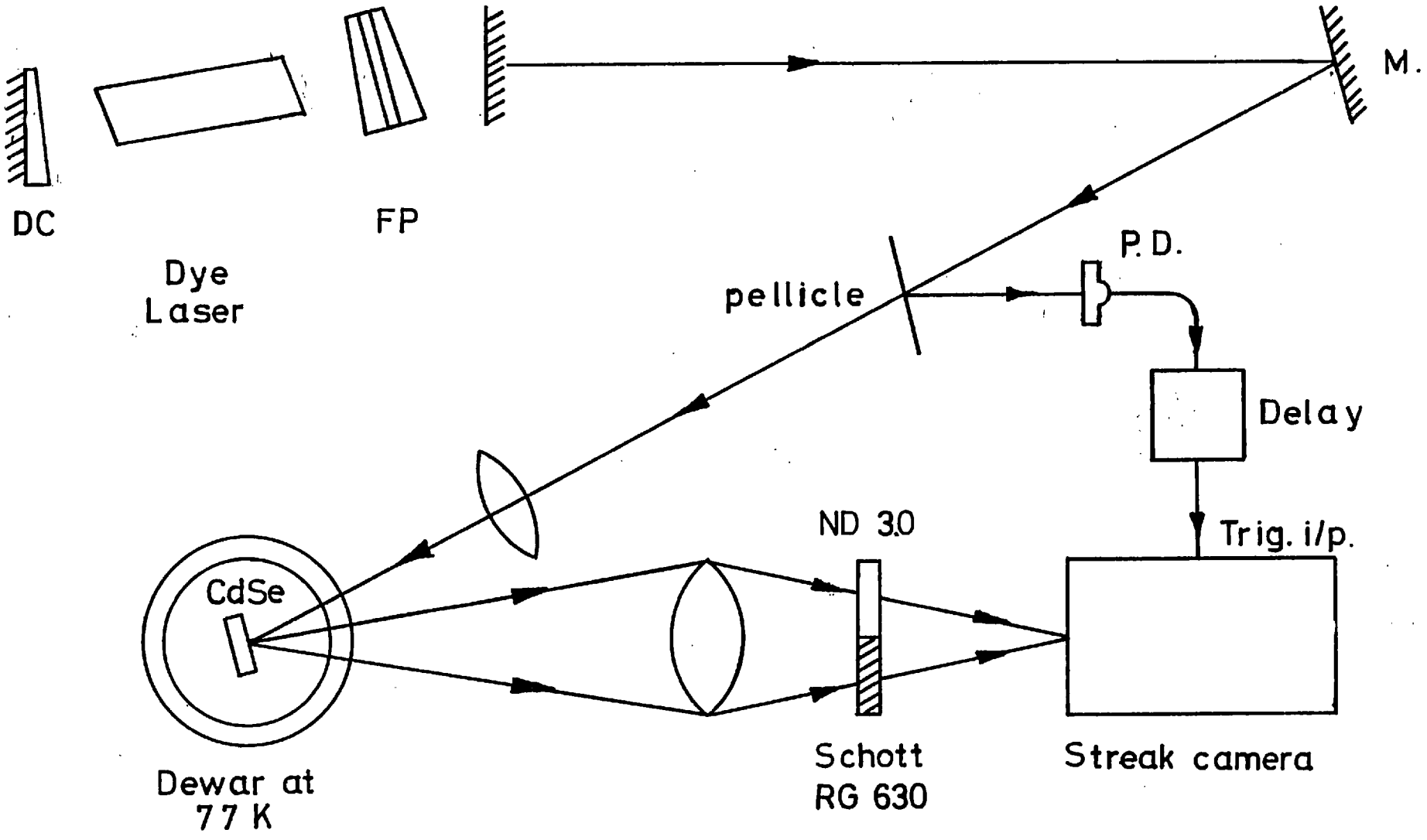

Fig.6.6 Experimental arrangement.

and on the nature of the luminescence spectrum. The laser pulses were reflected off the front and back surfaces of three 5 mm thick glass plates separated by 20 mm. Three pairs of sub-pulses with 50 psec separation were thus generated (cf Section 3.5). By streaking these subpulses the pulse duration ($\sim$ 4 psec) and writing speed of the camera (7×10^9 cm s^{-1}) were determined. Figure 6.7 shows a photograph of a typical streak image, and the corresponding intensity profile.

By substituting the slit of a Monospek 1000 spectrograph for the slit of the streak camera, in the arrangement described earlier for streaking the luminescence, the luminescence spectrum was recorded. The spectrum was found to be intensity dependent (Figure 6.8). As the intensity of the excitiation pulses was increased the $Pn=\infty$ line started to dominate. The position of this line is well known from the work of Liebling and others (144). The position of the A - LO line (corresponding to the radiative recombination of free excitons with the emission of a longitudinal phonon) and the E line (corresponding to exciton-electron interactions) were calculated using the formulae given in the literature (145-147). The energy of the A-exciton was determined by taking a reflection spectrum of the sample. The position of each of these lines is shown by an arrow in Figure 6.8.

6.3.4 Results

An example of a streak record showing both the laser pulse incident on the crystal, and the resultant luminescence is shown in Figure 6.9. By fitting a "best fit" curve through a microdensitometer trace of the streak, and allowing for the γ of the film we can derive the linear intensity

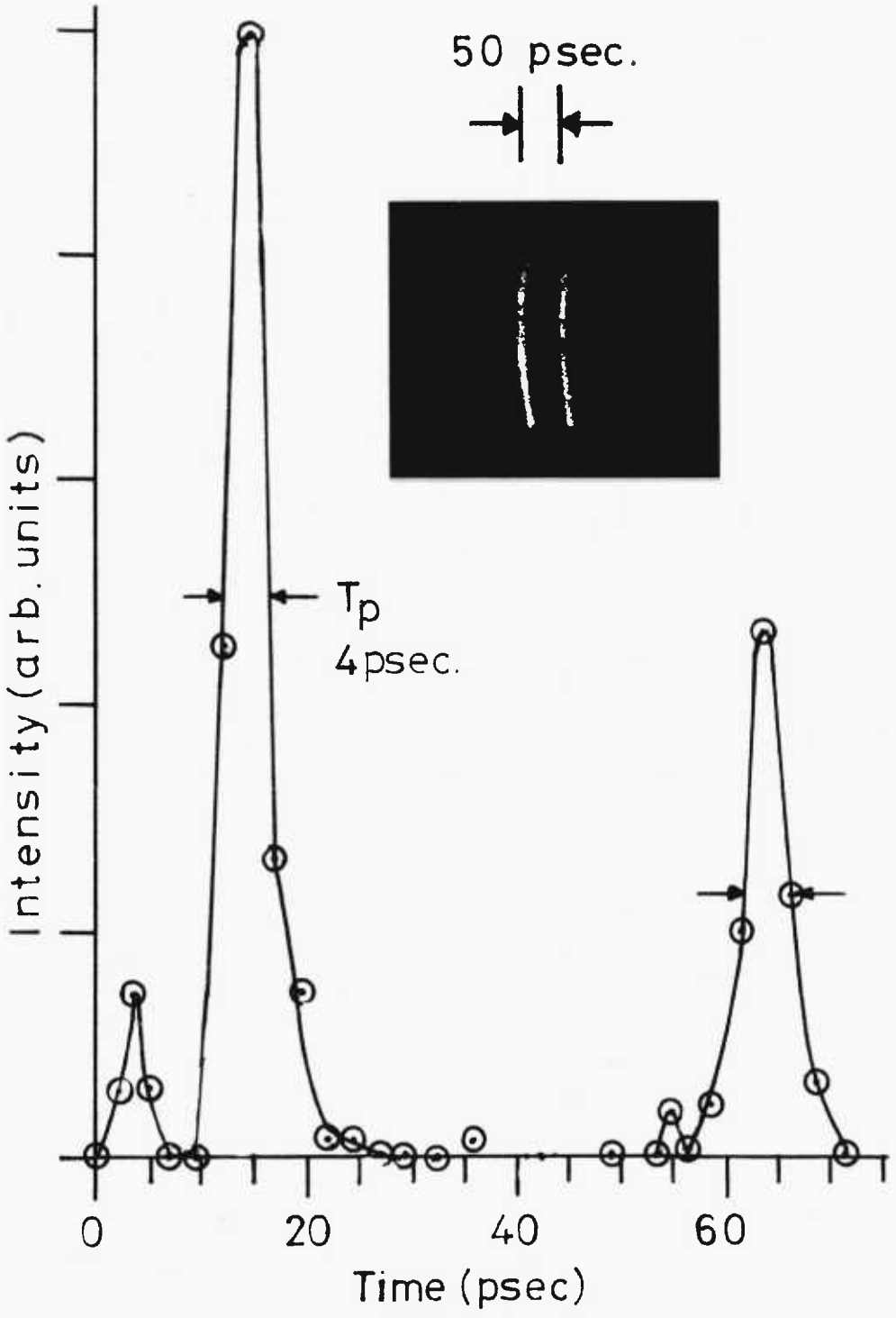

Fig.6.7 Laser pulse at 580 nm

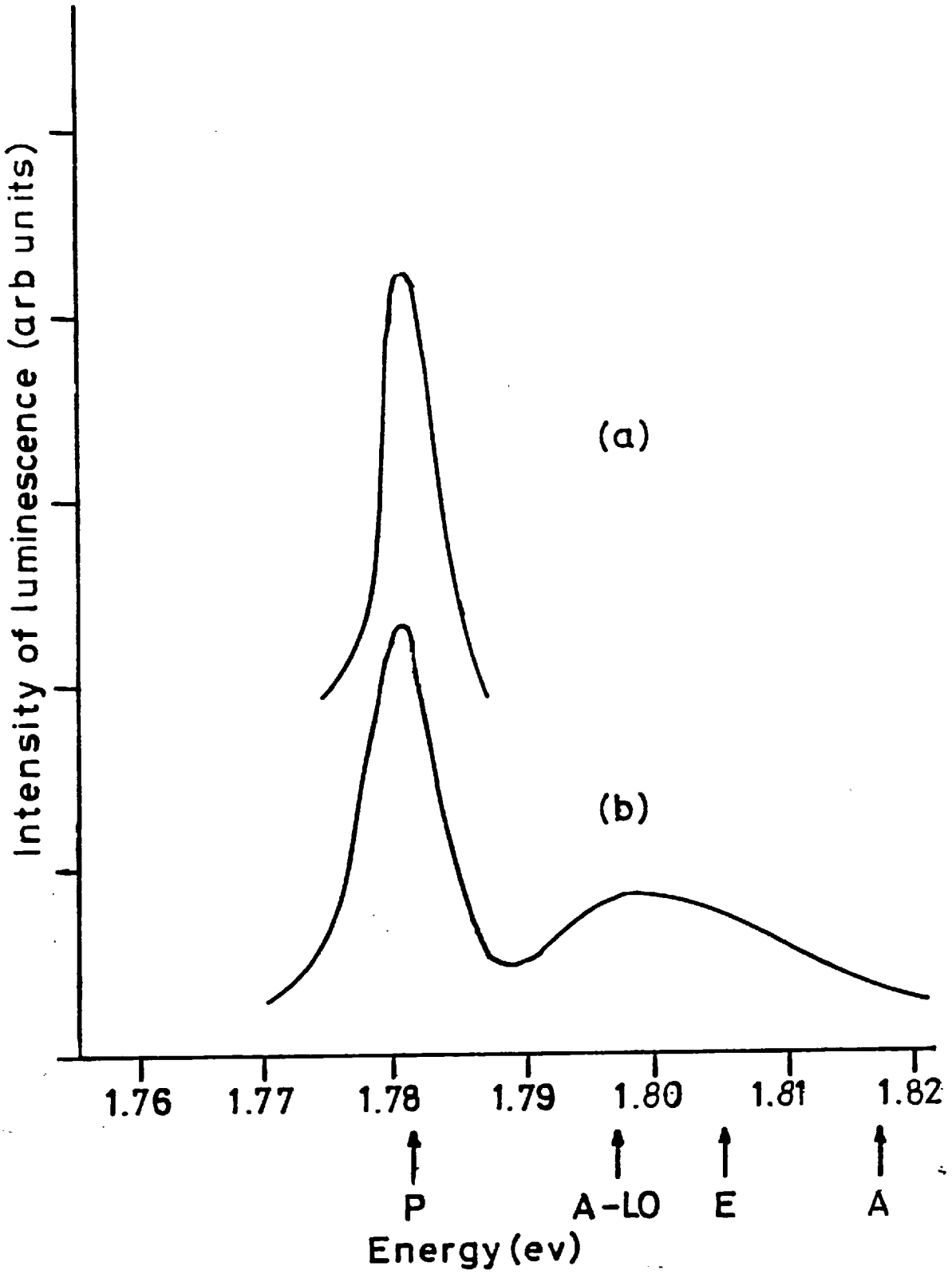

Fig.6.8 Luminescence spectrum

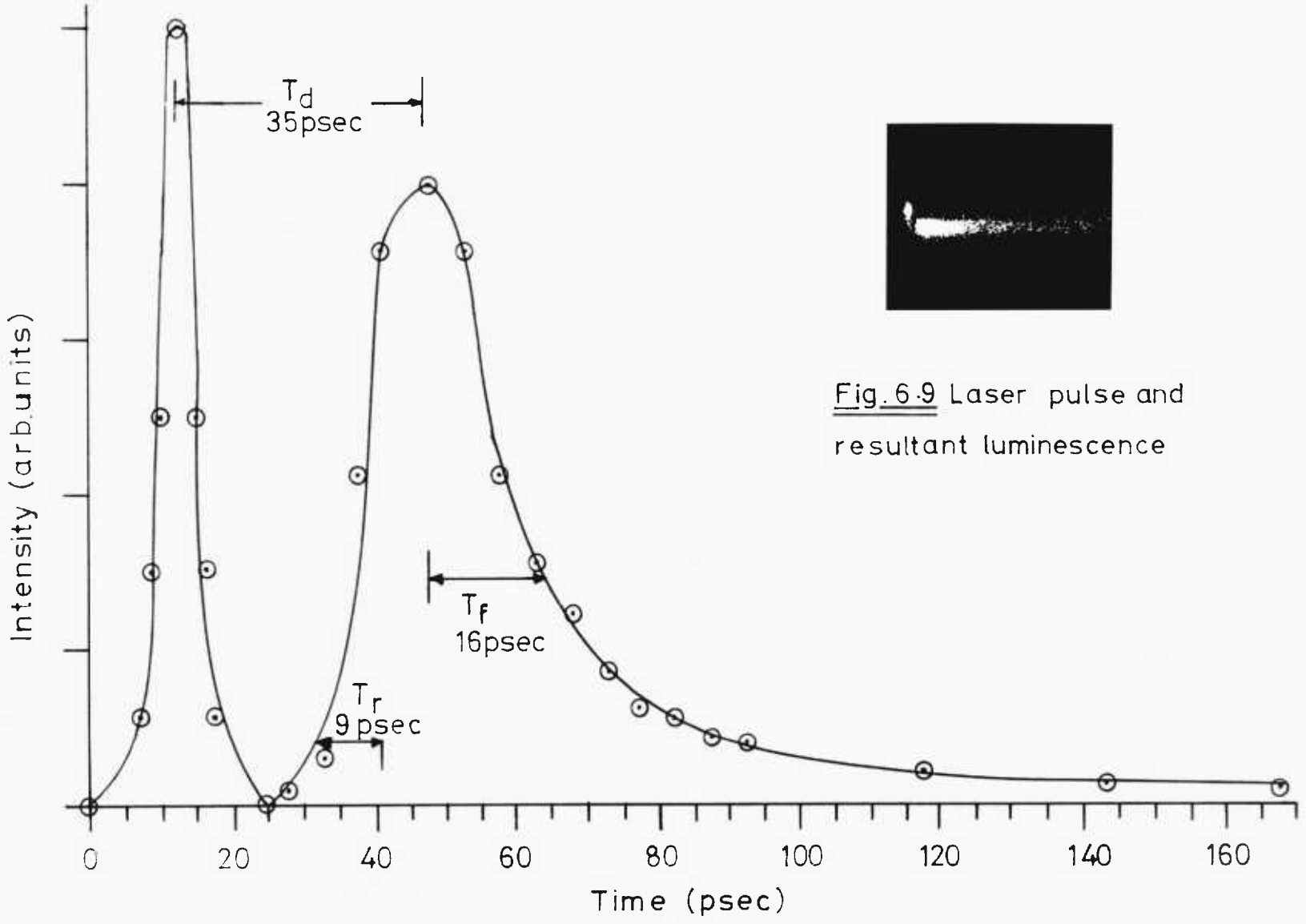

Fig. 6.9 Laser pulse and resultant luminescence

profile shown. The delay between the exciting pulse and the luminescence peak is 34 ± 6 psec. This represents an upper limit for the intraband relaxation time, and the time taken by a free carrier to be bound into an exciton. Two corrections to the measured delay must be considered. Firstly a correction for the dispersion in the optics, and secondly correction for the relative thickness of the two filters. The laser pulse at 580 nm and the luminescence at 680 nm both pass through $\sim$10 cm of glass. The change in refractive index of the more common glasses is $\sim 7.5 \times 10^{-3}$ between these two wavelengths (148), resulting in a relative delay of the laser pulse of ~ 2.5 psec. The Schott RG630 filter through which the luminescence passes is ~ 2 mm thicker than the gelatine neural density filter through which the laser pulse passes. This leads to a relative delay of the luminescence of ~ 3 psec. These two delays approximately cancel, and so no correction to the measured figure is required.

The risetime of the P-line was 9 ± 2 psec and the decay time corresponding to an intensity of $\frac{1}{e}$. I peak was 16 ± 3 psec. As can be seen from Figure 6.9 the slope of the decay curve changes at low intensities. This is indicative of a change in the recombination process, of the type indicated in Figure 6.8, at lower exciton densities. This however, can only be confirmed by taking a time resolved spectrum. It is planned to undertake this experiment in the near future.

6.3.5 Conclusion 2

The use of an ultrafast streak camera has enabled the measurement of the

luminescence decay time for the Pn=∞band in CdSe to be made with greater accuracy than had previously been possible, and has enabled a measurement of its risetime for the first time. This demonstrates the usefulness of a tunable picosecond dyelaser, and an ultrafast streak camera in this type of work. This research may readily be extended by altering the tuning range of the dye laser so that the resonant excitation of excitons may be studied. Such a study should enable the el imination of the intraband relaxation time, and the exciton creation time from the measured luninescence delay time.

CHAPTER 7

THE USE OF A VIDICON READOUT SYSTEM

7.1 Introduction

Previous work on the Mk.3 ultra-fast streak camera has relied on film as the recording medium. From measurements of the dynamic range of these cameras (Chapter 5) it was clear that up to the intensity level at which the photoelectron current limit was reached, the recording film was the only non-linear element in the system. Each piece of film used required individual calibration, followed by a lengthy processing procedure, which included microdensitometering the streak records in order to determine the pulse shape and duration.

The use of an optical multichannel analyser (OMA) in place of film as the recording medium for an ultra-fast streak camera has led to the production of a streak camera with a completely linear output. Although the time resolution of this camera appears to be slightly worse than its film counterpart there is a slight improvement in dynamic range.

Experiments have shown that provided a loss in dynamic range can be tolerated it is possible to dispense with the image intensifier, and couple the SIT vidicon of the OMA directly to the phosphor of the streak tube. Under these circumstances a time resolution of better than 3 psec is obtainable, and a dynamic range of > 25 measured for 4 psec pulses.

7.2 The Optical Multichannel Analyser

The optical multichannel analyser (OMA) measures and displays the intensity of the light incident on the detector head as a function of position. It is normally used as a one dimensional detector, integrating the light in the second dimension.

The light sensitive element of the Princeton Applied Research optical multichannel analyser (OMA) type 1205 is a silicon vidicon. Three types of detection head option are available:- the 1205B standard silicon vidicon, the 1205D Silicon intensified target vidicon (SIT), and the 1205I intensified silicon intensified vidicon (ISIT). The ISIT detector has roughly twice the sensitivity of the SIT detector, but only became available in the closing of this work. These detectors are based on the RCA 4532, 4804, and 4849 16 mm vidicon families respectively. Because of its greater sensitivity compared to the standard vidicon ($\sim$ 150 x) the SIT detector was chosen for this application.

A schematic diagram of a SIT vidicon is shown in Figure 7.1. The target (Figure 7.1(b))consists of a thin n-type silicon slice in which a matrix of p-type islands are diffused. Silicon oxide ($Si\ O_2$) covers the areas between the diodes, to isolate the n-type silicon from the reading beam, and the whole surface is covered by a semi-insulating film, to prevent the accumulation of charge on the oxide. The cathode of the read gun is biased to - 6V, and the target grounded. Scanning the target with the read gun charges the p-type islands to the cathode potential thus reverse biasing the p-n junction diodes.

The front end of the SIT vidicon is a conventional inverting image converter. Photoelectrons from the S-20 photocathode are accelerated and focused onto the silicon target, entering it at high energy, and

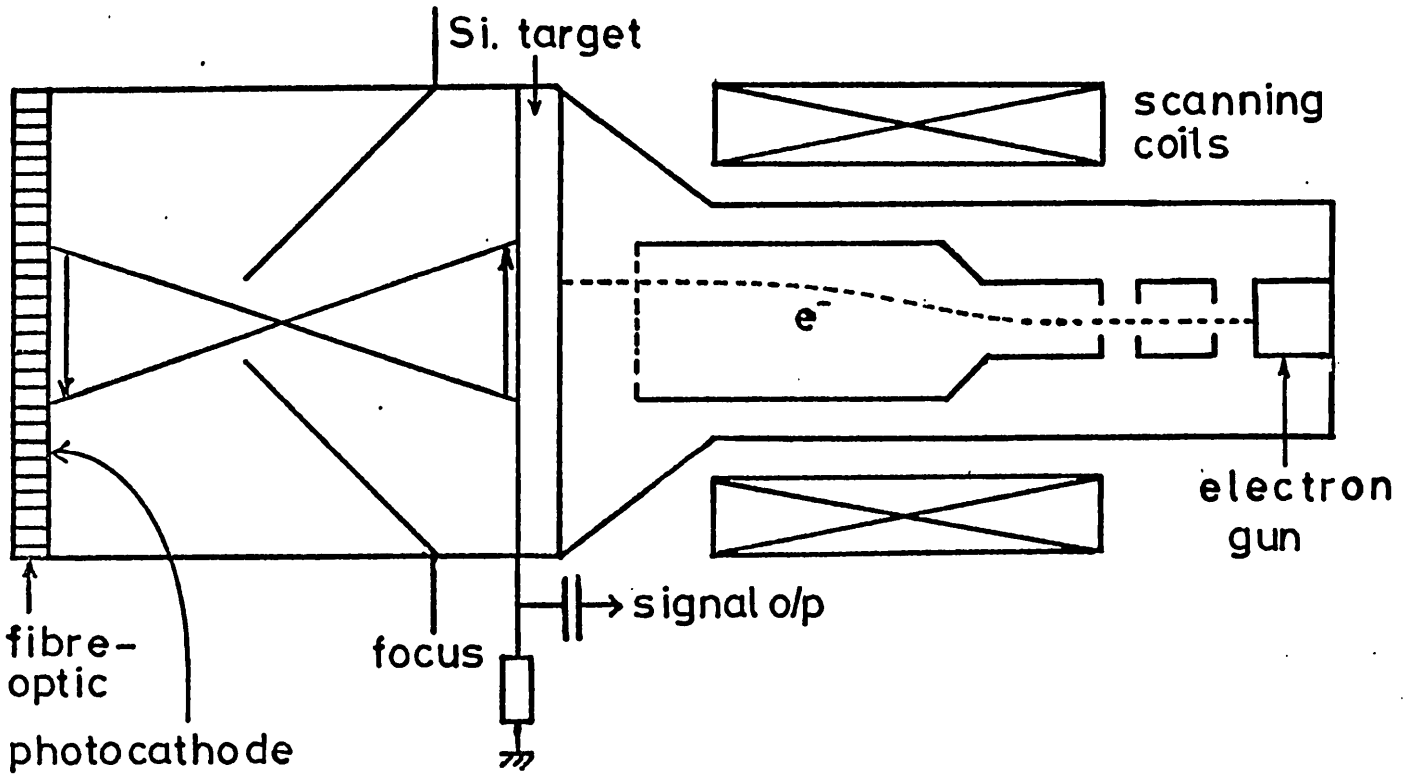

(a) Image tube

(b)Silicon target

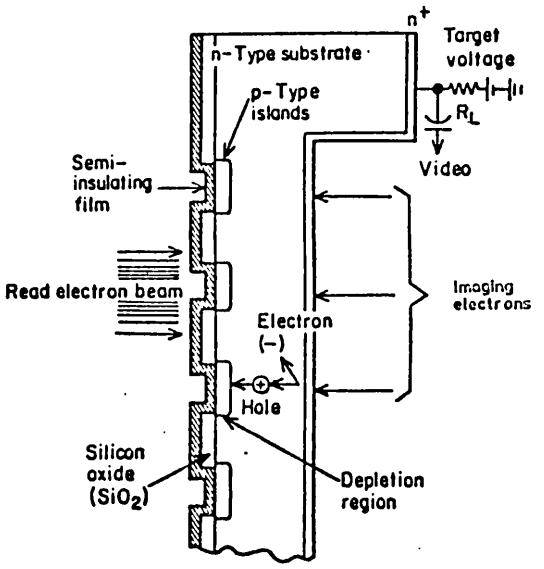

Fig. 7.1 SIT vidicon

creating electron-hole pairs. The holes are swept across the diode depletion regions, discharging them. By measuring the read gun current as it re-charges the diodes, the intensity corresponding to each image point is determined. Since each incident photoelectron enters the target with an energy $\sim$ 9KeV, and only 3.4eV are required to create an electron-hole pair, the charge pattern on the target is an amplified version of the original optical image. In principle, target gains of $\sim$ 2500 are possible, although in practice gains of $\sim$ 1500 are typical.

The vidicon is scanned in a normal T.V. raster. The OMA integrates the signal from each T.V. line, and after performing an analogue to digital conversion, digitally stores it. The image is thus divided up into 500 channels each corresponding to a T.V. line. The 5mm x 12mm active area of the photocathode is divided into two 2.5mm x 12mm regions, one designated the light area, used to detect the optical information, and the other,the dark area, used as a reference noise source. Care must be taken that information is only presented to the light half of the target. As each line is scanned, the signal from the dark area is subtracted from the signal derived from the light area. In this way the dark current, and any pre-amplifier off-set can be removed from the signal. The target may be scanned any number of times, and the signal at each channel digitally integrated.

In order to eliminate any error in the division of the target into two identical zones, and to allow a correction to be made for any background input signal, two 500 channel memories are provided. The desired signal plus the background is integrated in the 'A' memory, and the background only integrated in the 'B' memory. An A - B mode then permits operation on a signal :-

(signal + noise) - (noise)

The desired analogue signal (A, B, or A - B) is displayed on an oscilloscope monitor and may be printed out on a chart recorder to obtain a permanent record of the signal.

7.3 The Static Performance of the OMA

Whilst a comprehensive specification is available for the OMA, little detail is given regarding its use to record short single shot events (such as a phosphor illuminated by a picosecond pulse of electrons). A study of the performance of the OMA was thus carried out in order to determine the influence of the OMA characteristics on the parameters of the streak camera system as a whole.

The static performance of the OMA was examined by projecting a slit image onto the photocathode of the SIT vidicon and plotting a graph of recorded intensity (counts) as a function of optical attenuation (density). This graph is the transfer function of the OMA. The Kodak Wratten gellatin neutral density filters used for optical attenuation become more transparent towards the infra-red, and so it was necessary to restrict the spectral output of the tungsten lamp used for illumination, by passing the light through a Kodak type 54 glass filter (410 - 570 nm). In order to simulate a single shot event the photocathode of the vidicon was continuously illuminated, and the OMA gated on for $\sim$ 80 μs by the application of a -1200V pulse to the photo-cathode (which at all other times was held at the focus electrode potential). This pulse was derived from a gating generator similar to the one used to generate the +1200V for the channel plate intensifier (c.f. Section 4.6), except for small modifications to the output stage to reverse the pulse polarity.[1]

1. The phase of the two negative-going control pulses is reversed, the 820K resistance between the collector-emitter of the push-pull output transistors and ground is now connected to the EHT supply, and the circuitry to generate the +200V pulse is omitted.

The transfer characteristic of the OMA for 1 and 5 target scans is shown in Figure 7.2(a) and 7.2(b) respectively. The departure from linearity is clear. Increasing the number of scans to 20 (Figure 7.3), however, removes any non-linearities and enables the instrument to handle intensities corresponding to a maximum of 3000 counts/channel. This effect is known as target lag and arises from the exponential charging characteristics of the diodes in the target. The upper limit of 3000 counts is set by the type of A-D converter used in the instrument.

In order to determine the dynamic range of the OMA it is also necessary to measure its noise level. Extreme care has to be exercised in making this measurement due to the high sensitivity of the instrument. The front of the detector head was covered to exclude any light, and the background signal corresponding to 20 target scans accumulated into each memory in turn. By finding the R.M.S. value of the number of counts in 100 channels chosen at random, the noise level of the system was found to be $\pm$ 8 counts.

Order of magnitude calculations show this to be accounted for by Nyquist noise in the vidicon preamplifier stage. Since the first stage of this amplifier is a current to-voltage converter the noise current must be considered :-

$$\overline{i}^2 = 4kT\,\frac{B}{R} \qquad (A^2)$$

where $\overline{i}$ is the RMS current noise, k is Boltzman's constant, T is the

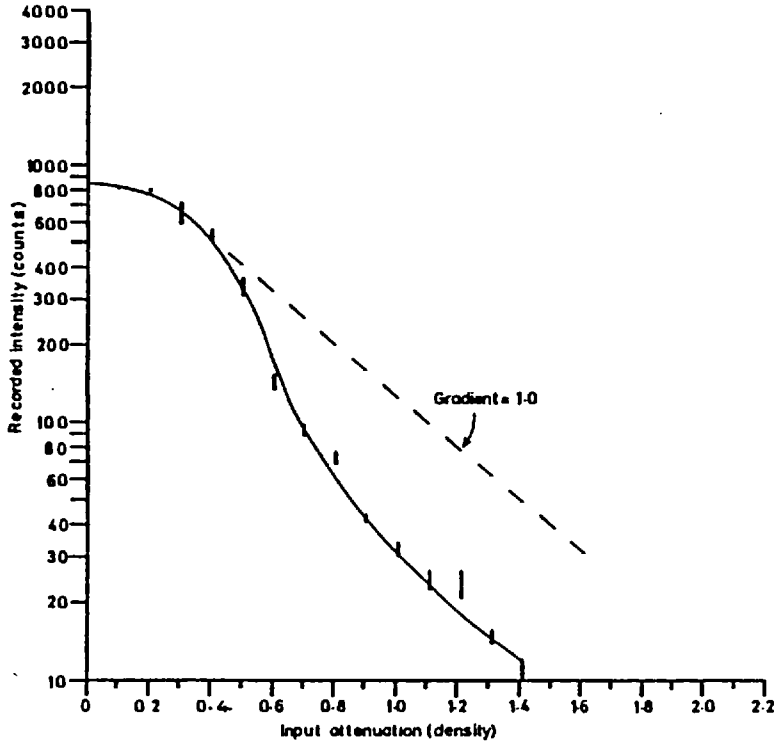

(a) 1 Scan

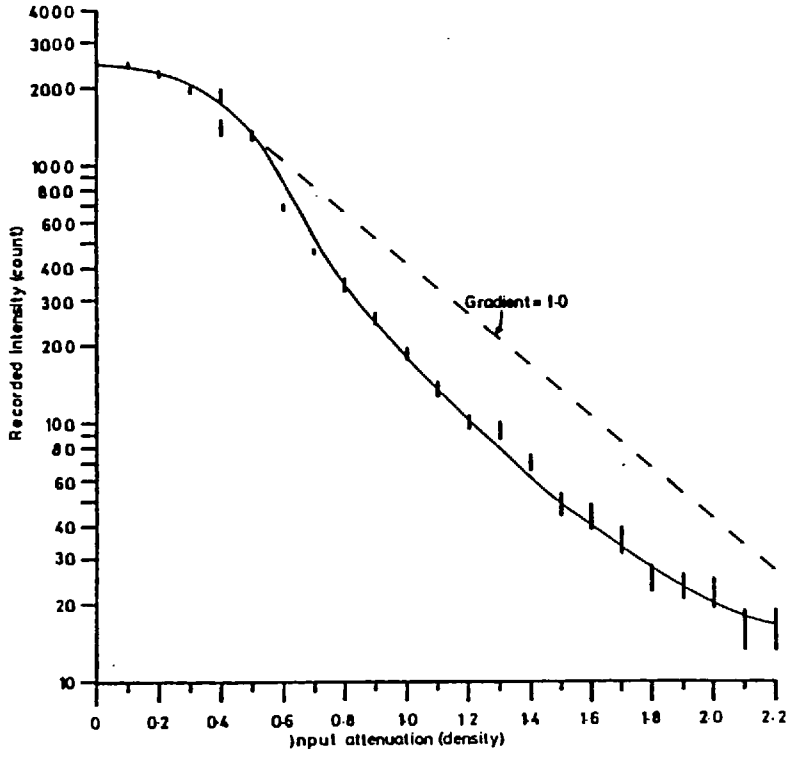

(b) 5 Scans

Fig 7·2 OMA transfer function

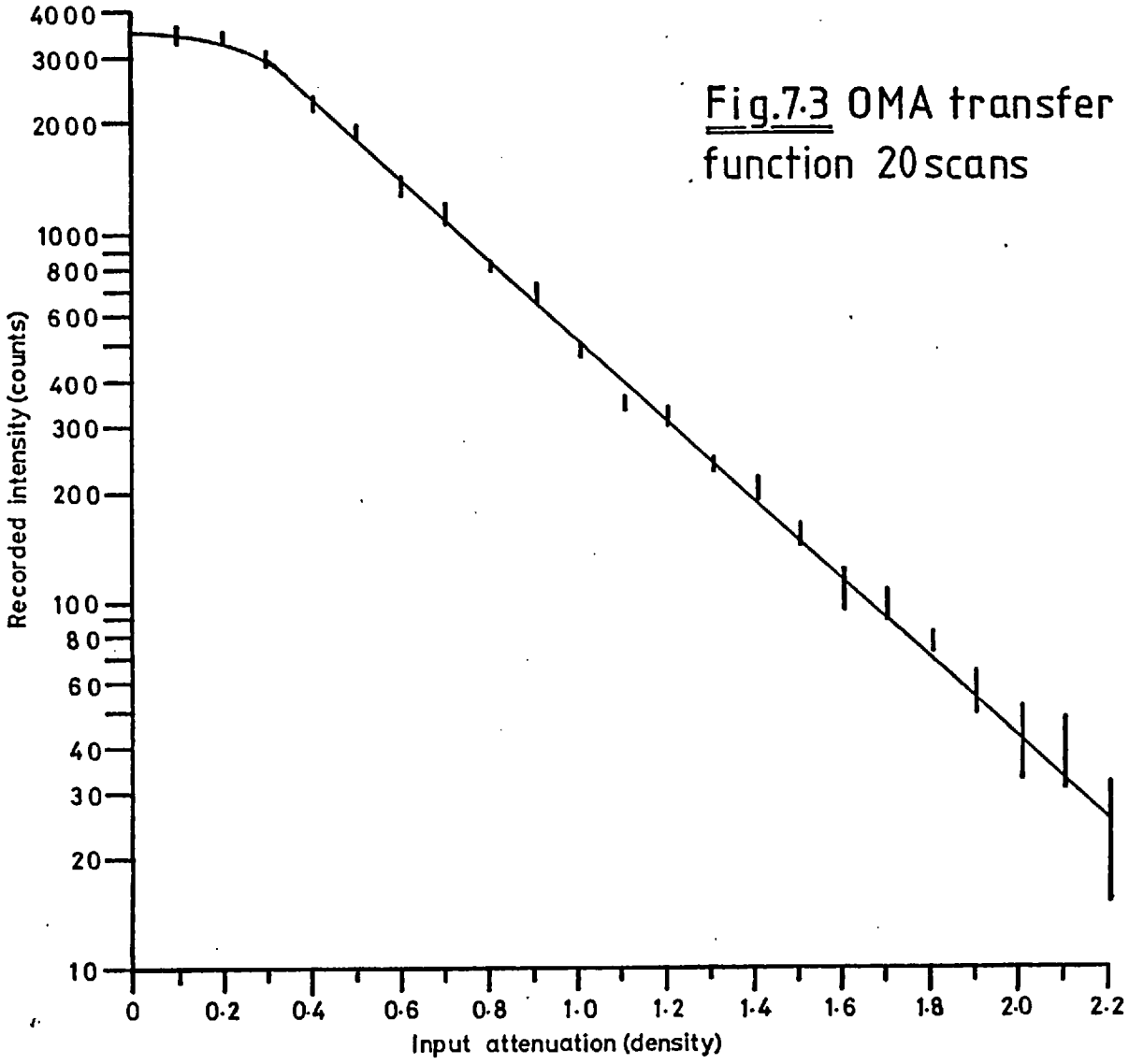

Fig.7.3 OMA transfer function 20 scans

temperature, B the amplifier bandwidth and R the amplifier input resistance. Taking the bandwidth to be twice the reciprocal of the time taken to read the signal from each line (tc) and converting the current to electrons this becomes :-

$$\overline{Ne}^2 = \frac{1}{C^2} \cdot 4\frac{kT}{R} \cdot \frac{2}{tc} \qquad (e^- s^{-1})^2$$

where $\overline{Ne}$ is the RMS number of electrons per second and C is the electronic charge.

The number of electrons per channel ($\overline{Nec}$) accumulated over Ns scans is then given by :-

$$\overline{Nec} = \frac{1}{C}\sqrt{\frac{8\,kT}{R\,tc}} \cdot Ns\,tc \qquad (e^- s^{-1})$$

This is equivalent to $\overline{Npe}$ photoelectrons, where

$$\overline{Npe} = \frac{1}{CG}\sqrt{\frac{8\,kT}{Rtc}} \cdot Ns\,tc \qquad (ph\ s^{-1})$$

and G is the target gain. Assuming a temperature of 300 K, a target gain of 1500, an input impedance of $10^8\ \Omega$, and that it takes 64 μs to read each line, the number of photoelectrons counted during 40 scans (20 scans for each memory) is 24.

Taking the manufacturer's figure of 2 photoelectrons per count this

indicates an RMS noise level of 12 counts which is in good agreement with the measured value. These numbers indicate a maximum dynamic range of ∿ 370 for the OMA when used in a single shot experiment.

The spatial resolution of the OMA was measured by masking off all but the variable spatial frequency wedge on a Baum chart (141), and projecting it onto the photocathode of the SITvidicon. A typical trace (Figure 7.4(a)) shows that the resolution at 50% modulation is ∿ 15 lp/mm, and the resolution at limiting resolution is ∿ 25 lp/mm.

7.4 The Linear Streak Camera (with intensifier)

The OMA was initially used as a direct substitute for film on the Mk.3 ultrafast streak camera, by lens coupling it to the back of the channel plate image intensifier. A pair of Canon 50 mm f/1.2 lenses mounted face to face were used to relay with unit magnification the image at the phosphor of the intensifier onto the photocathode of the SIT vidicon. The coupling efficiency of these lenses is estimated to be ∿ 16%, but there is more than sufficient light gain in the system to overcome this loss. This lens system can only cover an area ∿ 1.5 cm in diameter before vignetting becomes serious (86), but as the light sensitive portion of the OMA detector head is only 1.2 cm across this is not important. The coupling lenses were mounted in a fixed position relative to the image intensifier, and the system was focussed by altering the distance between the OMA and the lens.

It was extremely important that the slit of the streak camera be set perpendicular to the streak direction, and that the light sensitive channels of the OMA (the T.V. lines) were aligned along the slit. The former prevents slit walk-off, and the latter optimises spatial

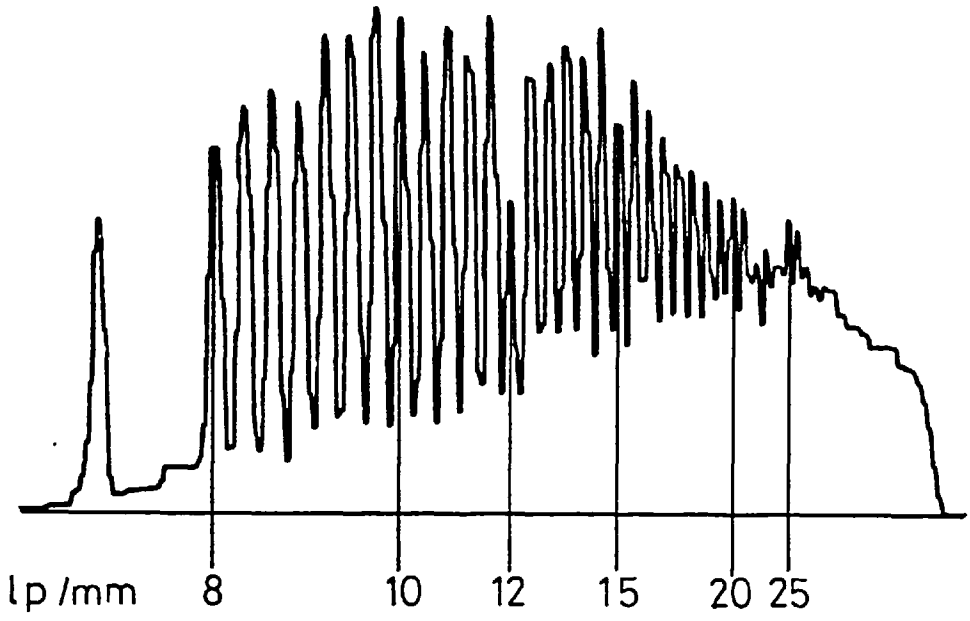

(a) OMA only

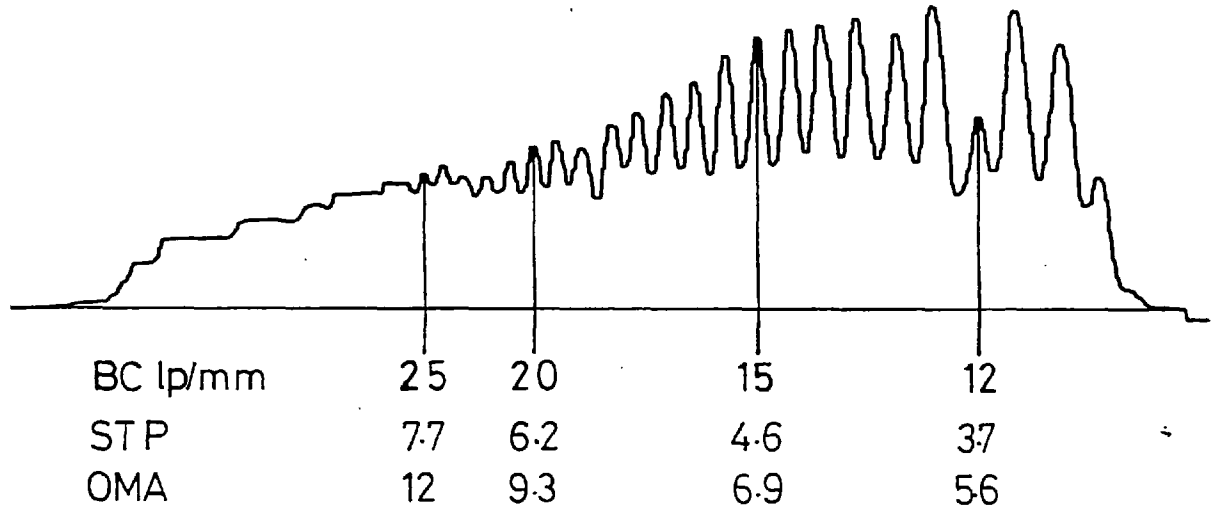

(b) Whole system – mag. at S.T. phos. 3·25

Fig. 7·4 System spatial resolution

resolution. The slit of the streak camera was illuminated by a white light source, and by deflecting the slit image from side to side, the streak direction was determined. A graticule was aligned along the streak direction and this was used to correctly align the slit. The OMA head was attached to the streak camera, and by alternately rotating it, and then adjusting the focus, the resolution was optimized.

To enable the system to be focussed the OMA has to be operated in the 'Real Time' mode, in which it displays information as it receives it, without any storage or other signal processing. The streak camera has to be set in the focus mode, and the channel plate intensifier repeatedly gated on to produce a quasi-continuous image at its output. Unless the gating of the channel plate intensifier and the scanning of the target of the OMA are synchronized, such that the intensifier is gated on during a (T.V.) frame flyback period two undesirable effects take place :-

(a) The channel plate gating pulse (+1200V) gives rise to R.F. radiation, which causes interference to the vidicon pre-amplifier.

(b) An effect known as skew lag occurs.
Channels scanned immediately before the image intensifier is gated on have been read more times than those scanned immediately afterwards. A sharp change in the amplitude of the displayed signal occurs at a position corresponding to the application of the gating signal. A confusing beat pattern hence runs through the displayed signal.

These effects may be elimated by using the FRBLANKD1 signal from the OMA to drive the channel plate gating generator. The FRBLANKD1 is a logical 1 signal during the frame flyback, and logical (zero) at all other times.

As the OMA target is continuously scanned it is necessary for the reasons stated above to synchronise the firing of the laser with the frame flyback period. This is accomplished by triggering the channel plate gating generator, and therefore the laser from the DELINHD1 signal from the OMA. Normally this signal is a logical 1. When the A Accumulate switch on the OMA consol is pressed to initiate a series of target scans, nothing happens until the start of next frame period. During the flyback DELINHD1 goes to logical zero, and remains at zero for the duration of the designated number of target scans, before returning to logical 1.

When the B accumulate switch on the OMA consol is actuated, to determine the system background noise, it is desirable that the channel plate intensifier be gated on without the laser firing. This is accomplished by using a latch (IC3a and 3b - Figure 4.6) to inhibit the laser trigger generator IC8.

By projecting a specially masked Baum pattern onto the photocathode of the shutter tube the static spatial resolution of the system was determined (Figure 7.4 (b)). The 40% MTF point corresponds to a resolution of $\sim$ 4 lp/mm at the phosphor of the streak tube, and the 15% MTF point to a resolution of $\sim$ 6 lp/mm (this corresponds to a resolution of $\sim$ 5.5 lp/mm and $\sim$ 9 lp/mm at the OMA photocathode).

7.5 Characteristics of the Linear Streak Camera

The curvature of the streak images produced by all ultra-fast streak cameras (c.f. Figure 6.2) complicates the setting up procedure of the streak camera when dynamic tests are being carried out. If an extended curved part of a streak image falls on the light sensitive area of the OMA detector, the effective temporal resolution of the streak camera is degraded. For optimum temporal resolution only the part of the streak with a tangent normal to the streak direction should be imaged onto the OMA photocathode. The part of the slit corresponding to the required part of the image was located from streak records taken on film. All but this 3 mm section of the slit (corresponding to 1.7 mm at the OMA) was then masked off, and by introducing magnetic deflection in the streak tube this part of the slit image was brought into alignment with the correct part of the OMA target. The magnetic deflection was provided by passing a current ~ 40 mA through two small solenoids[1] mounted close to the deflection plate connector pins. The use of magnetic deflection produced no noticable defocussing of the streak tube.

Using the system previously employed to measure the dynamic range of the Mk.3 streak camera (see Chapter 5) the dynamic range of this linear streak camera was determined both as a function of channel plate intensifier gain, and SIT vidicon target gain. Ultrashort test pulses were again generated from a dye laser modelocked with DQOCI, and tuned to 600 nm.

[1] The actuator coils from 2 R.S components type 7a 34y. 475 Ω relays.

With the gain of the channel plate intensifier nominally set at x 10^3, and a target gain of $\sim$ 1500 in the SIT vidicon, the recorded pulse duration was measured as a function of pulse intensity (counts). Figure 7.5 shows both the chart recorder trace and a photograph of the screen of the monitoring oscilloscope corresponding to a typical streak record. Vertical expansion of the display (Figure 7.6) shows that more of the detail of the low intensity pulses becomes available at the expense of the detail of the high intensity pulses. The separation of the sub-pulses from the etalon is $\sim$ 17.5 psec, and the recorded pulse duration is $\sim$ 3.7 psec. By illuminating the slit of the streak camera with white light and switching it to focus mode, the streak camera resolution limit can be plotted out on the same scale (Figure 7.7). A measurement of the halfwidth of this trace gives the limiting temporal resolution of the streak camera. With the OMA set to "Plot Rate 9" ($\sim$ 3 channels/sec), and a chart recorder speed of 120 mm/min the slit width is $\sim$ 3.5 mm, corresponding to a resolution of $\sim$ 2.6 psec at the writing speed used above (10^{10} cm s^{-1})at the streak tube phosphor). Including the photoelectron time dispersion at this wavelength then gives the instrument limited time resolution as $\sim$ 2.7 psec.

From a series of results similar to Figure 7.5 the transfer characteristic of the camera was plotted (Figure 7.8). It can be seen that a non-linear response only occurs at the OMA limit of $\sim$ 3000 counts. The background noise was measured with both camera and laser operating but unsynchronised. In this way photoelectrons scattered onto the phosphor of the streak tube were included in the noise figure. The background noise under these conditions was found to be $\pm$ 30 counts (RMS), indicating an instrument dynamic range of $\sim$ 100.

The SIT vidicon target gain was reduced from 1500 to 10 by reducing

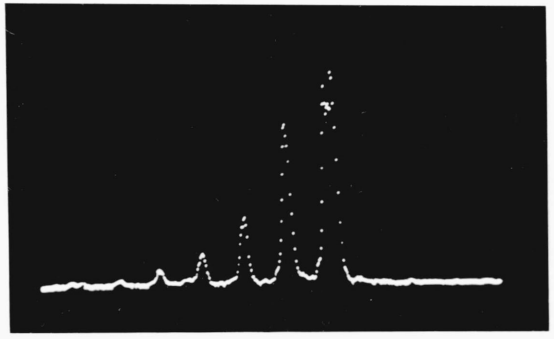

Fig. 7·5 OMA Output

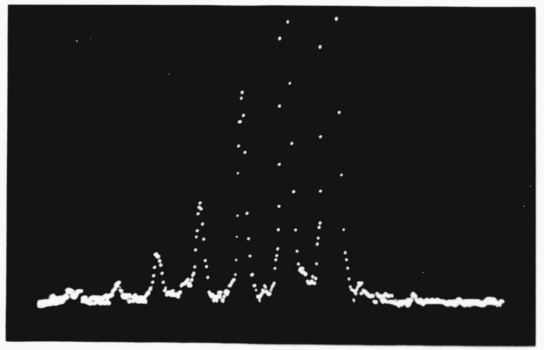

Fig. 7·6 OMA Output - fig. 7·5 expanded

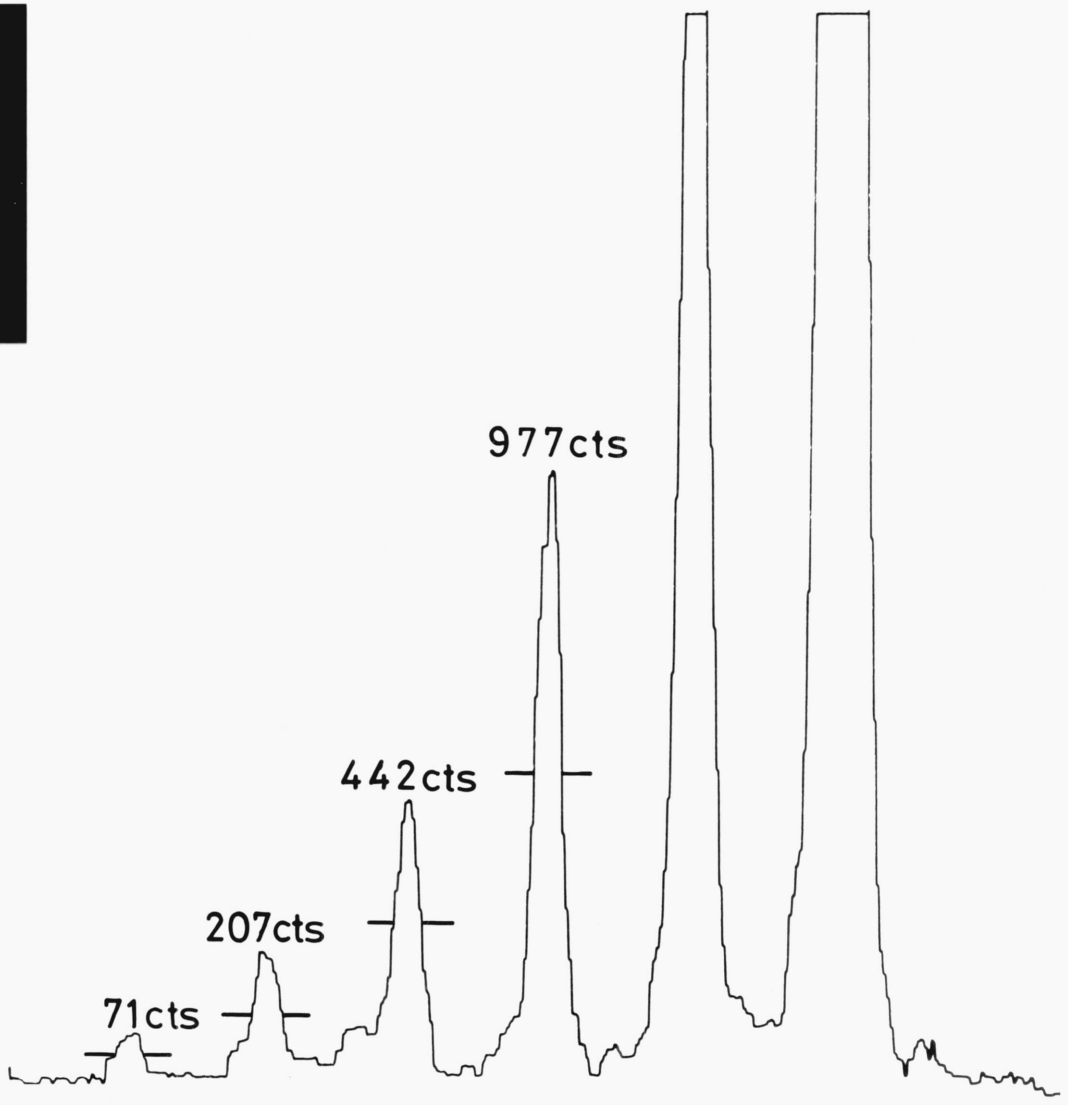

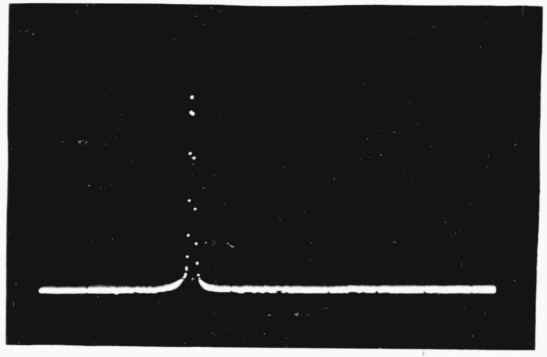

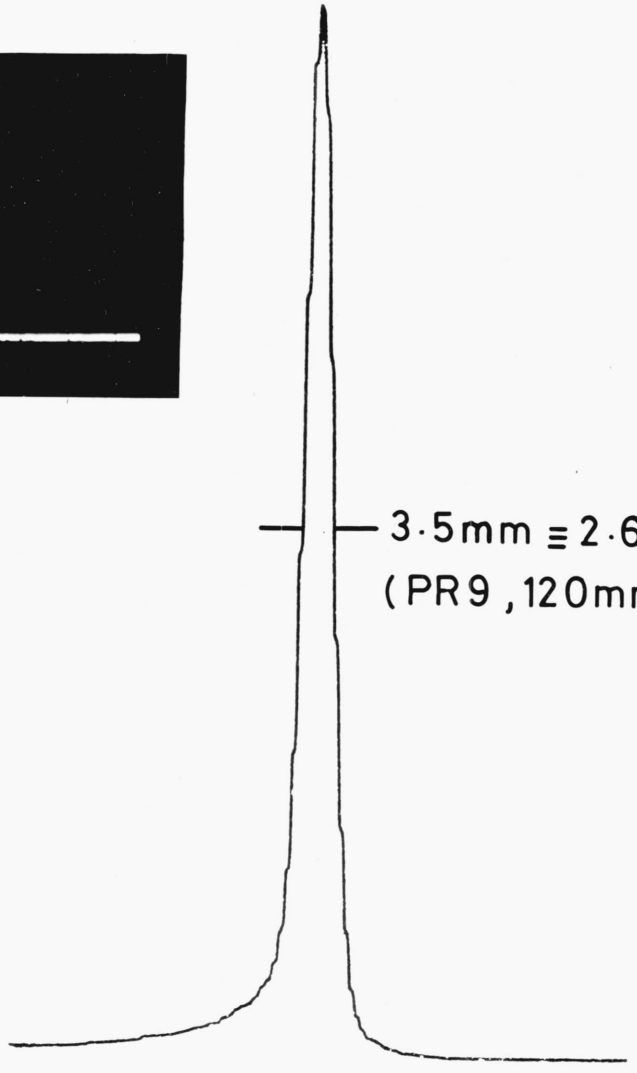

Fig.7·7 Static slit, complete system

Fig. 7·8 Dynamic range

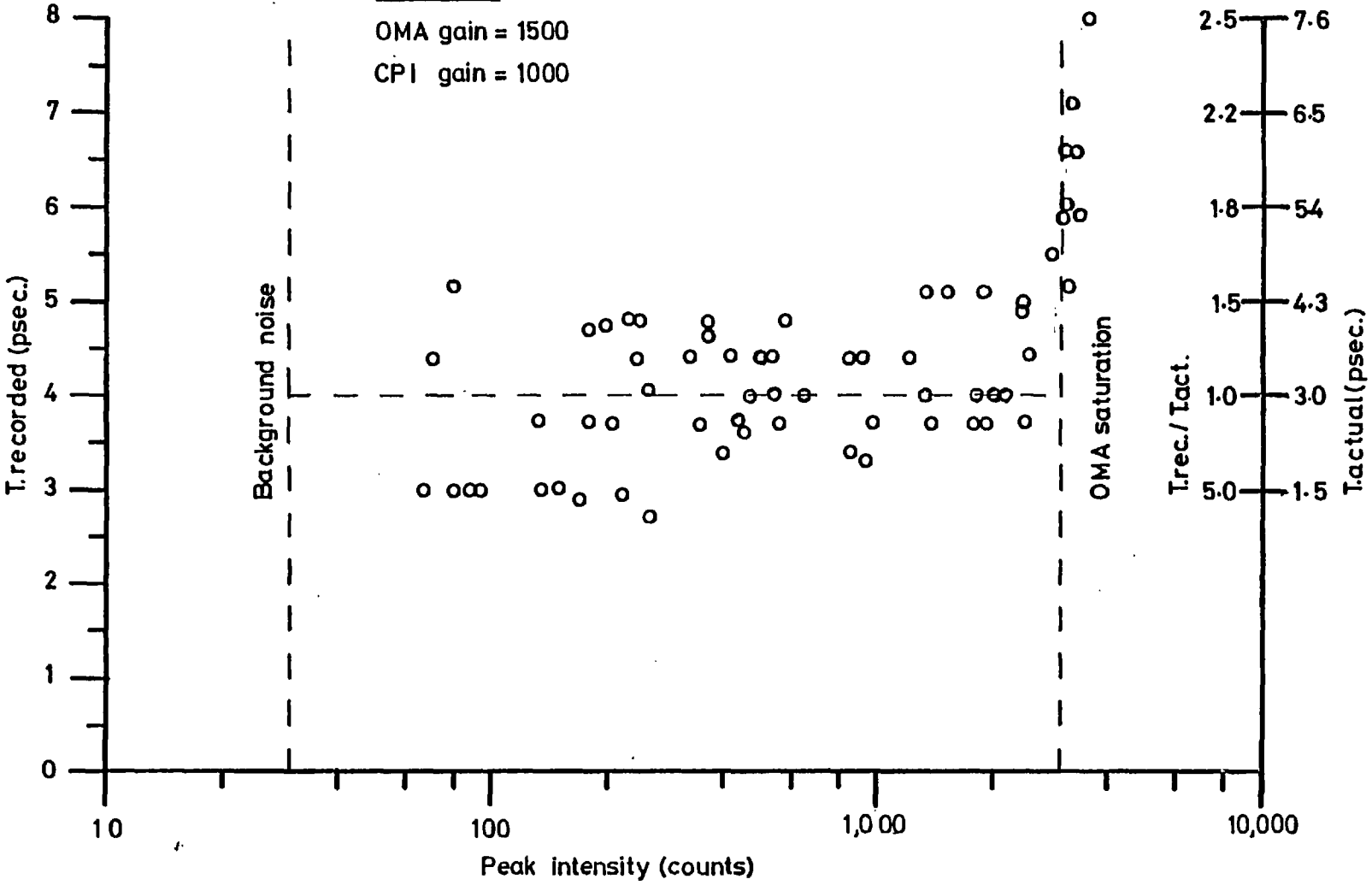

the voltage across the image converter stage in front of the silicon target. This simulated an OMA with a 1205B standard silicon vidicon detector head (a target gain of ∿ 10 is required to offset the quantum efficiency of the photocathode which is only ∿ 10%). To compensate for the loss of target gain, the gain of the channel plate intensifier was increased from x 10^3 to 10^5. The resulting transfer characteristic is shown in Figure 7.9. This is very similar to Figure 7.8, and shows that the upper intensity limit is again set by the A to D converter in the OMA. The background noise was again measured and found to be ± 20 counts indicating a slightly improved dynamic range of ∿ 150.

In order to determine the total dynamic range available in the absence of a limit imposed by the OMA electronics the gain of the image intensifier was reduced to x 10^4. The dynamic range curve (Figure 7.10) shows the characteristic sharp increase in recorded pulse duration, as the photoelectron current limit is reached at ∿ 1100 counts. The background noise however was also reduced to ∿ 10 - 15 counts, approaching the noise limit of the OMA, and indicating a dynamic range of ∿ 70:1.

This result implies that a factor of 3 in photoelectron current was available in the previous results indicating that such a system, with improved OMA electronics should be capable of a dynamic range of over 400.

7.6 The Linear Streak Camera (without intensifier)

The high sensitivity of the linear streak camera with the channel plate image intensifier was encouraging, and so experiments were performed to see if it would be possible to remove the image intensifier from the system. The removal of the intensifier gives a reduction in both cost

Fig.7.9 Dynamic range

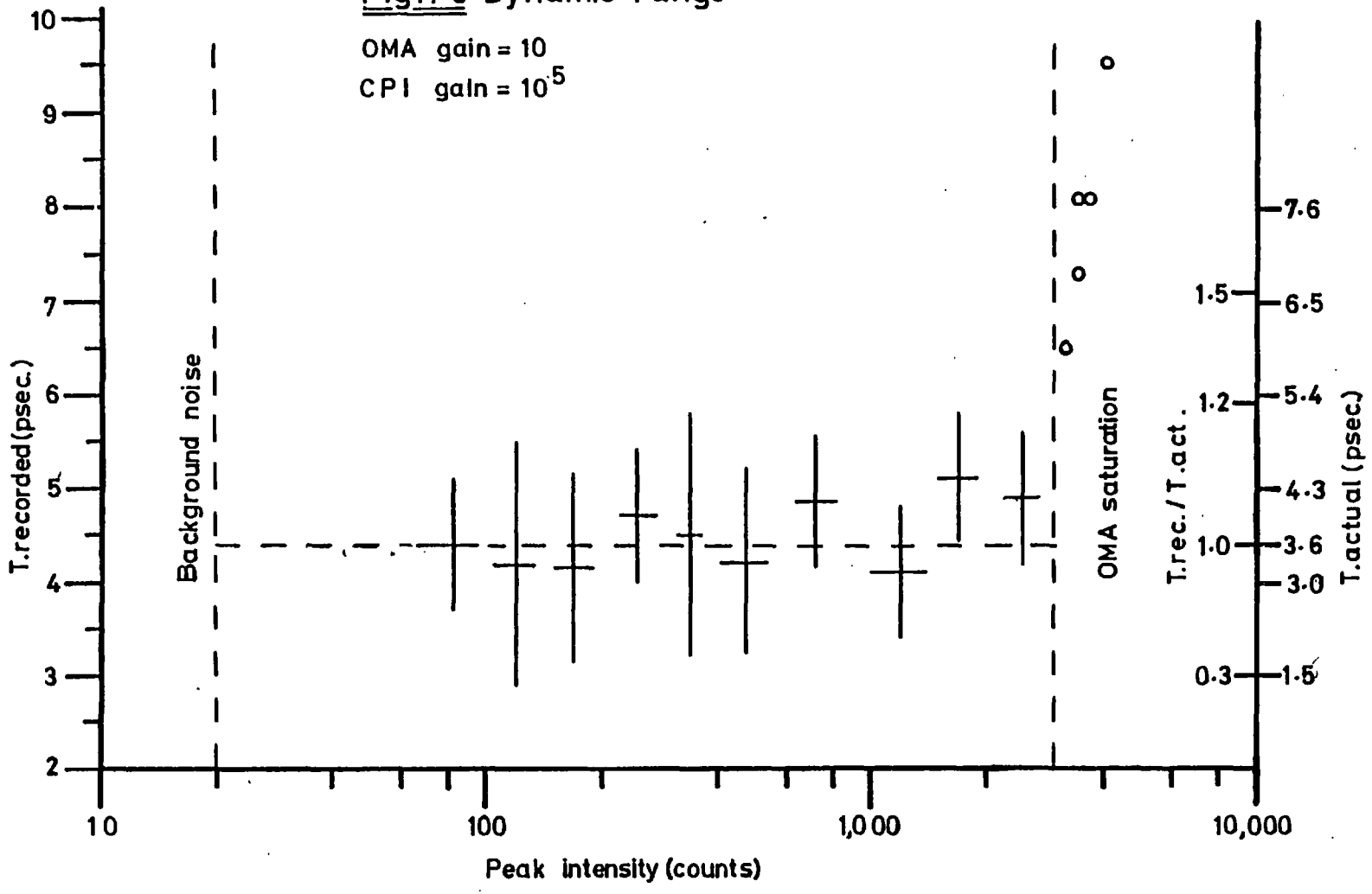

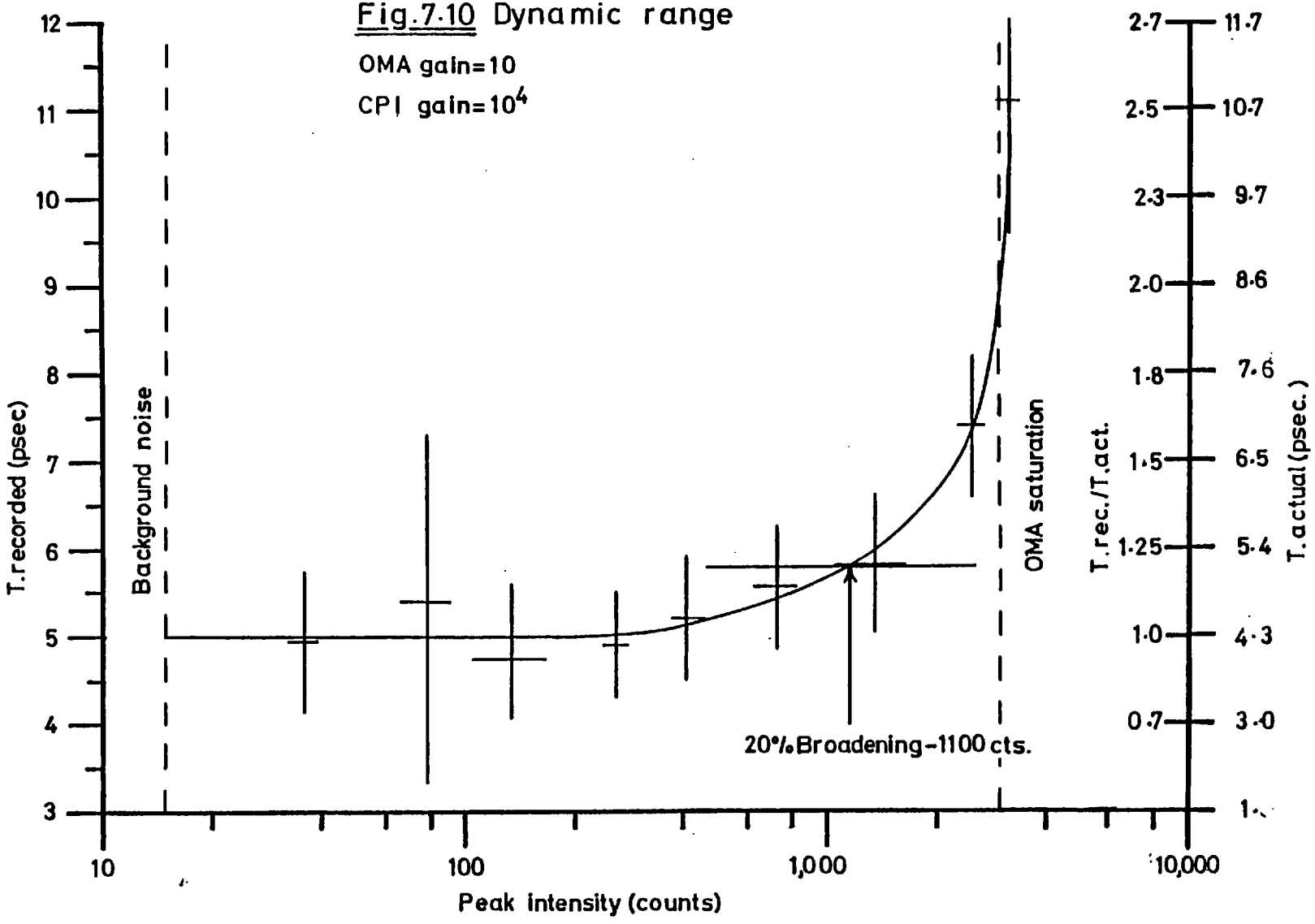
Fig.7.10 Dynamic range
OMA gain=10
CPI gain=10^4
T.recorded (psec)
Background noise
OMA saturation
20% Broadening-1100 cts.
T.rec./T.act.
T.actual (psec.)
Peak intensity (counts)
12
11
10
9
8
7
6
5
4
3
10
100
1,000
10,000
2·7
2·5
2·3
2·0
1·8
1·5
1·25
1·0
0·7
11·7
10·7
9·7
8·6
7·6
6·5
5·4
4·3
3·0

and complexity of the streak camera system, and enables a better appraisal of future systems such as streak tubes with internal silicon targets. It also enables an estimate to be made of the gain of the channel plate image intensifier.

The loss of the channel plate image intensifier means that the slit image at the OMA is increased in size by a factor of 1.5, and that the image is no longer inverted. In order to fill the same proportion of the OMA target as in previous experiments, the size of the active portion of the slit was reduced from 3mm to 2mm (corresponding to 70% of the OMA target). An adjustment to the current flowing in the magnetic deflection coils was also necessary.

Because it was no longer possible to simply remove the OMA and look at the output phosphor of the streak camera in order to obtain synchronisation (due to the much reduced optical gain), prelimary experiments were conducted with a writing speed of only 3×10^9 cm s^{-1} at the streak tube phosphor. Measurement of the static slit width (4 mm on the chart recorder - PR9, 120 mm/sec), indicated an instrument limited time resolution of $\sim$ 4.5 psec.

Using the Canon 50 mm f/1.2 lens pair to couple the OMA to the streak tube, and setting the OMA target gain to $\sim$ 1500 the dynamic range curve shown in Figure 7.11 was obtained for $\sim$ 4.3 psec pulses. The photoelectron current limit occurred at $\sim$ 210 counts, and the background noise was $\pm$ 14 counts indicating a dynamic range of $\sim$ 15.

By comparing Figure 7.10 with Figure 7.11 an estimate of the channel plate gain can be made. An estimate of the relative gains of the two

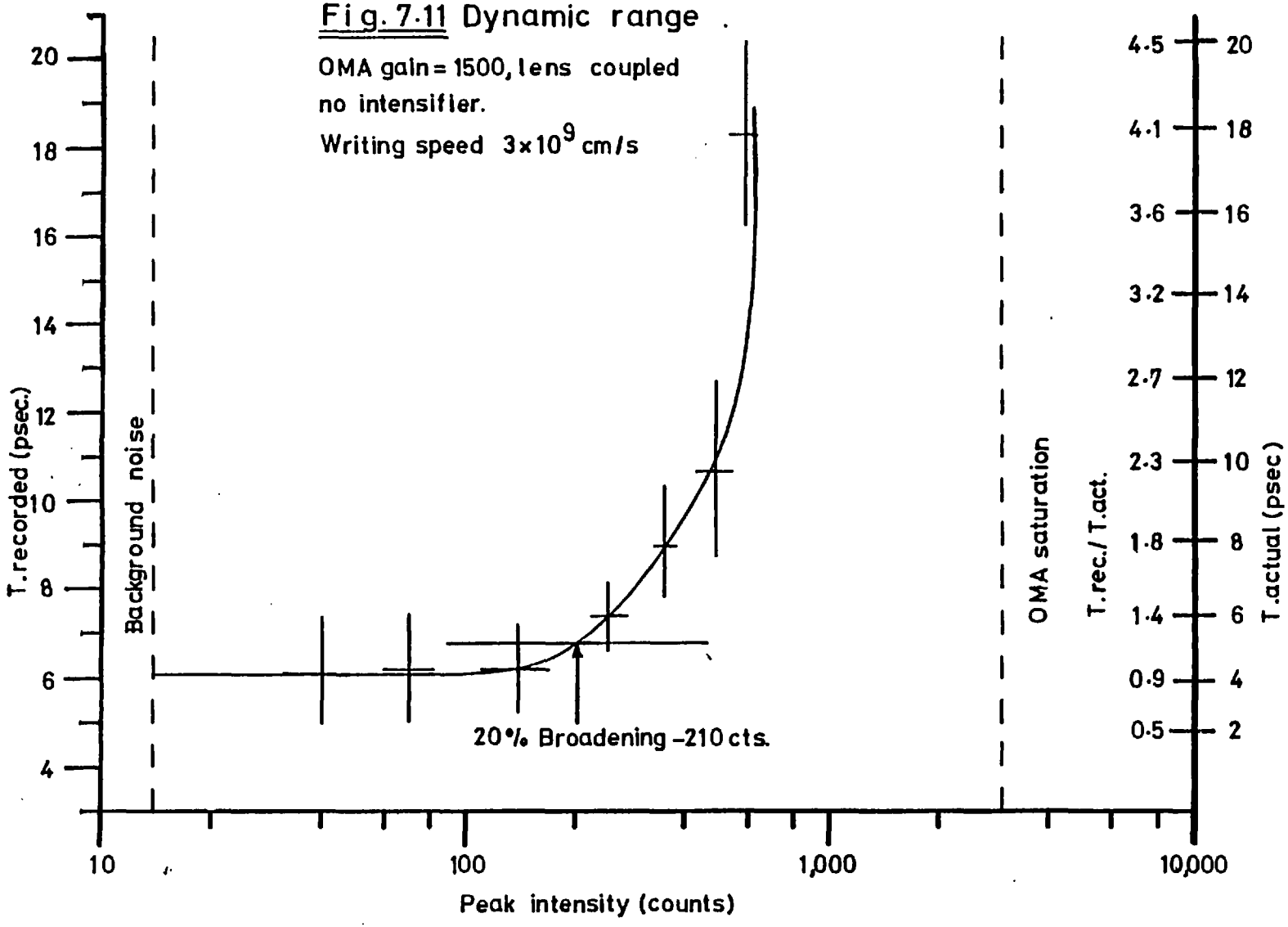
Fig. 7.11 Dynamic range
OMA gain = 1500, lens coupled
no intensifier.
Writing speed 3×10^9 cm/s
T. recorded (psec.)
20
18
16
14
12
10
8
6
4
Background noise
OMA saturation
20% Broadening -210 cts.
T. rec./ T.act.
4·5
4·1
3·6
3·2
2·7
2·3
1·8
1·4
0·9
0·5
T. actual (psec)
20
18
16
14
12
10
8
6
4
2
10
100
1,000
10,000
Peak intensity (counts)

systems, shown diagramatically in Figure 7.12, gives the effective gain of the system including the channel plate image intensifier as being $\sim$ 19 times the gain without it. Comparison of the number of counts corresponding to the streak photoelectron current limit for the two systems indicates a gain ratio of $\sim$ 5. This order of magnitude agreement is well within experimental error, and indicates that the gain of the channel plate image intensifier is indeed $\sim 10^4$ with a channel plate voltage of 1000 V.

The dynamic range of the streak camera was increased by changing from lens coupling to fibre-optic coupling between the streak tube and the OMA. Because the fibre optic faceplate of the SIT Vidicon is $\sim$ 14 mm inside the OMA housing, the fibre optic coupling took place via a 15 mm long 20 mm diameter fibre optic cylinder made from 6 μ m fibres of D14 glass (Teknis Ltd), in contact with both the SIT vidicon and the streak tube. Again an instrument-limited time resolution of $\sim$ 4.5 psec was measured. Measurements of streak camera dynamic range (Figure 7.13) showed that the photoelectron current limit occurred at $\sim$ 850 counts. The background noise was $\pm$ 20 counts, indicating a streak camera dynamic range of $\sim$ 40 for 4.3 psec pulses.

Comparison of the number of counts corresponding to the photoelectron current limit for lens coupling, and for fibre optic coupling show fibre optic coupling to be $\sim$ 4 times more efficient. This indicates that fibre optic coupling is more efficient than had previously been realized, since previous estimates (87) suggested a relative coupling efficiency of only $\sim$ 1.5.

The writing speed of the streak camera was increased to $\sim 6 \times 10^9$ cm s^{-1} at the streak tube phosphor. This corresponds to a writing speed at the

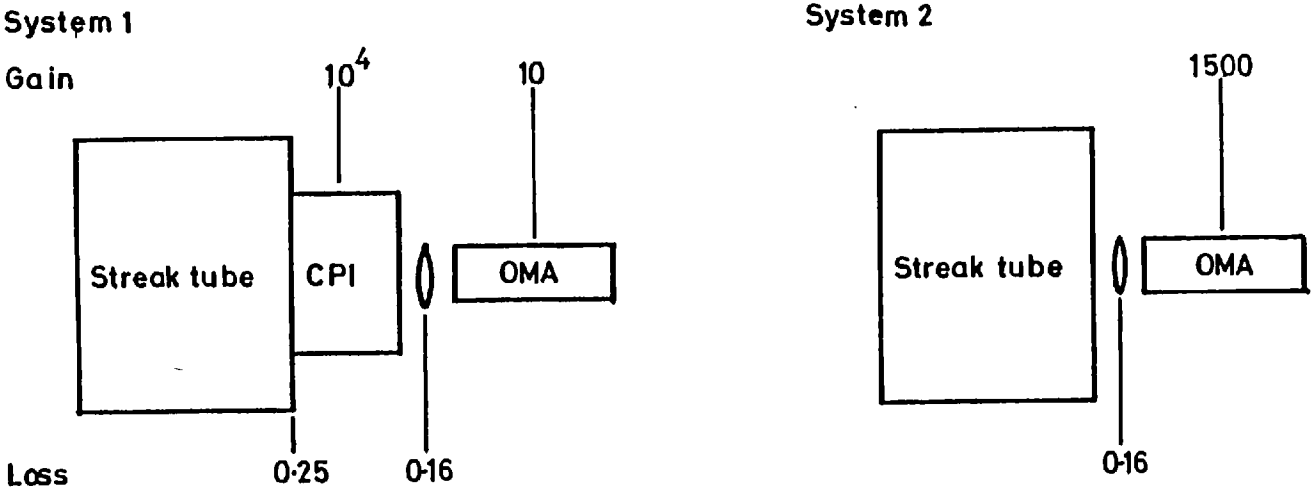

Overall gain	4000	240
Magnification	0·66	1
Writing speed	6×10^9 Cm/S	3×10^9Cm/S
Slit hight	3mm	2mm
Effective gain	4000	210
Gain1/Gain 2	~19	
20% Broadening	1100cts	210cts
Br1/Br2	~5	

Fig.7·12 Channel plate intensifier gain

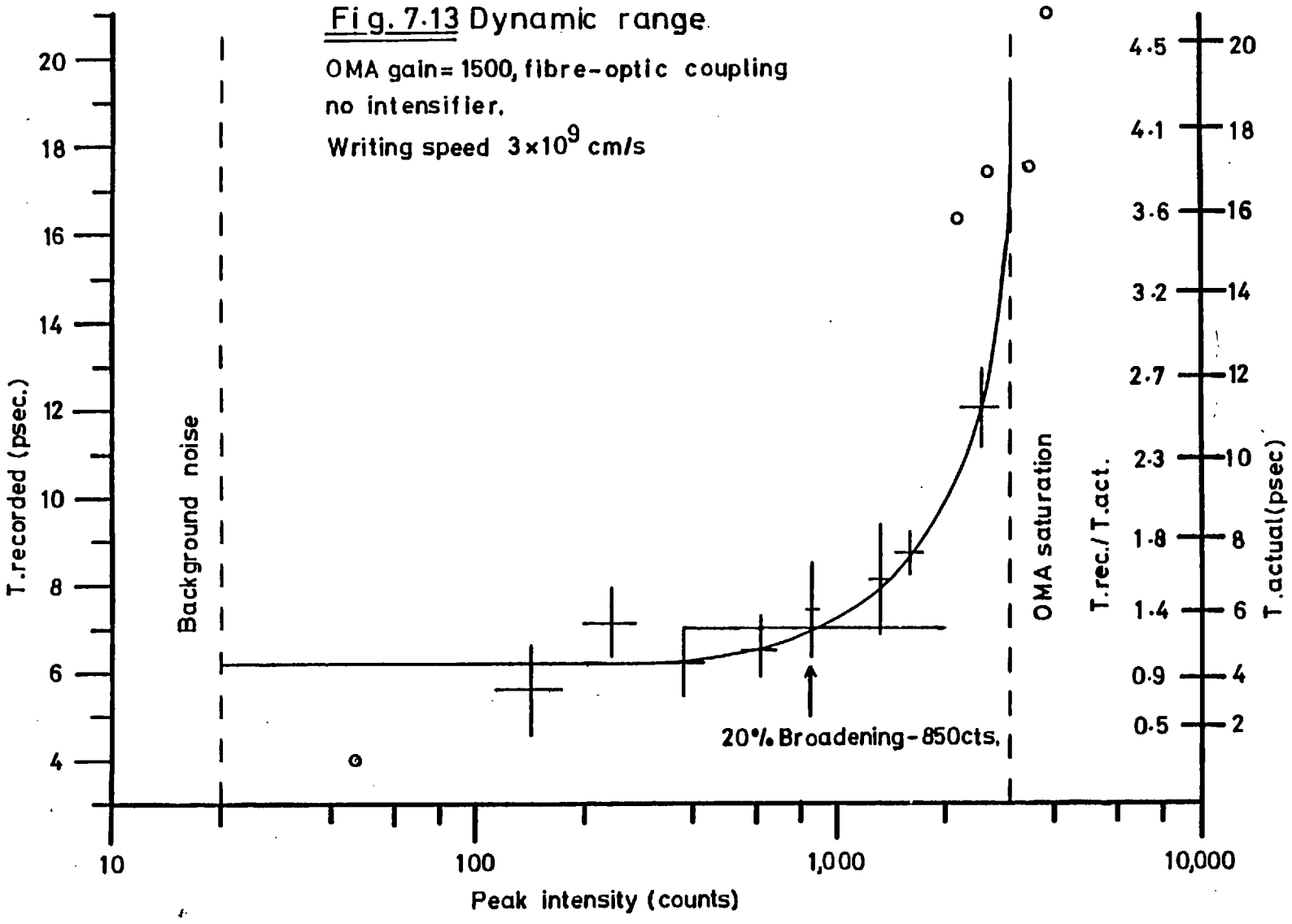
Fig. 7.13 Dynamic range
OMA gain= 1500, fibre-optic coupling
no intensifier.
Writing speed 3×10^9 cm/s
T.recorded (psec.)
Background noise
OMA saturation
20% Broadening - 850cts.
T.rec./T.act.
T.actual(psec)
Peak intensity (counts)
10
100
1,000
10,000
4
6
8
10
12
14
16
18
20
0.5
0.9
1.4
1.8
2.3
2.7
3.2
3.6
4.1
4.5
2
4
6
8
10
12
14
16
18
20

OMA, equal to the writing speed used with the streak camera, when it included an image intensifier (the magnification of the image intensifier being taken into consideration). The time resolution of the streak camera was hence reduced to $\sim$ 2.5 psec. An example of a streak record taken at this writing speed is shown in Figure 7.14. The dynamic range characteristic at this writing speed, for 4 psec pulses, is shown in Figure 7.15. This indicates a photoelectron current limit occurring at $\sim$ 520 counts, and a dynamic range of over 25. Although at first sight this figure appears poor, it should be seen in perspective by realizing that the dynamic range of a typical ultrafast single shot oscilloscope such as the Tektronix 7904 is only of this order.

7.7 Conclusion

A streak camera with a linear readout system has been constructed by coupling a commercial optical multichannel analyser to a Mk.3 Photochron streak camera. Besides introducing total linearity into the system, an improvement in dynamic range ($\sim$150) was achieved but the temporal resolution was reduced to $\sim$ 3 psec.

The high sensitivity of the SIT vidicon detector used enables the removal of the image intensifier, whereupon a time resolution of $\sim$ 3 psec is achieved, and a dynamic range of 25 measured for 4 psec pulses.

Because of the reduced "temporal window" of this system, arising from the small size of the vidicon target, a ramp generator with exceptionally low jitter is required before this system is brought into general usage. The development of a low jitter ramp generator must thus be given a high priority in the further development of this streak camera.

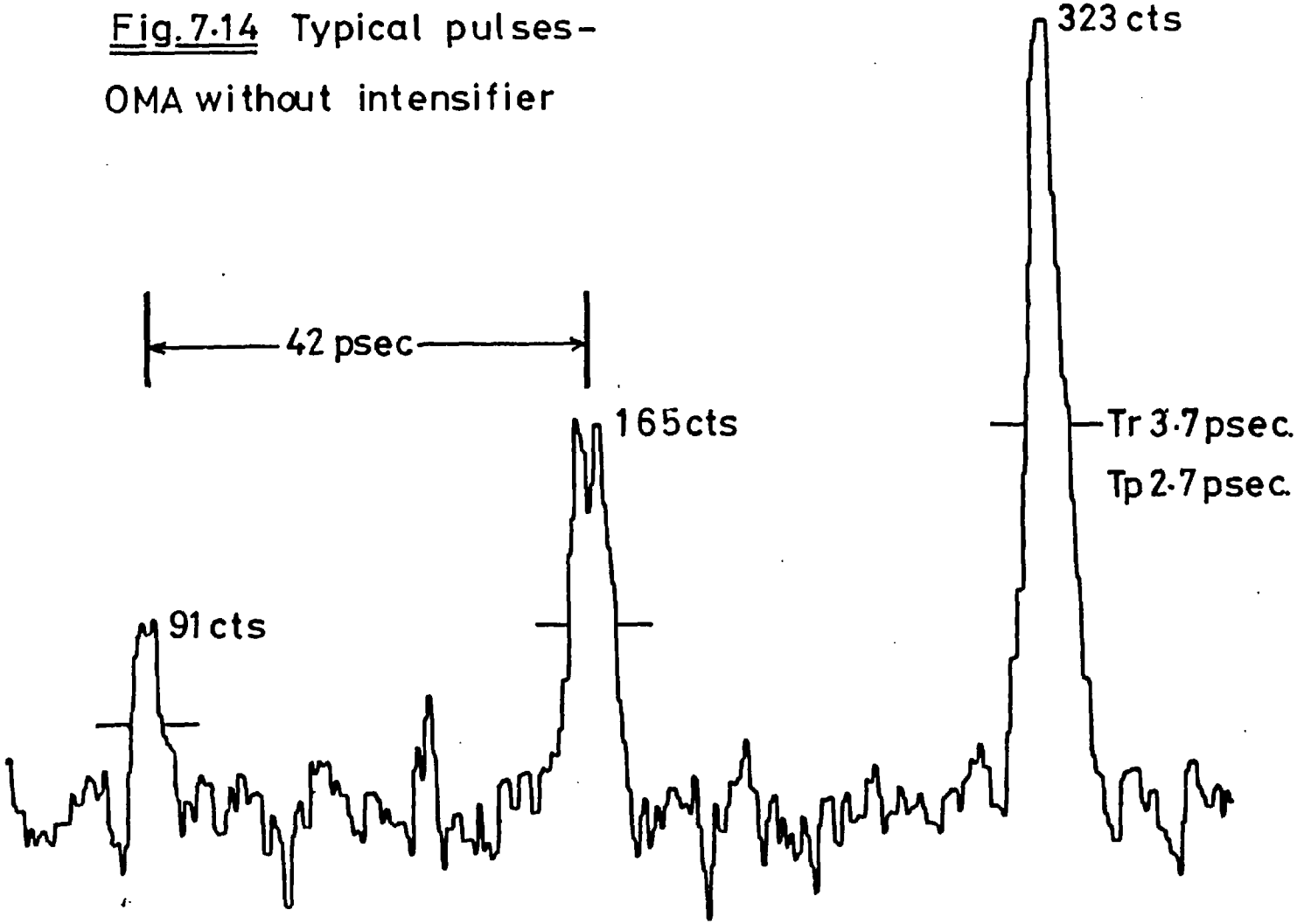

Fig. 7.14 Typical pulses-
OMA without intensifier

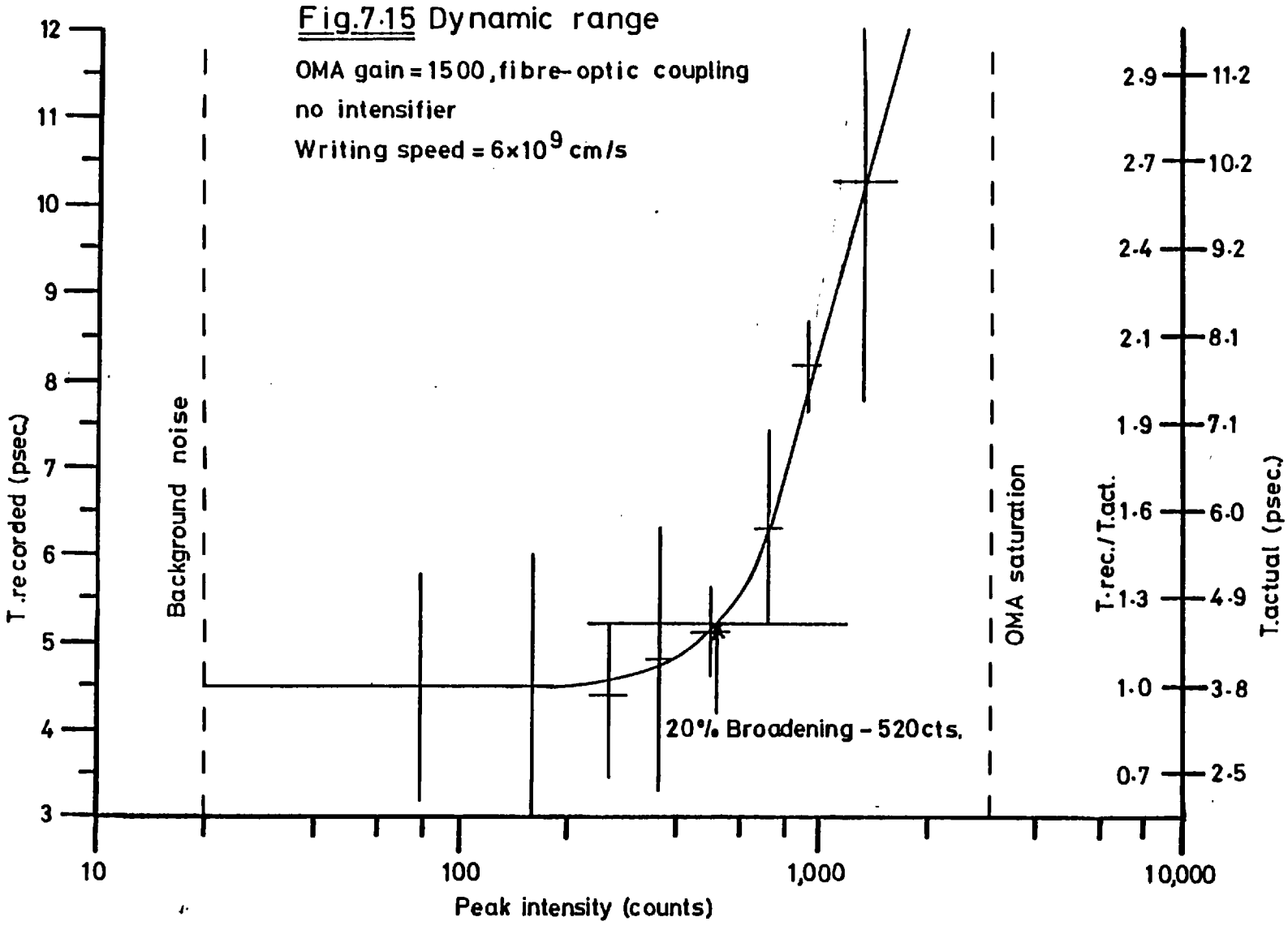
Fig.7·15 Dynamic range
OMA gain = 1500, fibre-optic coupling
no intensifier
Writing speed = 6×10⁹ cm/s
T.recorded (psec.)
12
11
10
9
8
7
6
5
4
3
Background noise
OMA saturation
20% Broadening – 520cts.
T·rec./T.act.
2·9
2·7
2·4
2·1
1·9
1·6
1·3
1·0
0·7
T.actual (psec.)
11·2
10·2
9·2
8·1
7·1
6·0
4·9
3·8
2·5
10
100
1,000
10,000
Peak intensity (counts)

CHAPTER 8

FUTURE DEVELOPMENTS IN PICOSECOND DIAGNOSTICS

8.1 The Ramp Generator

A significant improvement in the performance of the existing types of streak camera could be effected by reducing the jitter in the ramp generator. It has been found that even with a high quality control it is difficult to construct a Krytron based ramp generator with low jitter and a long operational life. The high voltage "semiconductor spark-gap" described by Auston (114) and Lee (116) could however be a suitable alternative. These switches incorporate a transmission line with a break in the signal carrying conductor bridged by a small chip of high resistivity semiconducting material such as silicon or Ga-As. A picosecond pulse from a laser induces conductivity in the semiconductor and thus closes the switch. Using silicon as the semiconductor such switches have been used to generate 10KV pulses in conjunction with an infra-red laser (151), and 1.5 KV pulses in conjunction with a visible laser (149). Risetimes as short as 25 psec have been demonstrated for this type of device. These voltages are perfectly adequate for use as a ramp generator in an ultrafast streak camera, and the devices are expected to have a low jitter.

There is an increased interest in the use of electronic readout devices in conjunction with these cameras (c f Chapter 7). Since these devices usually have a small window area, there is good reason to design new streak tubes having smaller phosphor-screen diameters ($\sim$ 15 - 25 mm). Under

these circumstances the deflection plates could be moved closer together increasing the deflection sensitivity of the tube to $\sim$ 100V cm^{-1}, whereupon a linear ramp voltage of $\sim$ 150V would be adequate.

Experiments have shown that it is comparatively easy to build an Auston switch with an output of 100V. These would be suitable for a reduced scan streak tube, or as a driver for a high voltage scan system, until a high voltage Auston switch becomes available. A more conventional ramp generator employing a tunnel diode trigger has been built by Cunin etal (143). This circuit has a jitter of $\sim$ 24 psec. It is possible however that a simple low voltage Auston switch could replace the complicated triggering stages used in this circuit.

A further improvement in streak tube deflection sensitivity may be possible by the introduction of travelling wave deflection (a system in which the deflection voltage follows the electrons down the streak tube - 152). Before this is implimented however the shape of the electron bunch as it passes through the deflection plates will have to be studied, since the time taken by the deflecting wave to traverse the electron bunch represents a fundamental limit to the time resolution of the streak tube.

8.2 Readout Systems

Although it is possible to reduce the size of the streak camera by introducing an internal channel plate gain stage (150) this would result in a streak tube with a higher noise figure. The noise figure is increased because the detection efficiency of a phosphor is $\sim$ 4 times that

of a channel plate. It is thus desirable to either retain the phosphor, or to use an electron detector with a high detection efficiency. The silicon diode matrix used as the target in a silicon vidicon is one such detector. Although the results obtained in Chapter 7 suggest that an internal silicon target may not be sufficiently sensitive, substantial advances have been made since this OMA was designed. Although the introduction of an internal silicon target would represent a technological improvement to the streak camera, from a production point of view it might be better to retain the phosphor, and use a commercial vidicon as a photon detector.

An alternative to a vidicon as a readout device is one of the solid-state arrays that are currently being developed. A thorough study of the comparative merits of the two systems is required before either is extensively developed.

8.3 The Streak Tube

Efforts to improve the streak tube are principally directed at reducing its size and cost, and improving its spatial resolution. Some form of scaling may reduce the size of the existing tube, although it may be necessary to adopt a different geometry such as that of the Pico-X tube.

An improvement in the spatial resolution of the system would both improve the time resolution of the tube, and its dynamic range. Efforts to improve the spatial resolution should however relate appropriately to the spatial resolution of both the image intensifier and the readout system capabilities.

If a time resolution of less than 0.5 psec is sought, the cathode-mesh structure will have to be redesigned, to further reduce the electron transit-time spread. Even at 0.5 psec a dynamic range of only 7 is to be expected, and an improved dynamic range would also be required. Efforts to improve the dynamic range should be directed as much to the photoelectron detection system as to the streak tube itself.

A redesigned cathode-mesh structure may well eliminate curvature of the streak image (caused by electrons off axis taking longer to reach the deflection plates than those on axis). This would be of great benefit when a vidicon was used as a readout device, since it would be possible to integrate the output signal over a long slit, and magnetic deflection within the streak tube would no longer be necessary (c f Chapter 7).

8.4 The Synchroscan System

Although the work described in this thesis has been restricted to the single-shot streak camera, some reference should be made to the synchroscan streak camera system (153). This type of streak camera, designed for use in conjunction with a modelocked CW laser, repeatedly overwrites the recorded streak image. No image intensifier is required, and a high dynamic range is to be expected. Although due to jitter in the deflection voltage the best time resolution so-far achieved is only $\sim$ 10 psec this type of camera may ultimately be capable of an extremely good dynamic range at very high time resolution.

8.5 Conclusion

These are probably the most significant areas where future development of streak cameras will be concentrated. During the next few years it would be reasonable to expect to have streak cameras with a dynamic

spatial resolution of >20 lp/mm, temporal resolution approaching 10^{-13} sec, and exhibiting complete linearity of both response and display.

APPENDIX I

ESTIMATE OF PHOTOELECTRON ENERGY DISTRIBUTIONS

The two principle methods by which photoelectrons loose energy prior to emission are lattice scattering and pair production (39). In the case of lattice scattering the energy loss per collision is small (typically 0.005 - 0.01 eV), because of the large difference in mass between the electron and the atoms of the crystal. When the excited electron has sufficient energy it can create a second electron - hole pair, loosing energy equal to or greater than the bandgap energy Eg. Typically the threshold for pair production will be ~ 3 Eg. Figure A 1.1 shows the form of the photoelectron energy distribution for these energy loss processes, and Table A1 lists the characteristics of the more common photocathodes.

At wavelengths above the pair production threshold, the energy distribution is normally gaussian like, with the average energy (Eav) corresponding to about half the maximum energy (Emax), i.e.

$$Eav \sim \frac{Emax}{2} \sim \frac{(h\nu - Eo)}{2}$$

where $h\nu$ is the photon energy. Comparing experimentally derived curves (26 - 31) with the gaussian probability function leads to the rough estimate that the halfwidth of the energy distribution (Δ E) is given

(a) Energy loss to lattice only

$h\nu \gtrsim 3E_g$

$E_{max} \simeq h\nu - E_o$

E_o = threshold

$E_{av} \simeq (h\nu - E_o)/2$

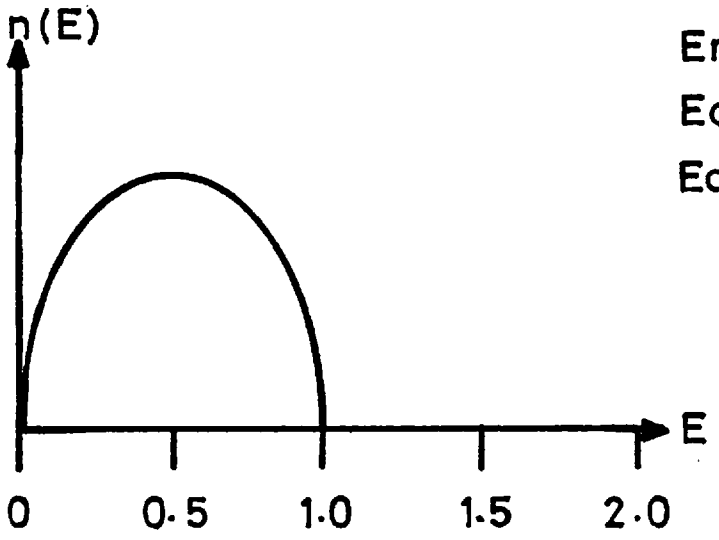

(b) Energy loss to pair-production and to lattice

$h\nu \gtrsim 3E_g$

$E_{max} \simeq h\nu - E_o$

$E_{av} \simeq 0.5$ eV

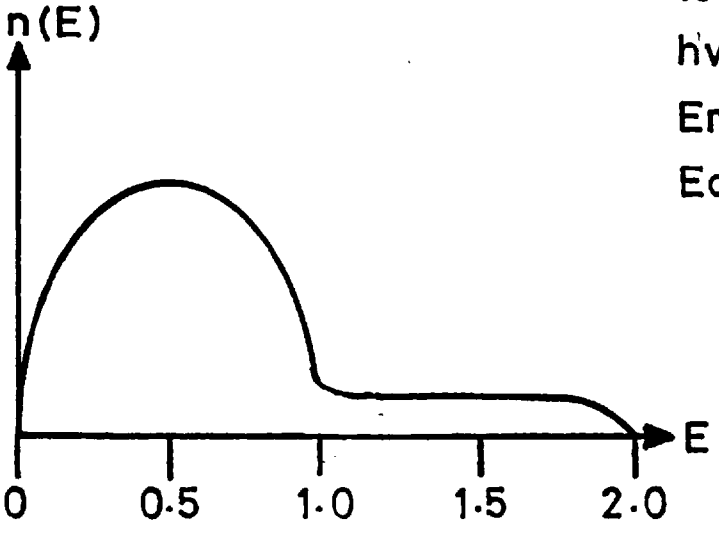

Fig. A1·1

Table A1

Cathode type		Eg	Ea	Pair production threshold	Threshold wavelength
S 1	Ag - O - Cs	0.3 ? eV	0.7 ? eV		1200 nm
S 11	Cs_3Sb on MnO	1.6 eV	∿0.45 eV	2.0 eV	650 nm
S 20	(Cs)Na_2KSb	1.0 eV	0.55 eV	3.0 eV	870 nm
Cs_2Te		Eg + Ea = 3.5 eV		> 7 eV	350 nm

by

$$\Delta E \sim \frac{E_{max}}{2}$$

From the above we can hence estimate the electron energy distribution for an S20 photocathode operating at 600 nm (2.05eV) (corresponding to the combination of the most sensitive wideband photocathode suitable for picosecond pulse measurement, and a modelocked R6G dye laser operating at its optimum wavelength). The threshold wavelength of an S20 is $\sim$ 870 nm (1.43eV), leading to estimates of $E_{av} \sim \Delta E \sim 0.3$ eV.

At wavelengths well below the pair production threshold, the average photoemission energy is to first order independent of wavelength. By examining the published experimental curves we can estimate $E_{av} \sim$ 0.5eV, $\Delta E \sim$ 1.0eV (26) in the case of the antimony based photocathodes, and $E_{av} \sim$ 0.25eV, $\Delta E \sim$ 0.5eV in the case of the S1 photocathode (31).

At intermediate wavelengths, the distribution broadens, and a better approximation becomes $\Delta E \sim E_{max}$, although this is always a rather pessimistic estimate.

GENERAL CONCLUSION

The range of wavelengths over which a Photochron 2 streak camera is sensitive has been extended into the VUV. This camera has been tested at 200 nm and was shown to have picosecond resolution. The camera was reduced in size by fibre-optically coupling a channel-plate image intensifier to its output. This camera has been thoroughly tested both statically and dynamically and has been shown to possess adequate diagnostic capabilities such that experiments requiring good time resolution and a high dynamic range have been successfully carried out. With the use of a commercial vidicon system the camera now has an entirely linear output as a function of both time and intensity. It has been shown that it is possible to extend the dynamic range of the camera by using it instead of recording film, or at the cost of dynamic range to dispence with the image intensifier.

REFERENCES

1. D J Bradley, F O'Neill
Journ. Opto-Elect. 1, 69, (1969)

2. E G Arthurs, D J Bradley, A G Roddie
Appl. Phys. Lett. 20, 3, (Feb 1972)

3. J R Taylor
Ph.D Thesis, The Queens University of Belfast (1974).

4. P R Bird, D J Bradley, W Sibbett
Proc. 11th Int. Cong. High Speed Photog., 112, (1974)

5. W Sibbett
Ph. D Thesis, The Queens University of Belfast (1973)

6. R S Adrain et al.
Optics Comm. 12, 136, (1974)

7. E P Ippen, C V Shank, A Dienes
IEEE J. Quant. Elect. QE-7, 178, (1973)

8. J Weber
Phys. Letts. 37A, 179, (1971)

9. J Weber
Phys. Letts. 45A, 35, (1973)

10. S A Tuccio, F C Strome
Appl. Optics 11, 64, (1972)

11. English Electric Valve Co
Hydrogen Thyratron Product Data (1972)

12. E G and G
Triggered Spark Gap Product Data (1974)

13. B B Snavely, F P Schafer
Phys. Letts. 28(a), 728, (1969)

14. F P Schafer, L Ringwelski
Zeit. Naturforsch 28(a), 792, (1973)

15. E G Arthurs, D J Bradley, A G Roddie
Appl. Phys. Lett. 19, 480, (1971)

16. D J Bradley, B Liddy, W E Sleat
Optics Comm. 2, 391, (1971)

17. E G Arthurs et al
Proc. 10th Int. Cong. High Speed Photog., 117, (1972)

18. D J Bradley
Methods of Generating Picosecond Light Pulses
(Ultrashort Light Pulses, Ed. S L Shapiro
Pub. Springer - Verlag (1977))

19. D J Bradley, W Sibbett
Appl. Phys. Lett. 27, 382, (Oct 1975)

20. D J Bradley, M H Key, J F Higgins
Appl. Phys. Lett. 16, 53, (1970).

21. A E Huston
Adv. in Elect. and Elect. Phys. 22B, 957, (1966)

22. W Sibbett
Private Communication

23. N Ahmad, B C Gale, M H Key
Adv. in Elect. and Elect. Phys. 28B, 999, 1969

24. B Liddy
Ph. D Thesis, The Queens University of Belfast (1971)

25. J D McGee
Photoelectronic Imaging Devices Ed.
Biberman and Nudelmand Pub. Plenum Press
Vol.2 Ch.6, 133, (1971)

26. W E Spicer
Phys. Chem. Solids 22, 365, (1961)

27. E Taft, L Apker
J Opt. Soc. America 43, 81, (1953)

28. E Taft, H Phillips
Phys. Rev. 115, 1583, (1959)

29. L Apker, E Taft, J Dickey
J. Opt. Soc. America 43, 78, (1953)

30. K S Neil
Ph. D Thesis, Southampton University (1968)

31. M Schelev, M Richardson, A Alcock
Rev. Sci. Inst. 43, 1819, (1972)

32. Leder, Simpson
Rev. Sci. Inst. 29, 571, (1958)

33. D J Bradley
U.K. Patent Spec 31167/70 (1970);
U.S. Patent 3761614 (1973)

34. Field Analysis ed D Vitkovitch
Pub. Van Nostrand (1966)

35. C Weber
Philips Res. Rep. Supp. 6, (1967)

36. V V Korobin, A A Maljutin, M Ya. Schelev
J. Photo. Sci. 17, 179, (1969)

37. E M Gordeev, S D Fanchenko
Inst. and Exptl. Tech. 19, 533, (1976)

38. V S Bulggin, Yu A Drozhbin, B M Stepanov
Sov. Phys. Tech. Phys. 21, 479, (1976)

39. W E Spicer, F Wooten
Proc. IEEE 8, 1119, (1963)

40. E K Zavoisky, S D Fanchenko
Appl. Optics 4,1115, (1965)

41. D J Bradley et. al.
Adv. in Elect. and Elect. Phys. 33B, 1145, (1972)

42. J R Taylor, W Sibbett, A J Cormier
App. Phys. Lett. 31, (Aug 1977)

43. S J Caughey
Ph. D Thesis, The Queens University of Belfast (1970)

44. H Kuroda, H Masuko, S Maekawa
Optics Comm. 18, 169, (1976)

45. D J Bradley, W Sibbett
Optics Comm. 9, 17, (1973)

46. P R Bird, D J Bradley, W Sibbett
Adv. in Elect. and Elect. Phys. 40a, 51, (1976)

47. W Friedman et. al.
Proc. 12th Int. Cong. High Speed Photog. 544, (1977)

48. W E Sleat
Ph. D Thesis, The Queens University of Belfast (1974)

49. G D Baldwin, E P Riedel
J. App. Phys. 38, 2726, (1967)

50. A Rose
Vision : human and electronic, Plenum Press, 20, (1973).

51. Informal Discussion on Dynamic Range
P 557, Ref. 47

52. S W Thomas, G E Phillips
P11, Ref. 47

53. S Majumdar
P24, Ref. 47

54. V V Krobkin, A A Malyutin, M Ya. Schelev
Proc. 9th Int. Cong. High Speed Photog., 232, (1970)

55. W Sibbett
P48, Ref. 5

56. K Jones
Private Communication

57. S W Thomas, G R Tripp, L W Colman
Adv. in Elect. and Elect. Phys. 40a, 451, (1976)

58. N Fleurot et al
P549, Ref. 47

59. E Lill, S Schneider, F Dorr
Optics Comm. 22, 107, (1977)

60. T R Royt, C H Lee, W L Faust
Optics Comm. 18, 108, (1976)

61. J P Ryan
Ph. D. Thesis London University (1978)

62. E Lill, S Schneider, F Dorr
App. Phys. 14, 399, (1977)

63. N Frigo, T Daly, H Mahr
IEEE J Q Elect. QE-13, 101, (1977)

64. E G Arthurs et al
Chem. Phys. Lett. 22, 230, (1973)

65. E G Arthurs, D J Bradley, A G Roddie
App. Phys. Lett. 23, 88, (1973)

66. G H C New, D H Rea
J. App. Phys. 47, 3107, (1976)

67. G H C New
IEEE J Q Elect. QE-10, 115, (1974)

68. Rentzepio
Chem. Phys. Lett. 2, 117, (1968)

69. Chuang, Eisenthal
J Chem. Phys. 59, 2140, (1973)

70. R K Jain, J P Heritage
App. Phys. Lett. 32, 41, (1978)

71. T R Royt, C H Lee
App. Phys. Lett. 30, 332, (1977)

72. T R Royt et al
App. Phys. Lett. 25, 514, (1974)

73. E G Arthurs, D J Bradley, A G Roddie
App. Phys. Lett. 20, 125, (1972)

74. E G Arthurs, D J Bradley, A G Roddie
App. Phys. Lett. 23, 88, (1973)

75. H Kuroda, S Shionoya
Optics Comm. 10, 74, (1974)

76. G A Boiko et al
Phys. Stat. Sol. (B) 85, 111, (1978)

77. P Schagen, H Bruining, J C Franken
Philips Res. Rep. 7, 119, (1952)

78. P Schagen
Adv. Image Pickup and Display Ed. B Kazan
Pub. Academic Press, 1, 58, (1974)

79. P Schagen, J Adams, B W Manley
Brit. Patent No. 1175599 (1967)

80. Commercial Literature from Mullard Ltd and from EMI Ltd.

81. M Aslam
Ph. D Thesis, London University (1965)

82. R.C.A Electro-Optics Handbook. 216, (1974)

83. W Sibbett and K Jones
Private Communication

84. C Weber
Philips Res. Rep. Supp. 6, (1967)

85. A J Guest
Acta Electronica 14, 79, (1971)

86. J D McGee et al
Adv. in Elect. and Elect. Phys. 22A, 113, (1966)

87. J Weber, Princeton Applied Research
Private Communication

88. G H C New
Optics Comm. 19, 117, (1976)

89. J N Elgin, G H C New
To be published

90. R B Miles, S E Harris
IEEE J. Quant. Elect. QE-9, 470, (1971)

91. A H Kung, J F Young, S E Harris
App. Phys. Lett. 27, 390, (1975)

92. R R Alfano, S L Shapiro
Phys. Rev. Lett. 24, 584, (1970)

93. A H Sommer
Photoemissive Materials, Pub. J Wiley (1968)

94. R Y Chiao, P L Kelley, E Garmire
Phys. Rev. Lett. 17, 1158, (1966)

95. M Matsouka, H Nakatsuka, J Okado
Phys. Rev. A12, 1062, (1975)

96. T R Royt, C H Lee, W L Faust
9th Int. Conf. Quant. Elect. Amsterdam (1976)
Reported at conference but not in abstract

97. J F Ward, G H C New
Phys. Rev. 185, 57, (1969)

98. D M Bloom et al
App. Phys. Lett. 26, 687, (1975)

99. D M Bloom, J F Young, S E Harris
App. Phys. Lett. 27, 390, (1975)

100. H Puell, G R Vidall
Optics Comm. 18, 107, (1976)

101. J R Taylor
Optics Comm 18, 504, (1976)

102. A I Ferguson, E G Arthurs
Phys. Lett. 58A, 298, (1976)

103. D M Bloom
App. Phys. Lett. 26, 687, (1975)

104. C R Vidal, J Cooper
J. App. Phys. 40, 3370, (1969)

105. P Dooley et al
P80, Ref. 47

106. S W Thomas, G R Tripp, L W Coleman
Adv. in Elect. and Elect. Phys. 40A, 451, (1976)

107. K B Eisenthal
P275, Ref.18

108. A J Campillo, S L Shapiro
P317, Ref. 18

109. D von der Linde
P204, Ref. 18

110. G I Bryakhnevitch et al
P17, Ref. 47

111. W D Friedman
P228, Ref. 4

112. C Loty
Acta Electronica 14, 107, (1971)

113. Image Tubes and Devices
Thampson - C.S.F. (1975)

114. D H Auston
P123, Ref. 18

115. D H Auston
App. Phys. Lett. 26, 101, (1975)

116. C H Lee
App. Phys. Lett. 30, 84, (1977)

117. Laser Program Annual Report - 1976
Lawrence Livermore Laboratory

118. H W Mocker, R J Collins
App. Phys. Lett. 7, 270, (1965)

119. A J DeMaria, D A Stetser, H Heynau
App. Phys. Lett. 8, 174, (1966)

120. E G Arthurs, D J Bradley, A G Roddie
Chem. Phys. Lett. 22, 230, (1973)
Optics Comm. 8, 118, (1973)

121. E G Arthurs et al
Optics Comm. 12, 360, (1974)

122. E G Arthurs et al
Optics Comm. 12, 136, (1974)

123. A Scavnnec
Optics Comm. 20, 335, (1977)

124. G H C New
To be published

125. V S Letoklov
Soviet Phys. JETP 28, 562, (1969)
Soviet Phys. JETP 28,1026, (1969)

126. J A Fleck
App. Phys. Lett. 12, 178, (1968)

127. J A Fleck
Phys. Rev. B 1, 84, (1970)

128. F De Martini et al
Phys. Rev. 164, 312, (1967)

129. R S Adrain
Ph. D Thesis, The Queens University of Belfast (1972)

130. I S Ruddock, D J Bradley
App. Phys. Lett. 29, 296, (1976)

131. C V Shank, E P Ippen
App. Phys. Lett. 24, 373, (1974)

132. J A Giordmaine et al
App. Phys. Lett. 11, 216, (1967)

133. H P Weber
J. App. Phys. 38, 2231, (1967)

134. M M Butslov et al
Proc. 4th Int. Cong. High Speed. Photog. 230, (1958)

135. Bradley et al
Optics Comm. 15, 231, (1975)

136. R Dupuy et al
P62, Ref. 47

137. G Clement, C Loty, J P Roux
P130, Ref. 4

138. C B Johnson et al
P56, Ref. 47

139. A J Lieber et al
P194, Ref. 47

140. K F Etherington
Mullard Tech. Comm. 136, 227, (1977)

141. Baum
Adv. in Elect. and Elect. Phys. 16, 391, (1962)

142. Hadland-Photonics Ltd, Bovingdon, Herts
Private Communication

143. B Cunin et al
P3, Ref. 47

144. A Liebing, P Mengel, W Ruppel
Phys. Stat. Sol. (B) 72, 431, (1975)

145. D Segall, G D Mahan
Phys. Rev. 171, 935, (1968)

146. E F Gross et al
Soviet Phys. Solid State, 8, 1180, (1966)

147. T Fisher, J Bille
J. App. Phys. 45, 3937, (1974)

148. Optical Industries Inc, Santa Ana
California - Catalogue

149. P Le Fur, D H Auston
App. Phys. Lett. 28, 21, (1976)

150. Hamamatsu Corporation Japan
Technical Specification

151. A Antonetti et al
Optics Comm. 23, 435, (1977)

152. C De Vere
Cathode-Ray Tubes, Tektronix Inc
Circuits Concepts Series (1967)

153. M C Adams, D J Bradley, W Sibbett
To be published.

ACKNOWLEDGEMENTS

I wish to thank Pro fessor D J Bradley, my supervisor, for his helpful advice and guidance during the course of this work.

I would also like to gratefully acknowledge the advice and assistance of all the members of the Laser Physics Group at Imperial College, particularly Drs. W Sibbett, J R Taylor and T H Williams.

I would like to thank academic visitors Proffessor V S Dneprovskii (Moscow State University) and Dr. E Lill (Munchen Technische Universitut) in conjunction with whom the experiments described in Chapter 6 were carried out.

I am grateful to the technical staff of the Physics Department at Imperial College for help in the design and construction of the apparatus used in these experiments, and to Mr N Jackson and Mrs B Bolt of the Photographic Section for their advice and assistance with the photography. I am also indebted to Mrs D Onslow for typing this thesis.

Finally I would like to thank my wife Jean for her unselfish tolerance and patience during the writing of this thesis.

PUBLICATIONS

SESSION L: NONLINEAR OPTICS II (vapors)

Chairman: Dr. R.C. Smith
The University, Southampton, UK

L1 SATURATION EFFECTS IN THIRD-HARMONIC GENERATION IN PHASE-MATCHED Rb–Xe MIXTURES

H. PUELL and C.R. VIDAL
Max-Planck-Institut für Extraterrestrische Physik, Garching, Fed. Rep. Germany

Third-harmonic generation in phase-matched Rb–Xe mixtures has been performed using 7 psec pulses of a mode locked Nd : glass laser with peak powers up to 200 MW. Maximum energy conversion efficiencies of 2% have been achieved, focusing the fundamental light beam with a confocal parameter of 47 cm into a concentric heat pipe filled with 1 torr Rb and 372 torr Xe over a length of 28 cm. At input intensities $\Phi_1 > 5 \times 10^{10}$ W/cm^2 the obserbed energy conversion was significantly smaller than expected from theory [1].

Detailed numerical calculations have shown that at these intensity levels the phase-matching condition is destroyed by an intensity dependent change of the refractive index of Rb. At an input intensity of 2×10^{11} W/cm^2, for instance, the second order Kerr-effect associated with the ground state of Rb gives rise to a mismatch of the wavevectors of the fundamental and the harmonic wave of $\Delta k = 3k_1 - k_3 = 2.3$ cm^{-1}. This large mismatch is reduced to $\Delta k = 1.7$ cm^{-1} by a population of the first excited 5P- and 4D-levels, which show different refractive indices and Kerr-constants with respect to the ground-state. Taking this into account, numerical calculations of the generated third harmonic energy show good agreement with the experimental results for input intensities up to 2×10^{11} W/cm^2.

It should be noted that, although the fundamental frequency is far off from the transition frequency to the 5P-level, a population of 4% is achieved by a transient excitation which is independent of the transition linewidth. This excitation results from the temporal variation of the incident field amplitude, which is fast compared to the energy relaxation rate of the 5P-level. It can be evaluated on the basis of the adiabatic following approximation or from a perturbation approach. A similar transient two-photon excitation is responsible for a population of 9% of the 4D-level.

The observed break-up of the phase-matching can be avoided to some extent by readjusting the Rb–Xe pressure ratio in such a manner that the initial mismatch compensates the intensity dependent changes of the refractive index close to the moment of maximum input intensity. For $\Phi_1 = 2 \times 10^{11}$ W/cm^2 our numerical calculations show that optimum phase-matching occurs at an initial mismatch of $\Delta k = -0.5$ cm^{-1}, corresponding to a pressure ratio of 1 torr Rb to 465 torr Xe. As a result an energy conversion efficiency of 11% is expected.

Due to the relatively large nonlinear refractive index of Rb ($n_2 \simeq 3.6 \times 10^{-31} N_0$ esu) the critical power for self-focusing becomes rather small (3×10^7 W). Nevertheless, self-focusing within the nonlinear medium can be avoided by increasing the beam diameter. In this case, however, the input power has to increase with the square of the input intensity and may become enormous. For our experimental conditions, for instance, an intensity of 10^{12} W/cm^2 requires an input power of 4×10^{11} W.

An upper limit to the input intensity is finally established by the multiphoton ionization. Estimates of the ionization probabilities showed that for $\Phi_1 > 10^{11}$ W/cm^2 the two-photon ionization of the 4D-level is nearly instantaneous. Together with the transient two-photon excitation of the 4D-level this leads to a considerable depletion of the ground-state at an intensity level of 5×10^{11} W/cm^2. As a result, the nonlinear medium is momentarily destroyed and generation of third harmonic radiation ceases.

Considering the limitations imposed on the third harmonic generation, the experimental conditions can be optimized by varying the length and the particle densities of the nonlinear medium. Model calculations indicate that energy conversion efficiencies of the order of 25% should be feasible.

Reference

[1] H. Puell and C.R. Vidal, Laser Spectroscopy, Proc. of the 2nd Int. Conf. Megève, 1975, eds. S. Haroche, J.C. Pebay-Peyroula, T.W. Hänsch and S.E. Harris (Springer Berlin, 1975) p. 461.

L2 THIRD-HARMONIC GENERATION OF PICOSECOND PULSES IN CALCIUM VAPOUR

W. SIBBETT, D.J. BRADLEY and S.F. BRYANT
Optics Section, Physics Department, Imperial College, London SW7 2BZ, UK

Detailed studies have been carried out of third-harmonic generation (~200 nm) in calcium vapour by picosecond pulses from a mode-locked dye laser. Unlike earlier investigations carried out with a mode-locked neodymium laser [1,2] in our experiments we have been able to tune close to a two-photon resonance

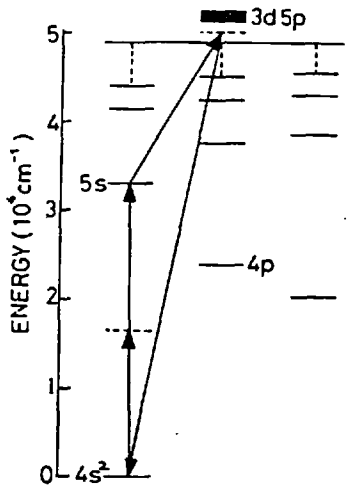

Fig. 1. Term-level diagram of calcium showing four-wave mixing resonance.

(fig. 1) so as to investigate the effects of resonant enhancement, saturation and the optical-frequeney Stark effect.

The picosecond pulses generated in a passively mode-locked flashlamp-pumped Rhodamine 6G dye laser [3] had durations of ~2 psec with energy ~50 μJ. Amplification to peak powers of ~300–400 MW was obtained in passing through a dye laser amplifier [4]. The whole pulse train was focussed, by a 30 cm focal length lens, into the centre of the 20 cm zone of calcium vapour, contained in the inner chamber of a concentric heat-pipe oven. The outer chamber of the oven also contained calcium with argon, at a pressure of 3 torr, acting as the buffer gas. The partial pressure of the calcium vapour in the inner cylinder was then equal to that of the outer chamber. The resulting laser pulse power density was $\sim 10^{10}$ Wcm^{-2} at the focus of the lens. A second, 30 cm focal length quartz, lens was employed to re-collimate the third-harmonic beam. Phase-matching of the fundamental and

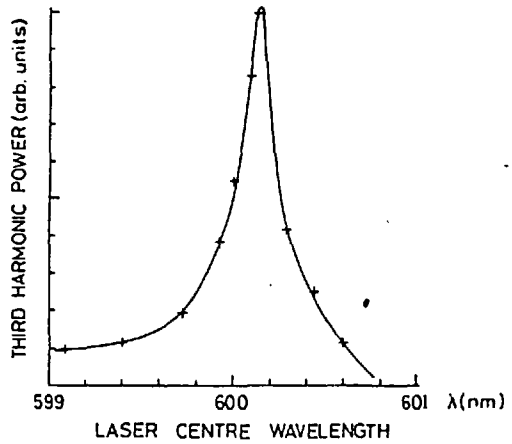

Fig. 2. Variation of third-harmonic generated power with laser wavelength.

harmonic frequencies was achieved by using xenon, at a pressure of ~10 torr. Fig. 2 shows how the conversion efficiency varies when the dye-laser frequency is tuned through resonance with the $4s^2$–4s5s transition.

Direct measurements have also been carried out of the thrid-harmonic pulse durations employing a Photochron II streak-camera [5] with a sapphire window and photocathode substrate. A pair of quartz prisms was employed to spatially separate out the 200 nm pulses from both the fundamental beam and light at 422 nm, arising from the 4s4p'P – $4s^2$ $^1S_0$ transition. Quantitative measurements of overall conversion efficiency and pulse shortening will be reported. Limits set by two-photon saturation and Stark shifts will be discussed and related to theoretical models.

References

[1] J.F. Young, G.C. Bjorklund, A.H. Kung, R.B. Miles and S.E. Harris, Phys. Rev. Letters 27 (1971) 1551.
[2] D.M. Bloom, G.W. Bekkers, J.F. Young and S.E. Harris, Appl. Phys. Letters 26 (1975) 687.
[3] D.J. Bradley, Opto-Electronics 6 (1974) 25.
[4] R.S. Adrain, E.G. Arthurs, D.J. Bradley, A.G. Roddie and J.R. Taylor, Opt. Commun. 12 (1974) 142.
[5] D.J. Bradley and G.H.C. New, Proc. IEEE 62 (1974) 313.

L3 TUNABLE PICOSECOND VACUUM-ULTRAVIOLET GENERATION IN Sr VAPOR USING SYNCHRONOUSLY PUMPED DYE LASERS

T.R. ROYT, Chi H. LEE and W.L. FAUST
Naval Research Laboratory, Washington, D.C. 20375, USA

We have conducted a series of experiments involving 4-wave parametric summing of 10 ps pulses in Sr vapor aimed at (1) demonstrating a particularly simple but efficient approach to the generation of tunable picosecond pulses in the VUV, (2) investigating the effects of temperature and additive gases on the efficiency of the conversion process in the vapor, (3) studying the most prominent autoionization resonance of Sr and its effect upon not only enhancement but phase-matching, and (4) testing for the existence of and measuring the relaxation time of a coherent state which might be created by two quantum excitation of a vapor resonance.

Third harmonic generation (THG) and sum frequency generation (SFG) in metal vapors have important advantages for the production of vacuum ultraviolet (VUV) radiation [1–2]. In order to make use of the resonant enhancement of $\chi^{(3)}$ in SFG, two waves each at frequency ω_1 are tuned to a two quantum transition of the vapor. Then they are added to a freely tunable third wave at ω_2 within the vapor to produce tunable VUV. It is necessary in general that the pulse at ω_1 be overlapped in time with the pulse at ω_2. The generation of picosecond pulses in the VUV, however, presents the problem of synchronizing the pulses from two independently tunable sources with picosecond accuracy. Overlap has been accomplished on a picosecond time scale without resonant enhancement by using wide bandwidth pulses from a parametric generator

STREAK CAMERA INVESTIGATION OF AN ACTIVELY MODE-LOCKED FLASHLAMP-PUMPED DYE LASER

E. LILL, S. SCHNEIDER and F. DÖRR
Institut für Physikalische und Theoretische Chemie der Technischen Universität München, D 8000 München 2, W. Germany

S.F. BRYANT and J.R. TAYLOR
Optics Section, The Blackett Laboratory, Imperial College, London SW7 2BZ, England

Received 6 October 1977

Direct measurements using a picosecond streak camera have shown that single pulses of 2–6 ps duration are obtained in the middle and latter stages of the output train of an actively mode-locked flashlamp-pumped dye laser. Measured pulse-widths showed no critical dependence on matching the cavity length to that of the driving master oscillator. In contrast pulses selected from the early stages of the train exhibited a complicated structure.

The use of a passively mode-locked flashlamp pumped dye laser to actively modulate the loss of a saturable absorber placed in the cavity of a second dye laser system to provide a synchronous mode-locked output has already been described [1]. A direct application of these variable time correlated mode-locked outputs has also been demonstrated in the measurement of the transmission decay times of several organic dyes [2]. Initial measurements using the two photon fluorescence technique showed the durations of the actively mode-locked pulses to be ~5 ± 3 ps. However, the TPF method necessitated the overall integration of all the pulses in the mode-locked train, thus providing no information on pulse development nor individual pulse structure. In this letter we report on the use of a picosecond streak camera to examine single pulses selected from various parts of the actively mode-locked train, and the effect of large mismatches of the driving and driven laser cavity lengths.

The experimental arrangement employed was similar to that described previously [1] and is schematically shown in fig. 1. Two identical laser systems were used. The cavity heads consisted of a bielliptical reflector accomodating two linear xenon flashlamps with a maximum total electrical input energy of ~100 J per lamp at 20 kV. In both systems the saturable absorber (1.5×10^{-4} M DODCI) was contained in a 2 mm length dye cell directly in contact with the plane wedged 100% mirror, and the optical cavity was terminated with a 50% plane wedged output reflector. The lasing medium in both laser systems was a 1.0×10^{-4} M water solution of Rhodamine 6G (+5% Ammonyx LO soap solution). Laser L 1 was passively mode-locked and was tuned using a narrow gap (~5 μm) Fabry–Pérot etalon (FP 1) to operate at 604 nm, where single pulse generation in the output train is rapid and the shortest pulses are obtained [3–5]. Approximately 50% of the output from laser 1 was reflected off mirror M_1 into the mode-locking dye cell of laser 2. Synchronization of the firing of both laser systems was achieved using a delay unit such that the peak of the ~1 μs mode-locked output of L_1 coincided with the rising edge of the flashlamp profile (fwhm 2.5 μs) of L_2 ~ 500 ns before its peak. The overall gain of system L_2 was kept below the lasing threshold. When the saturable absorber in L_2 is bleached by a pulse from the master oscillator L_1, the loss in system L_2 is reduced for approximately the aperture time of the saturable absorber [6]. If the amplification in the active medium of L_2 is sufficiently high then a rapid build up of the actively mode-locked pulse train occurs synchronously to the driving pulse train.

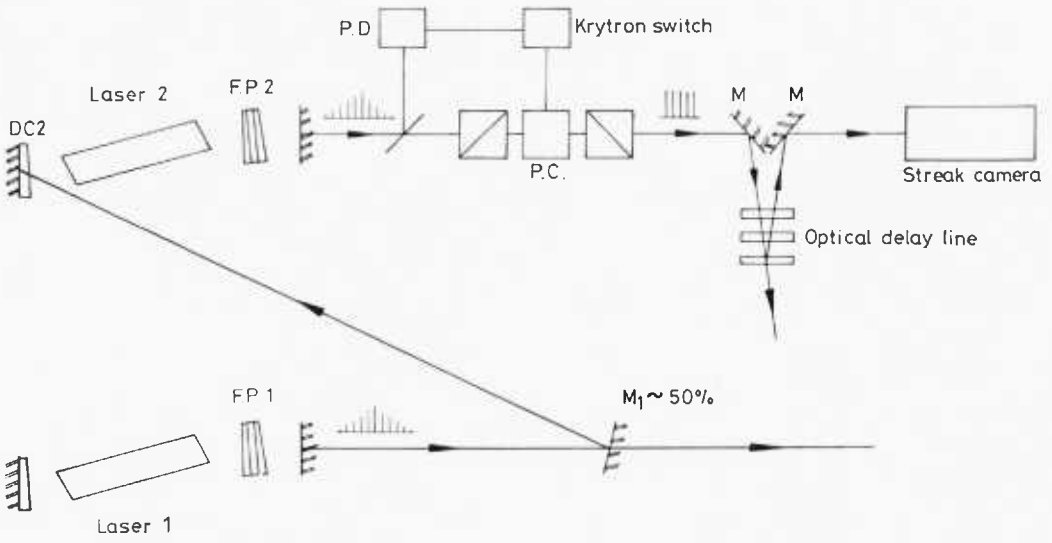

Fig. 1. Schematic of the experimental arrangement used in the generation and measurement of the actively mode-locked pulses.

Pulses were selected from various parts of the actively mode-locked train using a Pockels cell switch [7]. After passing through a calibrated optical delay line, single pulses were directed on to the S-20 photocathode of the Photochron II streak tube [8]. This tube was fibre optically coupled to a Mullard type 50/40 channel plate intensifier (operated at a gain of $\times 10^5$) and streaked images were recorded on photographic film (HP-5) which was in contact with the output face of the intensifier. At the laser wavelength used and with a camera writing speed of 10^{10} cm s^{-1}, the instrumental time resolution of the camera was 1.5 ps.

Previous experiments in active mode-locking using a frequency doubled Nd:Yag pumped dye laser system have shown a criticality in matching the driving cavity length to that of the actively mode-locked laser cavity [9]. However, in the work described here no attempt was made to accurately match the laser cavity lengths which has been described earlier [1]. For use as a source in providing two separately mode-locked frequency tunable sources with a variable time delay between pulses for applications in single shot excite and probe lifetime measurements for example, mismatches of the cavity are required [2]. Pulse quality and build-up was therefore examined for various cavity mismatches.

The passively mode-locked master oscillator was tuned to 604 nm. Fig. 2 shows a streak photograph and corresponding microdensitometer trace of a 2.5 ps pulse produced by this system. Typically pulses were in the range 2–4 ps with an energy content of ~80 μJ. Initially the actively mode-locked laser was tuned to operate at 595 nm and the cavity length was set at 580 mm. When operated passively at this wavelength mode-locked pulse formation occurs in a time of ~100 ns. The length of the driving master oscillator cavity was then varied in steps of ~66 ps mismatch over the range 520–620 mm and pulses were selected ~300 ns from the beginning of the ~800 ns long actively mode-locked trains. Fig. 3 shows microdensitometer traces of typical pulses for cavity lengths of laser L_1 of (a) 620 mm, (b) 560 mm and (c) 520 mm. It can be seen clearly that short pulses have evolved and that the pulse quality is relatively independent of the cavity lengths over this range of cavity mismatch. The pulses measured were of the order 2–7 ps.

The initial region of the actively mode-locked pulse train was also examined in a similar manner. In this case the actively mode-locked laser was tuned to operate at 585 nm, where under passive mode-locking conditions the build-up time of single pulses is relatively long ~150–200 ns. The pulses examined by the streak camera were selected ~80 ns from the beginning of the actively mode-locked train. A range of cavity mis-

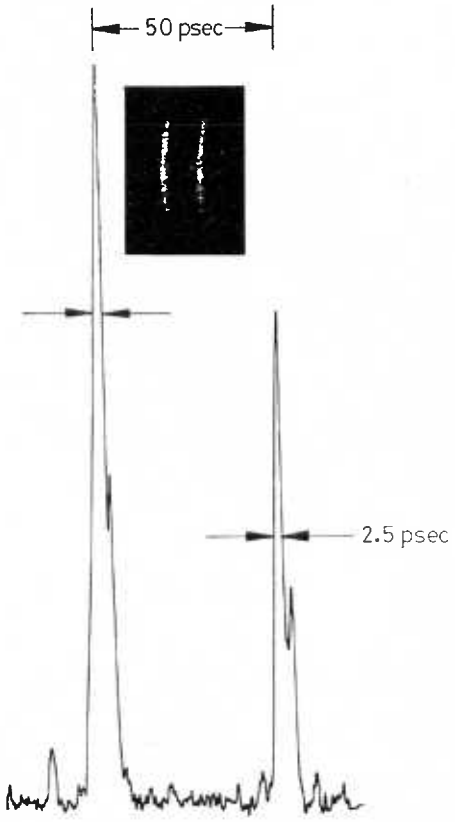

Fig. 2. Streak photograph and corresponding microdensitometer trace of a typical output pulse generated by the master oscillator (laser 1, see fig. 1).

matches from 540 to 620 mm for the driving oscillator was examined, with the cavity length of laser 2 constant at 580 mm. Fig. 4 shows typical microdensitometer trances of the pulses recorded over this range.

In general the results showed that single pulse development was not complete, although in most cases the pulses recorded showed the evolution of a single pulse with a duration of typically 2.5–6 ps. There was also a large amount of intrapulse structure, as can be seen in figs. 4(a), 4(c) and 4(d), which correspond to cavity lengths of 620, 580 and 560 mm respectively of laser L 1, the driving oscillator. Occasionally single pulses were recorded when the driving oscillator length was longer than that of the actively mode-locked cavity, (see fig. 4(b) recorded for L_1 cavity length of 600 mm). Slight variations in the pumping power or jitter in the switching caused by intensity variations most probably accounts for the appearance of a single pulse.

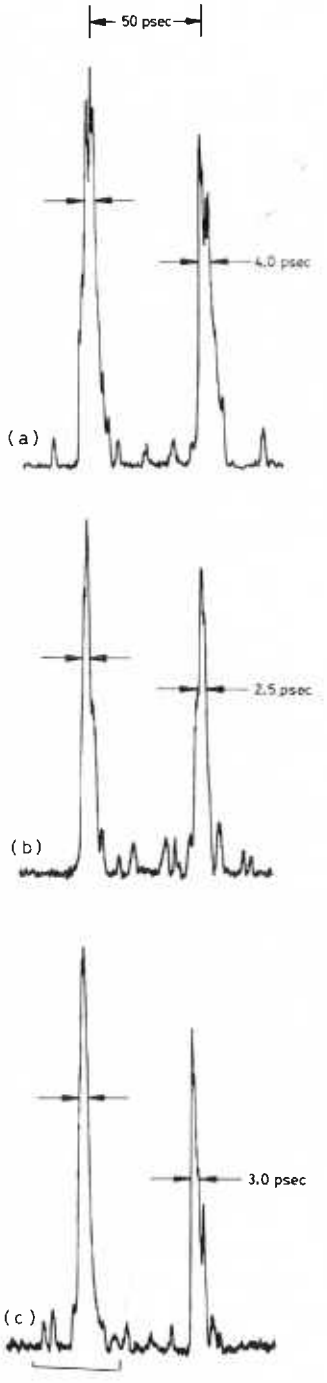

Fig. 3. Microdensitometer traces of pulses selected ~300 ns from the beginning of the actively mode-locked train for various cavity lengths of the master oscillator (a) 620 mm, (b) 560 mm and (c) 520 mm for a constant cavity length of the actively mode-locked laser of 580 mm.

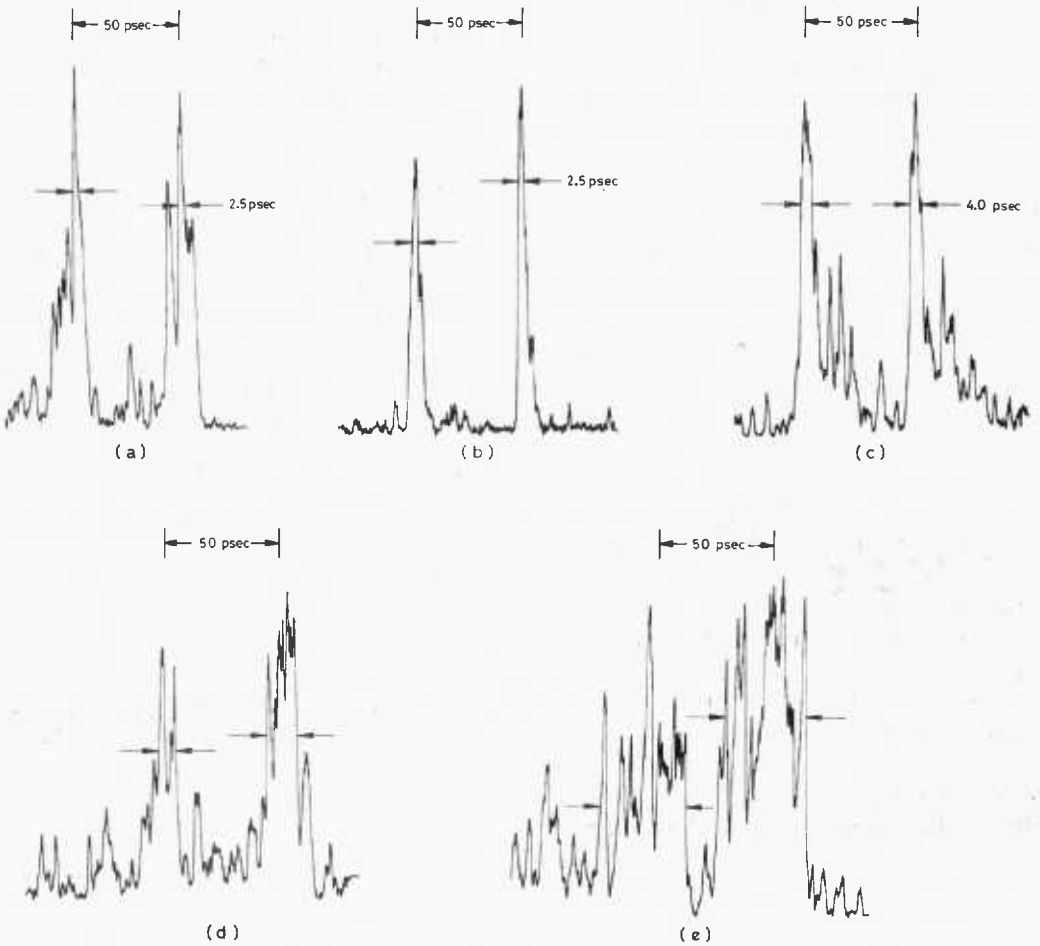

Fig. 4. Microdensitometer traces of typical pulses selected ~80 ns from the beginning of the actively mode-locked laser for driving cavity lengths of (a) 620 mm, (b) 600 mm, (c) 580 mm, (d) 560 mm and (e) 540 mm, with a constant actively mode-locked laser cavity length of 580 mm.

Usually the pulses recorded for the 600 mm cavity length of L_1 were similar to that of fig. 4(c), and single pulse evolution after this type of profile takes place in relatively few cavity round trips [5,10,11]. Fig. 4(e) shows typical pulse outputs recorded for a cavity length of 540 mm for laser 1. In this case the pulses were much longer and highly structured.

All the results of fig. 4 demonstrate that in the initial 100 ns of the activily mode-locked train single pulse evolution is incomplete, although oscilloscope traces would display single pulses and short TPF patterns would be obtained however with reduced contrast ratio. Therefore for use as a source of ultra short pulses, the initial region of the actively mode-locked train should not be used.

The dynamics of the development of a single pulse in the actively mode-locked train is complicated by several factors in the case of large mismatches in the cavity length. This is due to the fact that after the initial bleaching of the saturable absorber by the pulse from the passively mode-locked laser, in subsequent transits of the cavity, the actively mode-locked pulse in its build-up will "walk through" the "gate open time" of the saturable absorber caused by the driving laser, therefore getting out of step with it and giving rise to multiple pulses and high structure in the build-up re-

gion of the pulse trains. In the case where the cavities are perfectly matched or only a small (~ a few ps) mismatch is present, the build-up should be similar to that of the passively mode-locked laser [5] only occuring more rapidly. In the latter stages of the actively mode-locked output with mismatched cavities, single pulses are generated because saturable absorption and saturable amplification occur in the usual manner on the initial noise pulse created in the cavity by the driving oscillator which modulated the gain of the actively driven laser cavity.

The results have shown that short pulses are produced in the actively mode-locked laser for most of the output train. The fact that the build-up is rapid and the matching of cavity lengths is not critical, together with the high degree of tunability means that this method provides an excellent source of picosecond pulses for single shot excite and probe experiments. The study has however shown that the initial pulses in the train should not be used for this purpose. It is intended that a more detailed study will be carried out to determine the exact nature of the pulse evolution from noise for both the conditions of matched and mismatched cavities.

We would like to express our thanks to Professor D.J. Bradley for the provision of research facilities at Imperial College, and to Dr. W. Sibbett for experimental assistance and helpful discussions. The financial support granted by the Deutsche Forschungsgemeinschaft is gratefully acknowledged.

References

[1] E. Lill, S. Schneider and F. Dörr, Optics Comm. 22 (1977) 107.
[2] E. Lill, S. Schneider and F. Dörr, Applied Physics, in print,
[3] E.G. Arthurs, D.J. Bradley and A.G. Roddie, Appl. Phys. Letts. 19 (1971) 480.
[4] E.G. Arthurs, D.J. Bradley and A.G. Roddie, Appl. Phys. Letts. 20 (1972) 125.
[5] E.G. Arthurs, D.J. Bradley and A.G. Roddie, Appl. Phys. Letts. 23 (1973) 88.
[6] E.G. Arthurs, D.J. Bradley and A.G. Roddie, Chem. Phys. Letts. 22 (1973) 230.
[7] D.J. Bradley and W. Sibbett, Optics Comm. 9 (1973) 17.
[8] P.R. Bird, D.J. Bradley and W. Sibbett, Proc. 11th Intern. Congress on High speed photography (1974) p. 112.
[9] L.S. Goldberg and C.A. Moore, Lecture Notes in Physics 43 (1975) 248.
[10] G.H.C. New and D.H. Rea, J. Appl. Phys. 47 (1976) 3107.
[11] G.H.C. New, IEEE J. Quantum Elect. EQ-10 (1974) 115.

Intensity dependent time-resolution and dynamic range of Photochron picosecond streak-cameras

D. J. Bradley, S. F. Bryant, J. R. Taylor, and W. Sibbett

Optics Section, Blackett Laboratory, Imperial College, London SW7 2BZ, United Kingdom

(Received 25 August 1977; in final form, 26 September 1977)

The dynamic range of operation of Photochron I and Photochron II picosecond streak cameras is shown to depend upon the time-resolution employed. For events ~2 ps a useful dynamic range of 30 is obtainable, and this increases to a value of 180 for 30-ps events. No accumulative saturation effects occur at a time resolution as short as 2 ps.

I. INTRODUCTION

The Photochron type of image-tube streak-camera,[1–3] in which photoelectron time-dispersion spread is reduced by a high-potential planar mesh electrode close to the tube photocathode,[4] has been developed to the stage where a camera instrumental resolution of less than 1 ps can be obtained.[5] This high-field photocathode extraction electrode principle has since been almost universally adopted for picosecond streak cameras.[6] When the time-resolution limit was reduced to <10 ps for the first time[7] with a Photochron design of streak tube, it was noted that when the camera slit illumination was increased, time resolution deteriorated while spatial resolution was maintained.[8] Earlier[9] it had been demonstrated that picosecond exposure of a two-dimensional test pattern could be obtained without image distortion and with good spatial resolution, employing a gated four-stage cascade image-intensifier tube. It was postulated[8] that the loss of time resolution in the streak-tube arose from an intensity-dependent transit-time spread, probably arising from space-charge near the photocathode. Recently reported measurements of the magnitude of this effect in streak-tubes[10] have shown a dramatic loss of dynamic range in Photochron streak-tubes. If this peformance were characteristic of these tubes then it would not have been possible to have obtained the theoretically predicted time resolution[11,12] and good signal-to-noise ratio[2,8,13,14] over a wide range of wavelengths in the uv, visible, and ir spectral regions, and with sources varying in duration from nanoseconds to less than 1 ps. Streak-cameras are being increasingly employed in chemistry,[15] biology,[16] and condensed matter physics[17] where quantitative measurements of transient phenomena, with picosecond time resolution or better, are required. It was important therefore to carry out accurate measurements of the variation of temporal-resolution with input intensity, over as wide a range of time-resolution and operating wavelength as possible, to resolve the discrepancy between the results reported[10] and our earlier publications. As a result of measurements with two types of streak-camera systems we can now define the conditions under which streak cameras can be reliably employed for quantitative measurements of luminous phenomena. The dynamic range performance has been determined to be a factor of 10 better than that indicated by the results of Ref. 10.

II. EXPERIMENTAL ARRANGEMENTS

A. Photochron I camera with S1 photocathode

The two camera systems tested are shown schematically in Fig. 1. The Photochron I system, with optical coupling to a four-stage magnetically focused image-intensifier (EMI type 9694), has been extensively described in earlier publications.[1,3,5,8] The dynamic range was investigated with the arrangement of Fig. 2. A mode-locked Nd:phosphate–glass laser oscillator, operating in several transverse modes, was used to generate the test pulses. About five pulses were selected by a Pockels cell switch from the middle of the pulse train. In this manner signal-induced background, arising from the many pulses of the laser train, was reduced and the delay in the Krytron high-voltage ramp generator[18] could be conveniently accommodated. Each of the selected-out pulses was injected into an air-gap Fabry–

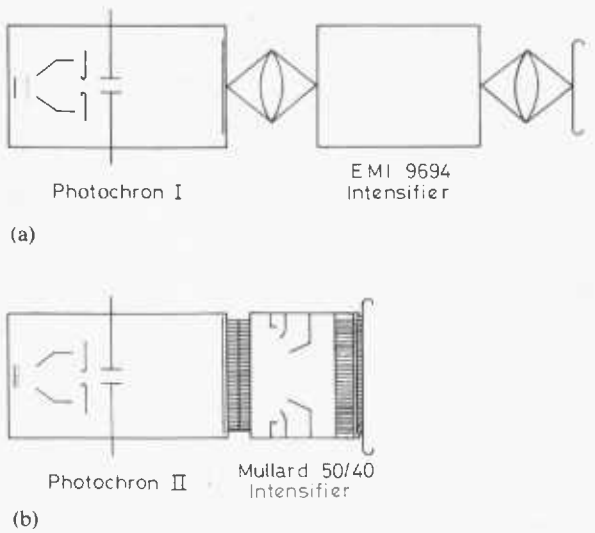

FIG. 1. The two types of streak cameras tested. In (a) the Photochron I streak tube had an S1 photocathode with absolute sensitivities of 0.36 mA/W at 1038 nm and 1.2 mA/W at 524 nm, respectively. In (b) the Photochron II tube had an S20 photocathode, of sensitivity 95 μA/lm.

 0034-6748/78/4902-0215$00.60

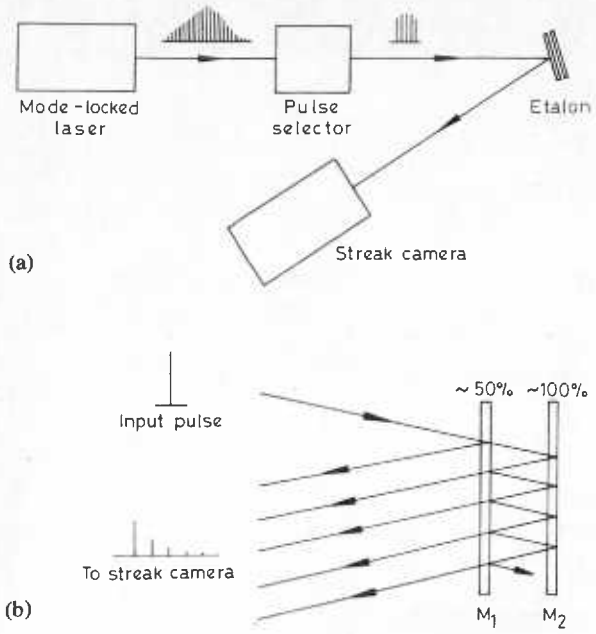

FIG. 2. Arrangement for generating a calibrated test source for the measurement of the intensity dependence of the streak-camera time resolution and the resultant useful dynamic range when the camera is operated at different instrumental time resolutions.

Perot etalon of mirror reflectivities 50% and 100% [Fig. 2(b)]. Thus a train of pulses of monotonically decreasing intensities, and separated by the double-transit time of the etalon, was generated from each incoming laser pulse. It was then necessary to record only such a sub-train of pulses in a single streak photograph, to obtain a direct measurement of the useful dynamic range of the camera. The time resolution of the camera was adjusted to match the duration of the pulse employed. A typical streak photograph and the corresponding calibrated microdensitometer trace is shown in Fig. 3. Before entering the Fabry–Perot etalon each of the laser pulses had an energy of ~1 mJ and the typical duration was 10 ps. The streak camera was set[18] to give a time resolution of 2.5 ps at a writing speed of 10^{10} cm s^{-1} at the streak-tube phosphor and the intensifier was operated at a gain of 10^6. The streak traces were photographed with Ilford HP5 film, developed to produce an ASA rating of ~3000 and a useable range of 1000 in exposed intensity. The film characteristic was determined for each series of exposures by employing a calibrated neutral density wedge. From records such as Fig. 3 it was possible to demonstrate that no significant broadening of the pulses with increasing intensity occurred at intensities less than 50 times the developed film fog level. The useful dynamic range of a streak camera can be defined as the range of intensity above fog level within which the measured pulse duration τ_r' (FWHM), after allowing for the low-intensity camera instrumental response, does not exceed the actual pulse duration τ_r by more than 20%. A convenient way of illustrating the intensity-dependent effects is to plot the ratio τ_r'/τ_r as a function of the pulse intensity. (The camera instrumental width is deconvolved from the records.) The variations of the ratio τ_r'/τ_r are shown in Fig. 4 for pulses of durations 10 and 35 ps. The longer duration pulses were produced by introducing into the laser resonator a bandwidth-limiting Fabry–Perot etalon of ~60 μm gap, and with mirrors of 70% reflectivity. For these longer pulses it was necessary to readjust the separation of the calibration etalon (of Fig. 2) to produce test pulses separated by 100 ps. The

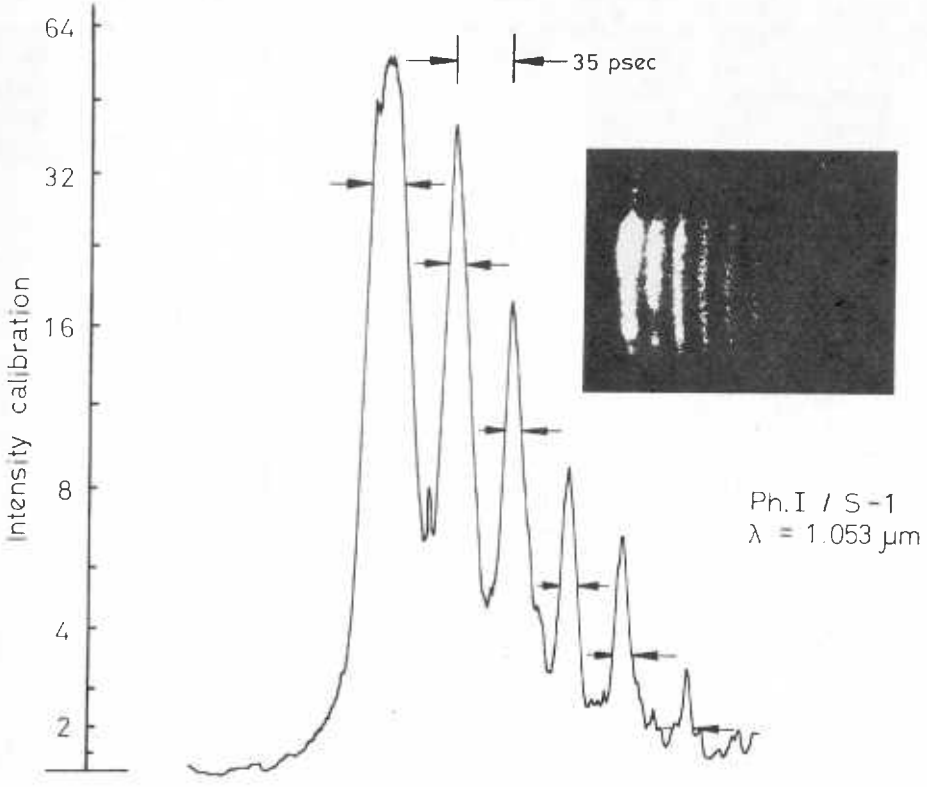

FIG. 3. Photograph and corresponding calibrated microdensitometer trace of streak-record obtained with arrangement of Fig. 2 with Photochron I tube, optically coupled to EMI 9694 intensifier. The laser pulse duration (Nd:phosphate–glass laser) was 10 ps and the camera instrumental resolution was 2.5 ps.

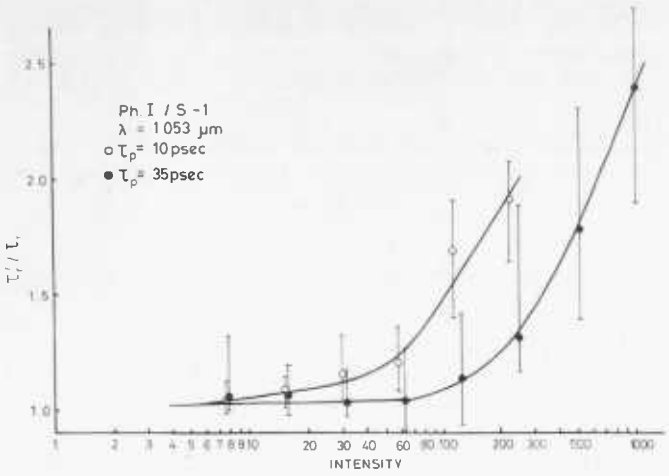

FIG. 4. Variation of ratio of recorded pulse duration to actual pulse duration (τ_r'/τ_r) as a function of laser pulse intensity as recorded by Photochron I, for 1.053-μm pulses of durations 10 ps and 35 ps, respectively.

camera writing-speed was reduced to 4×10^9 cm s^{-1} to allow all of the sequence of attenuated pulses to be displayed on the streak-tube phosphor-screen. The points on the graphs, which represent the most probable value for τ_r'/τ_r at a given intensity, were obtained from 20–25 separate streak records. The error bars indicate the maximum variations in the values derived from the microdensitometer traces. From Fig. 4 it can be seen that for the 10 ps pulses the incident intensity can be increased to ~55 × above the fog level before the ratio τ_r'/τ_r reaches the value 1.2. This corresponds to a variation of ±10% in the measured pulse duration for pulses falling within this range of intensity, i.e., a useful dynamic range of ~55. The authors of Ref. 10 reported a value of only 5 for the useful dynamic range, employing the same criterion, of an Imacon 675 camera (Hadland Photonics Ltd.) tested with 10 ps pulses at 1053 nm. This camera has a channel plate intensifier, with fiber-optic coupling between the streak tube and intensifier as well as between the intensifier and the film plane [as in Fib. 1(b)]. For an Imacon 600 camera with lens coupling and a three-stage magnetically focused intensifier, the same authors determined a dynamic range of ~15 for 30 ps pulses. From our measurements (Fig. 4) the dynamic range for a similar camera system is ~180, for 35-ps pulses, again ten times better performance.

As an independent check of our measurements, the camera response was also investigated with a Michelson interferometer arrangement. With this device two subpulses were produced from each incident laser pulse. By inserting calibrated neutral-density filters into the interferometer optical arms, a series of values of the τ_r'/τ_r ratio were determined over a range of pulse intensities, employing many separate laser firings. The dynamic range values for 10-ps pulses agreed to within 10% with the results of Fig. 4.

The dynamic range of the S1 photocathode camera was also measured at the second-harmonic wavelength (λ = 526 nm) of the Nd : phosphate–glass laser, by placing a 15-mm-long, 10-mm-aperture ADP crystal after the pulse selector. An etalon with the appropriate reflectivity mirrors at the visible wavelength generated the test signal. The camera resolution was reduced to ~4 ps by the increase in the spread of the photoelectron initial velocities from a S1 photocathode at this wavelength.[3] The second-harmonic frequency pulses were found to have durations of ~7 ps, but the dynamic range (Fig. 5) of ~60 was slightly better than that obtained with the 10-ps pulses at the laser fundamental frequency.

III. PHOTOCHRON II CAMERA WITH S20 PHOTOCATHODE

Dynamic range measurements were also carried out with the Photochron II camera system of Fig. 1(b). This second-generation streak-tube[11] had been constructed with an S20 photocathode on a sapphire substrate, a sapphire input window, and an output fiber-optic face plate, for the study[19] of the generation of third-harmonic (200 nm) pulses from a mode-locked dye laser. A Mullard type 50/40 channel-plate intensifier was fiber-optically coupled to both the streak tube and the recording photographic film. This electrostatically focused intensifier was operated at a gain of 10^5 and was gated open for an exposure of 100 μs. A flash-lamp pumped Rhodamine 6G dye laser, mode locked by DODCI[20] and tuned to operate at 605 nm, produced test pulses of durations ~5 ps. At the laser wavelength the S20 photocathode had a sensitivity of 24 mA/W. The camera was operated at a streak speed of 6×10^9 cm s^{-1} to give a time resolution of ~2 ps. A typical streak-photograph and the corresponding calibrated microdensitometer trace are shown in Fig. 6. Under these conditions the dynamic range was ~55. (Fig. 7). Pulses of duration 2 ps were generated[11] by employing DQOCI as a mode-locking dye in the laser. Increasing the camera streak writing speed to 10^{10} cm s^{-1} provided an instrumental time-resolution limit of 1.4 ps.[12] From Fig. 7 it can be seen that even for pulses as short as 2 ps the useful dynamic range remains as high as 30.

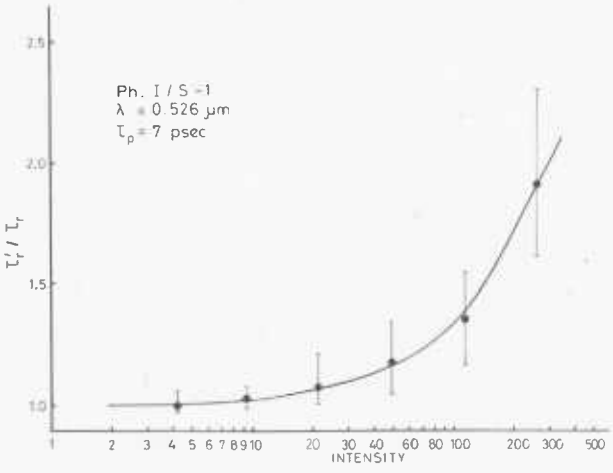

FIG. 5. Dynamic range, with second-harmonic frequency (526 nm) pulses of 7-ps duration for same camera as Fig. 4.

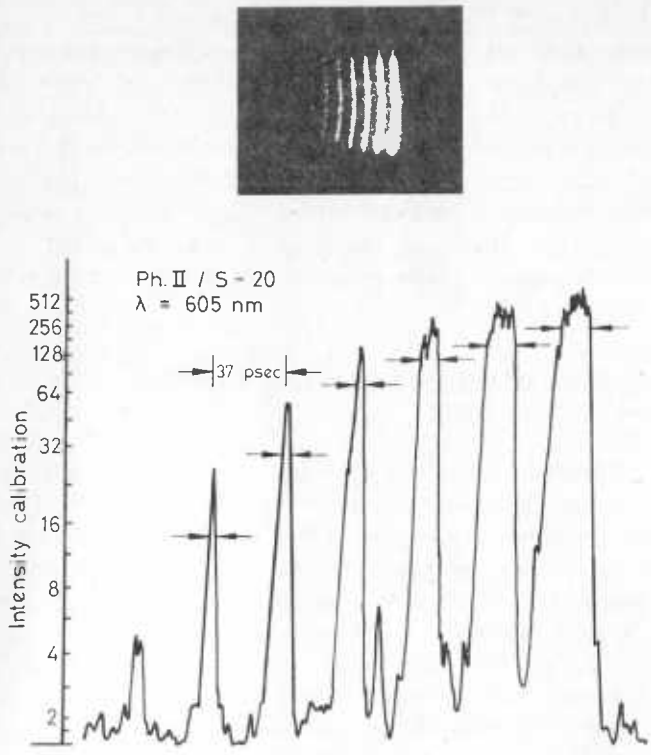

FIG. 6. Same as for Fig. 3 using a Photochron II streak camera with Mullard 50/40 image intensifier fiber-optically coupled to both the streak tube and the recording photographic film. Test pulses had durations of 5 ps at 605 nm.

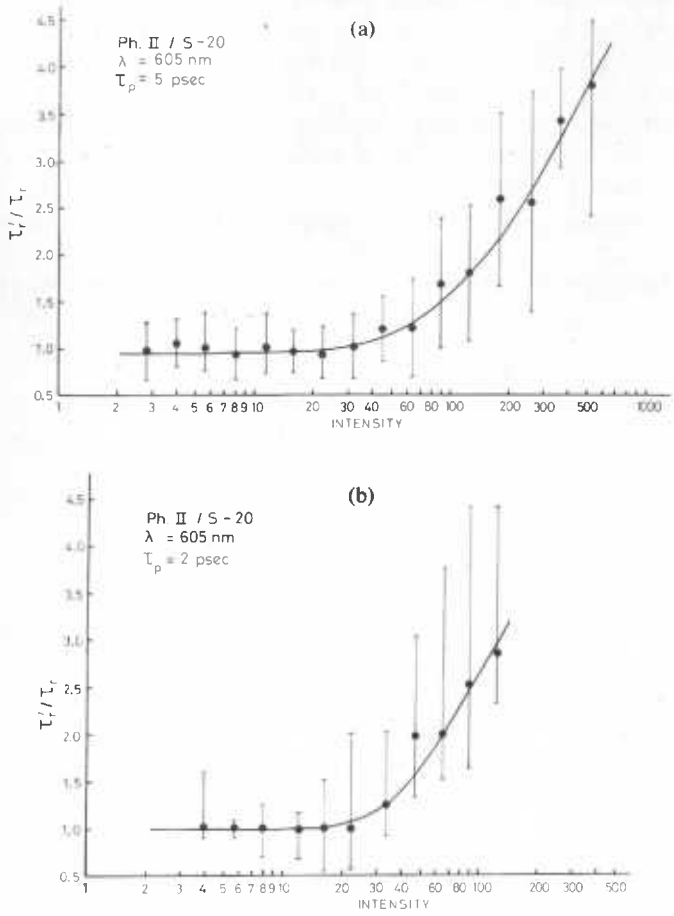

FIG. 7. Dynamic range of Photochron II streak-camera for (a) 5-ps pulses and (b) 2-ps pulses.

An accumulative effect on the measured pulse intensities was also reported in Ref. 10. The intensity recorded for successive pulses was influenced and reduced by the preceding pulses when three 30-ps pulses of equal intensity, spaced 120-ps apart, were recorded on single streaks. The effect apparently increased with increasing intensity of the incident pulses. We have repeated this type of measurement with a quartet of equal intensity 2-ps pulses, each separated by 8 ps, using the Photochron II camera system. The streak photograph and microdensitometer trace of Fig. 8 show that the camera faithfully reproduces the pulse profiles and confirms that there are no accumulative photocathode saturation effects on this time scale.

IV. DISCUSSION

Our results, summarized in Table I, have confirmed the original observation[8] that the time resolution of picosecond streak cameras deteriorates if the streak-tube photocathode is illuminated with too high an intensity. However, we have found that the useful dynamic ranges measured by us are considerably

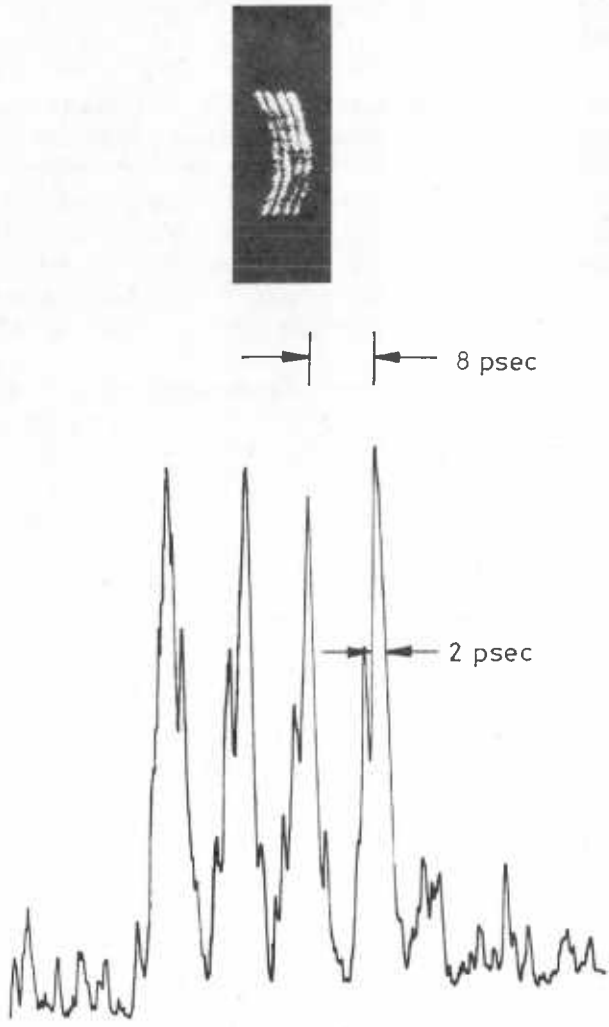

FIG. 8. Photograph and microdensitometer trace of streak images of a quartet of 2-ps pulses separated by 8 ps recorded by the S20/Photochron II streak camera. The pulses were generated in a mode-locked dye laser operating at 605 nm.

TABLE I. Summary of dynamic range measurements

Parameters	Photochron I (S1) camera			Photochron II (S20) camera	
Test laser pulse duration	30 ps	10 ps	7 ps	5 ps	2 ps
Wavelength	1.05 μm	1.05 μm	0.53 μm	0.6 μm	0.6 μm
Photocathode sensitivity	0.3 mA/W	0.3 mA/W	1.2 mA/W	24 mA/W	24 mA/W
Dynamic range measured	180	55	60	55	30

better than the values reported earlier, for similar camera systems.[10] The dynamic range of a shortened version of an S1 Photochron I image tube (ITL) has also been measured.[21] This system incorporates a four-stage magnetically focused intensifier in an arrangement similar to our S1/PhI camera. Based on a criterion of a broadening of 3 ps in their 50-ps test pulses (cf. 20% in this publication) these authors reported a dynamic range of 223 which is fairly consistent with our results of Table I.

The overall linearity of the streak camera is also substantiated by our results. The photographic film characteristic imposes the only nonlinearity in the responses of the systems. Work is now in progress to evaluate the performance of an optical multichannel array readout (PAR 1205D) as a replacement for film recording, with the aim of producing a completely linear response camera.

ACKNOWLEDGMENT

We are glad to acknowledge financial support from the Paul Instrument Fund of the Royal Society and from the Science Research Council.

[1] D. J. Bradley, B. Liddy, and W. E. Sleat, Opt. Commun. **2,** 391 (1971).
[2] D. J. Bradley, *Proceedings of the 11th International Congress on High Speed Photography*, edited by P. J. Rolls (Chapman and Hall, London, 1974), p. 23.
[3] D. J. Bradley and G. H. C. New, Proc. IEEE **62,** 313 (1974).
[4] D. J. Bradley, U. K. Patent Spec. 31167/70 (1970); U.S. Patent 3761614 (1973).
[5] D. J. Bradley and W. Sibbett, Appl. Phys. Lett. **27,** 382 (1975).
[6] See Ref. 2, pp. 32, 101, 107, 112, 118, 124, 130, and 136.
[7] D. J. Bradley, B. Liddy and W. E. Sleat. Paper read at Int. Conf. On Laser-Produced Plasmas (Moscow, USSR, November 1970). Report by S. D. Zakharov, in Sov. J. Quantum Electron. **1,** 310 (Nov/Dec 1971).
[8] D. J. Bradley, B. Liddy, A. G. Roddie, W. Sibbett, and W. E. Sleat, Adv. Electron. Electron Phys. **33B,** 1145 (1972).
[9] D. J. Bradley, J. F. Higgins, and M. H. Key, Appl. Phys. Lett. **16,** 53 (1970).
[10] W. Friedman, S. Jackel, W. Seka, and J. Zimmerman. *Proceedings of the 12th International Congress on High Speed Photography*. (SPIE **97,** Bellingham, Washington, 1977), pp. 544–548.
[11] P. R. Bird, D. J. Bradley, and W. Sibbett, Ref. 2, p. 112.
[12] P. R. Bird, D. J. Bradley, and W. Sibbett, Adv. Electron. Electron Phys. **40A,** 51 (1976).
[13] D. J. Bradley and W. Sibbett, Opt. Commun. **9,** 17 (1973).
[14] D. J. Bradley, *Ultra-short light pulses, Picosecond techniques and applications*, edited by S. L. Shapiro (Springer, Heidelberg, 1977), p. 17.
[15] K. B. Eisenthal, Ref. 14, p. 275.
[16] A. J. Campillo and S. L. Shapiro, Ref. 14, p. 317.
[17] D. von der Linde, Ref. 14, p. 204.
[18] D. J. Bradley, B. Liddy, W. Sibbett, and W. E. Sleat, Appl. Phys. Lett. **20,** 219 (1972).
[19] W. Sibbett, D. J. Bradley, and S. F. Bryant, Opt. Commun. **18,** 107 (1976).
[20] D. J. Bradley, Opto-Electronics **6,** 25 (1974).
[21] S. W. Thomas and G. E. Phillips, *Proceedings of the 12th International Congress on High Speed Photography* (SPIE 97, Bellingham, Washington, 1977), pp. 11–16.

INVESTIGATION OF THE RADIATIVE RECOMBINATION PROCESS IN CdSe (P-BAND) WITH 2-PICOSECOND TIME RESOLUTION

S.F. Bryant, V.S. Dneprovskii* and W. Sibbett

Optics Section

Physics Department

The Blackett Laboratory

Imperial College

London SW7 2BZ

UK

ABSTRACT

The characteristic delay, rise and decay times of recombination radiation at high exciton densities (P_∞-band) in CdSe monocrystal (77K) were measured with two picosecond time resolution and found to be 34 ± 6psec, 9 ± 2 psec and 16 ± 3 psec respectively. The values of the rate constants of the exciton-exciton interaction and of the binding of free carriers into excitons were estimated.

PACS numbers: 78.60.-b, 31.70.Hq

42.65.-k

* Visiting professor from Physical Department, Moscow State University

The delay, rise and decay times for recombination radiation from a CdSe monocrystal excited by picosecond laser pulses were measured with 2 psec time resolution.

Previously several methods have been employed to measure formation times and the relaxation times of excitons, biexcitons, and some exciton complexes in CdSe crystals. These include the use of an ultrafast shutter, with a variable delay line which was changed from shot to shot (1), a special laser spectrochronograph with 30 psec time resoltuion and an electron chronograph (3).

In this work a Photochron II streak camera with better than 2 psec time resolution was used (4), allowing the time resolved recombination radiation to be recorded in a single shot.

The experimental arrangement is shown in Figure 1. The platelet CdSe crystal, grown by resublimation of the charge, of stoichiometric composition was immersed in liquid nitrogen. The sample was excited by the complete train ($\sim$ 600 ns) from a flashlamp pumped dye laser, mode-locked with DQOCI (5) and tuned to 580 nm with a 5μm gap intra-cavity Fabry-Perot. This set $\frac{hc}{\lambda}$ - Eg $\simeq$ 0.34eV, where the bandgap of the crystal Eg $\simeq$ 1.8eV and λ is the laser wavelength.

The duration of the laser pulses was measured with the streak camera and it was found that the shortest pulses ($\sim$ 4psec) were recorded about 400 ns after the start of mode-locking. Figure 2 (a) is a photograph of the recorded streaks of the quasi-normal reflections of the laser pulses from a 5mm thick glass flat ($\equiv$ 50 psec). The intensity profile of these streak images is shown in Figure 2 (b). The focussed laser beam was incident at an angle of $\sim 75^0$ to the $(1\bar{2}10)$ plane of the crystal. The luminescence and the reflected part of the laser beam were focussed onto the slit of the streak camera with a f/1.0, 5 cm focal length lens. Part of this light

was passed through a Schott RG630 filter to eliminate the laser component, and the rest was attenuated with a large neutral density filter (ND 3.0). Images of both the laser pulse and the luminescence were thus simultaneously displayed on the phosphor of the streak camera. Part of the laser output was used to trigger the streak camera. This trigger was delayed by 400ns so that only the effects of short pulses were recorded.

Initially, a Monospeck 1000 spectrograph was substituted for the streak camera and the luminescence spectra of the CdSe crystal were studied. The recombination spectra at different excitation levels are shown in Figure 3. The position of the exciton-exciton interaction line (P_∞) was determined using the data of Liebing and others (6).

The positions of the maxima of the A-1O line (the line corresponding to the radiative recombination of free excitons with the emission of one longitudinal optical phonon) and the E-line (the line corresponding to exciton-electron interactions) were calculated using the formulae given in references 7 - 9. The energy of the A-exciton shown by an arrow in Figure 3 was determined from the reflection spectra of the sample.

An example of a streak record is shown in Figure 4. By fitting a 'best fit' curve through a microdensitometer trace of this streak, and then compensating for the non-linear intensity response of the film, we can derive the corresponding intensity profile shown in Figure 4 (b).

In addition to the decay time (2), the delay and the rise time of the luminescence could be measured with this ultra-fast streak camera.

The delay between the exciting pulse and the luminescence peak is 34 ± 6 psec. Consequently the intraband relaxation time for carriers and the time for the binding of free carriers into excitons must be less than this value. This result indicates that the process is very rapid, and is in agreement with those of the authors of references (2) and (10) each

of whom measured delay times of less than 100 psec.

The risetime of the P-line was 9 ± 2 psec and the decay time corresponding to an intensity of $\frac{1}{e} \cdot I_{peak}$ was 16 ± 3 psec. As can be seen from Figure 4 (b), the slope of the decay curve changes at low intensities probably indicating a change in the recombination process (Figure 3). This can only be checked however by taking time resolved spectra.

To estimate the reaction constant for the exciton-exciton interaction process (C), and the quadratic recombination coefficient of free carriers for direct recombination (γ), and for recombination via excitons (γ_{ex}) in CdSe at liquid nitrogen temperatures, the experimental curves for luminescent radiation were compared with the solution of the kinetic equations (c.f. ref. 10, the case of the dominating exciton-exciton interaction). The best fit of experimental data with calculated curves gives the following values for these parameters:

$$C \simeq 5.10^{-7} cm^3 s^{-1}, \gamma_{ex} = 0.1, \gamma \simeq 10^{-7} cm^3 s^{-1}$$

This experiment demonstrates the usefulness of the combination of a tunable picosecond dye laser and a high resolution streak camera in the investigation of fast exciton recombination processes. It is planned to extend this study by increasing the tuning range of the dye laser so that resonant excitation of excitons can be studied.

We would like to thank Professor D.J. Bradley for helpful discussions and the provision of research facilities and V.N. Chumash and V.S. Fokin (Moscow State University) for their help with measurement of the crystal reflection spectra. One of us, V.S. Dneprovskii, wishes to acknowledge the support of the British Council.

References

1. H. Kuroda, S. Shionoya, Opt. Commun. 10, 74, 1974; H. Kuroda and S. Shionoya, Technical Report of ISSP, Ser. A., N 603, 1974.

2. G.A. Boiko, V.S. Dneprovskii, M.V. Kraevskii, K. Marinova, S.M. Oak, E.K. Silina, V.S. Fokin, Phys. Stat. Sol., (B), 85, 111, 1978.

3. V.V. Egorov, A.N. Kurbatov, N.V. Soroko-Novitskii, Fiz. Teckn. Poluprov., 10, 7o3, 1976.

4. D.J. Bradley, S.F. Bryant, J.R. Taylor and W. Sibbett, Rev. of Sci. Instr., 49, 215, 1978.

5. P.R. Bird, D.J. Bradley and W. Sibbett. Proc. of 11th High Speed Photography Congress, 112, 1974.

6. A. Liebing, P. Mengel, W. Ruppel., Phys. Stat. Sol. (B) 72, 431, 1975.

7. D. Segall, G.D. Mahan, Phys. Rev. 171, 935, 1968.

8. E.F. Gross, S.A. Permogorov, B.S. Razbirin, Sov. Phys. Solid State, Vol. 8, No. 5, 1180, 1966.

9. T. Fisher, J. Bille, J. Appl. Phys. 45, 3937, 1974.

10. A.N. Kurbatov, A.I. Dirohka, A.D. Britov, A.N. Vlasov, N.N. Mochalkin, N.V. Soroko-Novitskii, Izvestiya Acad. of Sciences USSR, ser. Fizicheskaya, 37, 363, 1973.

Figure Captions

Figure 1 The experimental arrangement for exciting the CdSe crystal and streaking the laser pulse and resulting luminescence.

Figure 2 (a) A streak photograph of a pair of laser pulse images separated by 50 psec and (b) the corresponding intensity profile.

Figure 3 The recombination spectra of the CdSe crystal (a) at high intensities, and (b) at lower intensities.

Figure 4 (a) A streak photograph of both the excitation pulse and the luminescence from the CdSe crystal and (b) the corresponding intensity profile.

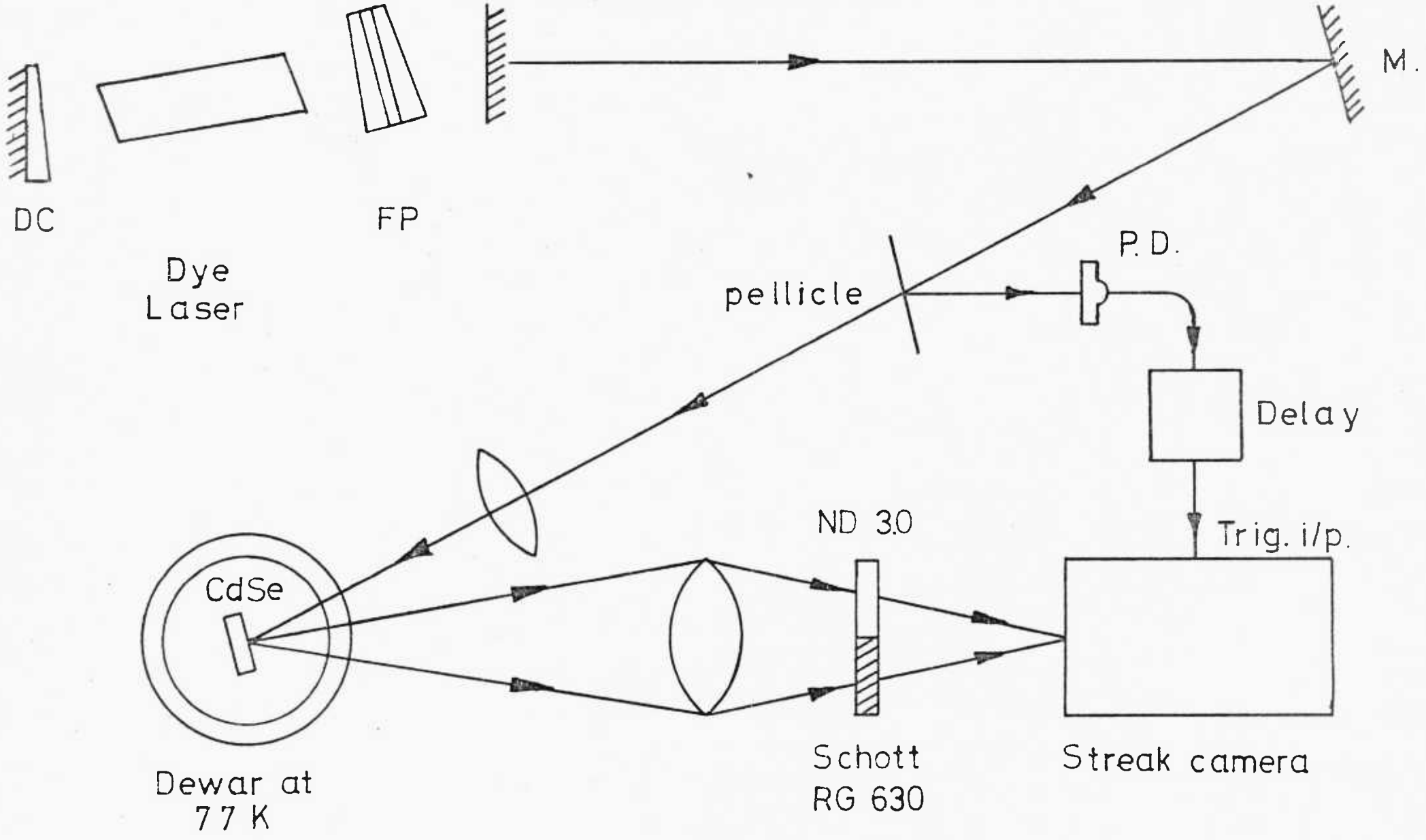
DC
Dye
Laser
FP
M.
pellicle
P.D.
Delay
Trig. i/p.
ND 3.0
CdSe
Dewar at
77 K
Schott
RG 630
Streak camera

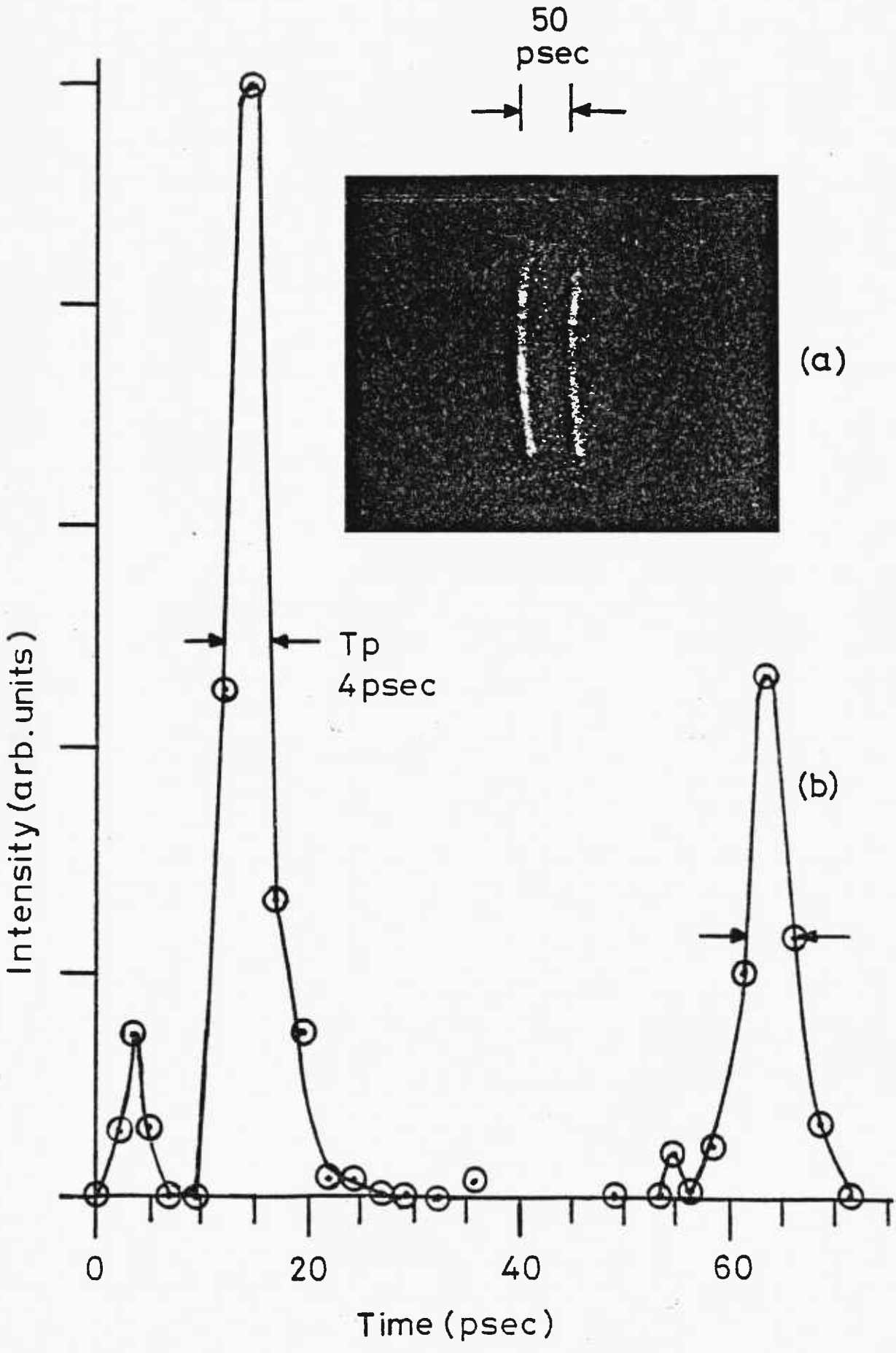
50
psec
(a)
Tp
4psec
(b)
Intensity (arb. units)
0
20
40
60
Time (psec)

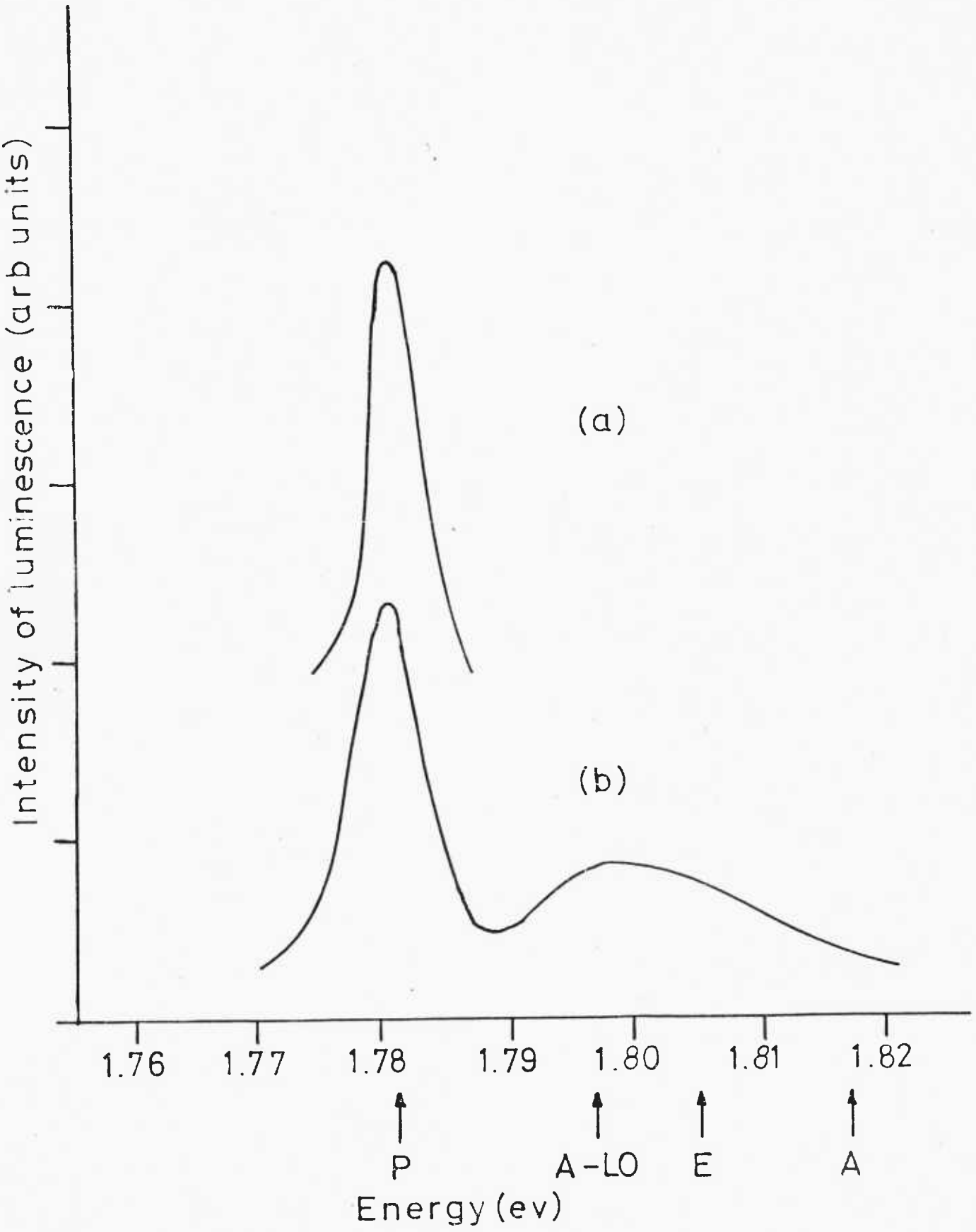
Intensity of luminescence (arb units)
(a)
(b)
1.76
1.77
1.78
1.79
1.80
1.81
1.82
P
A-LO
E
A
Energy (ev)

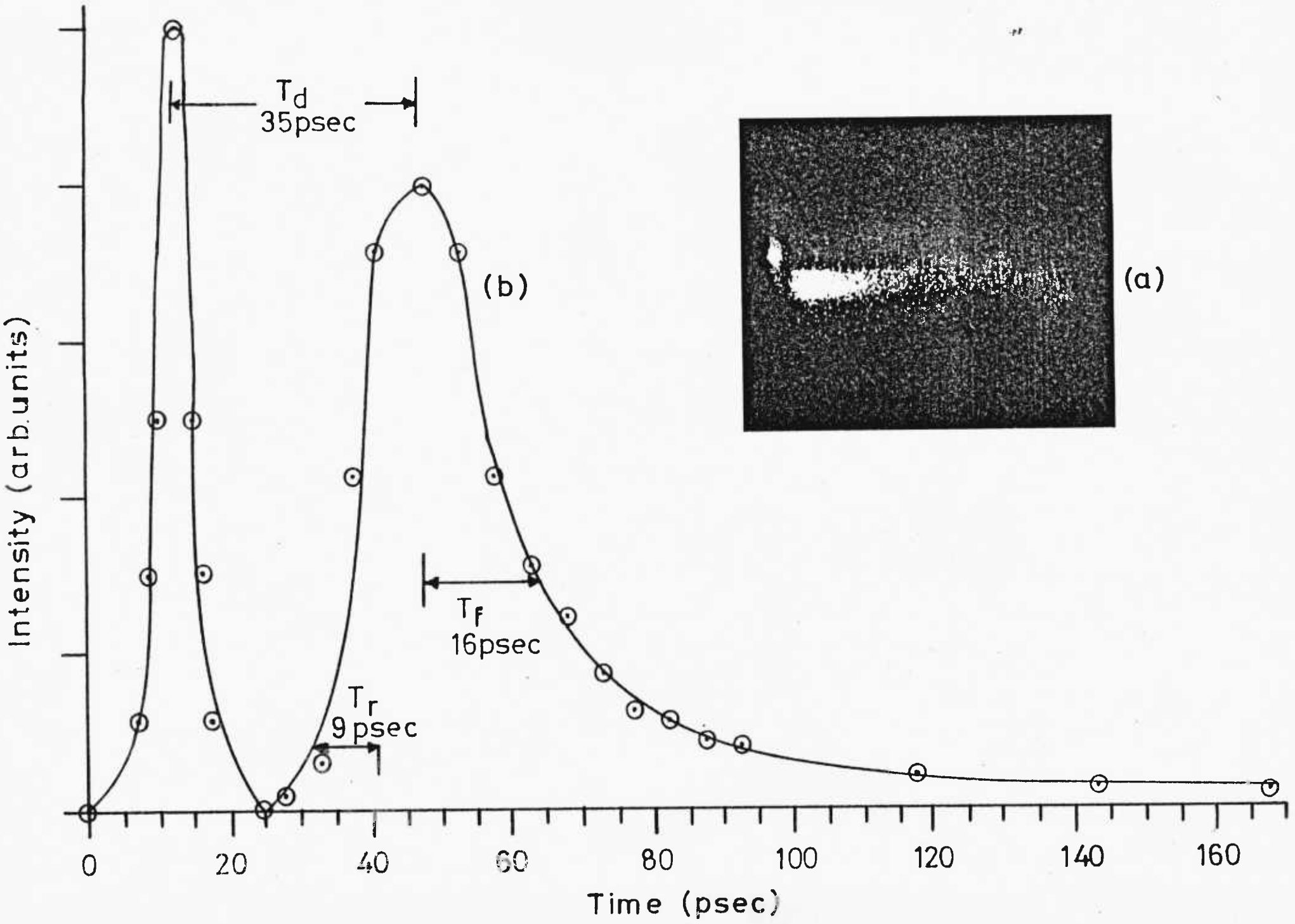
T_d
35psec
(b)
(a)
T_f
16psec
T_r
9psec
Intensity (arb.units)
0
20
40
60
80
100
120
140
160
Time (psec)